

TRANSITION AND STRUCTURAL DEVELOPMENT
OF THE NEAR FIELD OF A PLANAR
TURBULENT JET UNDER LOW LEVEL
ACOUSTIC EXCITATION

By

WILLIAM KIRK BRYZA

Bachelor of Science in Mechanical Engineering

Oklahoma State University

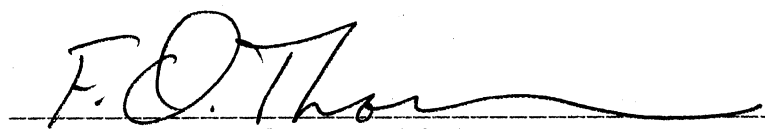
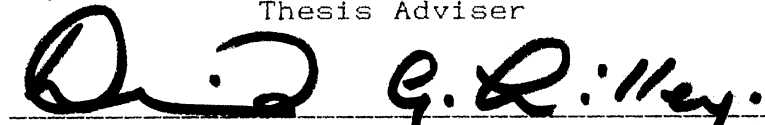

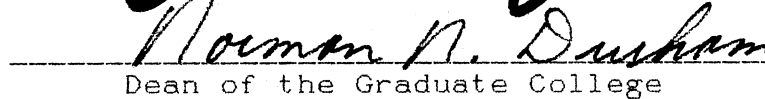
Stillwater, Oklahoma

1987

Submitted to the Faculty of
the Graduate College of
Oklahoma State University
in partial fulfillment of
the requirements for
the Degree of
MASTER OF SCIENCE
May, 1989

TRANSITION AND STRUCTURAL DEVELOPMENT
OF THE NEAR FIELD OF A PLANAR
TURBULENT JET UNDER LOW LEVEL
ACOUSTIC EXCITATION

Thesis Approved:


Thesis Adviser



Dean of the Graduate College

ACKNOWLEDGMENTS

I would like to express my sincere appreciation to my advisor, Dr. F. O. Thomas, for his invaluable help in preparing this thesis. I would like to thank him for help in taking, analyzing, and presenting the data that makes up the body of this thesis. Further, I thank him for giving me his time and efforts even after he left Oklahoma State for other academic efforts.

I would like to especially thank my wife, Deborah Bryza, for her patience, encouragement, and moral support while I completed the work required for my advanced degree. I would also like to thank my parents, William and Margaret Bryza, who provided constant support to me.

TABLE OF CONTENTS

Chapter	Page
I. INTRODUCTION	1
1.1 Introduction	1
1.2 Objectives of the Research	6
II. JET FLOW FIELD AND MEASUREMENT APPARATUS	7
2.1 The Planar Turbulent Jet	7
2.2 Facility Set-up and Measurement Apparatus	9
2.3 Validation of the Flow Field	14
2.3.1 The Unexcited Jet	14
2.3.2 The Effect of Acoustic Excitation	17
2.3.3 Velocity and RMS Fluctuation Variation	26
III. TRANSITION MECHANISMS OF THE JET	43
3.1 Application of Linear Theory	43
3.1.1 Linear Stability Theory	43
3.1.2 Linear Stability Techniques and Results	47
3.2 Power Spectral Measurements	60
3.2.1 Spectral Measurement Techniques	66
3.2.2 Spectral Development at $f_{ac} = 2650$ Hz	66
3.2.3 Spectral Development at $f_{ac} = 2200$ Hz	86
3.3 Digital Complex Demodulation	96
3.3.1 Digital Complex Demodulation Techniques	96
3.3.2 Digital Complex Demodulation at $f_{ac} = 2650$ Hz	98
3.3.3 Digital Complex Demodulation at $f_{ac} = 2200$ Hz	101
3.4 Bicoherence Spectra Measurements	104
3.4.1 Bispectral Techniques	104
3.4.2 Bicoherence Measurements at $f_{ac} = 2650$ Hz	108
3.4.3 Bicoherence Measurements at $f_{ac} = 2200$ Hz	123
3.5 Coherence and Phase Angle Measurements	128
3.5.1 Coherence and Phase Angle Techniques	128

Chapter	Page
3.5.2 Coherence and Phase Development at $f_{\omega} = 2650$ Hz	130
3.5.3 Coherence and Phase Development at $f_{\omega} = 2200$ Hz	141
3.6 Correlation Measurements	146
3.6.1 Correlation Techniques	146
3.6.2 Correlation Measurements at $f_{\omega} = 2650$ Hz	149
3.6.3 Correlation Measurements at $f_{\omega} = 2200$ Hz	158
IV. CONCLUSIONS AND RECOMMENDATIONS	170
4.1 Discussion of Results	170
4.1.1 The "Tuned" Jet	170
4.2.2 The "Untuned" Jet	175
4.2 Conclusions	178
4.3 Recommendations	180
REFERENCES	182
APPENDIXES	188
APPENDIX A - COMPUTER PROGRAM LISTINGS	189
APPENDIX B - UNCERTAINTY ANALYSIS	245

LIST OF TABLES

Table	Page
I. Comparison of Mean Flow Properties for Planar Jets	20
II. Jet Characteristics of Excited and Unexcited Profiles	42

LIST OF FIGURES

Figure	Page
1. Jet Schematic	2
2. Jet Schematic with Coordinates	10
3. Axisymmetric Calibration Jet Schematic	13
4. Example of King's Law	15
5. Momentum Thickness With Downstream Distance ($Fe = 0$ Hz)	16
6. Jet Widening With Downstream Distance ($Fe = 0$ Hz)	18
7. Mean Velocity Decay With Downstream Distance ($Fe = 0$ Hz)	19
8. Comparison of Momentum Thickness With Downstream Distance ($Fe = 0, 2650$ Hz)	23
9. Jet Widening With Downstream Distance ($Fe = 2650$ Hz)	24
10. Mean Velocity Decay With Downstream Distance ($Fe = 2650$ Hz)	25
11. Mean Velocity Profile at $x/D = 0.25$ ($Fe = 0$ Hz, $Fe = 2650$ Hz)	27
12. Mean Velocity Profiles at $x/D = 0.5, 1.0$ ($Fe = 0$ Hz, $Fe = 2650$ Hz)	28
13. Mean Velocity Profiles at $x/D = 1.5, 3.0$ ($Fe = 0$ Hz, $Fe = 2650$ Hz)	29
14. Mean Velocity Profiles at $x/D = 5.0, 7.5$ ($Fe = 0$ Hz, $Fe = 2650$ Hz)	30
15. Mean Velocity Profiles at $x/D = 10.0, 15.0$ ($Fe = 0$ Hz, $Fe = 2650$ Hz)	31
16. Longitudinal Fluctuation Intensity at $x/D = 0.25$ ($Fe = 0$ Hz, $Fe = 2650$ Hz)	33

Figure	Page
17. Longitudinal Fluctuation Intensity at x/D = 0.5, 1.0 (Fe = 0 Hz, Fe = 2650 Hz)	34
18. Longitudinal Fluctuation Intensity at x/D = 1.5, 3.0 (Fe = 0 Hz, Fe = 2650 Hz)	35
19. Longitudinal Fluctuation Intensity at x/D = 5.0, 7.5 (Fe = 0 Hz, Fe = 2650 Hz)	36
20. Longitudinal Fluctuation Intensity at x/D = 10.0, 15.0 (Fe = 0 Hz, Fe = 2650 Hz)	37
21. Comparison of Excited to Unexcited Shear Layer Fluctuation Intensities	39
22. Comparison of Excited to Unexcited Centerline Longitudinal Fluctuation Intensities	40
23. Plot of Delta Scaling	49
24. Amplification Rates Versus Beta	50
25. Phase Velocity Versus Beta	52
26. Theoretical Versus Experimental U Velocity at x/D = 0.5	54
27. Theoretical Versus Experimental U Velocity at x/D = 0.75	56
28. Theoretical Versus Experimental U Velocity at x/D = 1.0	57
29. Theoretical Versus Experimental U Velocity at x/D = 1.25	58
30. Theoretical Versus Experimental U Velocity at x/D = 1.5	59
31. Theoretical Versus Experimental Phase at x/D = 0.5	61
32. Theoretical Versus Experimental Phase at x/D = 0.75	62
33. Theoretical Versus Experimental Phase at x/D = 1.0	63
34. Theoretical Versus Experimental Phase at x/D = 1.25	64

Figure	Page
35. Theoretical Versus Experimental Phase at $x/D = 1.5$	65
36. Comparison of the Excited Power Spectra at $x/D = 0.25, 0.5, 0.75, 1.0$ ($F_e = 2650$ Hz)	67
37. Comparison of the Excited Power Spectra at $x/D = 1.25, 1.5$ ($F_e = 2650$ Hz)	70
38. Comparison of the Excited Power Spectra at $x/D = 1.75, 2.0$ ($F_e = 2650$ Hz)	72
39. Excited Power Spectrum at $x/D = 2.5$ ($F_e = 2650$ Hz)	73
40. Transformed Excited Power Spectrum at $x/D = 3.0$ ($F_e = 2650$ Hz)	75
41. Transformed Excited Power Spectrum at $x/D = 4.0$ ($F_e = 2650$ Hz)	76
42. Transformed Excited Power Spectrum at $x/D = 5.0$ ($F_e = 2650$ Hz)	77
43. Spectral Amplitudes For $F_e, F_e/2, F_e/4$	79
44. Spectral Amplitudes For F_e and Sidebands ($F_e = 2650$ Hz)	80
45. Spectral Amplitudes For $F_e/2$ and Sidebands ($F_e = 2650$ Hz)	82
46. Comparison of the Centerline Excited Power Spectra at $x/D = 1.0, 1.5, 2.0, 2.5$ ($F_e = 2650$ Hz)	83
47. Centerline Excited Power Spectra at $x/D = 3.0, 4.0$ ($F_e = 2650$ Hz)	85
48. Centerline Excited Power Spectrum at $x/D = 5.0$ ($F_e = 2650$ Hz)	87
49. Centerline Excited Power Spectrum at $x/D = 7.5$ ($F_e = 2650$ Hz)	88
50. Comparison of the Excited Power Spectra at $x/D = 0.25, 0.5, 0.75$ ($F_e = 2200$ Hz)	89
51. Comparison of the Excited Power Spectra at $x/D = 1.0, 1.25, 1.5$ ($F_e = 2200$ Hz)	91

Figure	Page
52. Comparison of the Excited Power Spectra at $x/D = 2.0, 2.5$ ($F_e = 2200$ Hz)	92
53. Excited Power Spectrum at $x/D = 3.0$ ($F_e = 2200$ Hz)	94
54. Spectral Amplitudes For F_e , $F_e/2$, and Sidebands ($F_e = 2200$ Hz)	95
55. Alpha and Beta Modulation Indices ($F_e = 2650$ Hz)	99
56. Alpha/Beta Modulations ($F_e = 2650$ Hz)	100
57. Alpha and Beta Modulation Indices ($F_e = 2200$ Hz)	102
58. Alpha/Beta Modulations ($F_e = 2200$ Hz)	103
59. Bicoherence Schematic	107
60. Bicoherence Spectrum at $x/D = 0.5$ ($F_e = 2650$ Hz)	109
61. Bicoherence Spectrum at $x/D = 0.75$ ($F_e = 2650$ Hz)	111
62. Bicoherence Spectrum at $x/D = 1.0$ ($F_e = 2650$ Hz)	113
63. Bicoherence Spectrum at $x/D = 1.25$ ($F_e = 2650$ Hz)	114
64. Bicoherence Spectrum at $x/D = 1.5$ ($F_e = 2650$ Hz)	116
65. Bicoherence Spectrum at $x/D = 1.75$ ($F_e = 2650$ Hz)	117
66. Bicoherence Spectrum at $x/D = 2.0$ ($F_e = 2650$ Hz)	119
67. Bicoherence Spectrum at $x/D = 2.5$ ($F_e = 2650$ Hz)	120
68. Bicoherence Spectrum at $x/D = 3.0$ ($F_e = 2650$ Hz)	121
69. Bicoherence Spectrum at $x/D = 4.0$ ($F_e = 2650$ Hz) .	122

Figure	Page
70. Bicoherence Spectrum at $x/D = 1.0$ ($F_e = 2200$ Hz)	124
71. Bicoherence Spectrum at $x/D = 1.25$ ($F_e = 2200$ Hz)	126
72. Bicoherence Spectrum at $x/D = 1.5$ ($F_e = 2200$ Hz)	127
73. Schematic for Coherence Probe Placement	131
74. Coherence and Phase at $x/D = 0.5$ ($F_e = 2650$ Hz)	132
75. Coherence and Phase at $x/D = 1.0$ ($F_e = 2650$ Hz)	134
76. Coherence and Phase at $x/D = 1.5$ ($F_e = 2650$ Hz)	136
77. Coherence and Phase at $x/D = 2.0$ ($F_e = 2650$ Hz)	137
78. Coherence and Phase at $x/D = 3.0$ ($F_e = 2650$ Hz)	138
79. Model of Upstream Influence	140
80. Coherence and Phase at $x/D = 0.5$ ($F_e = 2200$ Hz)	142
81. Coherence and Phase at $x/D = 1.0$ ($F_e = 2200$ Hz)	144
82. Coherence and Phase at $x/D = 1.5$ ($F_e = 2200$ Hz)	145
83. Coherence and Phase at $x/D = 3.0$ ($F_e = 2200$ Hz)	147
84. Correlation at $x/D = 0.25$ ($F_e = 2650$ Hz)	150
85. Correlation at $x/D = 0.5$ ($F_e = 2650$ Hz)	151
86. Correlation at $x/D = 1.5$ ($F_e = 2650$ Hz)	153
87. Correlation at $x/D = 2.5$ ($F_e = 2650$ Hz)	154
88. Correlation at $x/D = 4.0$ ($F_e = 2650$ Hz)	156

Figure	Page
89. Correlation at $x/D = 7.5$ ($Fe = 2650$ Hz)	157
90. Correlation at $x/D = 0.25$ ($Fe = 2200$ Hz)	159
91. Correlation at $x/D = 0.5$ ($Fe = 2200$ Hz)	161
92. Correlation at $x/D = 1.0$ ($Fe = 2200$ Hz)	162
93. Correlation at $x/D = 3.0$ ($Fe = 2200$ Hz)	163
94. Correlation at $x/D = 4.0$ ($Fe = 2200$ Hz)	164
95. Probe Schematic for Upstream Influence	165
96. Correlation at $x/D = 0.25$ and 3.0 ($Fe = 2200$ Hz)	167
97. Correlation at $x/D = 0.25$ and 3.5 ($Fe = 2200$ Hz)	168
98. Correlation at $x/D = 0.25$ and 4.0 ($Fe = 2200$ Hz)	169

NOMENCLATURE

A	constant in Eq. 2.3
a_m	amplitude of model signals
$A_1(t)$	modeled anemometer signal
$A_{m2}(t)$	modeled anemometer signal
B	constant in Eq. 2.3
$B[i, j]$	bicoherence spectrum
b	mean velocity half-width
$b[i, j]$	normalized bicoherence spectrum
C_1	virtual origin based on mean flow widening
C_{m2}	virtual origin based on mean velocity decay
C_r	phase velocity
C_{xy}	coincident spectral density function
D	nozzle slot width
E	mean voltage of anemometer
$E[]$	an expected (or mean) value
f_m	jet column mode (jet passage frequency)
f_{ac}	acoustic excitation frequency
f_d	frequency
f_j	frequency
f_{tr}	frequency

f_N	Nyquist frequency
G_{xy}	cross-spectral density function
K_1	jet widening rate
K_2	mean velocity decay rate
$n(t)$	a small amplitude random noise
P_x	power spectral density function of signal $x(t)$
P_y	power spectral density function of signal $y(t)$
Q_{xy}	quadrature spectral density function
Re_D	Reynolds number based on nozzle exit
R_{xy}	correlation function
t	time variable
T	total time period
U	mean longitudinal velocity
u^2	velocity fluctuation
U_m	local mean centerline velocity
U_0	initial jet exit mean velocity
x	longitudinal spatial coordinate
$x(t)$	a stationary time series
y	lateral spatial coordinate
z	vertical spatial coordinate
α_i	spatial growth rate
α_r	wave number
β_i	temporal growth rate
β_r	cyclic frequency
Ψ	wavy disturbance

ϕ	desired solution variable
η	similarity variable
θ	momentum thickness of low frequency mode
θ_{xy}	phase angle spectrum between two signals
γ_{xy}^2	spectral coherence function
Φ	transformation variable
τ	time delay
Δf	a narrow frequency interval
$*$	complex conjugate
$\omega_1, \dots, \omega_n$	angular frequencies

CHAPTER I

INTRODUCTION

1.1 Introduction

A planar jet is a flow in which the working fluid discharges from a two dimensional slot of width " D ", at an initial velocity of U_0 , into a stagnant environment. Figure 1 shows a schematic of the planar jet flow field. Two thin free shear layers develop from each lip of the nozzle and widen with downstream distance. The free shear layers bound a core of irrotational fluid known as the "potential core". The shear layers eventually engulf the potential core after approximately 3-4 nozzle slot widths. The region extending from the nozzle lip to the location where the shear layers merge is known as the "initial region". After the initial region, the shear layers begin to dynamically interact with one another in the "interaction" region. This region extends until the jet reaches a state of dynamic equilibrium. Following this region is the "similarity region" in which the mean velocity profiles collapse into a single profile when scaled by the proper length scales.

The majority of published work presented on the turbulent planar jet can be divided into two distinct

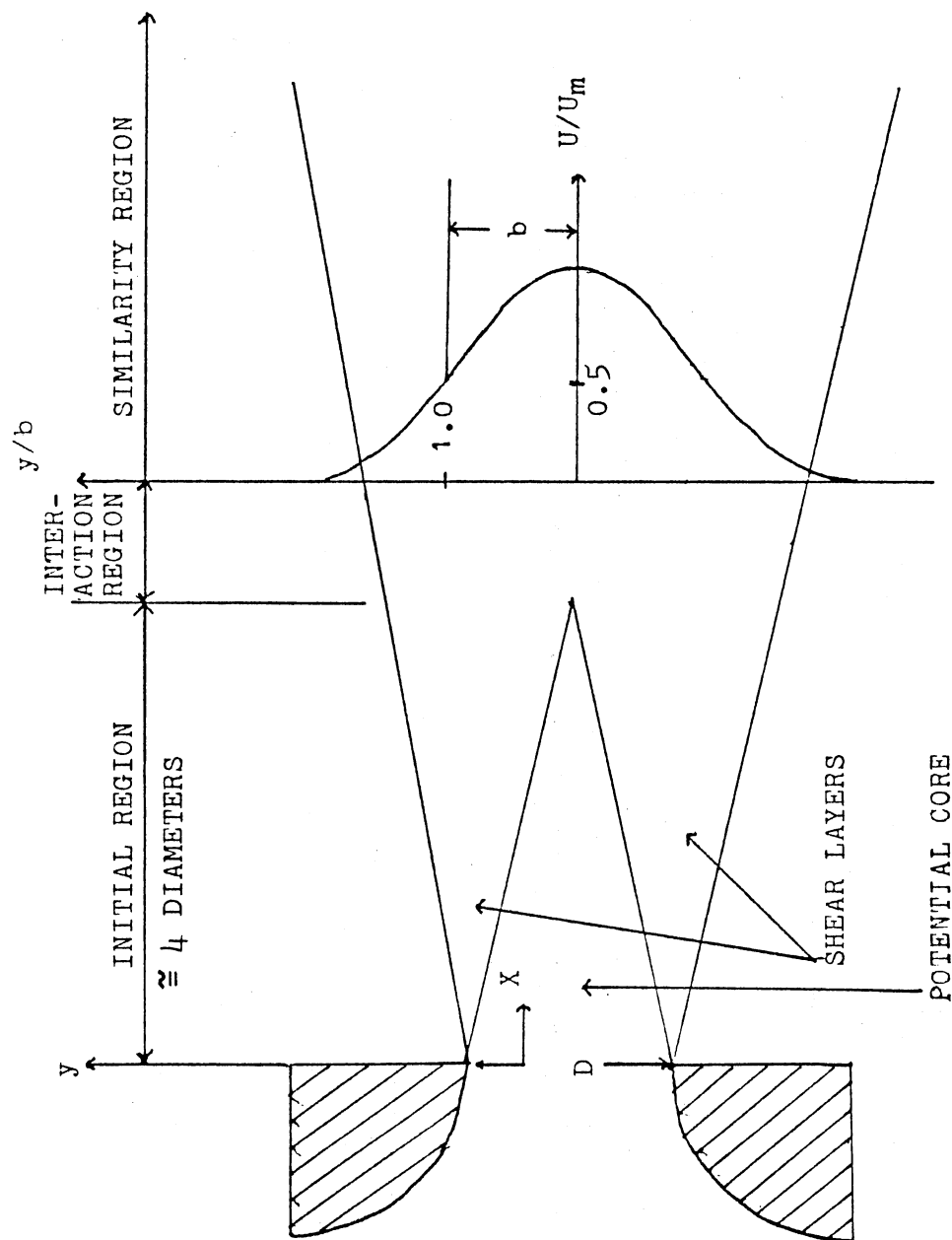


Figure 1. Jet Schematic

regions: the near exit region and the similarity region. A large volume of these works centers on the similarity region. Past work in this turbulent flow region documents the existence of large-scale coherent structures coexisting with fine grain turbulence. Townsend (1956) was one of the first researchers to describe large-scale coherent motions existing in free turbulent shear flow. Later work in plane mixing layers by researchers such as Brown & Roshko (1971, 1974), Winant & Browand (1974), and Browand & Weidman (1976) have clearly illustrated the presence of large, essentially two-dimensional roller vortices with axis perpendicular to the plane of mean shear. Due to works such as these, there has been a gradual shift in the approach taken to turbulent fluid mechanics research. It has become clear that much of what has been traditionally considered as a completely random phenomenon actually contains certain deterministic aspects. Authors taking this new deterministic approach to research have clearly established that large-scale structures do exist and should be included in modeling turbulent shear flows. Oler and Goldschmidt (1984) have provided a kinematic model of the large-scale structures in the planar turbulent jet. Their findings suggest that coherent structures extend across the entire width of the flow and are quite similar to a Karman-Vortex-Street.

Other work in the similarity region involves

documentation of what was initially referred to as the "flapping" phenomenon. The shear layers in the near exit region were noted to flap like that of a flag in a strong wind. This phenomenon has been reported in the planar turbulent jet by researchers Bradbury (1965), Goldschmidt & Bradshaw (1973), Gutmark & Wygnanski (1976), Cervantes (1980), Antonia et al. (1983), Thomas & Goldschmidt (1986), Thomas & Brehob (1986), and has been demonstrated to be the strongest indication of large-scale vortices rotating in opposite directions in the self-preserving region (i.e. similarity region) in a Karman-Vortex-Street arrangement. It should be noted here that not all researchers agree that the antisymmetric coherent structures are arranged in a Karman-Vortex-Street pattern, but instead suggest that a multiple structural form may be indicated. This flapping phenomenon, due to the antisymmetric large-scale structures, is easily detected by measuring the correlation function between the fluctuating longitudinal velocities at symmetric points on either side of the jet centerline.

Work centered on the near field of the planar turbulent jet can be put into a single category: instability wave interaction measurements that characterize transition. The main objective of transition type measurements is to document the wave interactions of the shear layers during transition to turbulence. It has

been shown by Michalke (1965), Sato & Okada (1966), Browand (1966), and Freymuth (1966) that inviscid linearized theory can be applied to free shear flows when the amplitude of the velocity fluctuations are small. When the amplitude of velocity fluctuations become sufficiently large, the linear theory is no longer valid due to nonlinear interactions taking place in the flow field. Investigations of the stability interactions of the planar turbulent jet have been performed by Tatsumi & Kakutani (1958), Sato (1960), Sato & Sakao (1964), and Browand (1966). Results of these investigations led to conclusions that observed values of the amplification rate, the propagation velocity and the amplitude distribution of small-amplitude velocity fluctuations are in good agreement with the theoretical results predicted by stability calculations.

The above mentioned instability calculations are based on linear equations and are only valid for low amplitude flows which only truly occur at low Reynolds numbers. Therefore it has been desirable to obtain nonlinear stability equations for those flows where parallel flow does not exist. The difficulty in solving for the stability characteristics of a non-parallel flow lies in the evaluation of the eigenvalues of a set of partial differential equations. An assumption must be made that non-parallel effects are of higher order than parallel

effects. Attempts to apply nonlinear stability theory to the planar turbulent jet by such researchers as Ling & Reynolds (1973) and Garg (1979) have shown some agreement in measured values. It would be helpful to future researchers to have a better understanding of the exact nature of nonlinear interactions involved in transition.

Research by Sato (1970, 1975, 1978), Motohashi (1979), Miksad et al. (1983), and Chang (1987) have investigated the quantitative features of nonlinear interactions during transition. Their results point to the importance of low-frequency fluctuations produced by sum and difference-mode interactions. Also important in the transition process is the presence of vortices in the shear layer. Winant & Browand (1974) have shown the importance of vortex interactions in determining shear layer development. They showed that an interaction takes place whereby two neighbouring vortices coalesce to form a single, larger vortex and the spacing between vortices then roughly doubles. Continuous repetition of this 'pairing' process is responsible for the entrainment of surrounding fluid, and controls the growth of the mixing layer.

1.2 Objectives of the Research

The primary objective of this research is to document the transition and structural development of the near field of a planar jet under the influence of low level

acoustic excitation. To accomplish this objective, techniques used in the above mentioned research papers will be used. Linear stability calculations will be performed and compared to theory in the near region of the jet, linear and non-linear effects of the jet will be documented and examined, and the role of downstream structure influence on the near exit region will be studied. It is the goal of this research to leave little question as to the mechanisms of transition involved in the planar turbulent jet.

CHAPTER II

JET FLOW FIELD AND MEASUREMENT APPARATUS

2.1 The Planar Turbulent Jet

A schematic of the planar turbulent jet is shown in Figure 1 on page 2. The coordinate system which describes the jet flow field is as follows: x - longitudinal coordinate which is non-dimensionalized by the jet diameter D , y - lateral coordinate which is non-dimensionalized by the mean velocity half-width b which is defined as the lateral distance from the jet centerline to the location where the mean velocity is one half that of the mean centerline velocity (see figure), and z - coordinate in direction of mean flow homogeneity. The jet flow field, as mentioned in Chapter I, can be divided into three regions: initial region, interaction region, and similarity region. Several generalizations can be mentioned about the similarity region. When the mean velocity profiles in this region are normalized by the maximum local velocity and the proper length scale they will collapse into a single profile shape. All mean velocity profiles and turbulence quantities will be normalized by the local mean centerline velocity, U_m , and the mean velocity half-width b . The jet widening rate in

the similarity region behaves in a linear fashion. The widening rate, b/D , is given by the relationship

$$b/D = K_1 (x/D - C_1) \quad (2.1)$$

where $K_1 = d(b/D)/d(x/D)$ = the non-dimensional widening rate and C_1 = the virtual origin based on jet widening. The mean velocity decay rate in the similarity region is also a linear relationship and given by the equation

$$(U_m/U_o)^{-2} = K_2 (x/D - C_2) \quad (2.2)$$

where $K_2 = d((U_m/U_o)^{-2})/d(x/D)$ = the non-dimensional mean velocity decay rate and C_2 = the virtual origin based upon mean velocity decay. In the initial region U_m remains relatively constant, while in the interaction U_m gradually decays until the similarity region is reached.

2.2 Facility Set-up and Measurement Apparatus

The experimental facility used in this study is shown schematically in Figure 2. The jet is driven by a three horse-power centrifugal blower which supplies air to a cubic plenum chamber of 4 feet on a side. The blower and plenum are coupled by means of flexible rubber duct for vibration isolation. A 5 inch thick slab of fiberglass insulation material is used within the plenum to both filter the air and to insure that any blower pulsation is decoupled from the exit jet flow. A rectangular duct of

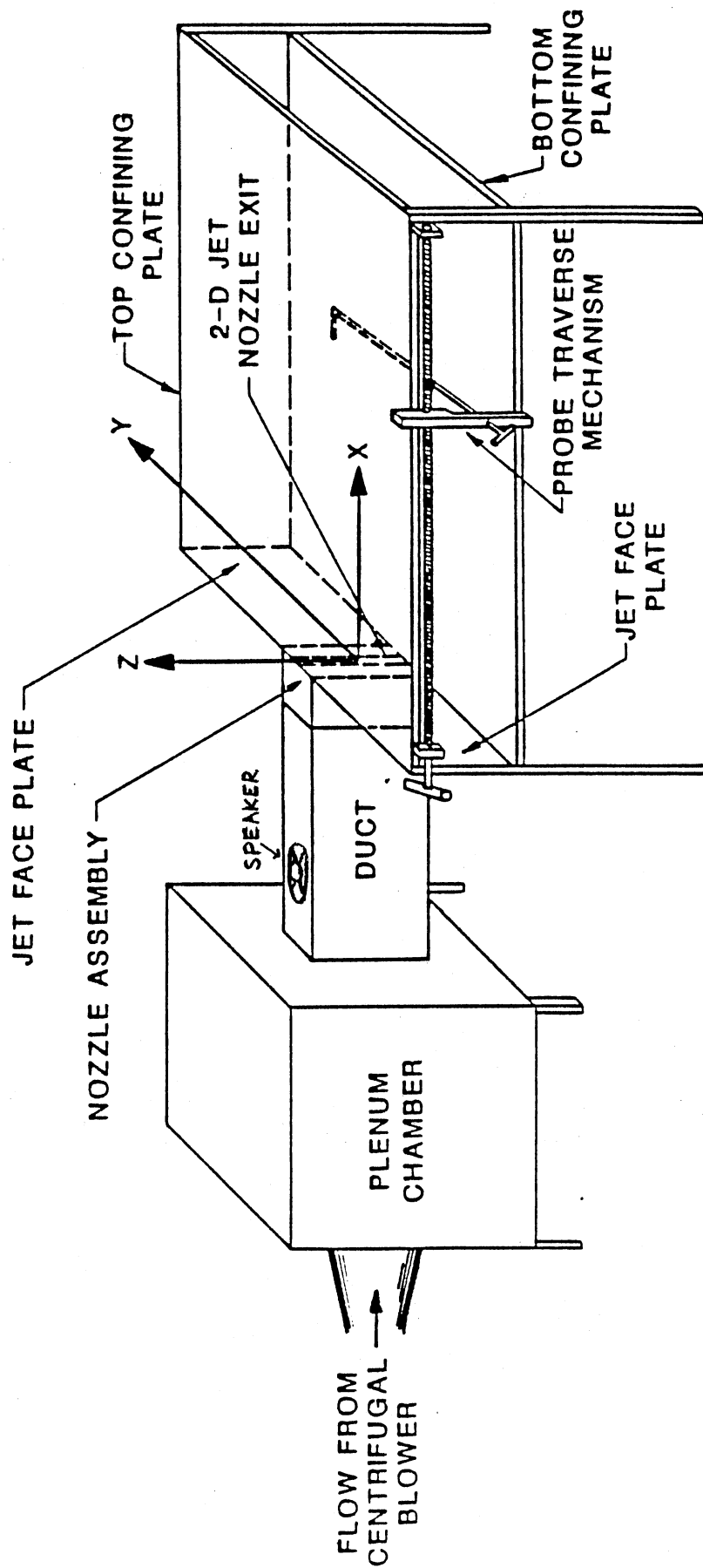


Figure 2. Jet Schematic with Coordinates

dimensions 2.5 feet in length, 1.5 feet in height, and 8 inches in width connects the plenum to the nozzle assembly. The duct assembly contains flow straighteners and turbulence reducing screens. The two-dimensional nozzle has a contraction ratio of 16:1 and ends in a slot that is 0.5 inches in width and 18 inches height. The nozzle contour is based on a design by Jordinson (1961).

In order to keep the flow field two-dimensional, two large horizontal plates are mounted parallel to one another. These plates are of dimensions 5 feet by 7 feet and are separated by an 18 inch air gap. The inner surface of these plates have been sanded and waxed to insure a smooth surface. Twin stainless steel faceplates are mounted flush with the nozzle assembly and extend laterally to the edge of the flow field. The rest of the flow field is unrestricted. The probe traversing mechanism is attached to a sturdy angle iron frame that supports the set-up. The probe traversing mechanism allows probe positioning in three dimensions accurate to 0.03 inch. Lateral probe positioning is accurate to 0.001 inch.

The jet exit velocity is measured by a pitot static probe mounted in the nozzle exit plane near the top plywood plate. The accuracy of the pressure reading was 0.01 inch of water (corresponds to 6.68 ft/s).

In order to introduce controlled sinusoidal

longitudinal velocity perturbations into the exit flow, a loudspeaker is mounted in the rectangular duct assembly. The loudspeaker is driven by an audio-oscillator. The frequency of the oscillation is monitored by a digital frequency counter, while the rms amplitude of the excitation is monitored by a digital true rms voltmeter. Jet facility was constructed by Brehob (1986).

All measurements to be reported were made with commercial hot-wire anemometers operating in the constant temperature mode at 220°C which corresponds to an overheat ratio of approximately 1.6. Standard straight wire probes were used. The analog signals from the probes were passed through anti-alias filters and were digitized with an HP-98640A A/D board which has a maximum sampling rate of 18 microseconds. A HP-9920S minicomputer processed the digital signals and performed all data reduction.

The hot wires were calibrated using an axisymmetric calibration jet facility. The calibration jet is shown schematically in Figure 3. The calibration jet facility has an exit diameter of 0.6 inches. The calibration jet is powered by compressed air which is controlled by a valve allowing precise velocity setting to 0.005 inches of water. The anemometer D.C. bridge voltage is recorded for each velocity setting and calibration is obtained by using King's law

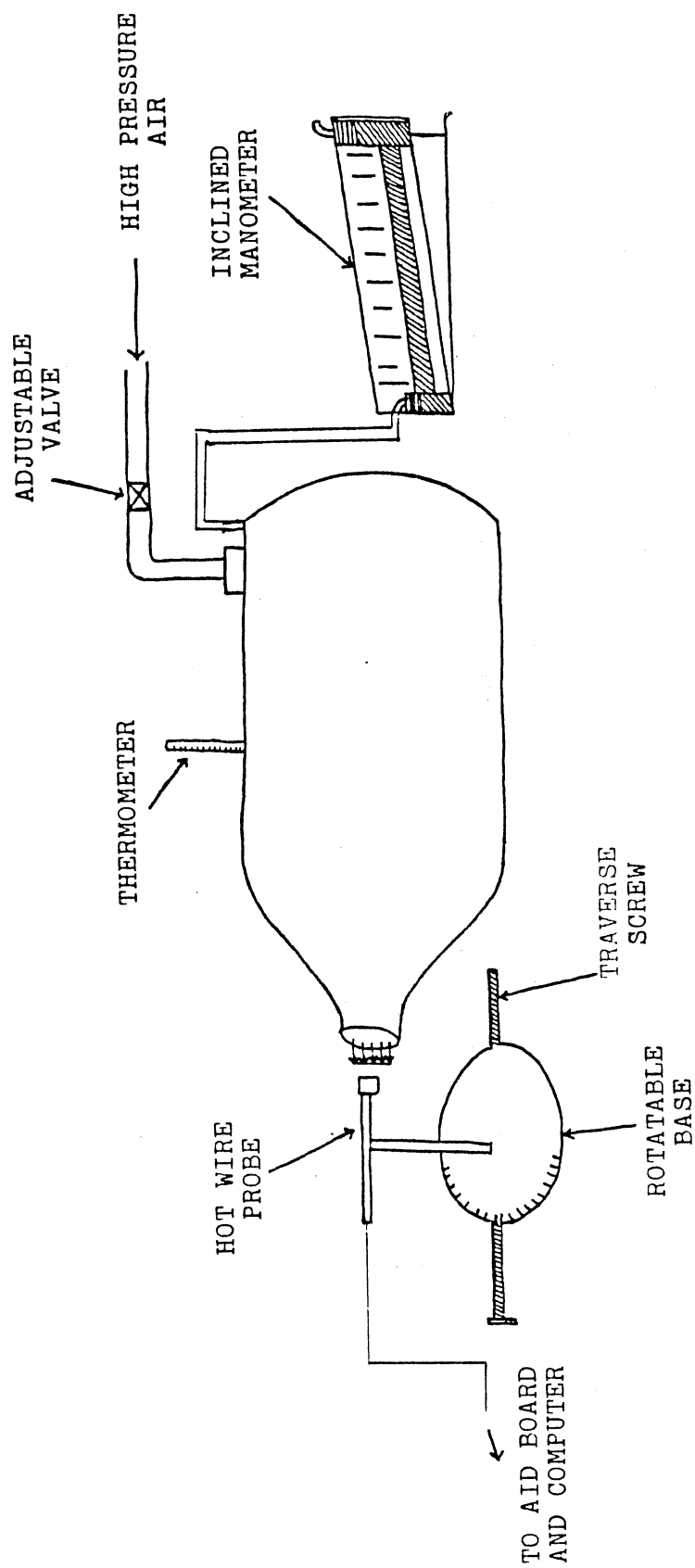


Figure 3. Axisymmetric Calibration Jet Schematic

$$E^2 = A + BU^{0.45} \quad (2.3)$$

where E is the mean D.C. bridge voltage, and U is the mean velocity. A and B are the then experimentally determined calibration constants. Figure 4 shows the typical calibration fit.

2.3 Validation of the Flow Field

In this section experimental results will be presented that document the basic development of the jet. These results will be used to show that the jet exhibits no unusual behavior that would invalidate the conclusions of this research. All results are obtained at a Reynolds number of 16700. This corresponds to an exit velocity of 63 ft/s.

2.3.1 The Unexcited Jet

The basic development of the natural (unexcited) jet is presented in this section. The exit centerline fluctuation intensity is found to be low (0.101 percent). The initial momentum thickness of the shear layer is measured to be 0.1033 mm. The downstream variation of the momentum thickness, θ , is shown in Figure 5. Localized increases in the momentum thickness can be seen at $x/D = 1.5$ and $x/D > 5.0$. A linear relation is noted for $x/D > 7$. This slope is defined as $d(\theta/\theta_0)/d(x/D) = 2.891$.

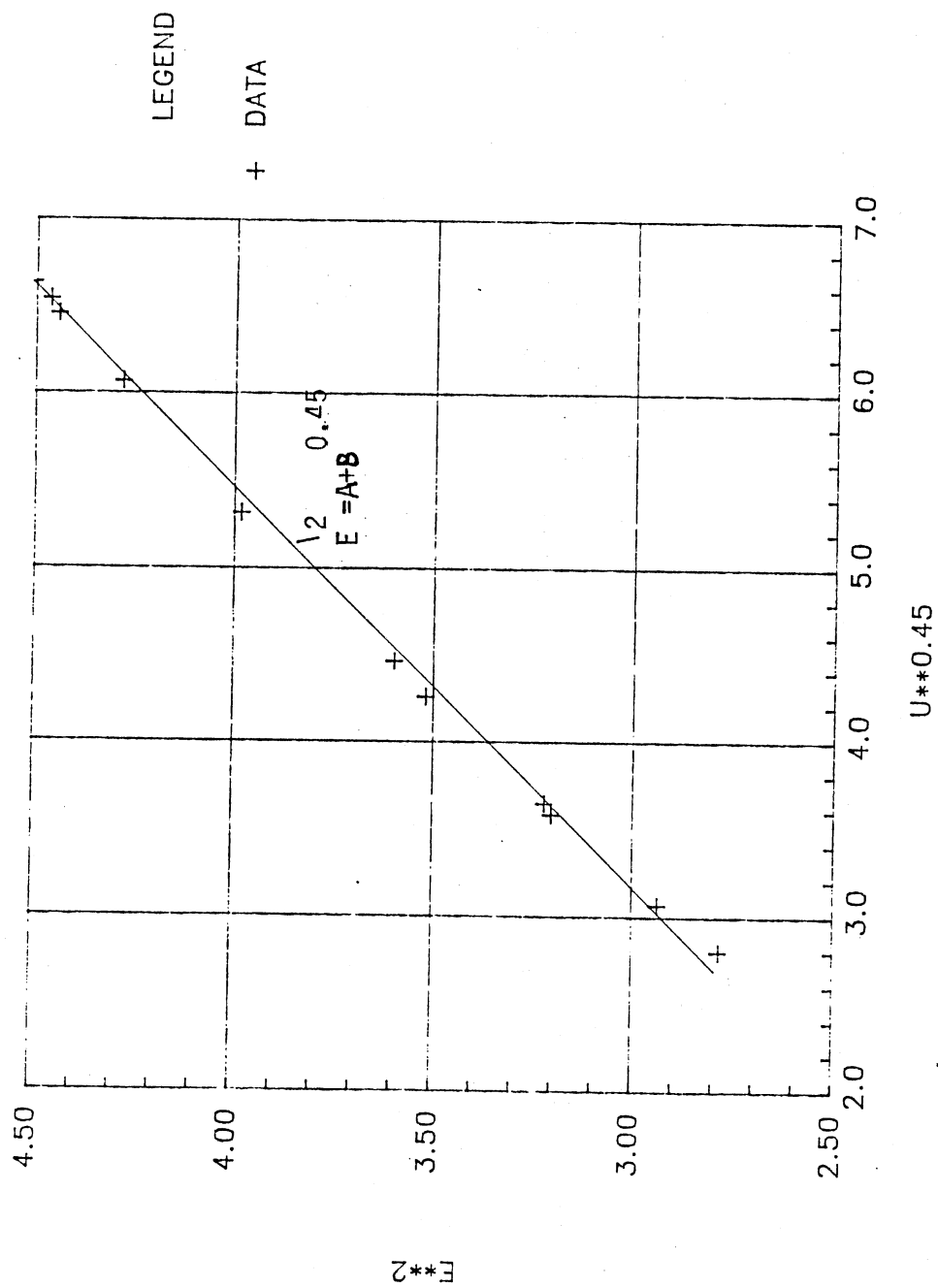


Figure 4. Example of King's Law

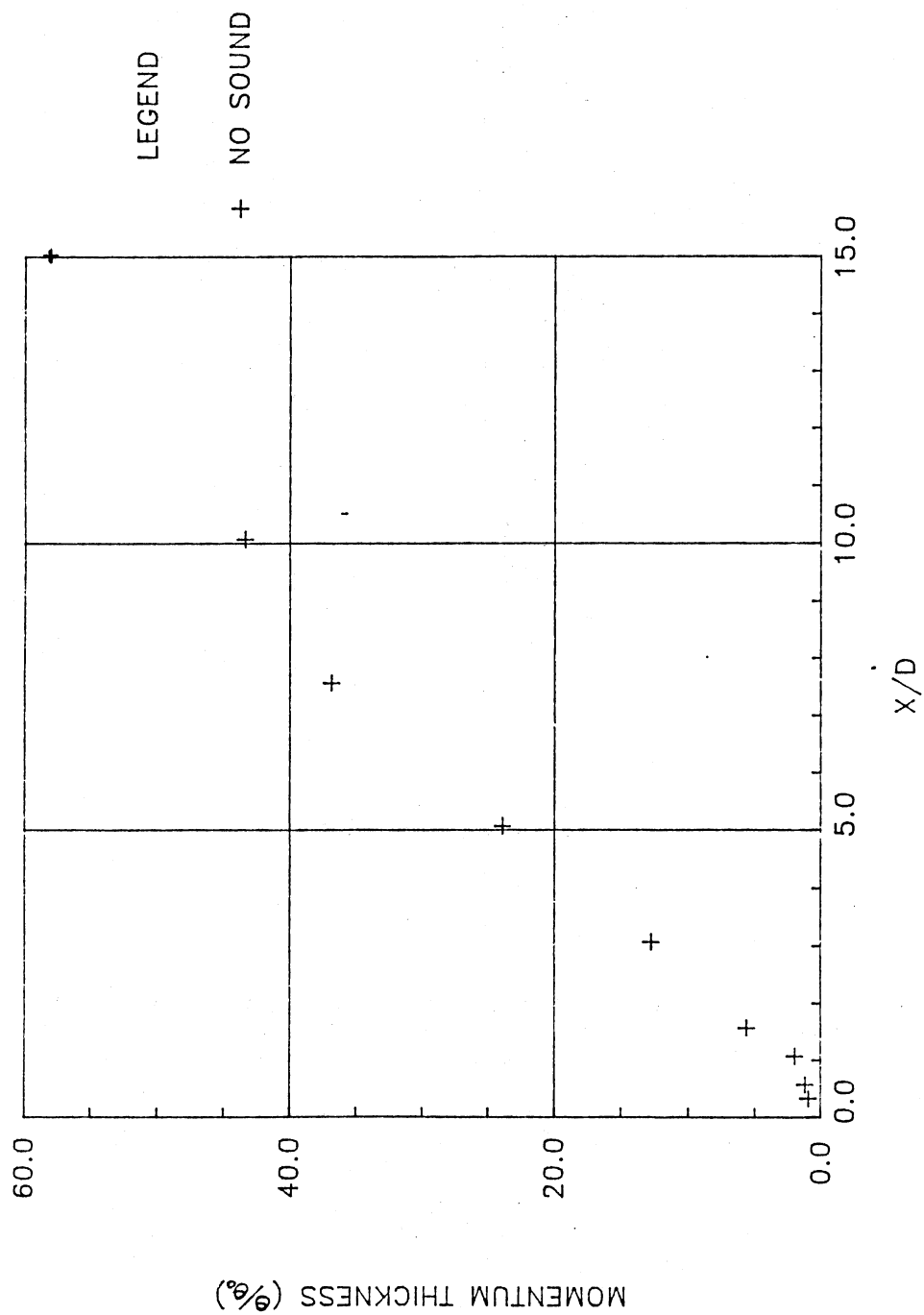


Figure 5. Momentum Thickness With Downstream Distance ($f_e = 0$ Hz)

Figure 6 presents the widening of the jet. The plot shows the widening rate b/D as a function of downstream distance x/D . Localized increases in widening are noted at $x/D = 1.5$ and $x/D = 3.0$. For $x/D > 5.0$ a linear variation is seen. This linear variation of the widening rate is expected in the similarity region as described in section 2.1. The non-dimensional widening rate (defined in section 2.1) is $K_1 = 0.099$, with the geometric virtual origin $C_1 = -1.7307$. Figure 7 shows the mean velocity decay with downstream distance x/D (decay is shown as a positive slope). This figure shows constant mean velocity in the potential core of the initial region, increased decay in the interaction region, and linear increases in the similarity region. In this linear region, the mean velocity decay rate is $K_2 = 0.1706$ and the kinematic virtual origin $C_2 = -1.3812$. These results agree favorably with previously measured values shown in Table 1 on page 20.

2.3.2 The Effect of Acoustic Excitation

It is well known that the properties of jet flows may be controlled by the application of periodic forcing. Low level acoustic excitation can be utilized in order to introduce a controlled perturbation into the flow in order to facilitate study of transition to turbulence. In this study, low level sinusoidal excitation is used to

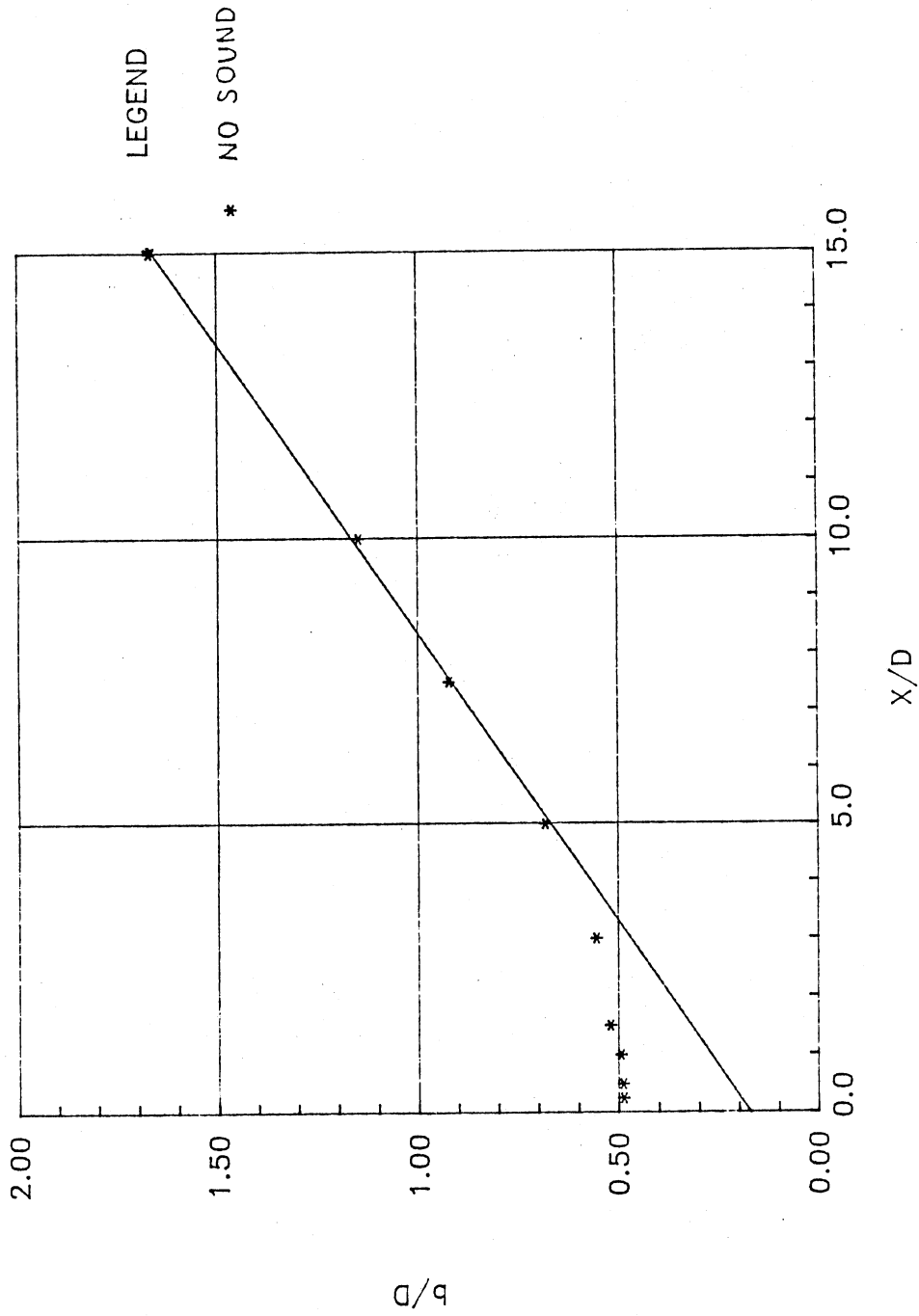


Figure 6. Jet widening with downstream distance
($f_e = 0$ Hz)

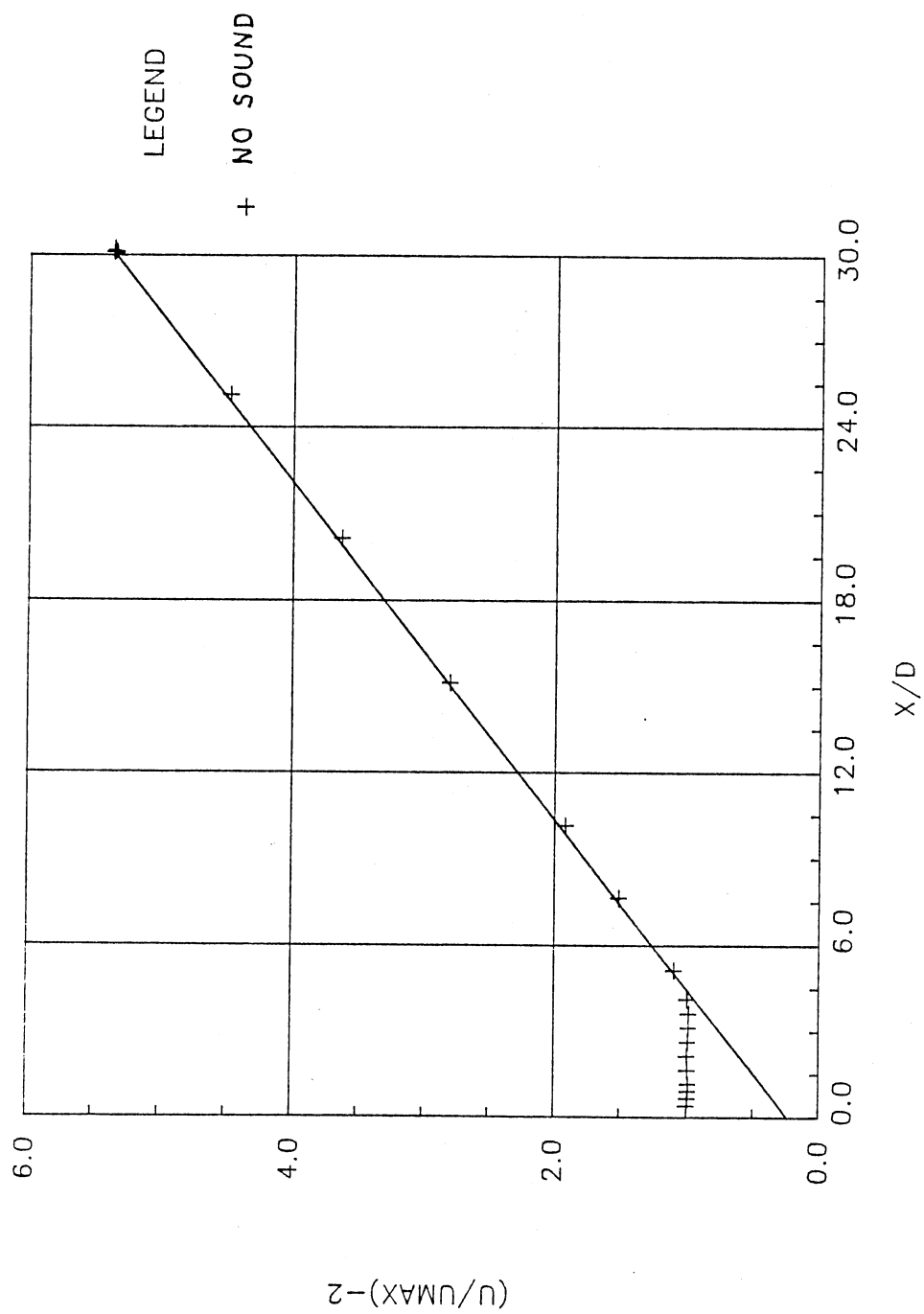


Figure 7. Mean Velocity Decay With Downstream Distance ($f_e = 0$ Hz)

TABLE I
COMPARISON OF MEAN FLOW PROPERTIES FOR PLANAR JETS

Reference	Re _D	K ₁	K ₂	c ₁	c ₂
van der Hegge Zijnen (1958)	1.33 x 10 ⁴	0.100	0.205	0.000	-1.700
Foss (1965)	5.50 x 10 ⁴	0.085	0.257	-2.000	6.500
Flora (1969)	2.00 x 10 ⁴ to 3.00 x 10 ⁴	0.109 to 0.130	0.158 to 0.227	-15.000	2.000
Kaiser (1971)	6.00 x 10 ³	0.101	0.208	-2.600	0.000
Ott (1972)	1.00 x 10 ⁴	0.097	0.228	-3.000	7.000
Jenkins (1974)	1.45 x 10 ⁴	0.085	0.160	-6.100	4.000
Mulej (1975)	1.60 x 10 ⁴	0.095	0.185	-0.789	13.200
Gutmark & Wygnanski (1976)	3.00 x 10 ⁴	0.100	0.170	-2.000	4.700
Chambers (1977)	6.00 x 10 ³	0.100	0.190	-3.500	-3.200
Cervantes (1978)	1.00 x 10 ⁴	0.083	0.240	-6.600	4.500
Thomas (1980)	6.00 x 10 ³	0.106	0.214	-3.500	-0.913
Thomas (1983)	6.00 x 10 ³	0.100	0.220	-3.200	-1.600
Thomas & Brehob (1986) *	1.50 x 10 ⁴	0.086	0.253	-4.711	10.371
Frakash (1986) *	7.70 x 10 ³	0.104	0.180	-1.800	-0.354
Chang (1987) *	8.20 x 10 ³	0.104	0.220	-1.542	-0.597
Current (1986) *	1.67 x 10 ⁴	0.099	0.171	-1.731	-1.381

* same nozzle geometry

introduce a controlled instability into the flow that can be documented throughout the transition region. Using the theory of Michalke (1965) discussed in section 3.1, the range of unstable frequencies is determined. The jet is to be acoustically excited at the theoretically determined most unstable frequency. This excitation is accomplished by the means of the loudspeaker mounted in the duct assembly upstream of the nozzle exit.

The range of unstable frequencies shifts toward lower frequencies as one travels downstream in the jet. This fact leads to the most unstable frequency at $x/D = 0.75$ being chosen to excite the jet. The frequency at this x/D location is chosen since it amplifies significantly both upstream and downstream of $x/D = 0.75$. This frequency is used extensively throughout this research except where noted. This frequency is determined to be $f_{\omega} = 2650$ Hz. The amplitude of the excitation is chosen such that at the nozzle exit the rms amplitude $u(f_{\omega})$ of the excited mode does not exceed the amplitude of the natural background fluctuations. The longitudinal fluctuation intensity at the excitation frequency f_{ω} was measured to be 0.0092 percent while the exit longitudinal fluctuation intensity at the same frequency for the natural jet was 0.0061 percent. This corresponds to a very low level excitation that should not significantly change the exit flow field. The total longitudinal turbulence intensity at the nozzle

exit when excited is 0.1013 percent, compared to 0.1006 percent for the unexcited jet. This translates to a 0.7 percent difference.

In order to document the effects of the low level excitation, measurements are presented that directly correspond to those presented in the section 3.2.1. Figure 8 gives the momentum thicknesses for the excited case plotted along with the natural case. Very little difference is seen in the near exit region of the jet. However, downstream at $x/D > 7$, the slope of the excited momentum thickness is not as steep as in the natural jet. The excited momentum variation for $x/D > 7$ is $d(\theta/\theta_{\infty})/d(x/D) = 2.555$ compared to 2.891 for the natural jet. Comparison values of momentum thicknesses can be found in Table 2 on page 42.

Figure 9 documents the widening of the excited jet. For $x/D > 5$ a linear variation is noted as in the unexcited jet. The non-dimensional widening rate is found to be $K_1 = 0.105$, while the geometric virtual origin is found to be $C_1 = -1.1031$. Figure 10 documents the mean velocity decay of the jet centerline. Again a linear variation is noted for $x/D > 5$. The mean decay rate is given by $K_2 = 0.1747$, while the kinematic virtual origin is $C_2 = -1.1646$. The widening rate of the excited jet shows a slight increase of 5.7 percent over the unexcited jet, while the centerline mean velocity decay showed a 0.6

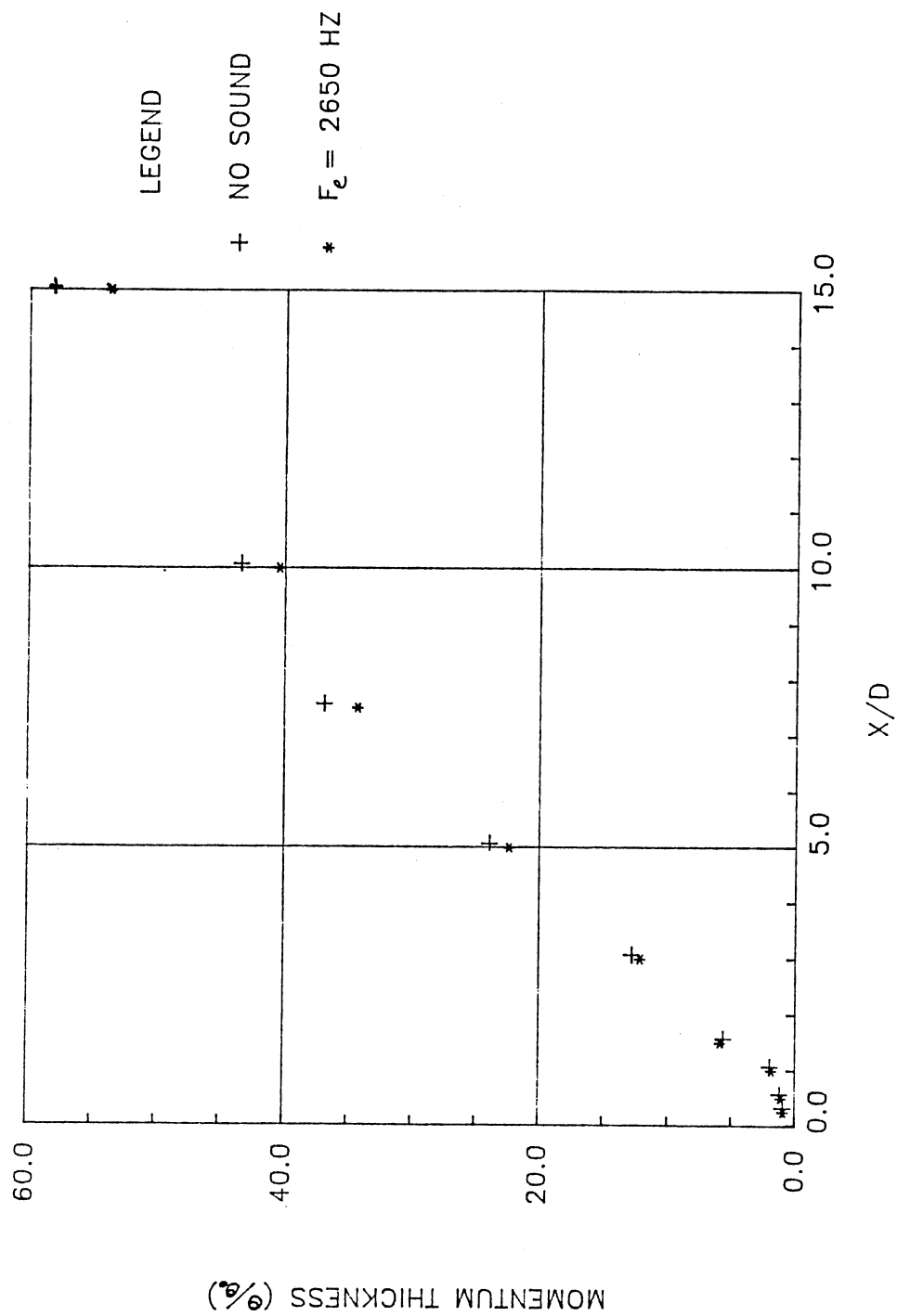


Figure 8. Comparison of Momentum Thickness With Downstream Distance ($f_c = 0, 2650$ Hz)

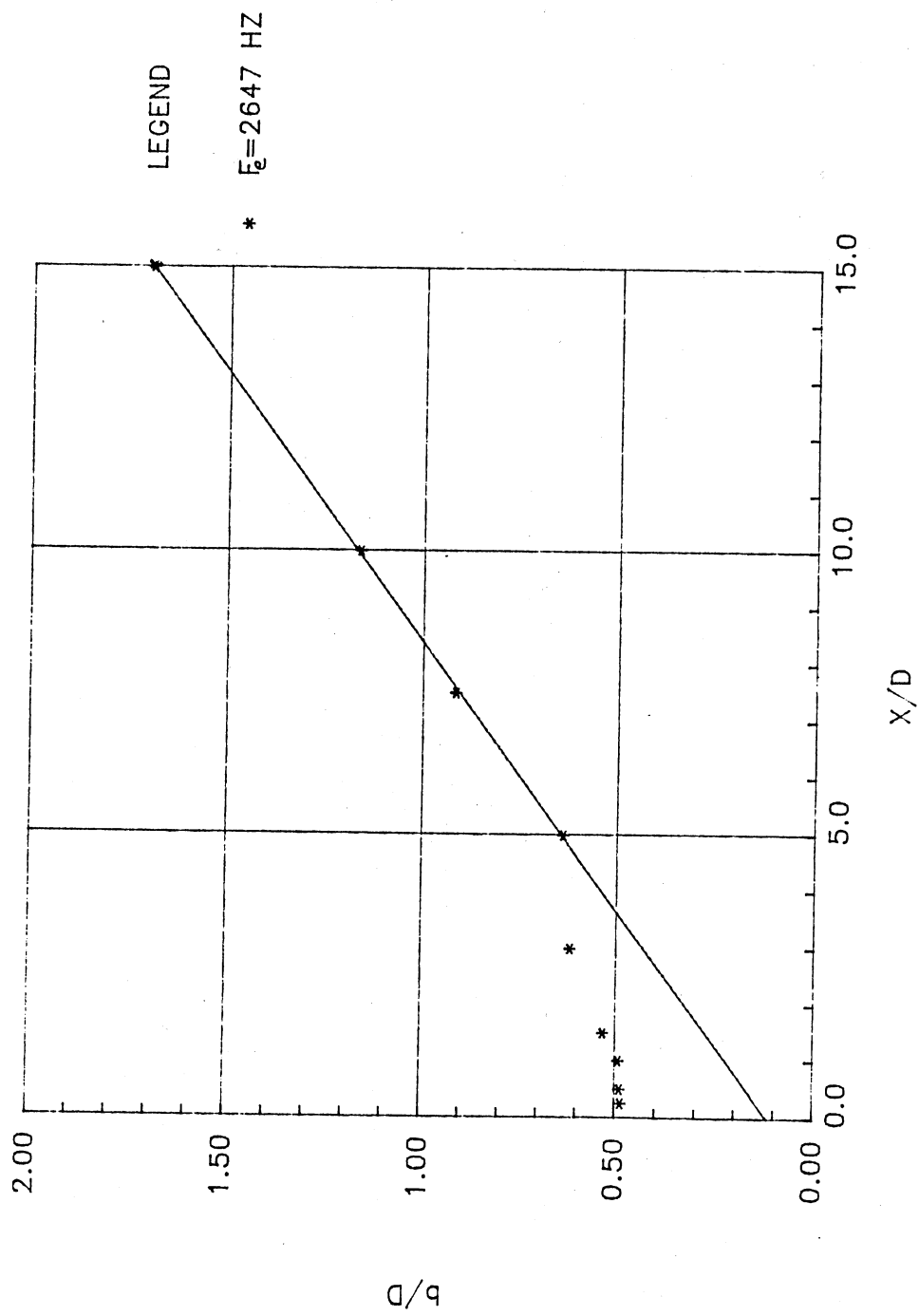


Figure 9. Jet Widening With Downstream Distance
($f_e = 2650 \text{ Hz}$)

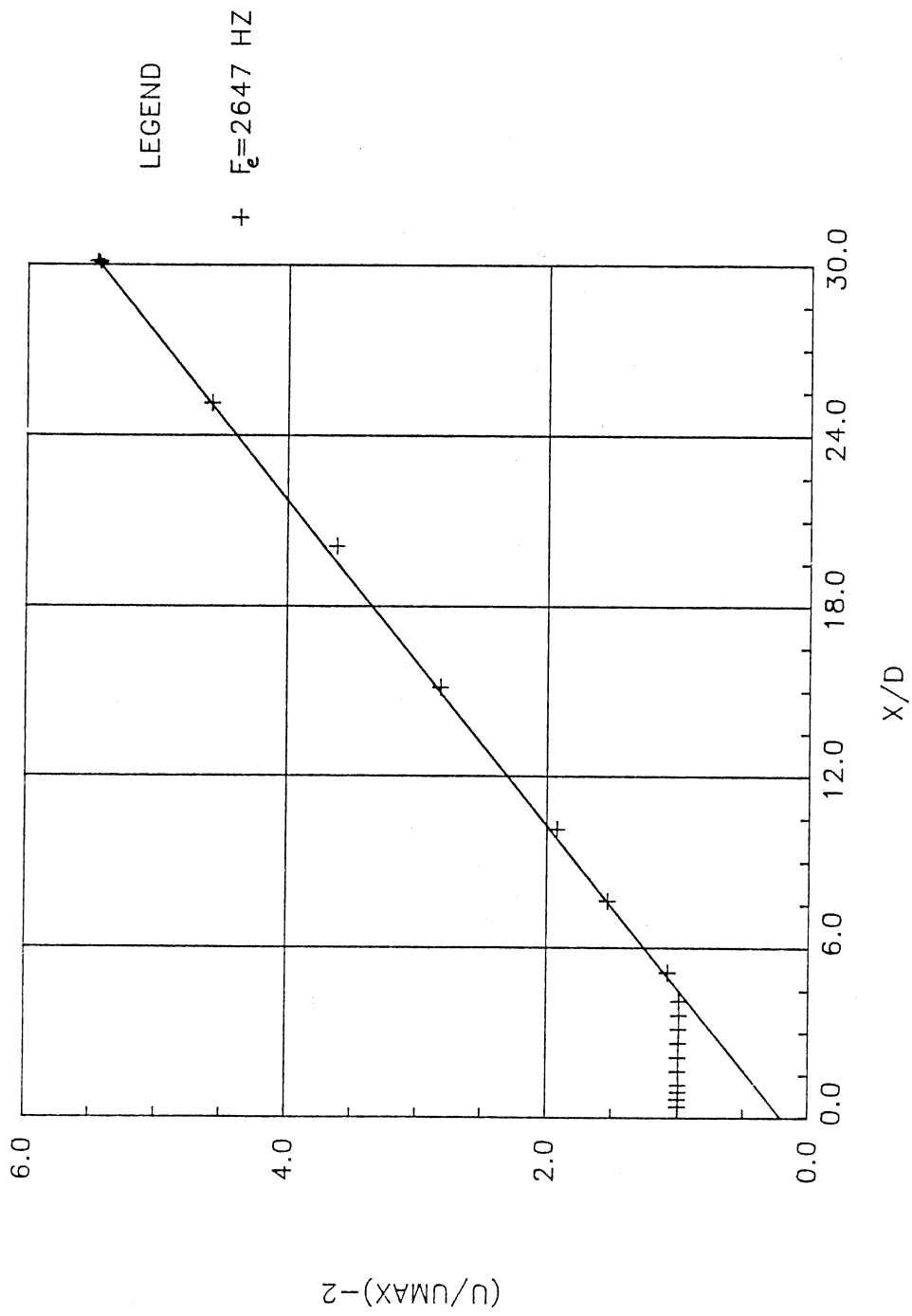


Figure 10. Mean Velocity Decay With Downstream Distance ($f_e = 2650 \text{ Hz}$)

percent increase. Overall, the basic characteristics of the excited jet behave very similarly to the unexcited jet.

2.3.3 Velocity and RMS Fluctuation Variations

The mean velocity profile development is shown in Figures 11-15. The natural jet is directly contrasted with that of the acoustically excited jet. Figure 11 shows the mean velocity profile at $x/D = 0.25$. No significant difference between the two cases is observable. The mean velocity profiles for $x/D = 0.5$ and 1.0 is shown in Figure 12. Again the profiles are very similar. The initial region of the jet profile is seen to be flat across the potential core. The variation of velocity is shown to be completely within the shear layers. The shear layers are shown to be very thin on either side of the irrotational potential core. Figure 13 (x/D locations 1.5 and 3.0) clearly shows the widening of the shear layer to engulf the potential core. The potential core is completely engulfed by approximately $x/D = 3.5$. The interaction region is very small and extends from $x/D = 3.5$ to $x/D = 5.0$. Figures 14 and 15 show the mean velocity profiles in the similarity region. The profiles, as predicted, are collapsed into one similar profile. The similarities between the excited and unexcited profiles are obvious. The main differences lie

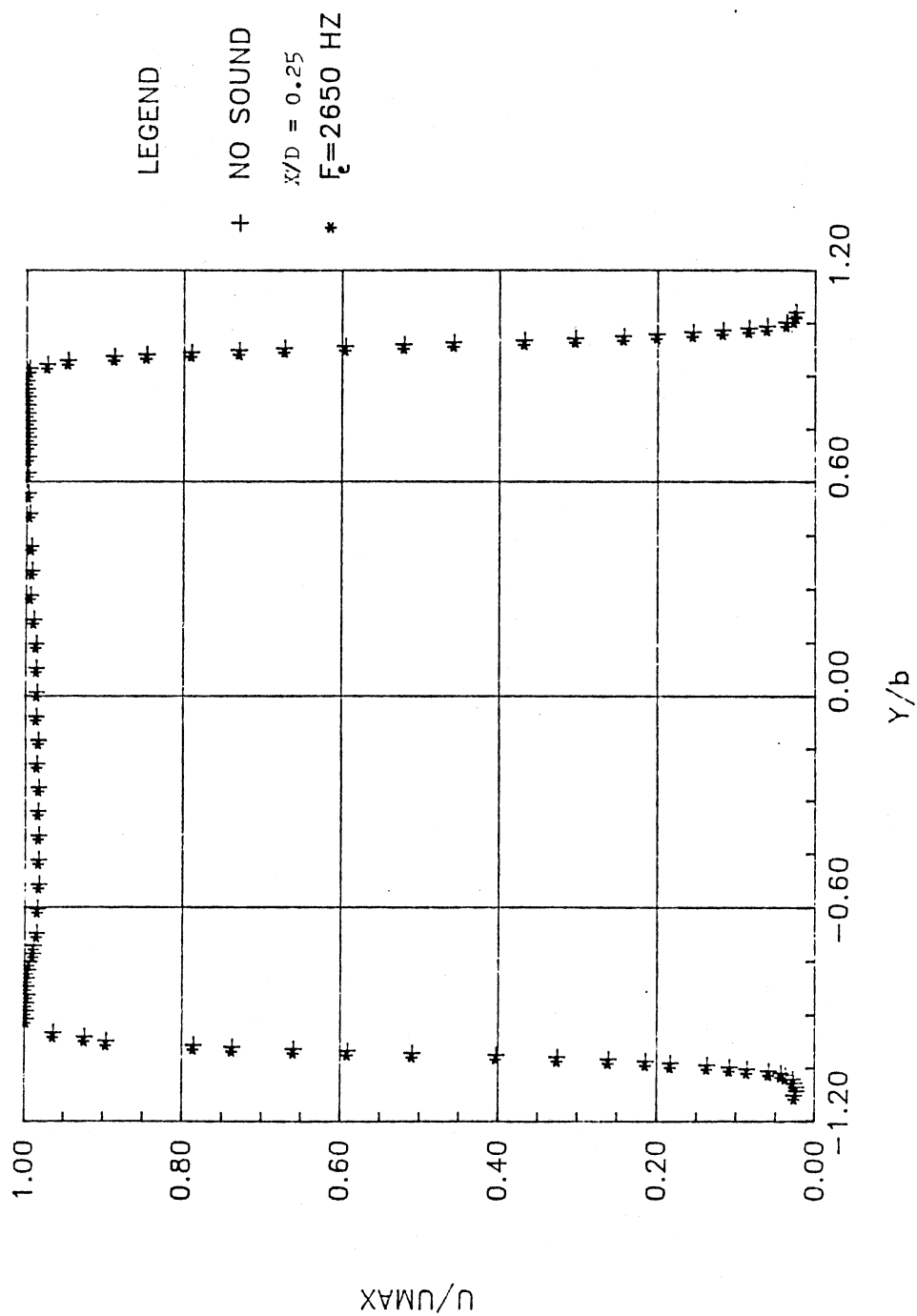


Figure 11. Mean Velocity Profile at $x/D = 0.25$
($f_e = 0$ Hz, $f_e = 2650$ Hz)

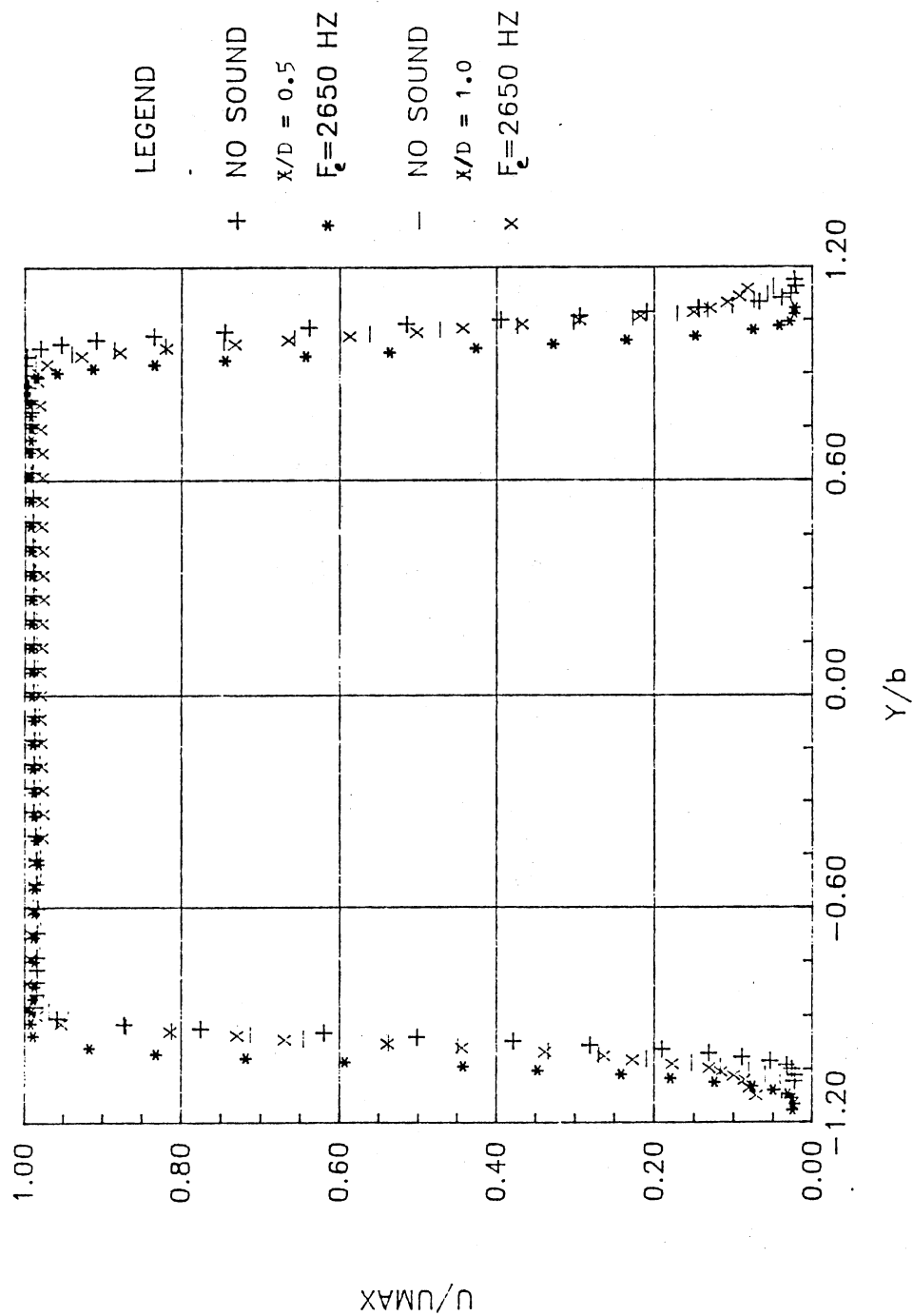


Figure 12. Mean Velocity Profiles at $x/D = 0.5, 1.0$
($f_e = 0$ Hz, $f_e = 2650$ Hz)

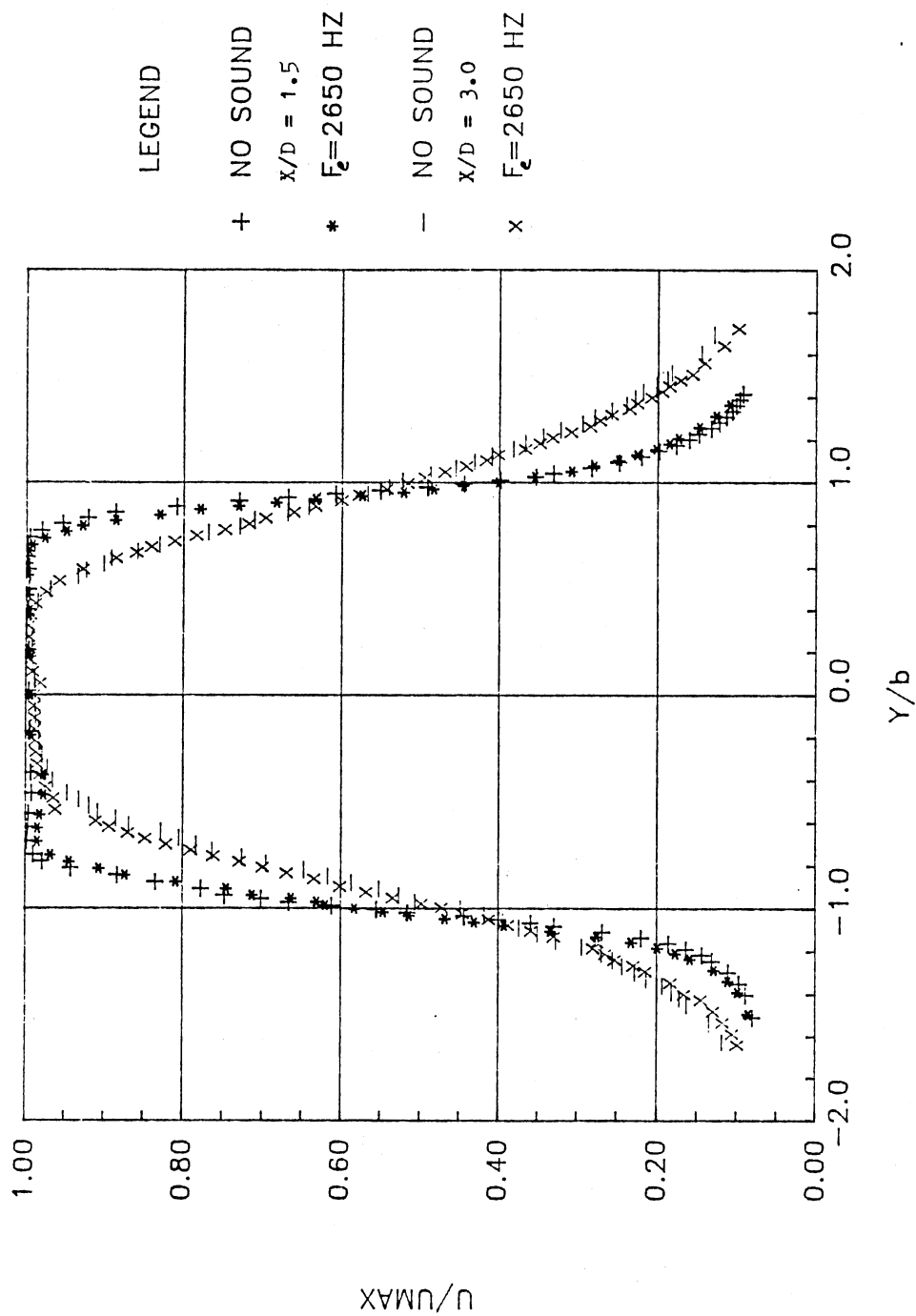


Figure 13. Mean Velocity Profiles at $x/D = 1.5, 3.0$
($f_e = 0$ Hz, $f_e = 2650$ Hz)

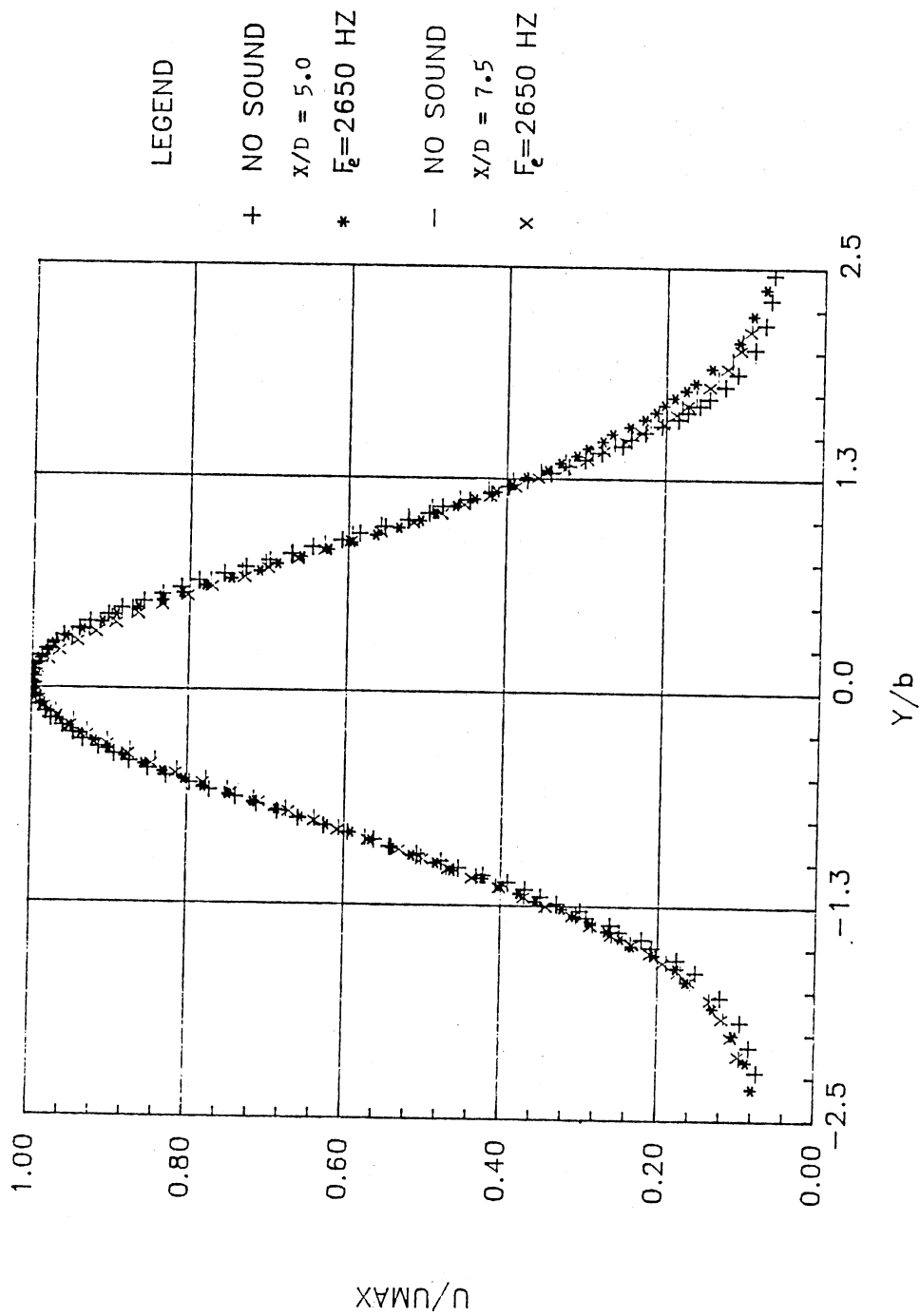


Figure 14. Mean Velocity Profiles at $x/D = 5.0, 7.5$
($f_e = 0$ Hz, $f_e = 2650$ Hz)

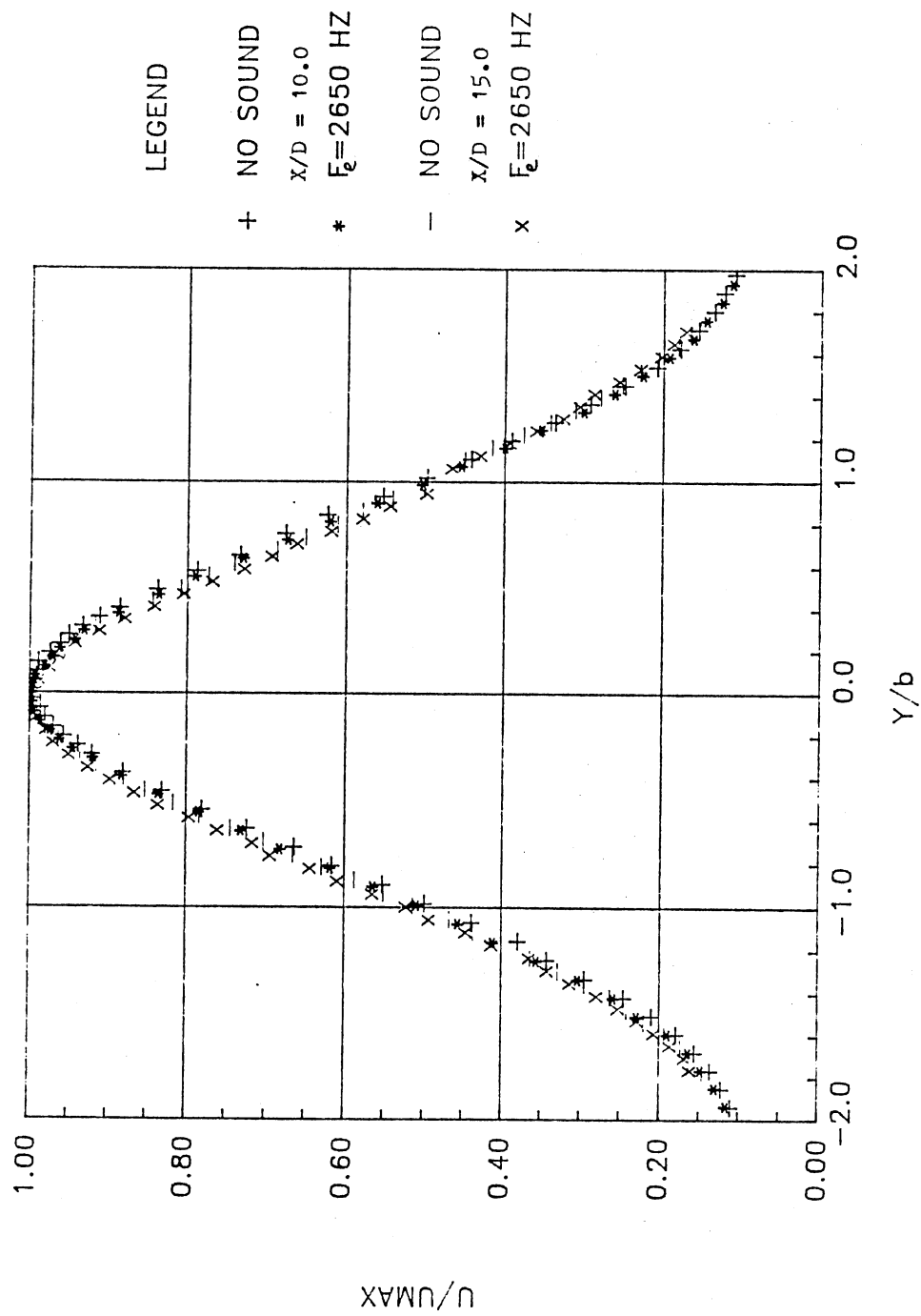


Figure 15. Mean Velocity Profiles at $x/D = 10.0, 15.0$
($f_e = 0$ Hz, $f_e = 2650$ Hz)

in the non-dimensional mean velocity half-width, b/D .

Table 2 on page 42 gives these values for the excited and unexcited cases.

Along with the presented mean velocity profiles, longitudinal fluctuation intensity profiles were taken in order to document their growth and development in the natural flow. These intensities are normalized by the local centerline velocity, U_m , and scaled by the local jet half-width, b , as were the mean velocity profiles. Figures 16-20 present these intensities. As in the mean profiles, the intensity profiles are presented in a manner to allow direct comparison of the excited jet to the natural jet. Figures 16 ($x/D = 0.25$) and 17 ($x/D = 0.5$ and 1.0) show that the initial intensities are very low in the potential core and are relatively constant. The intensities peak near the center of the shear layer ($y/b = 1.0$) which is the location of maximum mean shear dU/dy . It can be easily seen that the intensity levels in the center of the shear layers grow rather rapidly with downstream distance. The excited jet intensities are very similar in form to the natural jet intensities, but they show higher levels. From Figure 18 ($x/D = 1.5, 3.0$) it can be seen that the turbulence intensity from the shear layers "diffuses" toward the centerline. This gives the intensity profiles a characteristic "saddle" shape. In Chapter 3.1, the u velocity fluctuations calculated by

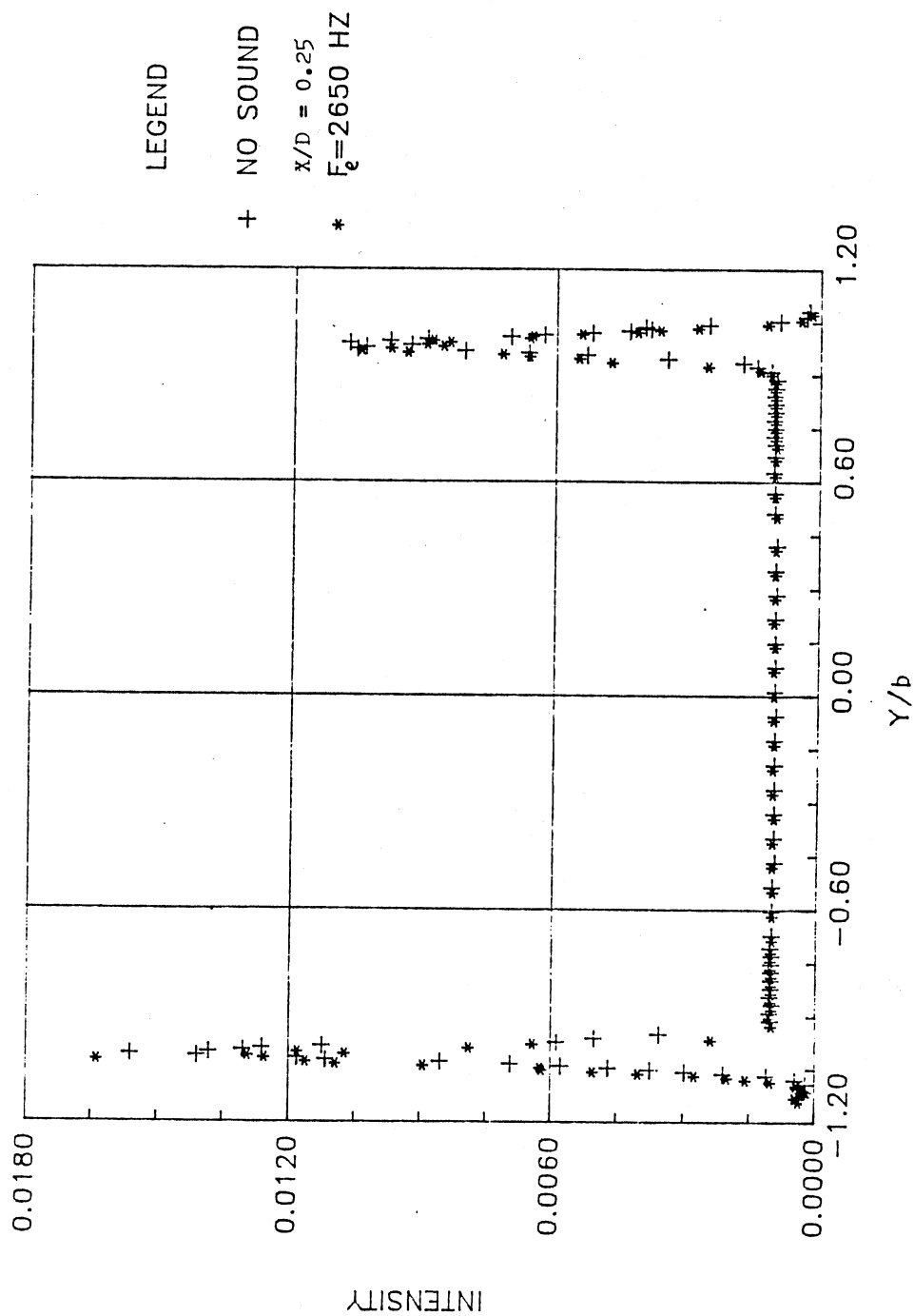


Figure 16. Longitudinal Fluctuation Intensity at
 $x/D = 0.25$ ($f_e = 0$ Hz, $f_c = 2650$ Hz)

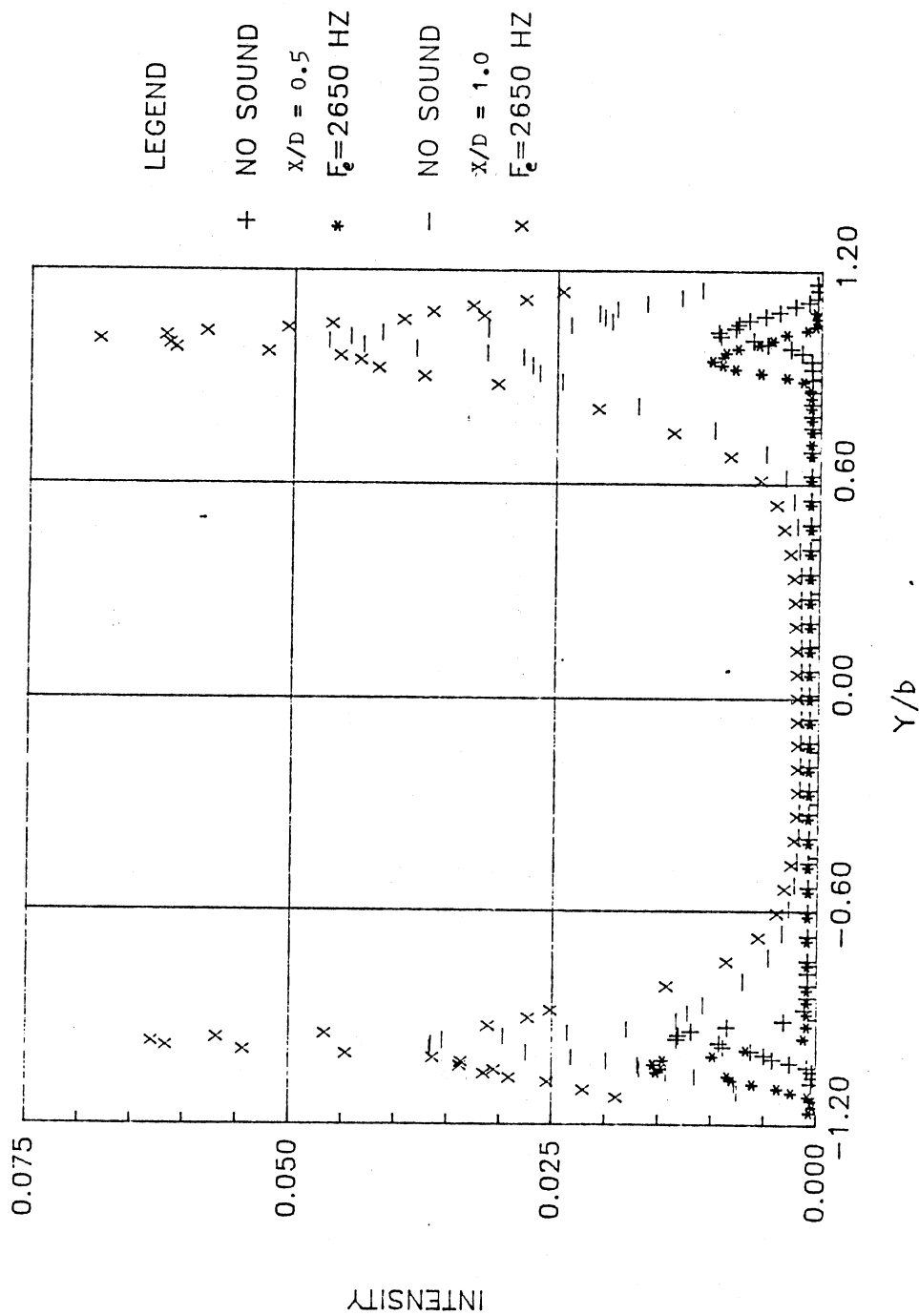


Figure 17. Longitudinal Fluctuation Intensity at $x/D = 0.5, 1.0$ ($f_e = 0$ Hz, $f_e = 2650$ Hz)

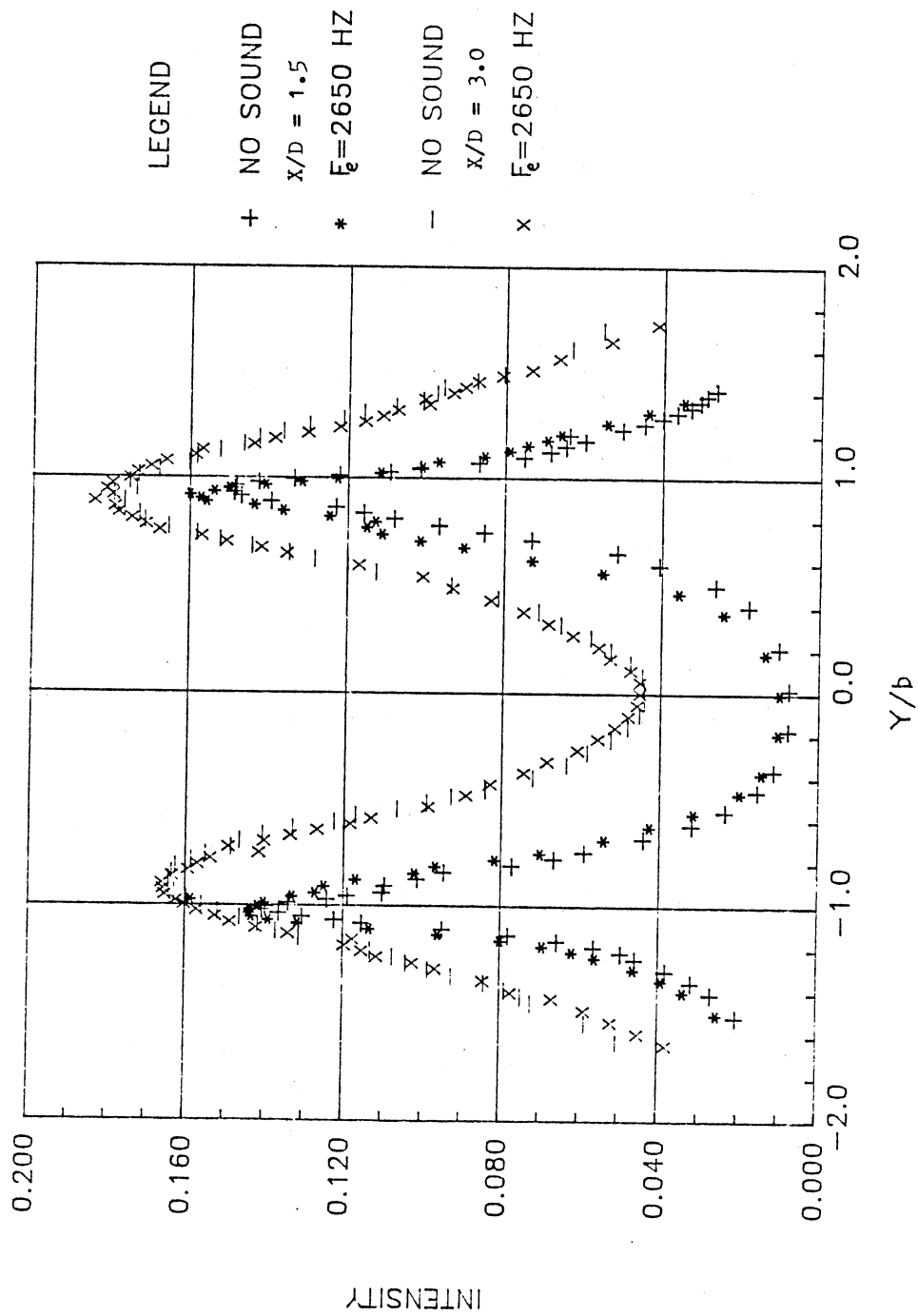


Figure 18. Longitudinal Fluctuation Intensity at $x/D = 1.5, 3.0$ ($f_e = 0$ Hz, $f_e = 2650$ Hz)

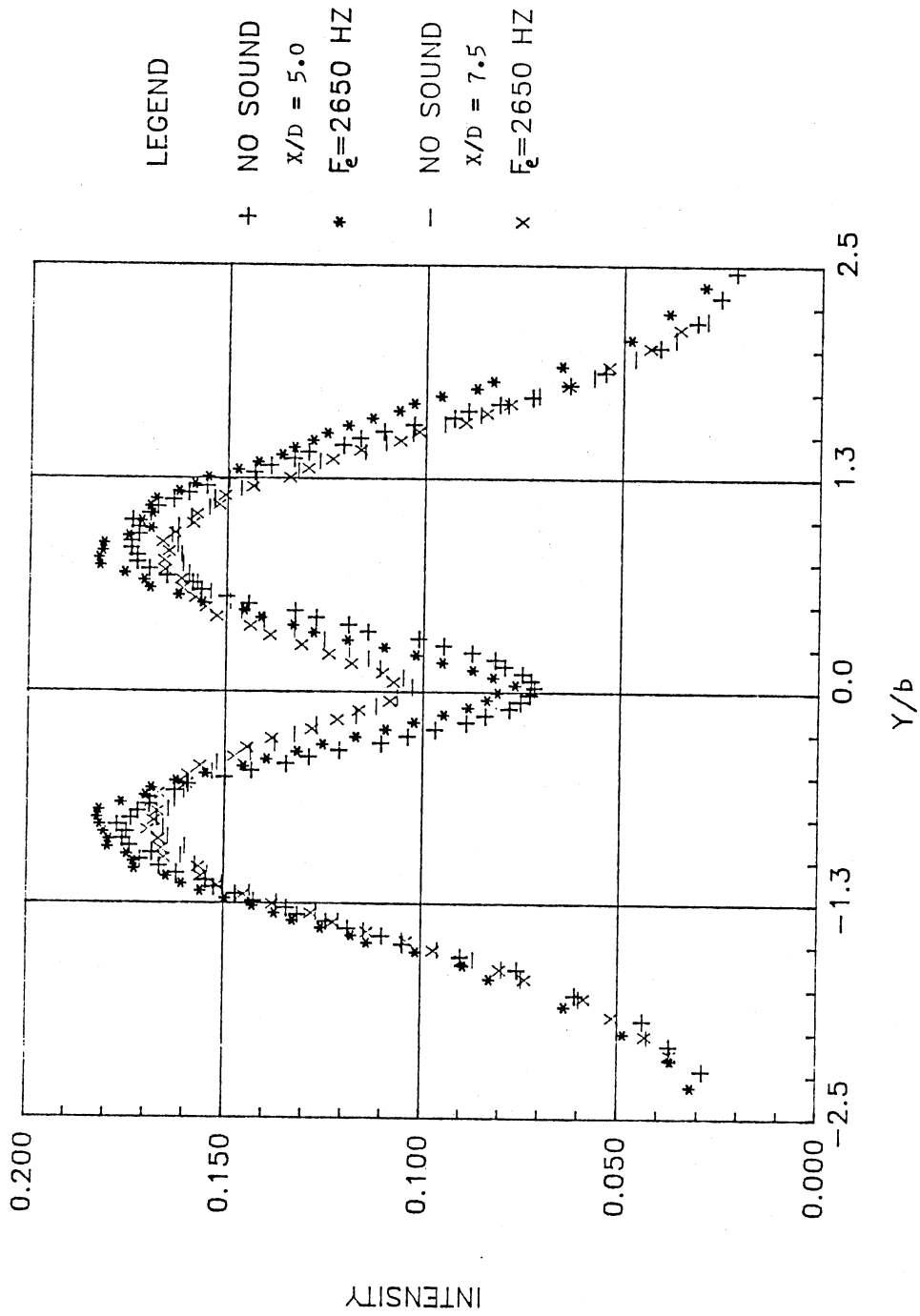


Figure 19. Longitudinal Fluctuation Intensity at
 $x/D = 5.0, 7.5$ ($f_e = 0$ Hz, $f_e = 2650$ Hz)

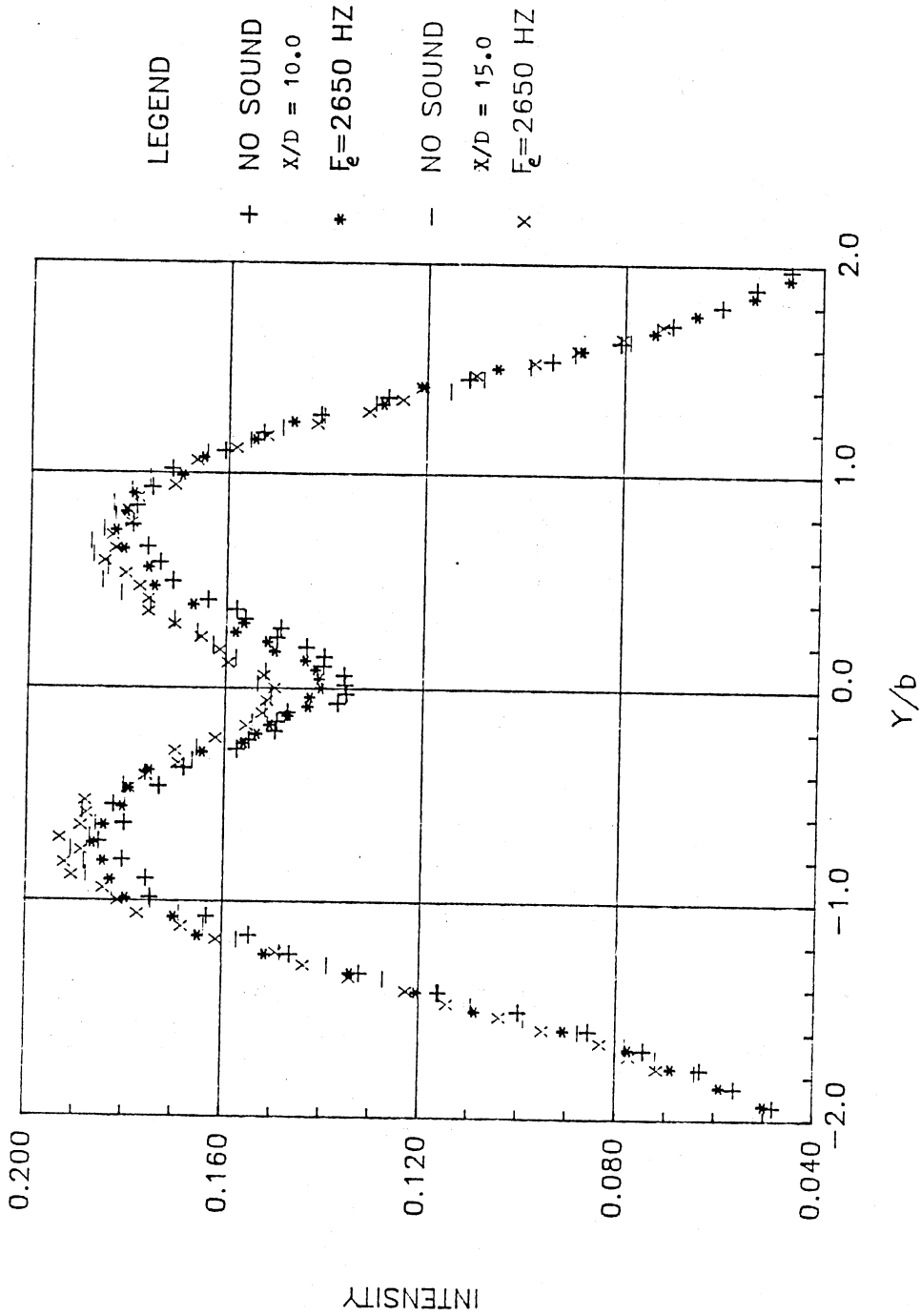


Figure 20. Longitudinal Fluctuation Intensity at $X/D = 10.0, 15.0$ ($f_c = 0$ Hz, $f_c = 2650$ Hz)

linear stability theory will be very similar in form to the longitudinal fluctuation intensity profiles shown here, the difference being that the fluctuations in Chapter 3.1 are the results of a single instability wave while the fluctuations in this chapter are the result of the entire spectrum of disturbances. Figures 19 ($x/D = 5.0$ and 7.5) and 20 ($x/D = 10.0$ and 15.0) show the intensity profiles in the similarity regions. It is interesting to note that the intensity profiles do not give evidence of self-similar behavior as did the mean velocity profiles. However, further downstream (by $x/D = 20.0$) the intensity profiles exhibit self-similar behavior as reported by Bradbury (1965) and Gutmark and Wygnanski (1976). This type of behavior where the mean velocity profiles show self-similar behavior before that of the intensity profiles is also seen in plane mixing layers. The only difference in the excited jet turbulence intensities from that of the natural jet turbulence intensities is found to be the maximum amplitude of these intensities. Figure 21 shows the maximum amplitudes of the natural and excited jet with downstream distances, while Table 2 on page 42 lists these values.

Figure 22 presents the longitudinal turbulence intensity variation with downstream distance x/D measured on the centerline of the jet for the natural and excited cases. The figure shows the strongest growth to occur in

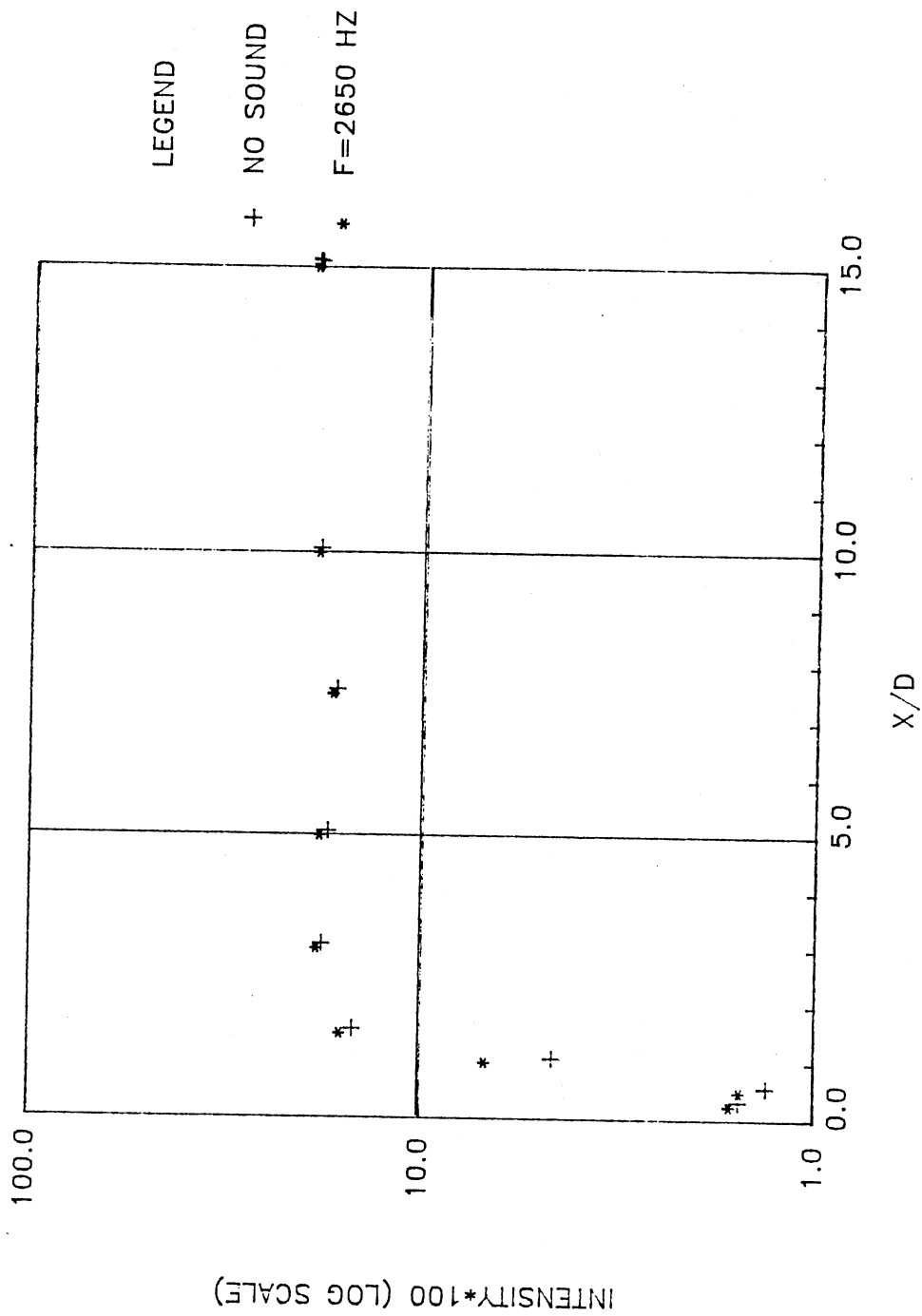


Figure 21. Comparison of Excited to Unexcited Shear Layer Fluctuation Intensities

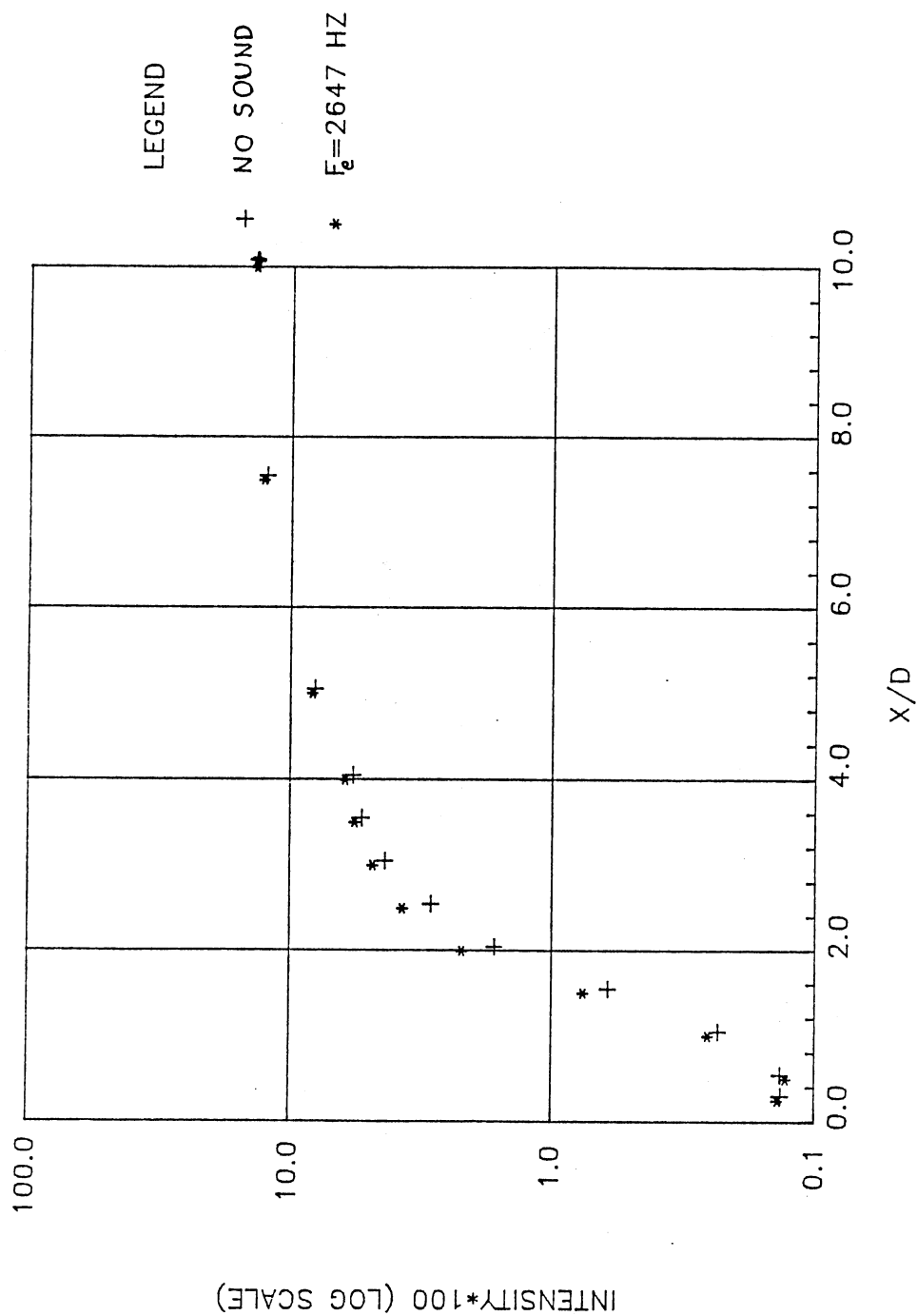


Figure 22. Comparison of Excited to Unexcited Centerline Longitudinal Fluctuation Intensities

the range $1.0 < x/D < 4.0$. In the similarity region of the jet the intensities are equal. The intensity increases at $x/D = 1.0$ and becomes approximately constant around $x/D = 7.5$. At $x/D = 4.0$, the end of the potential core, it is interesting to note that the intensity is less than a curve fit of the data would indicate. The intensity profiles show nothing out of the ordinary happening in the jet.

The results of this chapter show the overall behavior jet to behave as expected. It can be concluded that any results obtained in this research will be completely obtainable in all similar planar jets.

In the next chapter the transition mechanisms of the jet will be documented by several different measurement techniques. The following techniques will be used to accomplish the documentation: application of linear theory (Michalke, 1965), power spectral measurements, digital demodulation measurements, bicoherence measurements, coherence measurements, and correlation measurements. Each of these measurement techniques will be described before the data is presented.

TABLE 2
JET CHARACTERISTICS FOR EXCITED AND UNEXCITED PROFILES

x/D	NO SOUND			f _{exc} =2650 Hz		
	b/D	θ/θ_0	Turb. Iten.	b/D	θ/θ_0	Turb. Iten.
0.25	0.488	1.000	0.0156	0.486	1.000	0.0164
0.50	0.489	1.244	0.0133	0.489	1.205	0.0155
1.00	0.495	2.024	0.0468	0.493	1.932	0.0686
1.50	0.521	5.634	0.1490	0.533	5.955	0.1600
3.00	0.556	12.707	0.1795	0.619	12.205	0.1847
5.00	0.684	23.756	0.1744	0.639	22.455	0.1824
7.50	0.906	36.610	0.1671	0.917	34.318	0.1701
10.00	1.149	43.098	0.1854	1.163	40.500	0.1867
15.00	1.670	58.293	0.1911	1.698	53.727	0.1937

CHAPTER III

TRANSITION MECHANISMS OF THE JET

In this chapter the primary results of the experimental measurements utilized in the research are presented. Transition mechanisms measurements are presented along with the application of linear stability theory to the jet shear layers.

3.1 Application of Linear Theory

This section compares the results of linear theory predictions to the actual jet behavior. Linear stability theory is first discussed before the results are presented.

3.1.1 Linear Stability Theory

In order for linear stability to be applicable the following criteria must be met:

1. Very low amplitude velocity fluctuation
2. Mean velocity profile has an inflection point
3. Must be an inviscid type flow
4. The Reynolds number must be sufficient to produce parallel flow.

If the above criteria is met the linear stability theory

introduced by Michalke (1965) is applicable. The general equation that must be solved is obtained by restricting the flow to wavy disturbances of the form

$$\Psi(x, y, t) = R[\phi(y)e^{i(\alpha x - \beta t)}] \quad (3.1)$$

where Ψ is a disturbance wave function, α and β are constants, and $R[\]$ refers to the set of real numbers. This gives the celebrated Rayleigh equation

$$(U - \beta/\alpha)[\phi'' - \alpha^2\phi] - U''\phi = 0 \quad (3.2)$$

For unbounded velocity profiles the disturbances must vanish at infinity making the boundary conditions

$$\phi(-\infty) = \phi(\infty) = 0 \quad (3.3)$$

Since the velocity profile is unbounded

$$\lim_{y \rightarrow \pm\infty} U'' = 0 \quad (3.4)$$

and from (3.2) and (3.3) the asymptotic behavior of ϕ' is

$$y \rightarrow +\infty \quad \phi' = -\alpha\phi \quad (3.5)$$

$$y \rightarrow -\infty \quad \phi' = +\alpha\phi \quad (3.6)$$

The order of the differential equation (3.2) can be reduced if we use the following transformation

$$\phi = \exp \left[\int \Phi dy \right] \quad (3.7)$$

Using the transformation (3.7) we obtain from equation (3.2) the corresponding Riccati equation in $\Phi(y)$

$$\Phi' = \alpha^2 - \Phi^2 + U''/(U-\beta/\alpha) \quad (3.8)$$

With (3.5) and (3.6) the appropriate boundary conditions become

$$\Phi(+\infty) = -\alpha; \quad \Phi(-\infty) = +\alpha \quad (3.9)$$

The constants $\alpha = \alpha_r + i\alpha_i$ and $\beta = \beta_r + i\beta_i$ are in general complex. α_r is the wave-number, β_r the cyclic frequency or angular velocity of the disturbance and α_i and β_i the spatial and temporal growth rates respectively. For the application of linear theory to the planar turbulent jet, Freymuth (1966) has shown that it is appropriate to assume spatial amplification only giving $\beta_i = 0$.

Equation (3.8), along with boundary conditions (3.9), has to be integrated for real values $\beta > 0$. An eigenvalue problem must therefore be solved first in order to determine

$$\alpha = \alpha(\beta) = \alpha_r + i\alpha_i \quad (3.10)$$

α and β can be limited to the following values of $\alpha_i < 0$, and $\beta > 0$ due to the fact that we are only interested in disturbances traveling and growing in the basic flow direction. The eigenvalues are then determined by numerical integration via a Runge-Kutta-Gill procedure.

The computer code to accomplish this can be viewed in Appendix A.

With the computed eigenvalues known the eigenfunctions ϕ can be found by integration of equation (3.8). Since the eigenfunctions are determined except for an arbitrary multiplicative constant alone, the initial values are normalized to

$$\phi_r(0) = 1; \quad \phi_i(0) = 1 \quad (3.11)$$

The initial gradient is found from (3.7) to be

$$\phi'(0) = \phi_r(0) + i\phi_i(0) \quad (3.12)$$

Equation (3.8) along with initial values (3.11) and (3.12) is solved via a Runge-Kutta-Gill procedure program shown in Appendix A. Once the solution to these equations is known the u' and v' velocity fluctuations can be calculated by the proportion

$$u' \propto (\phi_r^2 + \phi_i^2)^{1/2} \quad (3.13)$$

$$v' \propto (\phi_r^2 + \phi_i^2)^{1/2} \quad (3.14)$$

with the phase angle between them given by

$$u' \text{ phase } \propto \tan^{-1}(\phi_i/\phi_r) \quad (3.15)$$

$$v' \text{ phase } \propto \tan^{-1}(\phi_i/\phi_r) \quad (3.16)$$

In the next section the techniques used to apply linear

stability theory to the planar turbulent jet is discussed.

3.1.2 Linear Stability Techniques

and Results

In order to use linear stability theory, very accurate mean velocity profiles must be obtained. The excited mean profiles shown in section 2.3 are the profiles that will be used to obtain the theoretical predictions of the u velocity fluctuations and u phase variation.

The excitation frequency used in this research to produce a controlled perturbation is of the same frequency as the most unstable frequency at a given x/D location in the near field of the jet. This frequency must first be found. Unexcited mean velocity profiles are taken in the initial region. The Rayleigh equation (equation 3.2) that is to be solved requires the mean local velocity and the second derivative of the mean local velocity as inputs. In order to obtain a second derivative of the mean velocity, a family of curve fits is suggested by Cohen and Wygnanski (1978)

$$0.5\{1 + \tanh\eta[1 + \operatorname{sech}^2\eta(-C_1\tanh\eta + C_2)]\} \quad (3.14)$$

$$\eta = 0.5C_2[y - y(0.5)]^{1/8} \quad (3.15)$$

is fitted to the mean velocity profile. The constants C_1 and C_2 are constants describing the symmetric and antisymmetric corrections, respectively, to the classical

hyperbolic tangent profile. The constant C_3 is related to the other constants by

$$C_3 = 1 - 2/3(C_2) - 2/35(C_1)^2 - 2/15(C_2)^2 \quad (3.16)$$

After the profiles are fitted and a second derivative is found, the Rayleigh equation is solved. The eigenvalues $\alpha = \alpha(\beta)$ are obtained where α is the wave number and β is the cyclic frequency. The excitation frequency is found from the relationship

$$f = \beta U_{\infty} / 2\pi\delta \quad (3.17)$$

where U_{∞} is the maximum velocity at the nozzle exit and δ is found as in the Figure 23. At $x/D = 0.75$ the maximum amplification rate ($-\alpha_1$) corresponds to a cyclic frequency of $\beta = 0.275$ or $f = 2650$ Hz. This location of $x/D = 0.75$ is chosen because the corresponding frequency at this location amplifies at upstream locations and several downstream locations as well. This frequency is chosen to excite the flow throughout this paper except where noted.

Using the frequency given above, the excited mean profiles are generated as presented in section 2.3. Curve fits are generated for the positions $x/D = 0.5, 0.75, 1.0, 1.25$, and 1.5 . The eigenvalues are then found for each of these cases. Figure 24 shows the amplification rates versus the nondimensional frequency beta. A shift in the range of frequencies is noted in the curves for $x/D = 1.25$

MEAN VELOCITY VARIATION IN SHEAR LAYER

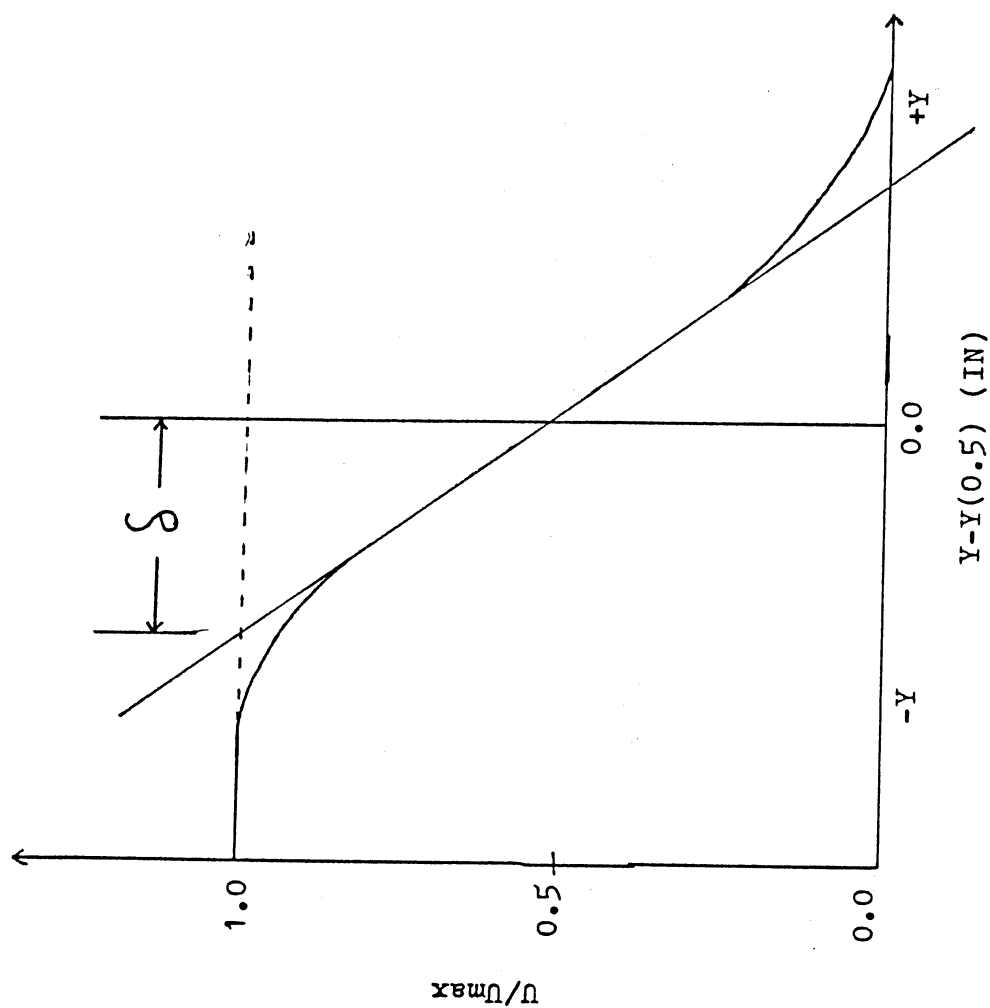


Figure 23. Plot of Delta Scaling

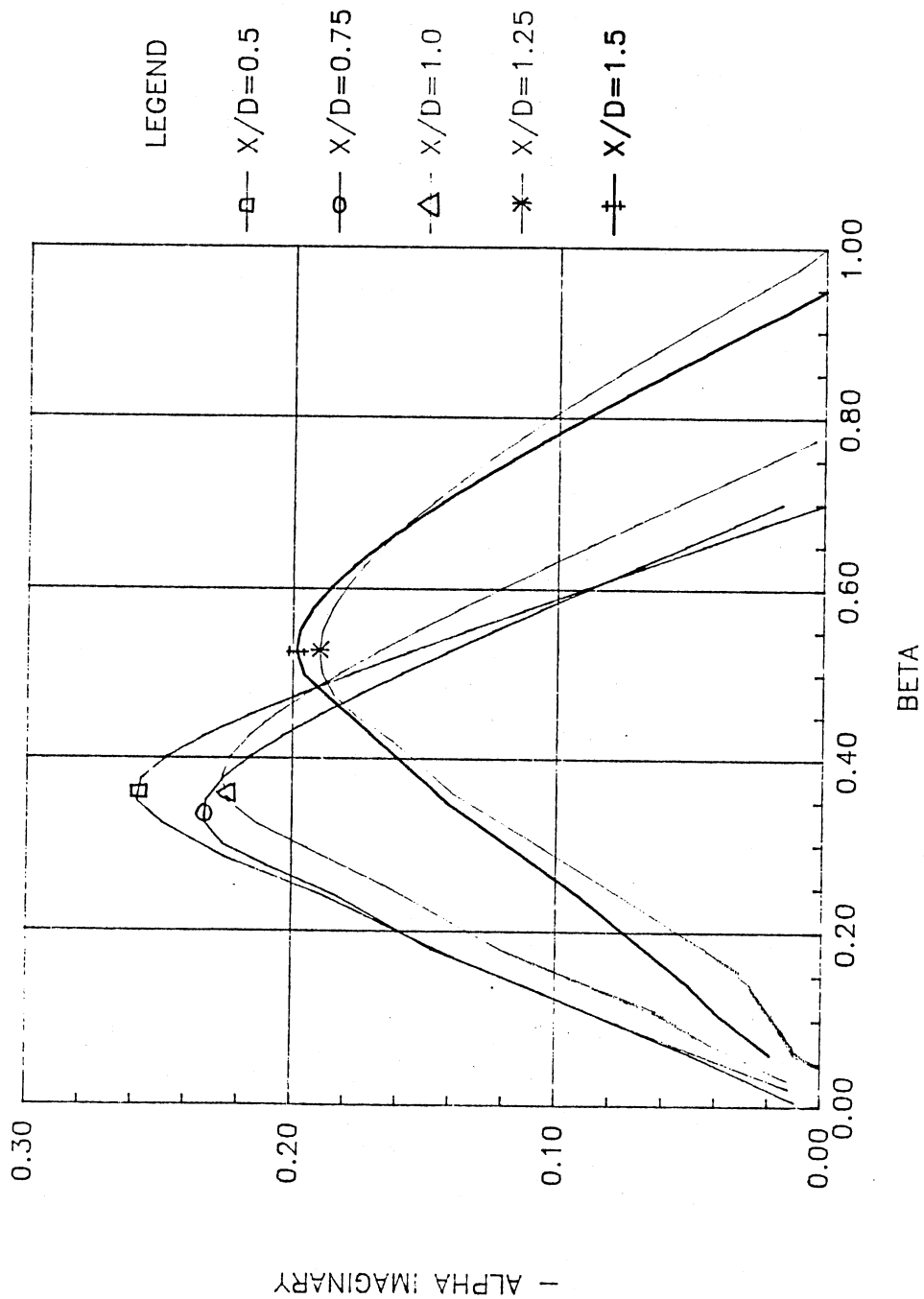


Figure 24. Amplification Rates Versus Beta

and $x/D = 1.5$. The reason for this shift is that the excitation used slightly changes the mean velocity profiles at these locations from the natural profiles while the upstream locations are not affected by the excitation. Since the eigenvalue calculations are very sensitive to the second derivative of velocity, small changes in the mean velocity profile can have a significant effect on the solution. As expected, the farther downstream from the exit, the lower the maximum unstable frequency becomes. Figure 25 shows the phase velocity c_r as a function of β . The phase velocity is defined as $c_r = \beta_r / \alpha_r$. Now that the eigenvalues are known, the eigenfunctions can now be determined. From these eigenfunctions the u and v velocity fluctuations can be calculated for the profile.

The flow field is excited at the predetermined frequency of 2650 Hz. The u disturbance measurements are taken with a standard hot-wire probe used in the constant temperature mode. The hot-wire signals pass through filters and are then digitized by an HP-98640A analog/digital conversion board. A total of 512 samples is recorded for each ensemble. Each sample is phase locked with the inputted excitation frequency by sampling only when the sinusoidal periodic excitation is at a maximum peak. The phase locking allows the comparison of

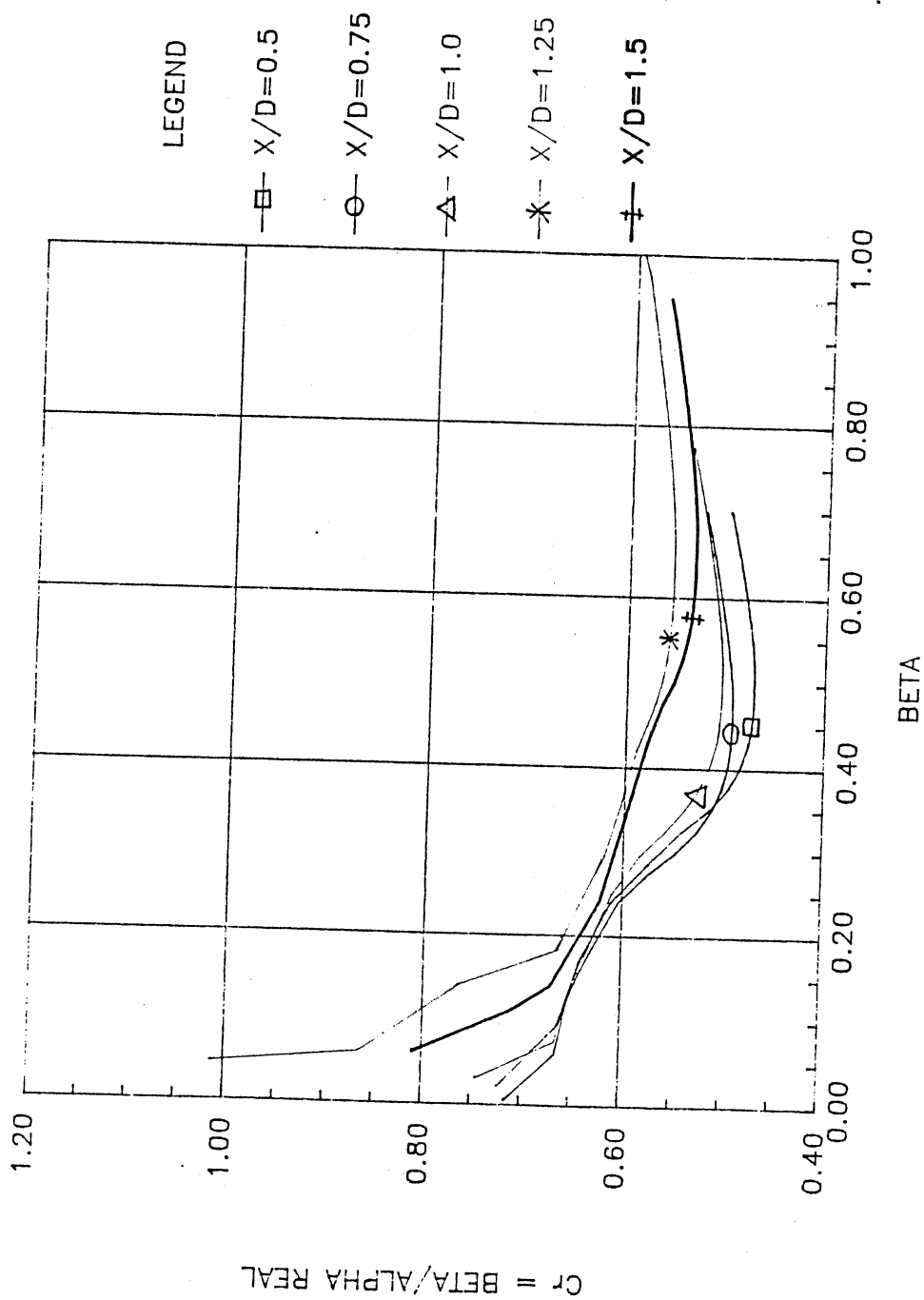


Figure 25. Phase Velocity Versus Beta

the theoretical u velocity fluctuations at a certain β frequency to the spectral measurements at $f_{ex} = 2650$ Hz. A total of 50 ensembles is used to assure a smooth spectrum. A Nyquist frequency of 6000 Hz is used for each spectrum. A Fast Fourier Transformation algorithm is used to compute the spectral density function from the inputted signal. Appendix A contains the computer program used to accomplish the above.

In order to convert the spectral density function to the desired u velocity fluctuations, the local mean velocity is needed for each location the spectral density is taken. The spectral density function can then be converted to u velocity fluctuation by the following relationship

$$(u^2)^{ms} = (e^2)^{ms} dU/dE \quad (3.17)$$

where e^2 is the integrated area of the spectral density over a 50 Hz bandwidth centered on the excitation frequency and dU/dE is the derivative of equation (2.3). The results are then normalized to the maximum value obtained to allow direct comparison to the theoretical curve that is also normalized to its maximum value.

Figure 26 shows the results of the theoretical u velocity versus the experimentally measured u velocity at $x/D = 0.5$. The location $y = 0$ is the location in the shear layer where $U/U_{free} = 0.5$. Good results are obtained

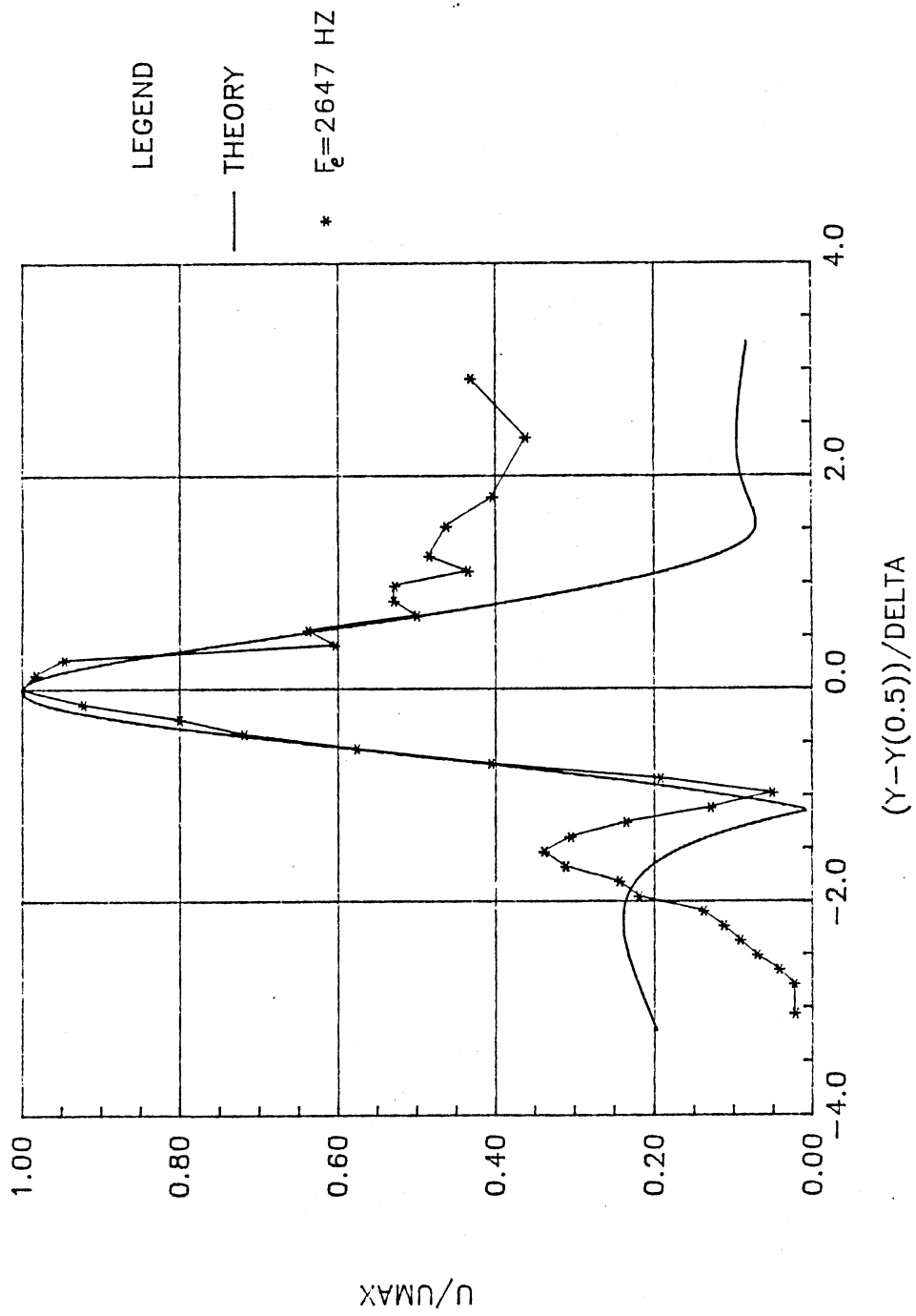


Figure 26. Theoretical Versus Experimental U Velocity at $x/D = 0.5$

from the phase reversal at $y = -1.2$ up to a location $y = 1$. Theoretical u velocity fluctuation overpredicts on the low speed side of the shear layer and underpredicts on the high speed side. The discrepancy on the low speed side is expected due to limitations in measuring with hot wires in zones where low velocities cause flow intermittency. The discrepancy on the high speed side is seen to occur at the location where the intensity of the u velocity fluctuations reach a maximum. However, the relative shape of the theoretical curve on the low and high speed sides are in good agreement with the experimental curves.

Figures 27 and 29 show the results at x/D locations of 0.75 and 1.0. Again good results are obtained near the center of the shear layer. The curves show near perfect agreement from $y = -1.5$ to $y = 1.0$. As in the case of $x/D = 0.5$, the slope of the curve on the low and high speed sides are consistent although they do not agree in magnitude. The discrepancies between the measured and calculated u fluctuations are expected to become greater the farther downstream one travels since the amplitude of fluctuations increases with downstream distance.

Figures 29 and 30 show the results at x/D locations 1.25 and 1.5. The results show very little agreement. At these locations the intensity levels are at significant levels to invalidate linear theory. From the results obtained it would seem that linear theory can only be used

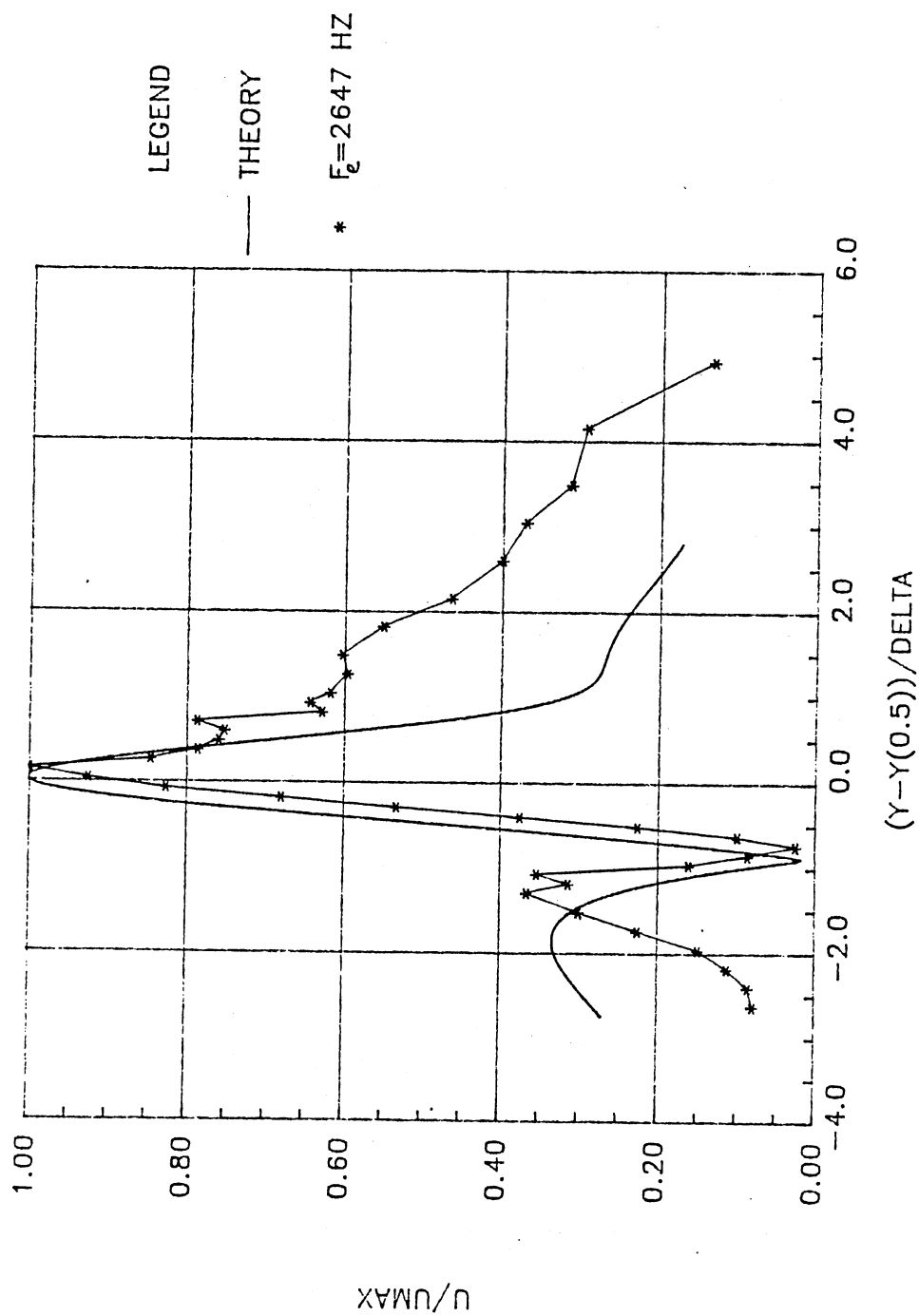


Figure 27. Theoretical Versus Experimental U Velocity at $x/D = 0.75$

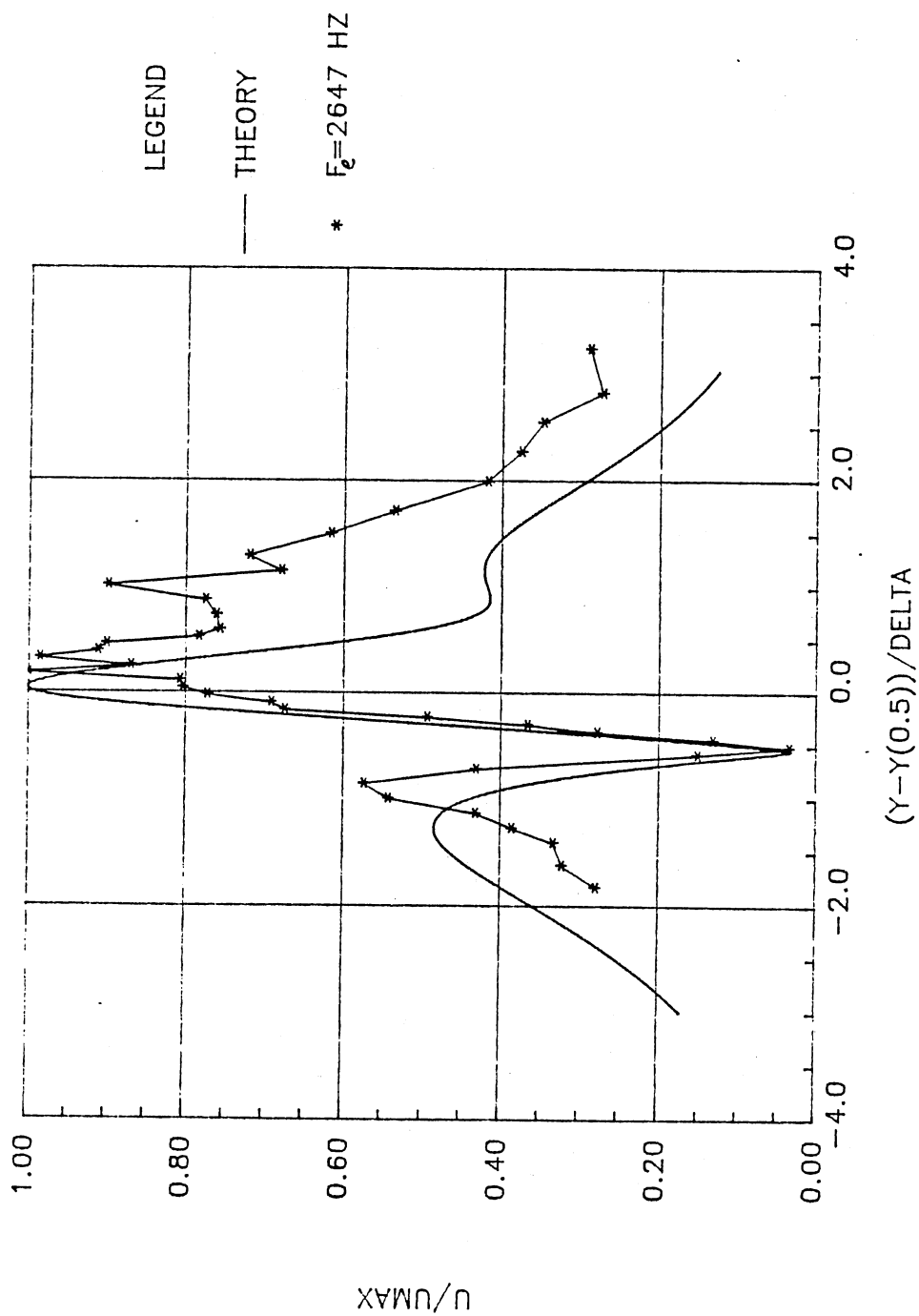


Figure 28. Theoretical Versus Experimental U Velocity at $x/D = 1.0$

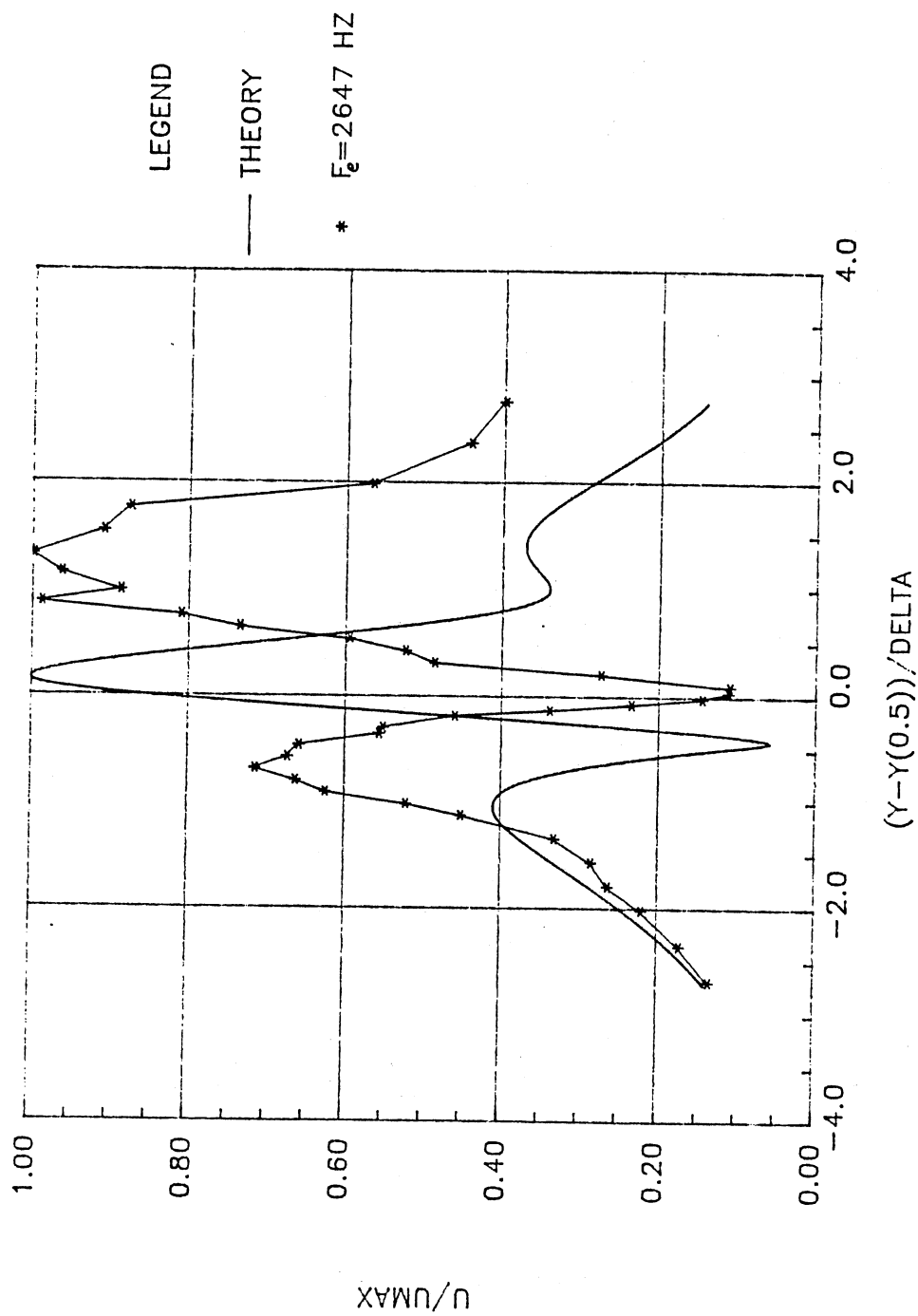


Figure 29. Theoretical Versus Experimental U Velocity at $x/D = 1.25$

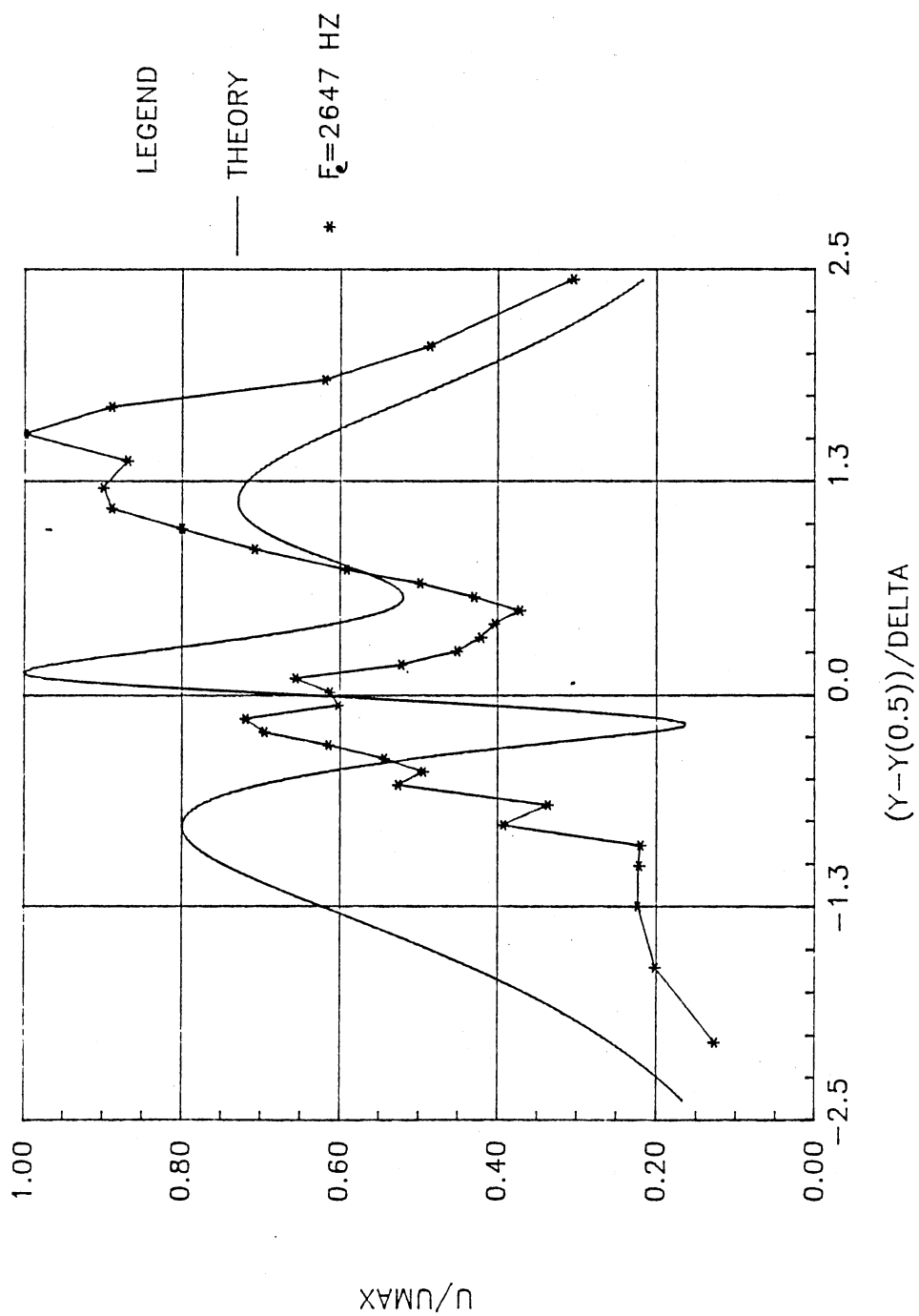


Figure 30. Theoretical Versus Experimental U Velocity at $x/D = 1.5$

at locations where the turbulent intensity is less than 10 percent. At x/D locations less than 0.5, the frequency chosen would not significantly amplify to obtain experimental curves.

Figures 31-35 present the results of the phase angles at x/D locations 0.5, 0.75, 1.0, 1.25, and 1.5. The results at x/D locations 0.5, 0.75, 1.0 show agreement with theoretical calculations. The phase shift and general slope of the phase is seen precisely at all three locations. Very little agreement is seen at x/D locations 1.25 and 1.5 although the general slope of the phase is indicated. This is expected since the u velocity fluctuation curves at these two locations are not in good agreement due to large amplitudes of velocity fluctuations.

3.2 Power Spectral Measurements

This section presents power spectral measurements documenting the spectral evolution of the jet under two different excitation conditions. The first acoustic excitation will be at the most unstable frequency at location $x/D = 0.75$, $f_{\text{max}} = 2650$ Hz (determined in section 3.1). The second case of frequency excitation to be used will give what is referred to as an "untuned jet". An untuned jet refers to a jet that has been acoustically excited at a frequency that is not a multiple of the jet

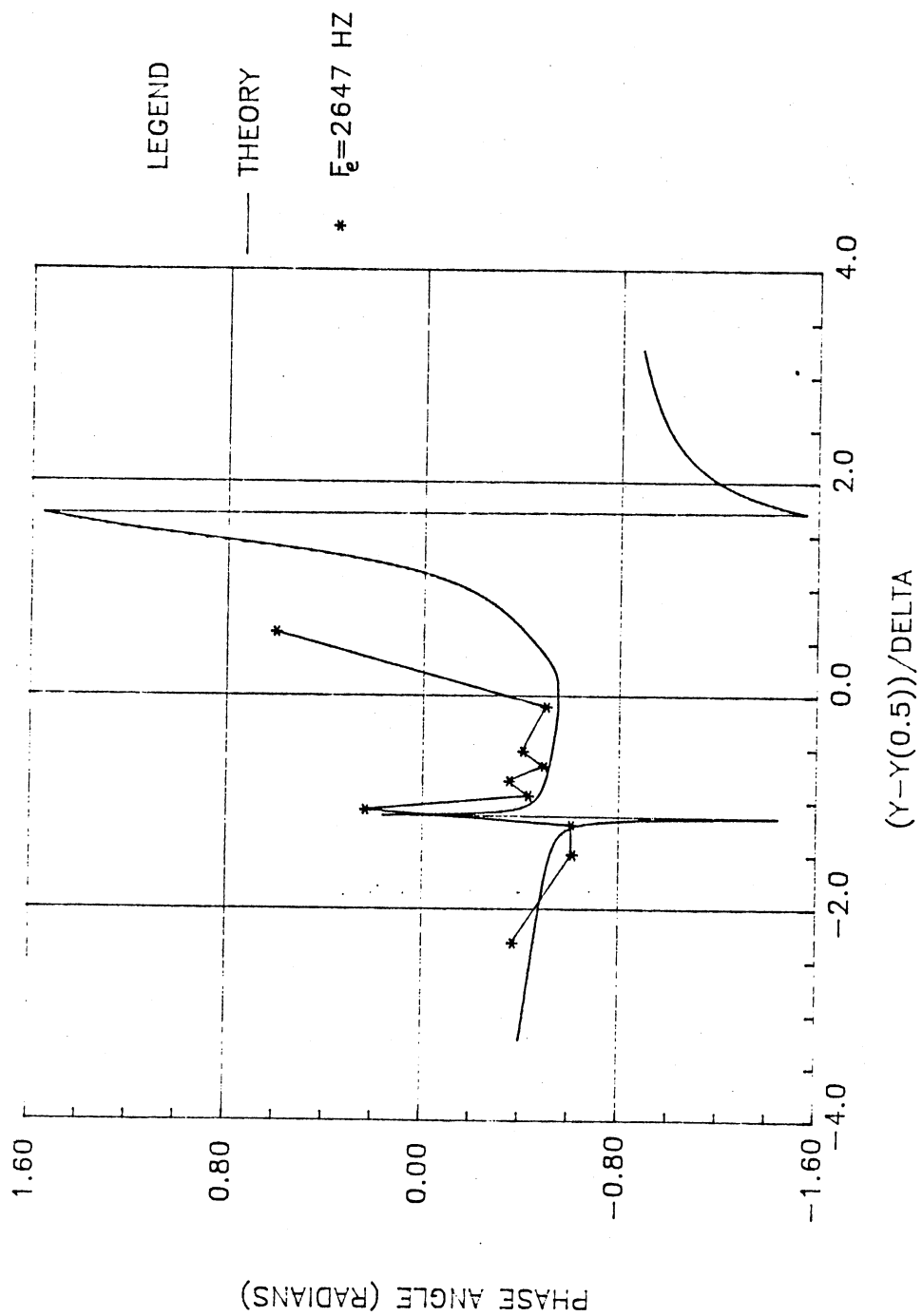


Figure 31. Theoretical Versus Experimental Phase
at $x/D = 0.5$

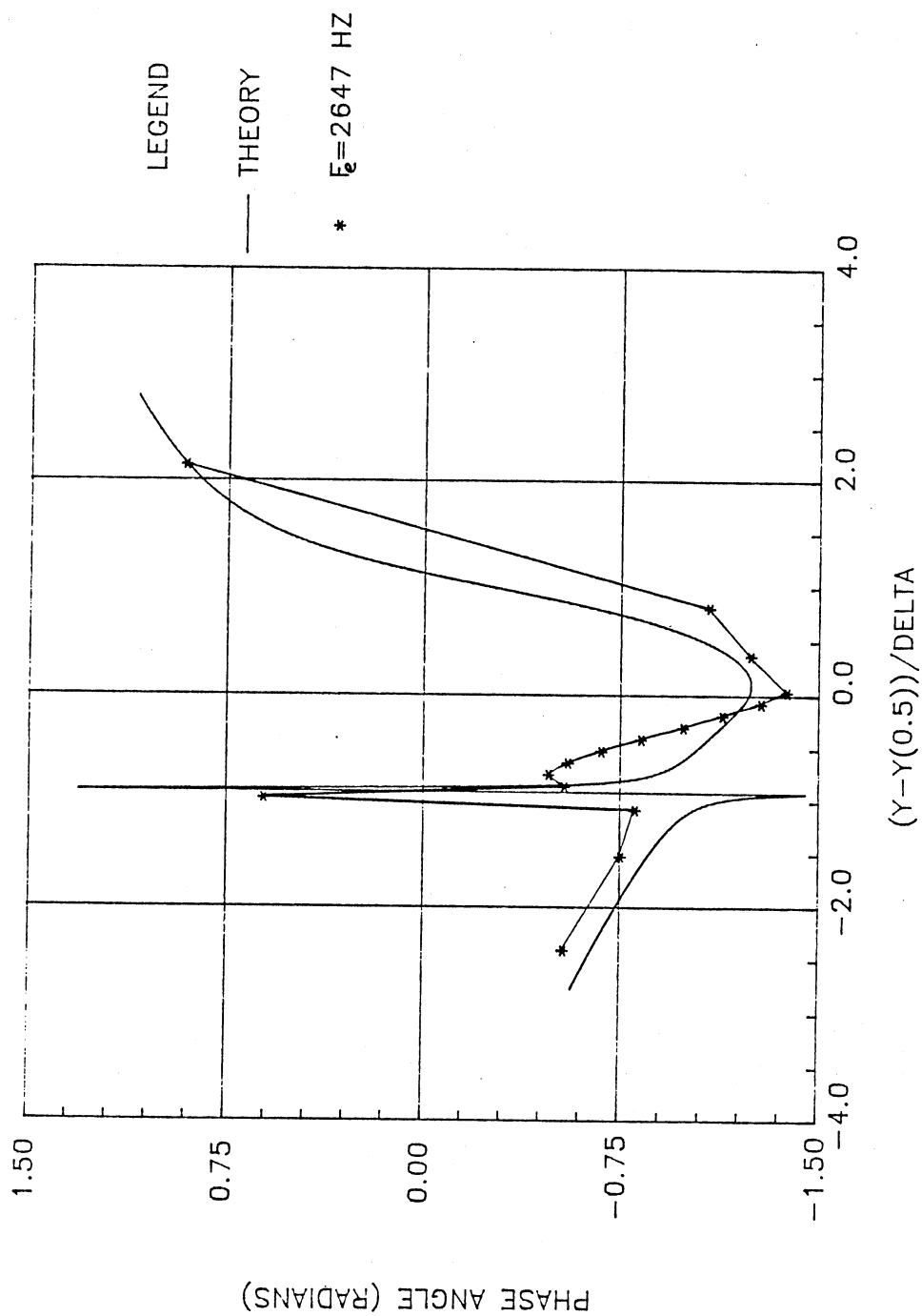


Figure 32. Theoretical Versus Experimental Phase
at $x/D = 0.75$

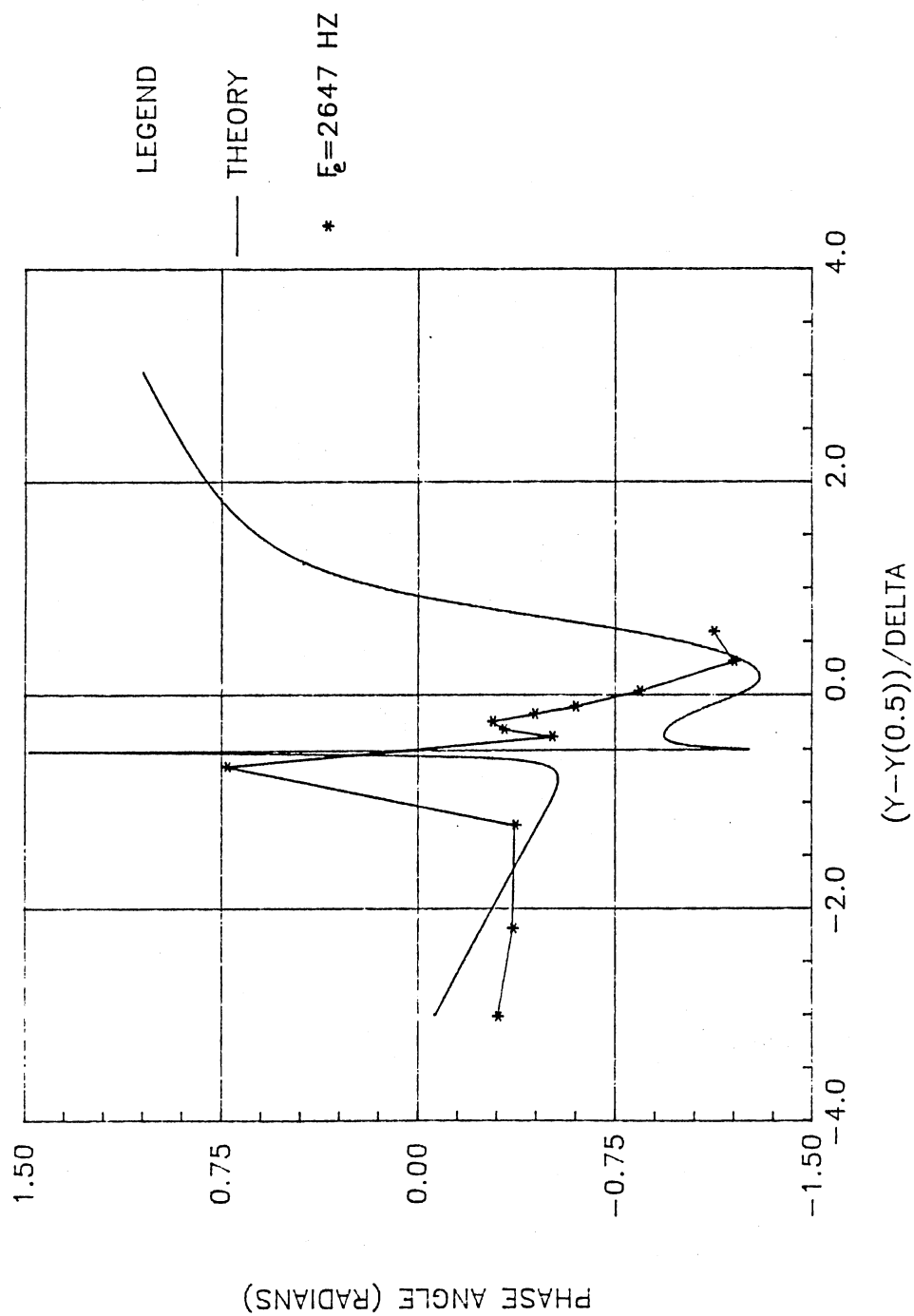


Figure 33. Theoretical Versus Experimental Phase
at $x/D = 1.0$

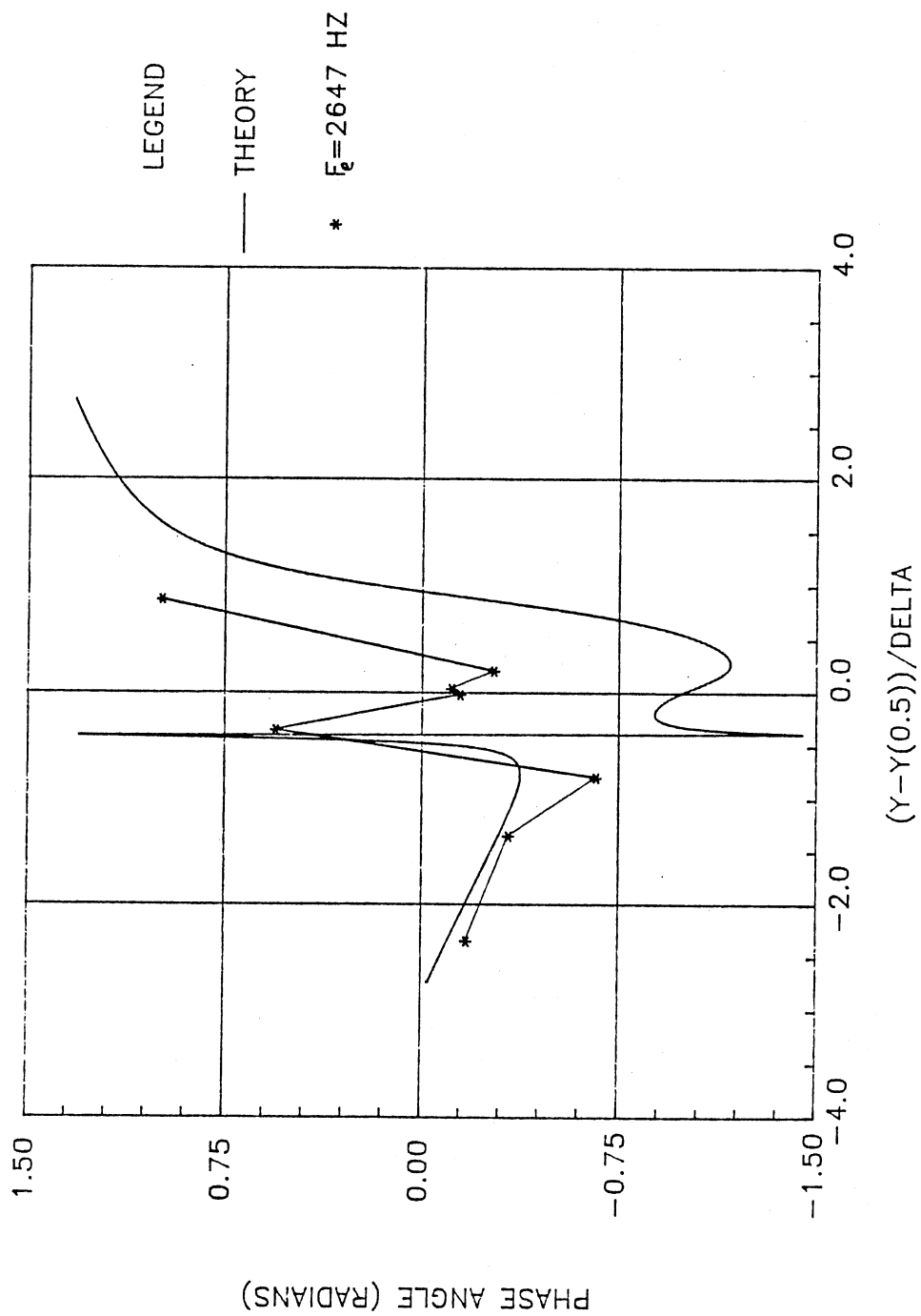


Figure 34. Theoretical Versus Experimental Phase
at $x/D = 1.25$

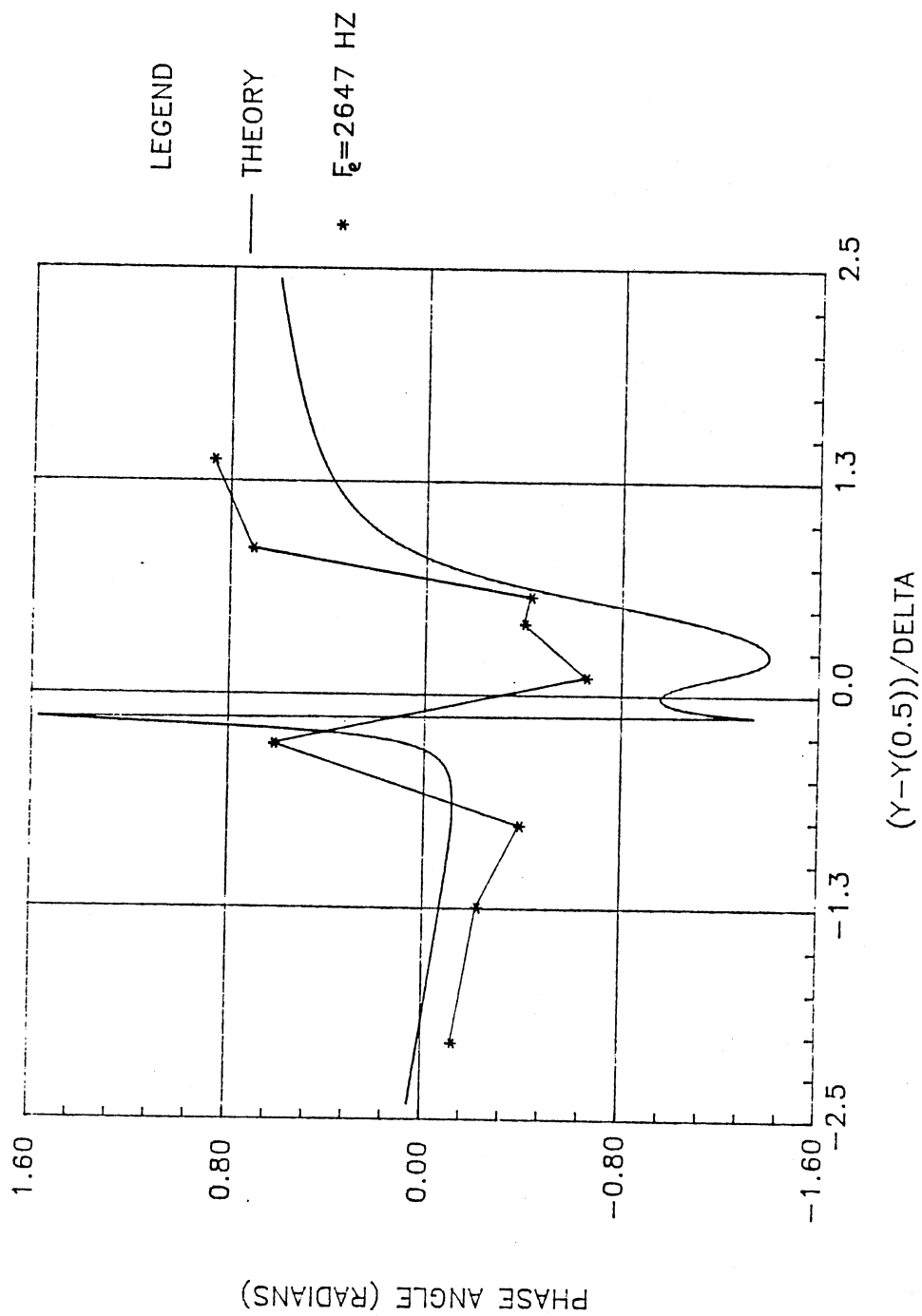


Figure 35. Theoretical Versus Experimental Phase
at $x/D = 1.5$

column mode (passage frequency of large-scale vortices at the end of the potential core). A sample frequency that provides an untuned jet is that of $f_w = 2200$ Hz. Power spectra are obtained on the jet centerline and in the developing shear layers for x/D locations 0.25 to 5.

3.2.1 Spectral Measurement Techniques

For the spectral measurements a standard "straight wire" probe was used in the constant-temperature mode. The signal from the hot-wire is AC-coupled and passed through anti-alias filters and then digitized by an HP-98640A analog/digital conversion board with 512 samples recorded for each ensemble. The number of ensembles increased with downstream distance, with the typical value being 100 ensembles. The Nyquist frequency used is 6000 Hz. A Fast Fourier Transformation algorithm is then used to compute the spectral density function. The program used can be viewed in Appendix A.

3.2.2 Spectral Development at $f_w = 2650$ Hz

All spectral measurements in this section correspond to the jet acoustically excited at frequency $f_w = 2650$ Hz. Figure 36 presents the power spectra in the excited jet shear layer at $x/D = 0.25, 0.5, 0.75$, and 1.0 . The energy levels at $x/D = 0.25$ are very low, but definite peaks are observed. A low level peak occurs at the most unstable

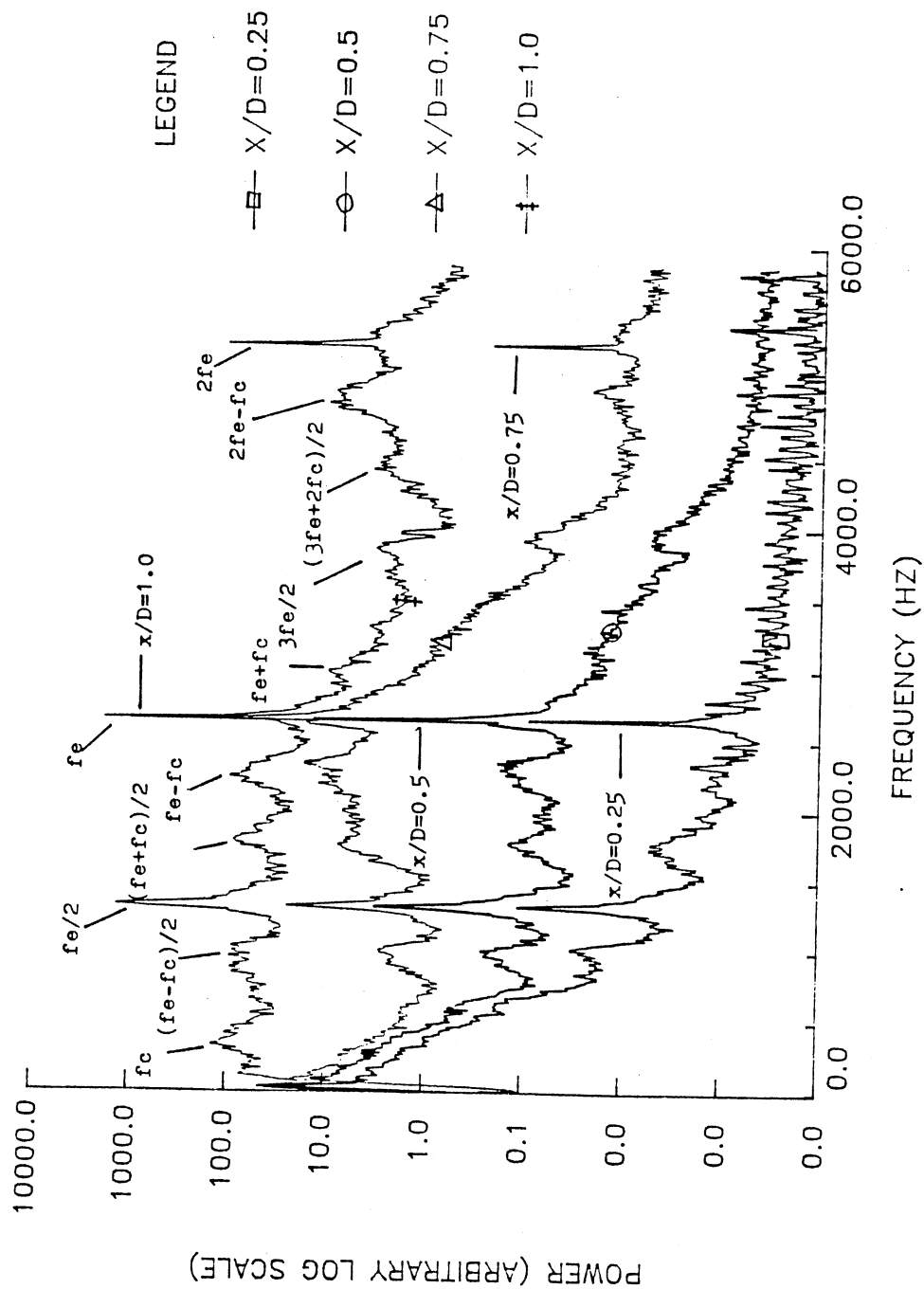


Figure 36. Comparison of the Excited Power Spectra
at $x/D = 0.25, 0.5, 0.75, 1.0$ ($f_e = 2650$ Hz)

jet shear layer frequency of 2650 Hz. This peak occurs due to the low level excitation of the jet. Already at this near exit streamwise location, the spectrum indicates nonlinear wave interactions. A definite peak is observed at the subharmonic frequency $f_{\omega}/2 = 1325$ Hz. Sidebands about the fundamental and subharmonic frequencies are also being generated, suggesting modulation effects. These sidebands help to distribute the energy throughout the shear layer. The modes present in the power spectrum suggest that interactions between the excitation frequency and the jet column mode f_c are occurring. The jet column mode is defined as the passage frequency of large-scale vortices at the end of the potential core. This frequency is measured to be $f_c = 390$ Hz. A Strouhal number can be found from the jet column mode and is given by

$$St = f_c D / U_{\infty} \quad (3.18)$$

The Strouhal number is $St = 0.26$. A very important mode formed by the interaction of the fundamental and the jet column mode is seen at $f_{\omega} - f_c$. The beginnings of other modes formed by interaction of f_{ω} with f_c are found at $(f_{\omega} - 2f_c)/2$ and at $(f_{\omega} + 2f_c)/2$.

At $x/D = 0.5$, the modes found at $x/D = 0.25$ are still evident only at higher energy levels. The emergence of the difference mode at $f_{\omega} - f_c$ can clearly be seen at this location. At location $x/D = 0.75$, the excitation

frequency shows large growth over the previous location. The previously defined modes are still in evidence. The harmonic frequency ($2f_{\omega}$), although very low in energy, begins to form at $f = 5300$ Hz. By $x/D = 1.0$ the spectrum shows growth of energy levels throughout the entire frequency band. Other modes are forming at f_c , $(f_{\omega} + f_c)$, and $(2f_{\omega} - f_c)$.

Figure 37 presents the development of the power spectrum from $x/D = 1.25$ to 1.5 . At $x/D = 1.25$, the spectrum shows very large and dominant growth of the subharmonic frequency. The harmonic frequency is still in evidence, although it has less amplitude than at the previous upstream location. Growth of modes $(3f_{\omega} - f_c)/2$ and $(3f_{\omega} + 2f_c)/2$ are noted along with a large growth of $3f_{\omega}/2$. Downstream at $x/D = 1.5$, the majority of the energy in the flow is being shifted to the lower frequencies. The second subharmonic frequency $f_{\omega}/4$ is seen at this location. The harmonic frequency is decreasing in amplitude to a very low amplitude, along with the modes surrounding it. The subharmonic frequency is still the dominant frequency, although a peak at $(f_{\omega} - 3f_c)/2$ is emerging as a dominant frequency. The modes on either side of the excitation frequency have exhibited growth. This growth is seen in the entire range of frequencies less than 3000 Hz. The peak at $(f_{\omega} - 2f_c)/2$ is no longer evident at this location.

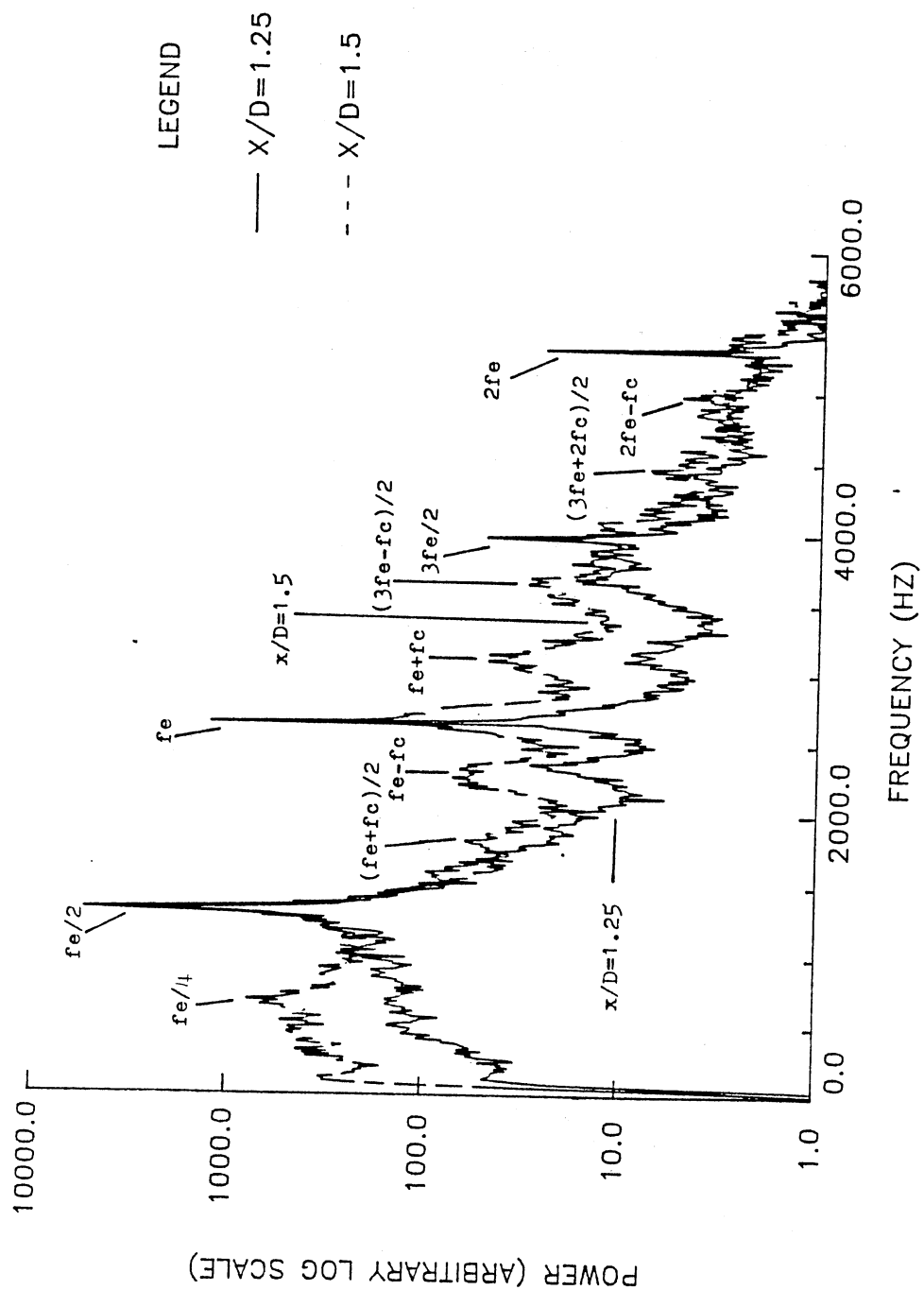


Figure 37. Comparison of the Excited Power Spectra
at $x/D = 1.25, 1.5$ ($f_e = 2650$ Hz)

Figure 38 documents the development in the shear layer from $x/D = 1.75$ to 2.0 . At $x/D = 1.75$ it is very interesting to note that the fundamental excitation frequency is the dominant peak. However, the spike is very thin with all the energy concentrated right at the excitation frequency. Again it is noted that the majority of the energy has been shifted to the lower frequencies. The subharmonic is still visible, but like the fundamental it is very thin. The majority of the energy at $x/D = 1.75$ is centered at the mode $f_{\infty}/4$. Since the harmonic frequency has completely disappeared, the scale on the frequency is adjusted to show the lower frequencies better. It is also interesting to note that the distinct modes, besides modes mentioned above, observed at the previous upstream location are no longer noticeable. Energy has transferred to the valleys between the modes. This is characteristic of the growth of random instabilities which occurs when transition to turbulence begins. At $x/D = 2.0$ the frequency centered at mode $f_{\infty}/4$ has grown to be the dominant peak containing the majority of the energy in the spectra. The other observable peaks are those at the fundamental and subharmonic frequencies. The subharmonic has shown growth while the fundamental has shown significant reduction in amplitude.

Figure 39 documents the spectra at locations $x/D = 2.5$. At $x/D = 2.5$ the fundamental excitation frequency is

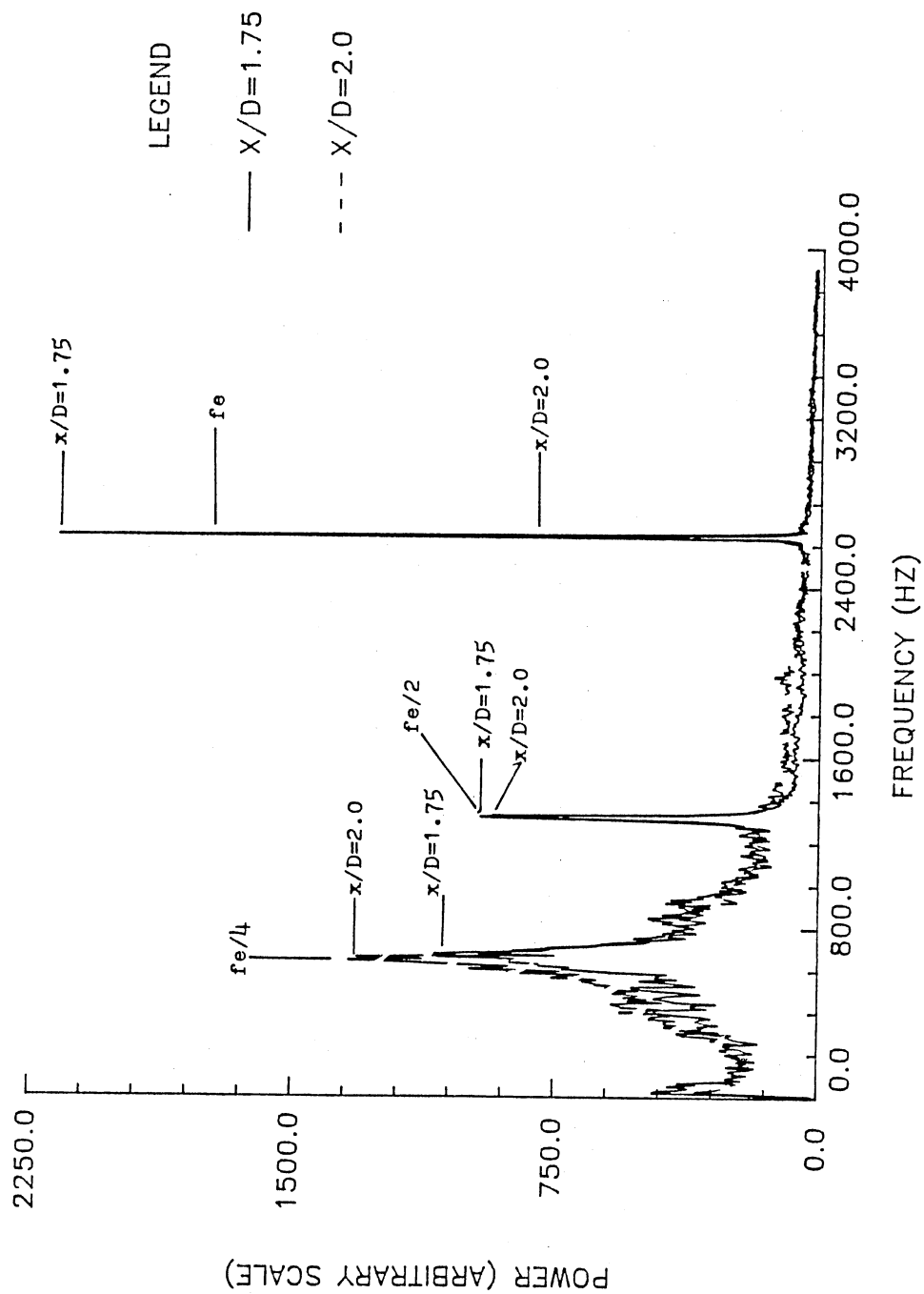


Figure 38. Comparison of the Excited Power Spectra
at $x/D = 1.75, 2.0$ ($f_e = 2650$ Hz)

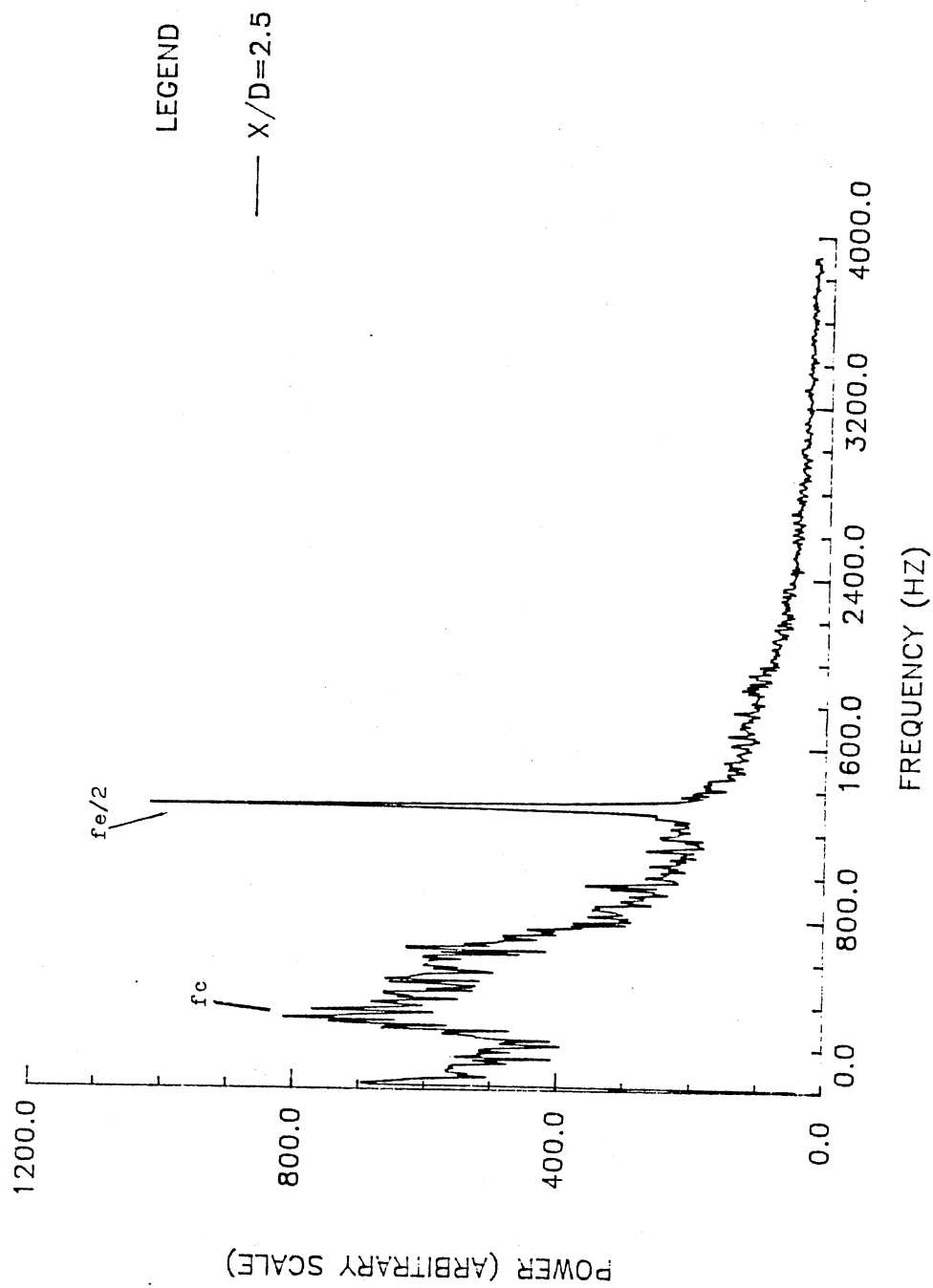


Figure 39. Excited Power Spectra at $x/D = 2.5$
($f_e = 2650$ Hz)

no longer evident. The mode that was centered at $f_{w}/4$ has broken down from a centered peak to a broad peak. The jet column mode is now observable. The subharmonic frequency is still evident, but as before it is very thin with all the energy located at the frequency itself. The spectrum has almost all of the energy at the lower frequencies and has begun to resemble a broadband spectra.

In order to determine more about the power spectra at downstream locations where the spectra has begun to resemble a broadband spectra, a simple transformation will be used. The energy in the spectrum is given by

$$E = \int S(f) df \quad (3.19)$$

where f is the spectrum frequency and $S(f)$ is the spectrum value at a particular frequency. If we let $x = \log f$ and $dx = df/f$, then $df = f d(\log f)$. This gives the energy in the spectrum as

$$E = \int f S(f) d(\log f) \quad (3.20)$$

Figure 40 documents the transformed spectrum at location $x/D = 3.0$. This figure clearly shows the increase of the mode at $f_{w}/4$. The peak at the jet column mode is also clearly visible. Figure 41 shows the transformed spectrum at location $x/D = 4.0$. At $x/D = 4.0$ the subharmonic frequency has completely decayed. The peaks clearly visible exist at modes $f_{w}/4$ and f_{c} . Figure 42 presents

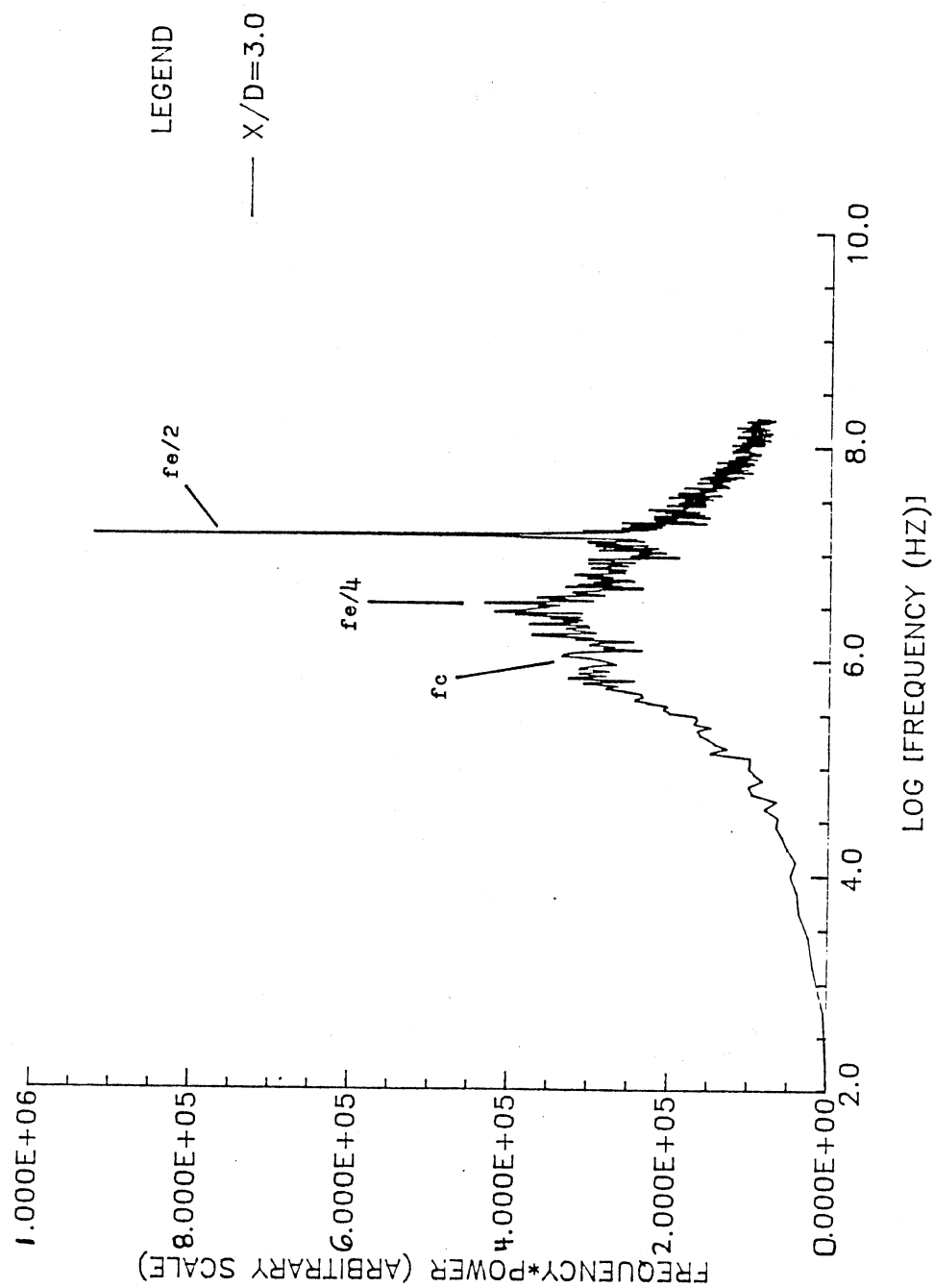


Figure 40. Transformed Excited Power Spectra
at $x/D = 3.0$ ($f_e = 2650$ Hz)

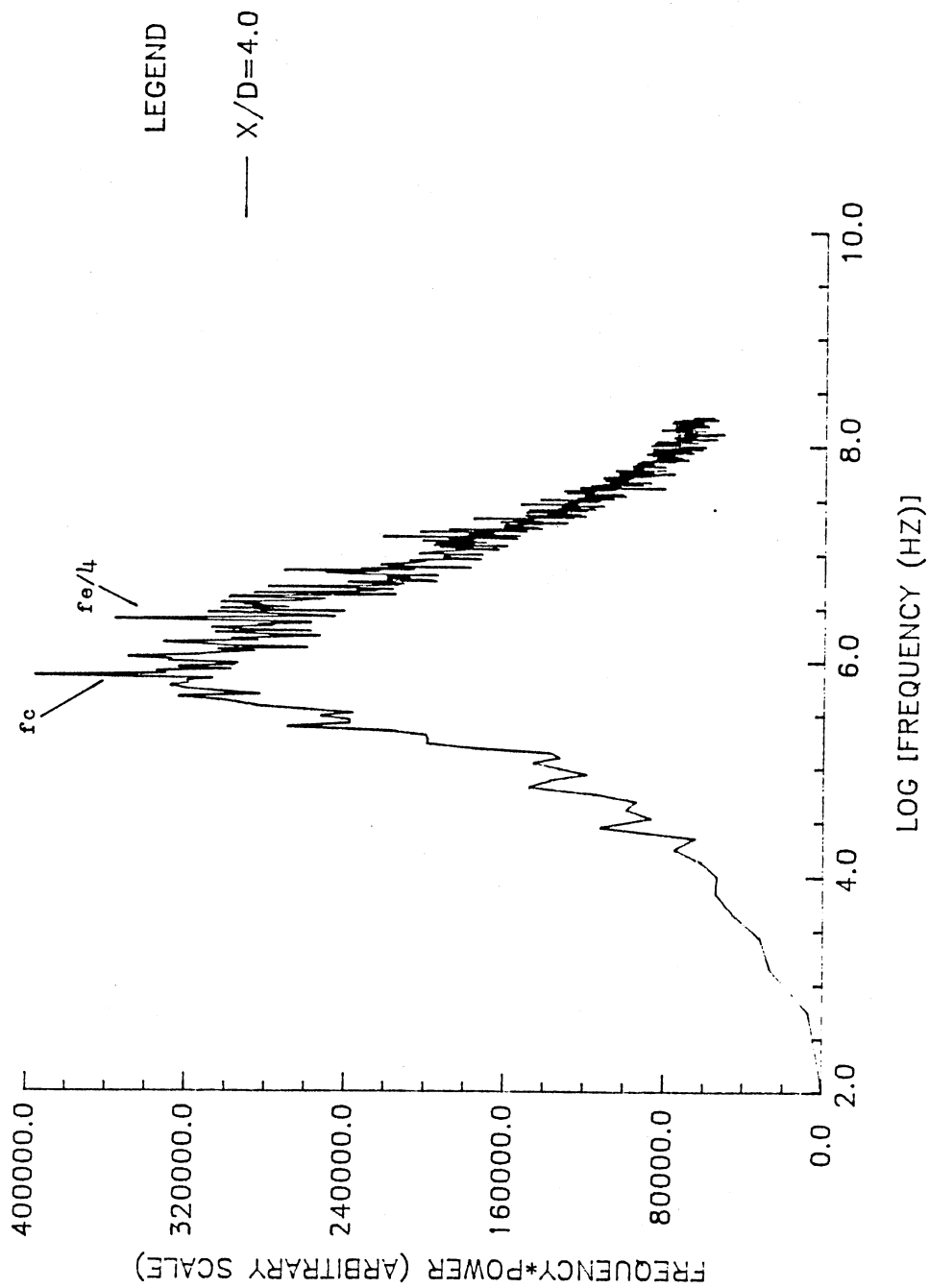


Figure 41. Transformed Excited Power Spectra
at $x/D = 4.0$ ($f_e = 2650$ Hz)

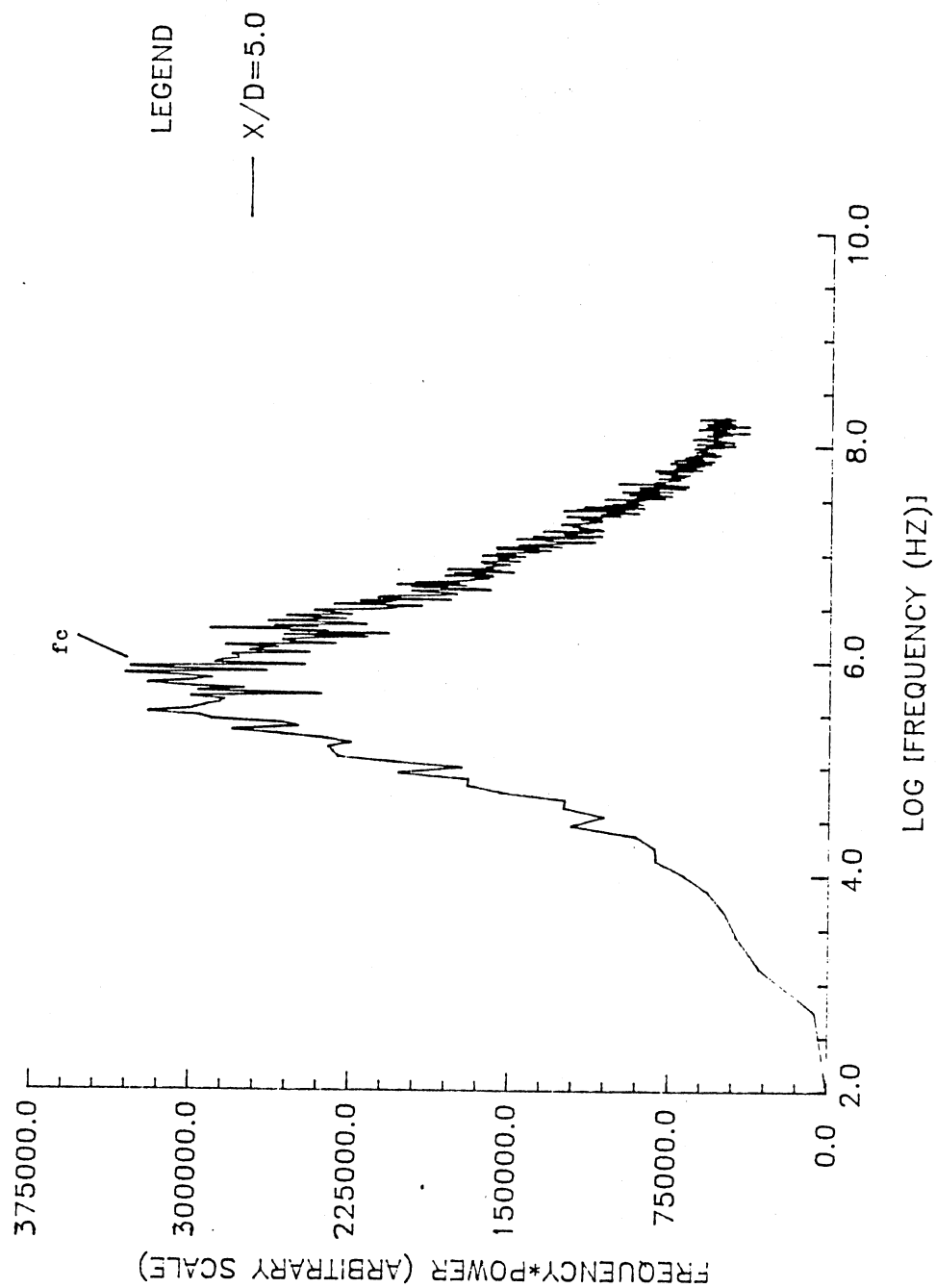


Figure 42. Transformed Excited Power Spectra
at $x/D = 5.0$ ($f_e = 2650$ Hz)

the transformed spectrum at location $x/D = 5.0$. The peaks at $f_w/4$ and f_w are still visible with a new peak showing up at $f_w/2$.

By plotting the spectral density amplitudes of the modes observed in the previously presented power spectra with downstream distance x/D , an effective picture of what is happening in the shear layer can be presented. Figure 43 presents the spectral density amplitudes versus downstream distance for modes f_w , $f_w/2$, and $f_w/4$. It can be noted from this figure that the growth of the fundamental mode is linear for $x/D < 1.0$. The saturation of the fundamental occurs at $x/D = 1.0$. The saturation of the fundamental is associated with the rapid growth on the subharmonic which saturates at $x/D = 1.25$. The subharmonic growth is significantly larger than the fundamental growth beyond $x/D = 1.0$. An interesting deviation appears between x/D locations 1.5 and 1.75. The subharmonic decays while the fundamental shows a significant growth. Also present between these locations is the growth of the second subharmonic. By $x/D = 2.0$, the second subharmonic frequency is the dominant frequency. After $x/D = 1.75$ the fundamental shows dramatic reductions, while the subharmonic does not show significant decay until after $x/D = 3.0$.

Figure 44 shows the spectral amplitudes versus downstream distance for the excitation frequency and the

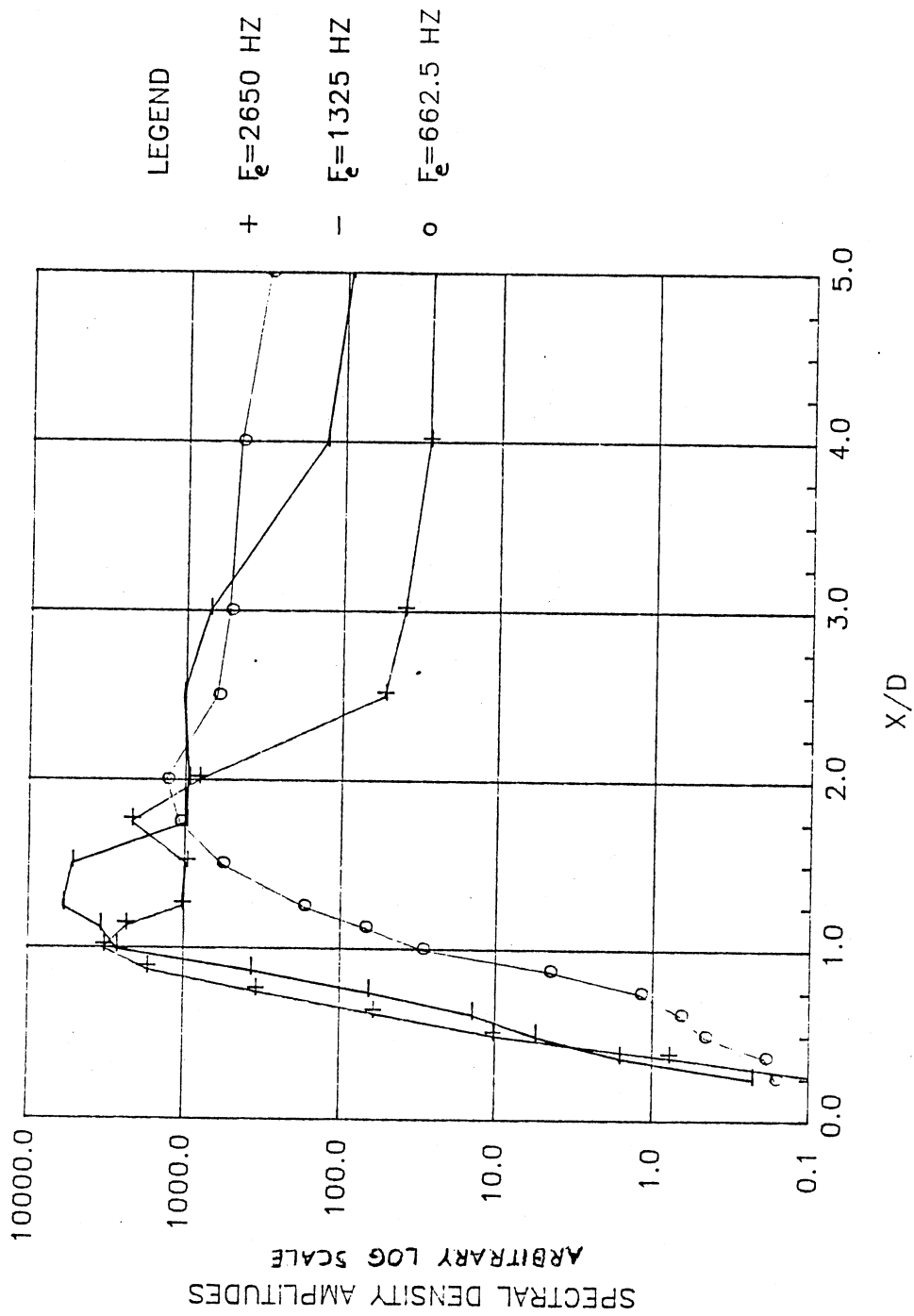


Figure 43. Spectral Amplitudes For f_e , $f_e/2$, $f_e/4$
($f_e = 2650$ Hz)

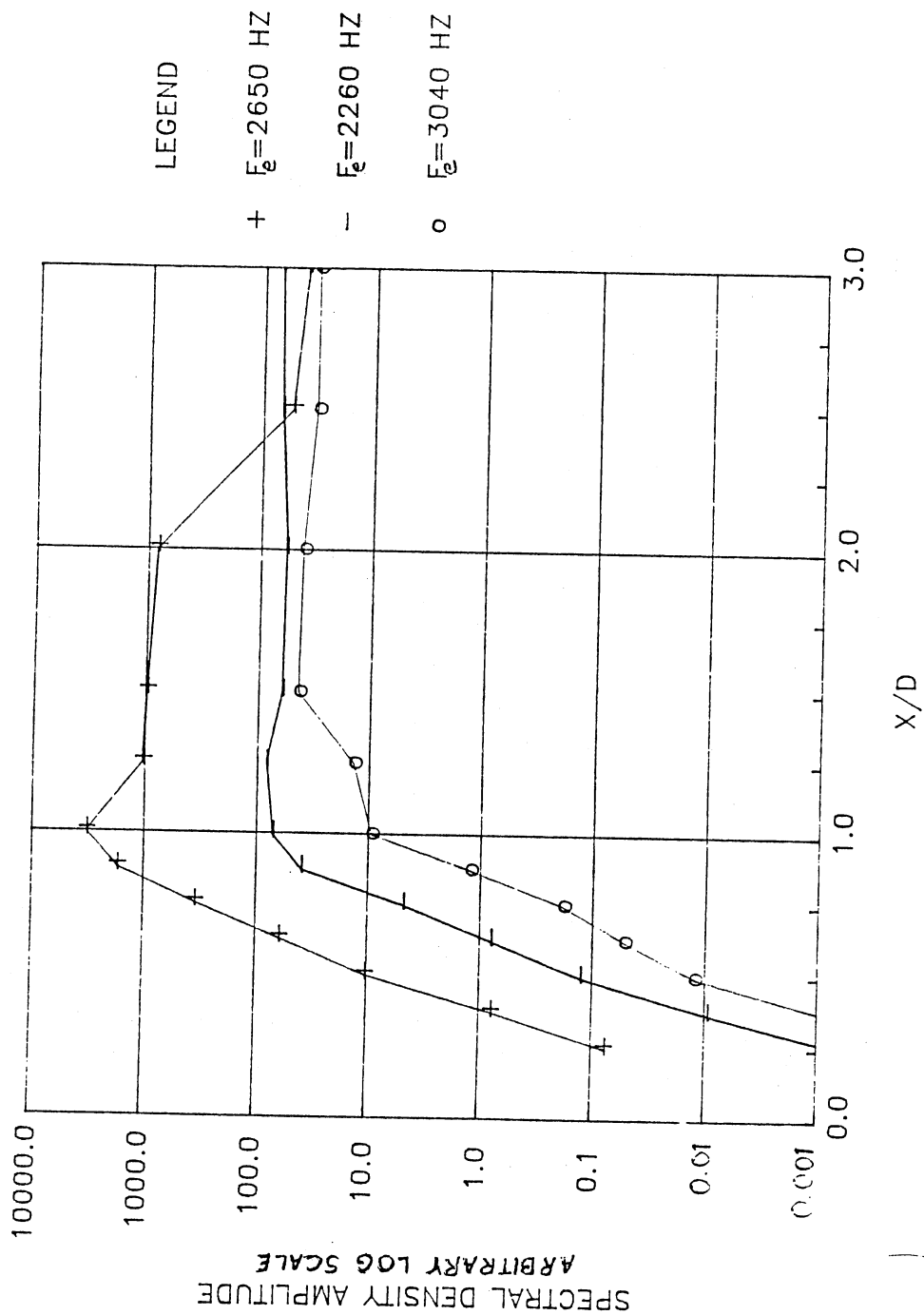


Figure 44. Spectral Amplitudes For f_e and Sidebands ($f_e = 2650$ Hz)

sidebands on either side of it ($f_{\omega} \pm f_{\omega}$). Although significantly less in the magnitude, the sidebands appear to be directly related to the excitation frequency. Both of the sidebands show linear growth at the same x/D locations as the excitation and both sidebands deviate from linear growth at the same location as the harmonic. It is interesting to note that the lower sideband is favored over the upper sideband. The only location where any deviations of the sidebands from the harmonic appear is at $x/D = 1.0$ where the upper sideband shows continued growth where the harmonic decays and at $x/D > 2.0$ where both sidebands show constant amplitudes where the fundamental decays.

Figure 45 shows the spectral amplitudes versus downstream distance for the subharmonic frequency and the sidebands on either side of it ($f_{\omega}/2 \pm f_{\omega}$). As in the fundamental and its sidebands, the subharmonic and its sidebands appear to be directly related. Similar growth is shown for $x/D < 1.0$ and growth trends continue to be present further downstream.

Information about the shear layers' influence on the centerline of jet can be found by looking at the power spectra on the jet centerline. Distinct peaks should be observable farther downstream due to lower turbulent intensities on the centerline. Figure 46 shows the centerline power spectra for $x/D = 1.0, 1.5, 2.0$, and 2.5 .

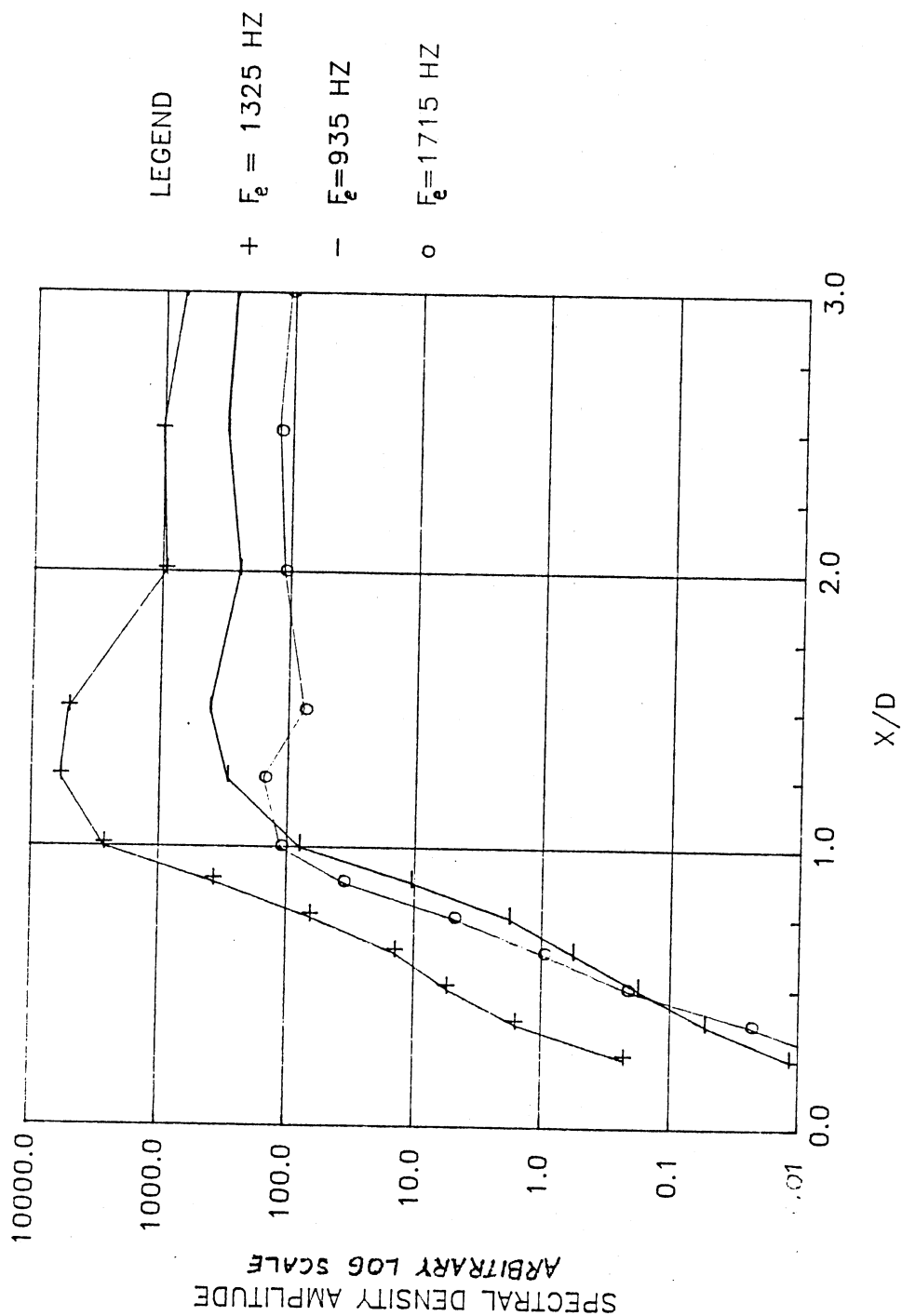


Figure 45. Spectral Amplitudes For $f_e/2$
and Sidebands ($f_e = 2650$ Hz)

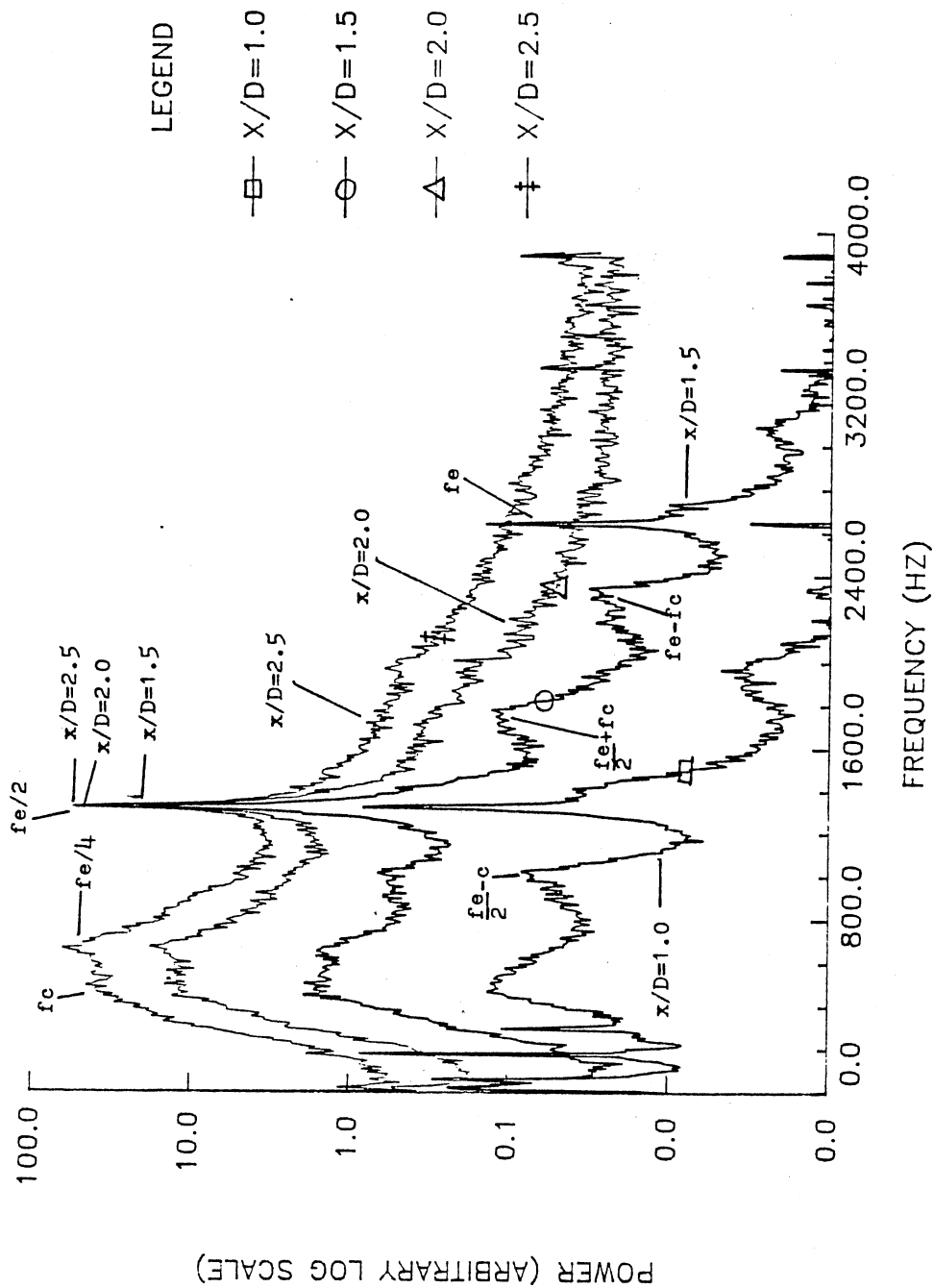


Figure 46. Comparison of the Centerline Excited Power Spectra at $x/D = 1.0, 1.5, 2.0, 2.5$ ($f_e = 2650$ Hz)

No noticeable energy shows up at locations upstream of $x/D = 1.0$. At $x/D = 1.0$, the energy levels are very low. Several modes begin to appear at this point. A very thin, almost nonexistent peak appears at the excitation frequency. The dominant peak in the spectrum appears at the subharmonic frequency $f_{sc}/2$. Other observable peaks are at the jet column mode f_{sc} and a peak forming at $(f_{sc} - 2f_{sc})/2$. By $x/D = 1.5$, all the peaks have grown considerably. The fundamental, although still low in energy, is now observable. The subharmonic is still the dominant peak in the spectrum. New modes are observable at locations $(f_{sc} + 2f_{sc})/2$ and $f_{sc} - f_{sc}$. All of these modes were observable in the shear layer spectra at higher amplitudes. This suggests the peaks observed on the centerline reflect the presence of the shear layer modes.

At $x/D = 2.0$ there are only two modes present. All of the energy at the higher end of the spectrum has now been shifted to the lower end. The only modes observable are the subharmonic frequency and at a frequency $f_{sc}/4$. The only change at $x/D = 2.5$ is that the modes grow. Figure 47 shows the centerline power spectra at $x/D = 3.0$ and 4.0 . The majority of the energy is showing up in between the modes f_{sc} and $f_{sc}/4$. The subharmonic frequency is still a visible mode, although it has diminished in energy. At location $x/D = 4.0$ the only mode present is the jet column mode. This signifies the end of the potential core and

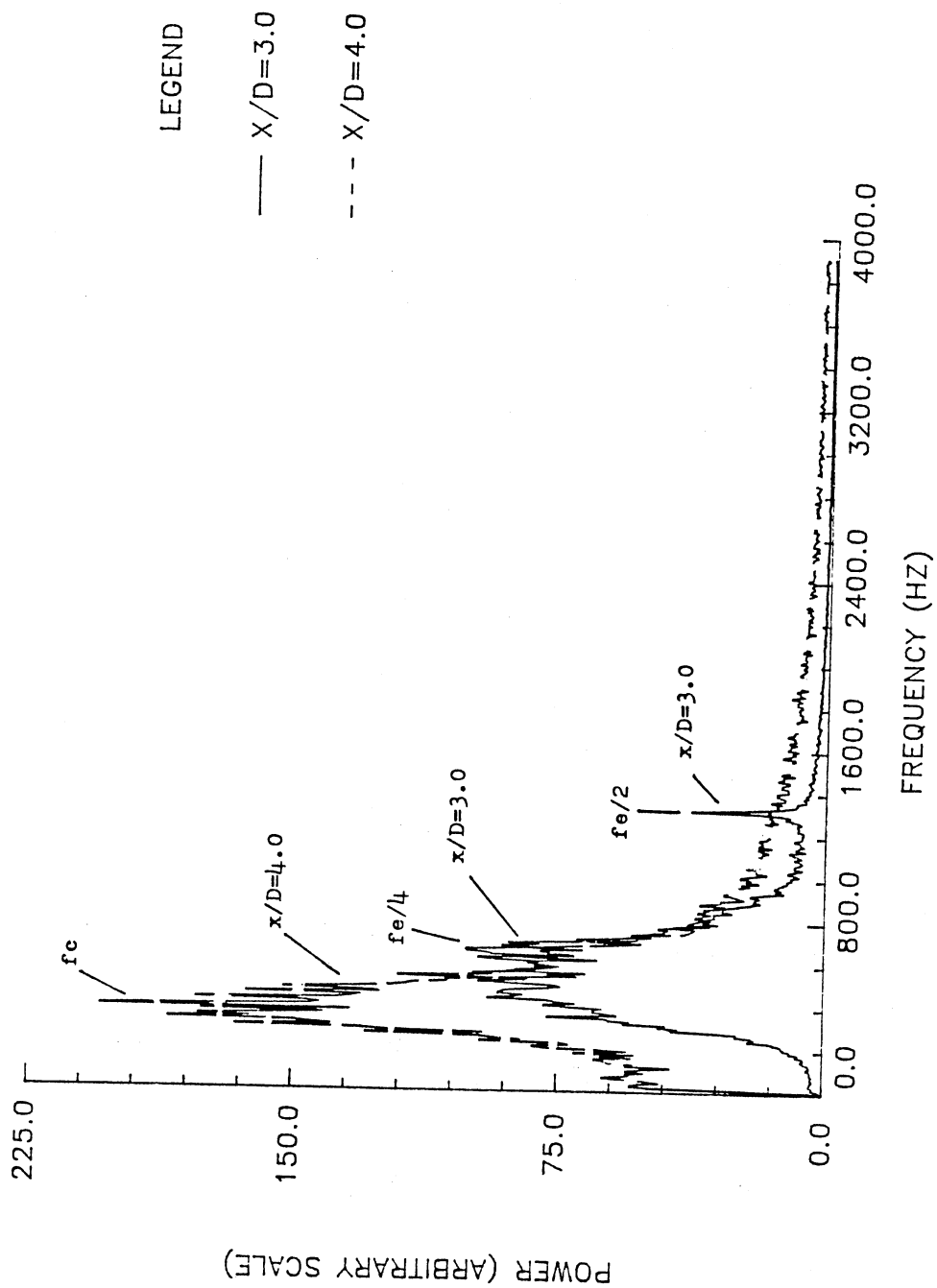


Figure 47. Centerline Excited Power Spectra at $x/D = 3.0, 4.0$ ($f_e = 2650$ Hz)

shows the passage frequency of the large vortical structures. Figure 48 is the transformed (equation 3.20) centerline spectrum at location $x/D = 5.0$. The jet column mode is again the dominant mode showing growth over the previous x/D location. Figure 49 shows the transformed centerline power spectrum at $x/D = 7.5$. The jet column mode is still the dominant frequency, but the remaining energy in the flow has shifted to lower frequencies. We will now look at the power spectrum for what is referred to as an "untuned" jet. An untuned jet is obtained by exciting the jet at a frequency that is not a multiple of the jet column mode. For the case just examined $f_{exc}/8 = 331$ Hz which is close to the jet column mode $f_c = 390$ Hz. If the jet is excited at an arbitrary frequency of $f_{exc} = 2200$ Hz, the multiples of the excitation frequency will be $f_{exc}/4 = 550$ Hz and $f_{exc}/8 = 275$ Hz, neither close to the jet column mode frequency. In the next section the way the jet responds to this untuned case will be examined.

3.2.3 Spectral Development at $f_{exc} = 2200$ Hz

Exciting the jet at a frequency that is not a multiple of the jet column mode ($f_c = 390$ Hz) gives a different exit flow field. The power spectrum measurement technique is applied to the jet, acoustically excited at $f_{exc} = 2200$ Hz, in this section.

Figure 50 presents the power spectra for the untuned

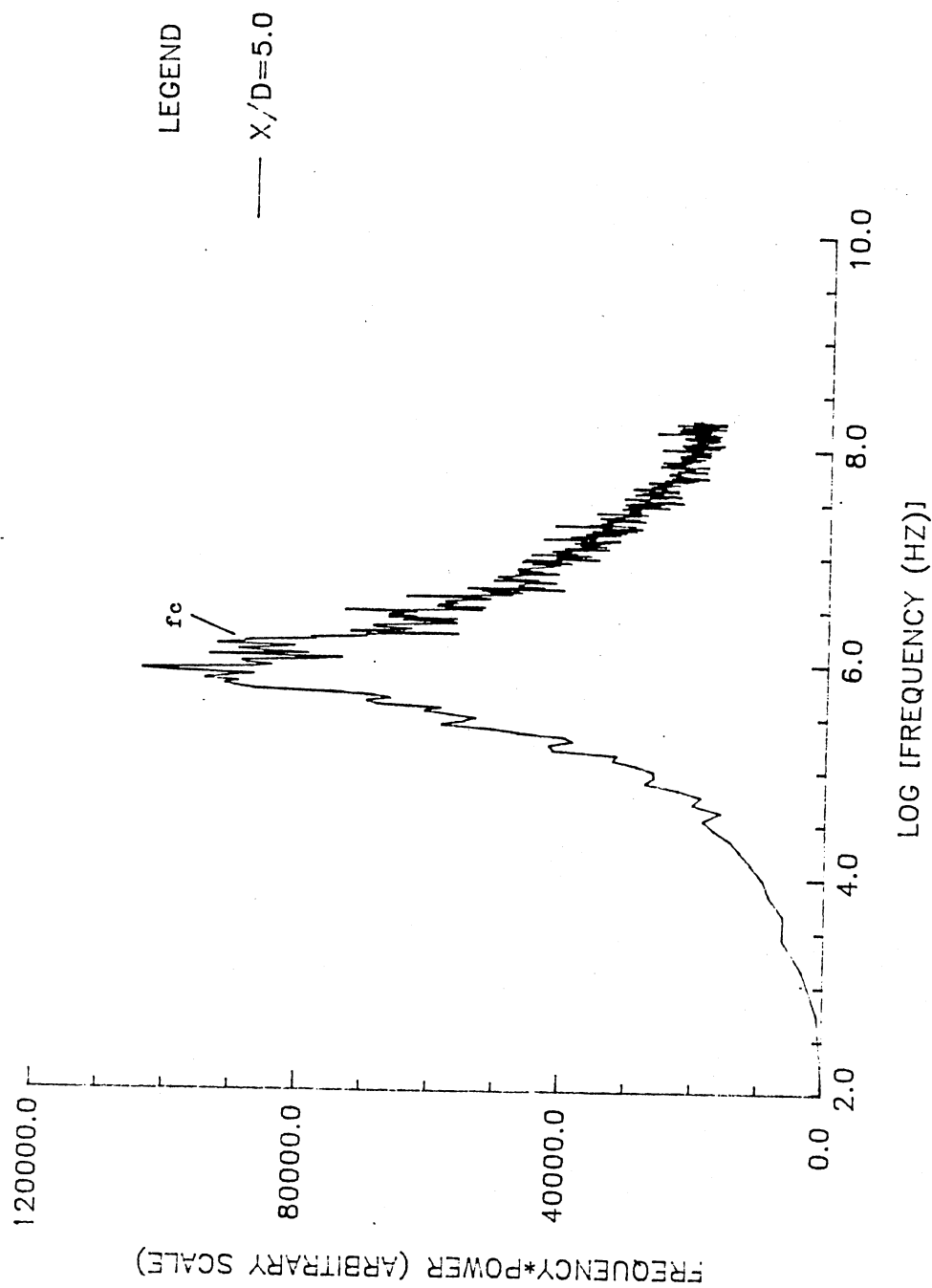


Figure 48. Transformed Excited Power Spectra
at $x/D = 5.0$ ($f_e = 2650$ Hz)

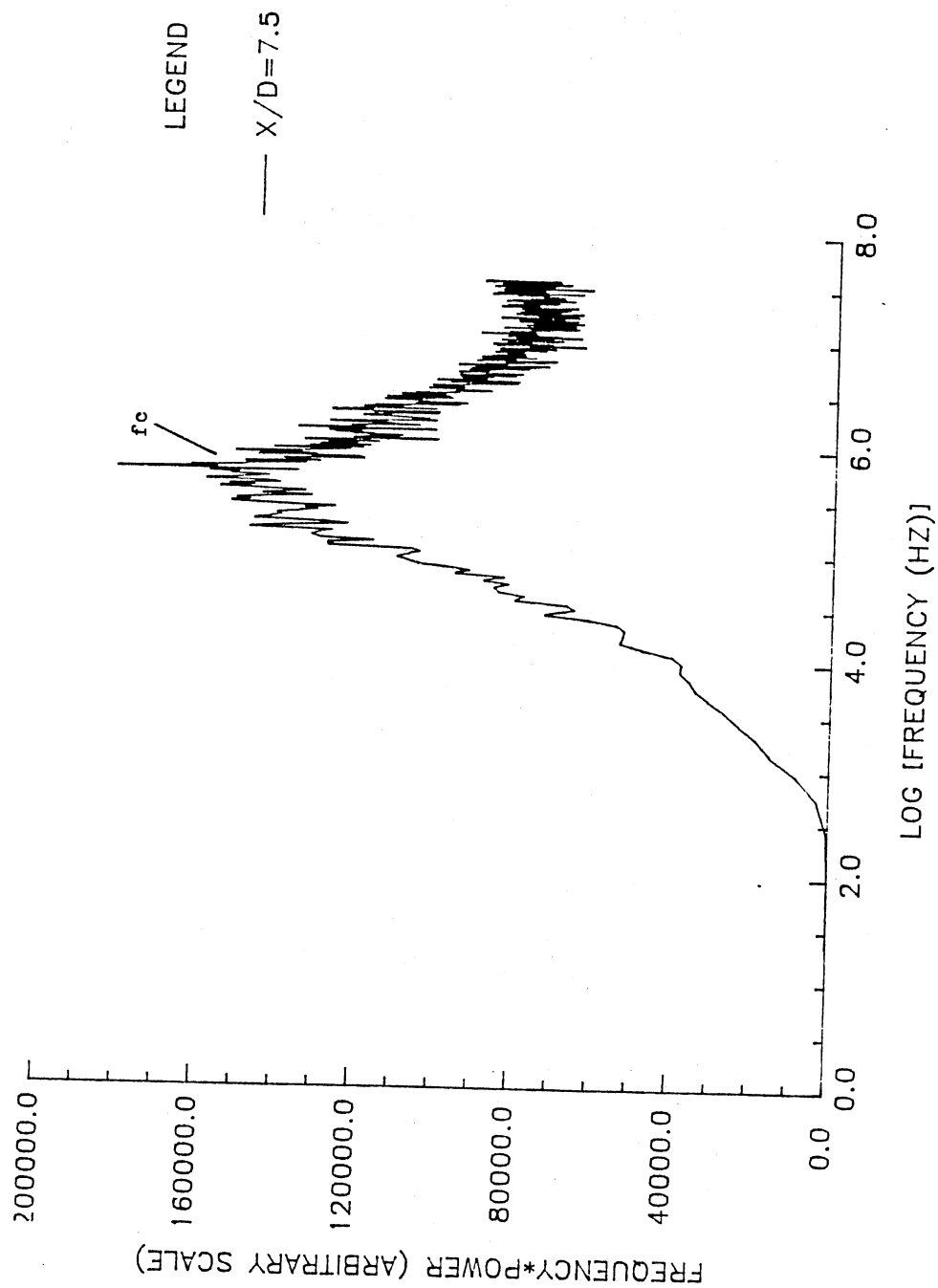


Figure 49. Transformed Centerline Excited Power Spectra
at $x/D = 7.5$ ($f_e = 2650$ Hz)

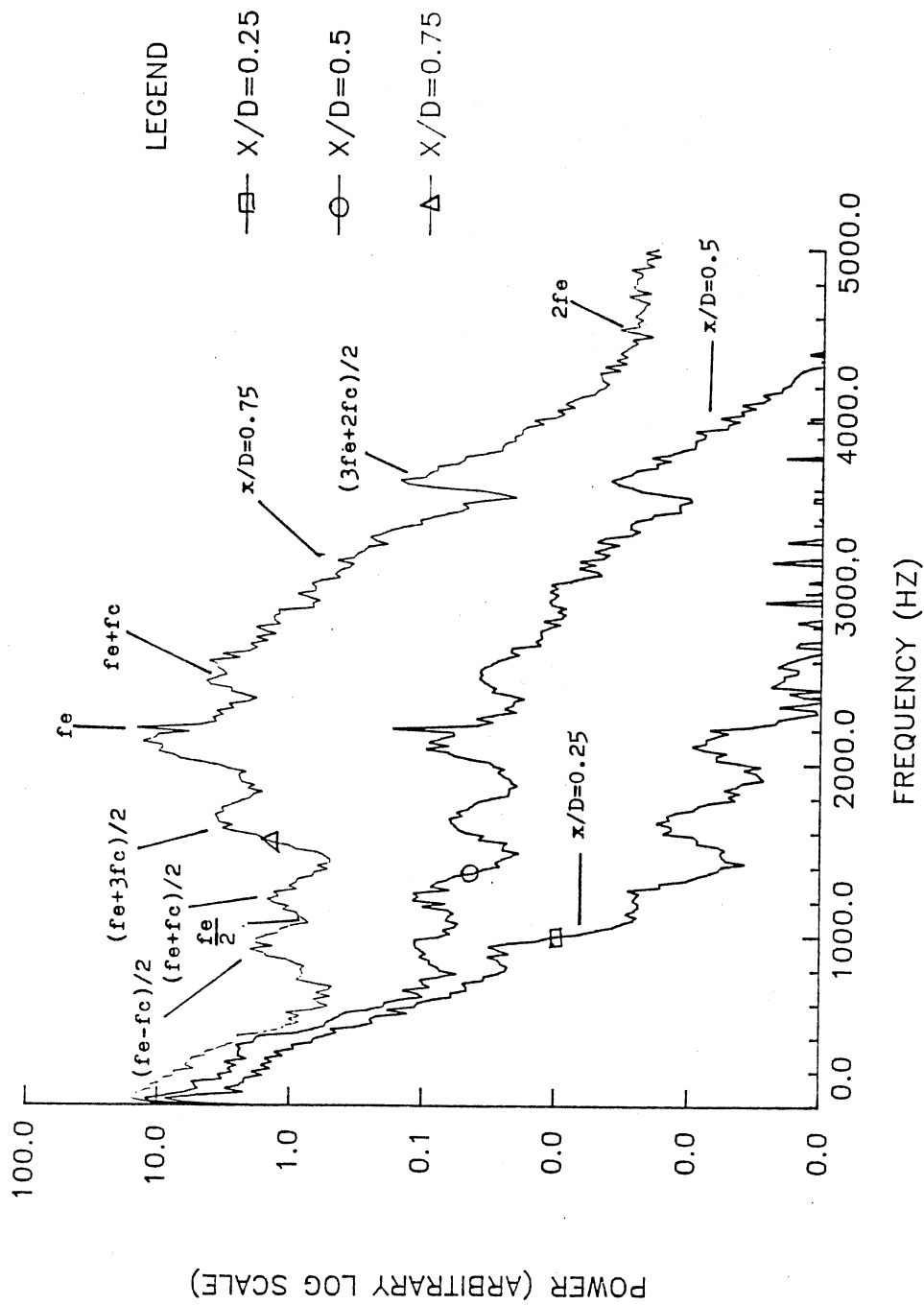


Figure 50. Comparison of the Excited Power Spectra
at $x/D = 0.25, 0.5, 0.75$ ($f_e = 2200$ Hz)

jet for locations $x/D = 0.25, 0.5, \text{ and } 0.75$. It is obvious from this figure that the untuned jet behaves differently than that of the tuned jet. The peaks observed in the power spectrum do not show the sharp concentration of energy as in the tuned case. The peaks of energy are rounded, spreading the energy over a greater frequency band. By $x/D = 0.75$ the following energy peaks are noticeable: f_{ω} , $(f_{\omega}+3f_{\omega})/2$, $(f_{\omega}-f_{\omega})/2$, $(f_{\omega}+f_{\omega})/2$, $f_{\omega}+f_{\omega}$, and $3f_{\omega}/2+f_{\omega}$. It is very interesting to note the fact that the subharmonic frequency does not show up as a peak, but instead has a peak on either side of it. Also interesting is the peak at $f = 2100 \text{ Hz}$.

Figure 51 presents the power spectra for the untuned jet for locations $x/D = 1.0, 1.25, \text{ and } 1.5$. The spectra at these locations show basically the same peaks at higher energy levels as in the previous location $x/D = 0.75$. At $x/D = 1.25$ the jet column mode f_{ω} becomes evident. New peaks are located at $2f_{\omega}-f_{\omega}/2$ and $2f_{\omega}+f_{\omega}/2$. As in the subharmonic frequency, the peaks do not occur at the harmonic but rather at either side of the harmonic. By $x/D = 1.5$ a few changes in the spectrum is noticed. The peak at $(f_{\omega}+3f_{\omega})/2$ is no longer present and the two peaks located on either side of the subharmonic are not as pronounced as in previous locations.

The power spectra for $x/D = 2.0 \text{ and } 2.5$ are shown in Figure 52. At $x/D = 2.0$ only two peaks are noticeable. A

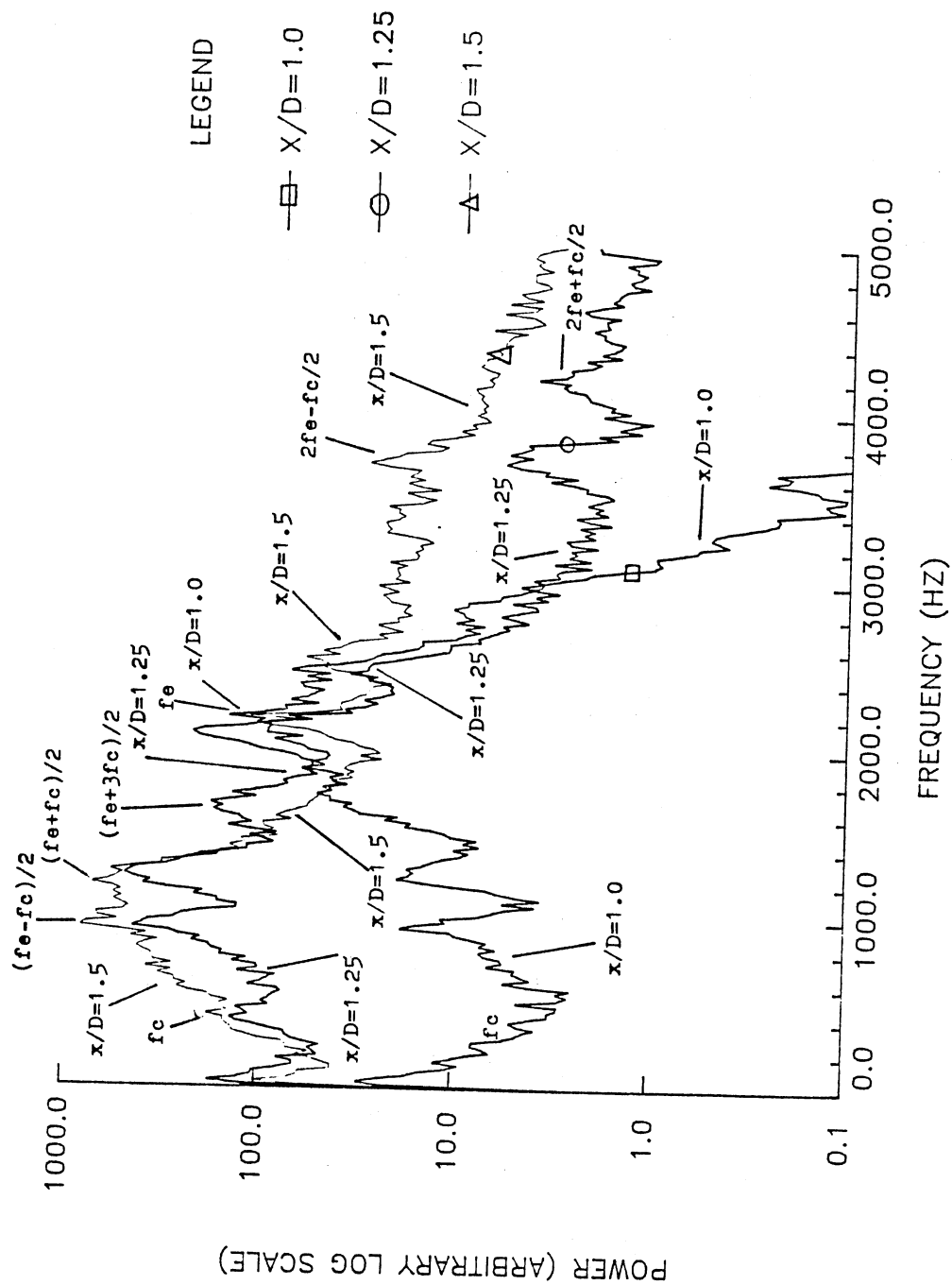


Figure 51. Comparison of the Excited Power Spectra
 at $x/D = 1.0, 1.25, 1.5$ ($f_e = 2200$ Hz)

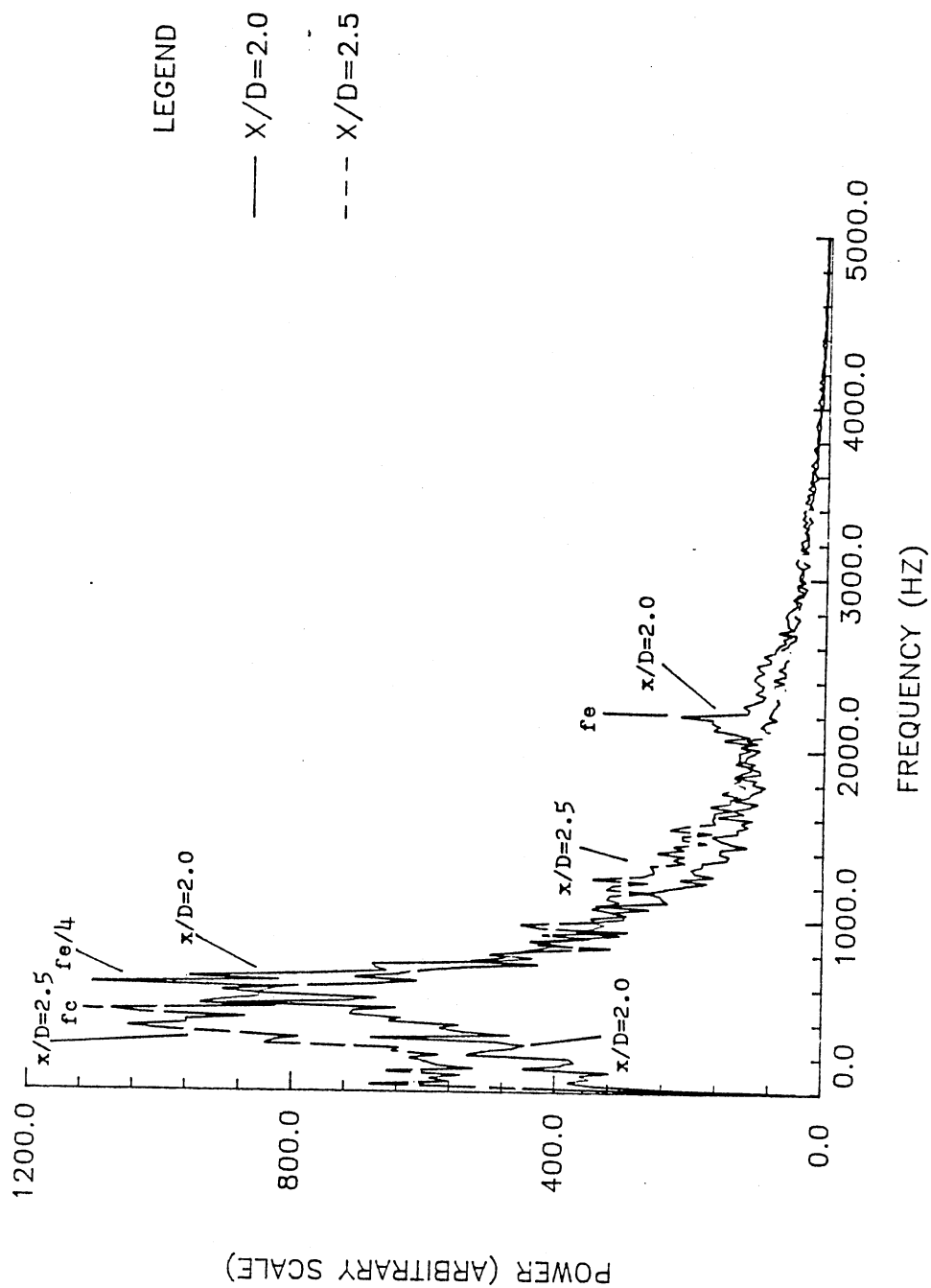


Figure 52. Comparison of the Excited Power Spectra
at $x/D = 2.0, 2.5$ ($f_e = 2200$ Hz)

low energy peak exists at the excitation frequency. Most of the energy in the shear layer is located in a peak centered at $f_{sw}/4$. By $x/D = 2.5$ the only peak present is the peak at the jet column mode f_{sc} . The transformed power spectrum (equation 3.20) for $x/D = 3.0$ is shown in Figure 53. The dominant peak at this location is shown to be the jet column mode.

The power spectra for the untuned jet have shown a different distribution of the energy in the shear layer than that of the tuned jet. The difference is due to the jet redistributing the energy in the shear layer to allow efficient passage at the end of the potential core.

Figure 54 shows the spectral density amplitudes versus downstream distance for the fundamental, subharmonic, and the two modes on either side of the subharmonic $(f_{sw} \pm f_{sc})/2$. The fundamental frequency shows linear growth for $x/D < 1.0$, with saturation occurring at $x/D = 1.0$. Even though the sidebands of the subharmonic frequency are greater in amplitude than the subharmonic itself, the sidebands seem to be directly related to the subharmonic. Growth patterns are consistent for the subharmonic and its sidebands throughout the entire range of x/D locations.

In the next section digital complex demodulation measurements will be presented.

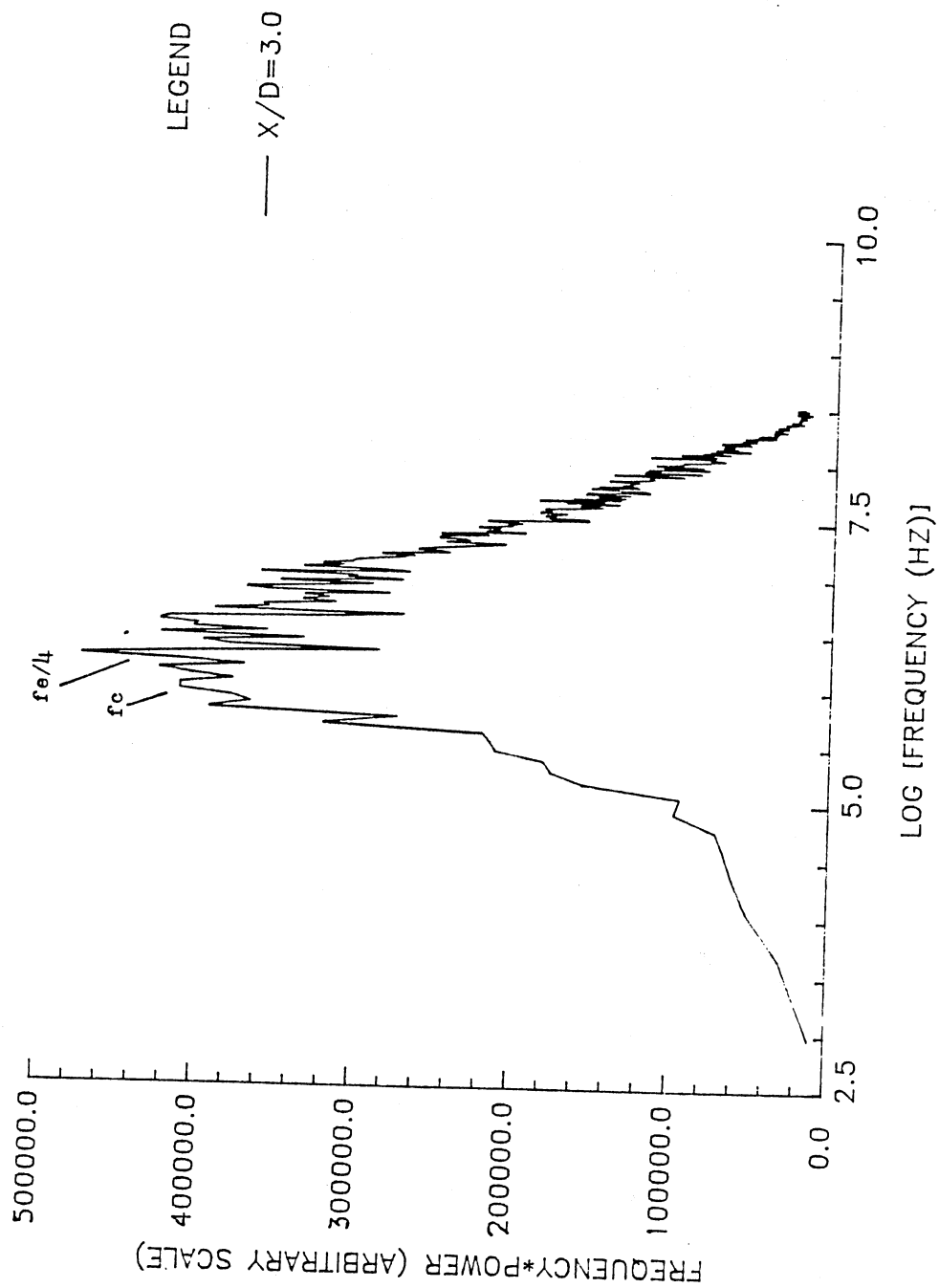


Figure 53. Transformed Excited Power Spectra
at $x/D = 3.0$ ($f_e = 2200$ Hz)

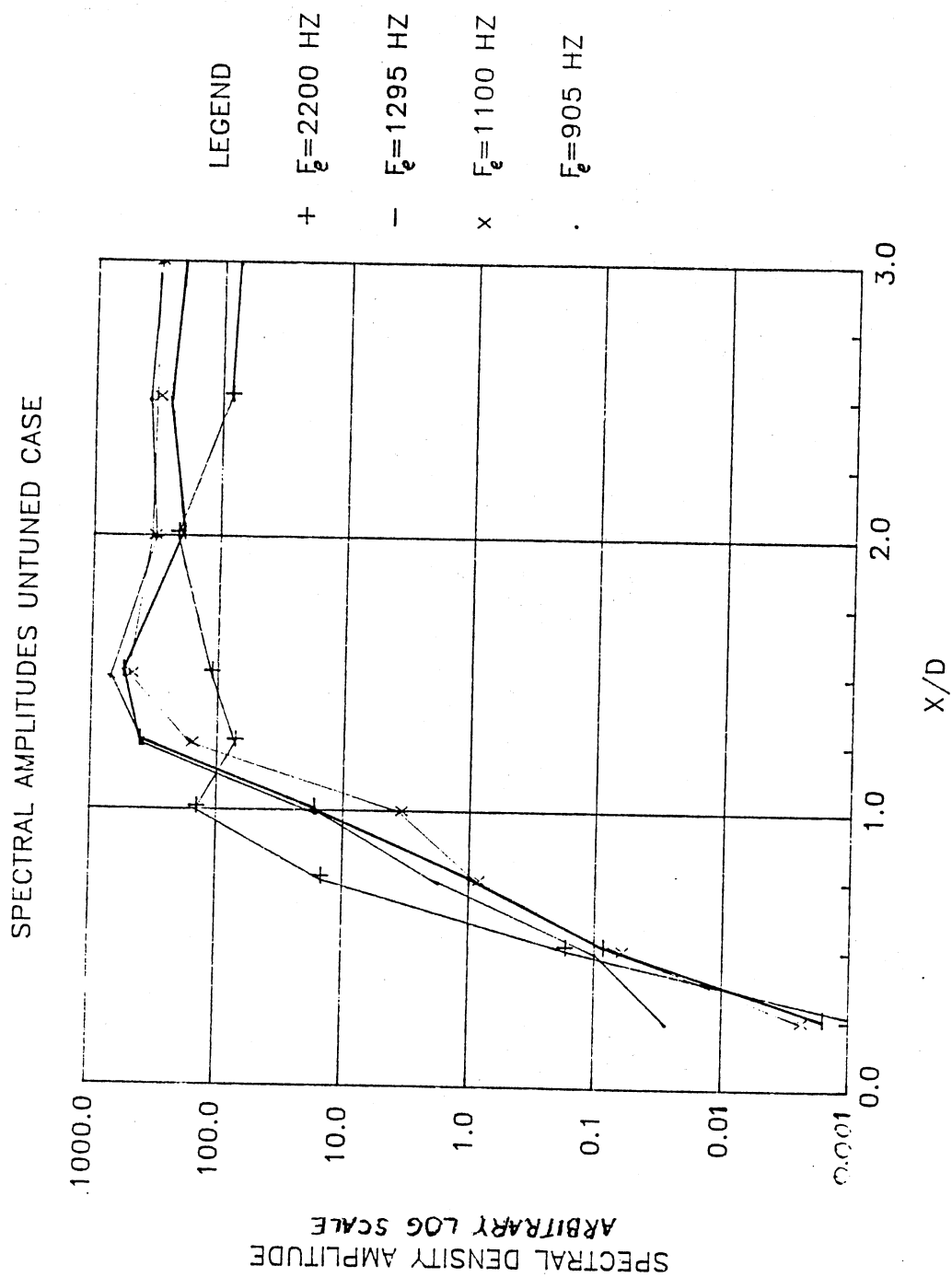


Figure 54. Spectral Amplitudes For f_e , $f_e/2$, and Sidebands ($f_e = 2200$ Hz)

3.3 Digital Complex Demodulation

Complex demodulation enables the experimentalist to obtain quantitative measurements of the amplitude and phase modulation characteristics of unsteady flow. Background and theory will be presented before the measurements are presented.

3.3.1 Digital Complex Demodulation

Techniques

The presence of wave modulation is easy to detect in power spectra measurements since a modulated wave is portrayed in terms of its "carrier wave" and upper and lower sidebands. However the power spectra give little to no information on whether the carrier wave is amplitude modulated, phase modulated, or both. Digital complex demodulation technique enables one to directly recover both the time traces of amplitude and phase modulation of a carrier wave with a center frequency ω_c .

$\Phi(x, t)$ denotes the unsteady signal measured at point x . With starting point $x=0$, assume that $\Phi(t)$ is an amplitude and phase modulated wave described by the following equation

$$\begin{aligned}\Phi(t) &= a(t) \cos[\omega_c t + p(t)] \\ &= a(t)/2 \{ \exp[i\omega_c t + ip(t)] + \exp[-i\omega_c t - ip(t)] \} \quad (3.21)\end{aligned}$$

where $a(t)$, $p(t)$, and ω_c refer to amplitude modulation,

phase modulation, and carrier frequency, respectively.

Equation (3.21) is then multiplied by an exponential term $2\exp(-i\omega_d t)$, where ω_d is the demodulation frequency, to obtain

$$2\Phi(t)\exp(-i\omega_d t) = a(t)\{\exp[i(\omega_c - \omega_d)t + ip(t)] + \exp[-i(\omega_c + \omega_d)t - ip(t)]\} \quad (3.22)$$

Set $\omega_d = \omega_c$ and feed the result into a digital lowpass filter with a cut-off frequency less than $2\omega_c$. This will give the complex demodulation $c(t)$

$$c(t) = a(t)\exp[ip(t)] \quad (3.23)$$

Since $c(t)$ is a complex number expressed as $c_r(t)$ and $c_i(t)$ the instantaneous amplitude and phase modulation are found by computing

$$a(t) = [c_r^2(t) + c_i^2(t)]^{1/2} \quad (3.24)$$

$$p(t) = \tan^{-1}[c_i(t)/c_r(t)] \quad (3.25)$$

From computer-generated values of the instantaneous amplitude and phase modulation we can determine the degree of modulation by computing the modulation indices

$$\alpha = \langle (a - \langle a \rangle)^2 \rangle^{1/2} / \langle a \rangle \quad (3.26)$$

$$\beta = \langle p^2 \rangle^{1/2} \quad (3.27)$$

where α and β denote the amplitude and phase modulation

indices respectively, and the angular bracket denotes a time average. The computer code used can be viewed in Appendix A.

3.3.2 Digital Complex Demodulation

at $f_{\text{exc}} = 2650$ Hz.

The technique discussed above is used at an excitation frequency of $f_{\text{exc}} = 2650$ Hz. The hot wire probe is placed in the shear layer at the location $U/U_{\text{free}} = 0.6$. The Nyquist frequency is $f_N = 6000$ Hz. The excitation frequency of $f_{\text{exc}} = 2650$ Hz is also the frequency of demodulation. The digital low-pass filter is set to a frequency bandwidth $\Delta f = 0.03$ and a cutoff of 35 db.

Figure 55 shows the amplitude (alpha) and phase (beta) modulation indices. These indices quantitatively measure the changes in the intensity of the amplitude and phase modulations. It can be seen from this figure that the shear layer is undergoing both amplitude and phase modulation. Even though both amplitude and phase modulation exist, phase modulation is clearly dominant. It has been shown by researchers such as Miksad, et al. (1982) that phase modulation is preferred when nonlinear interactions are occurring. This is due to the more efficient spectral-energy redistribution properties of phase-modulated waves. The ratio of the two indices can be viewed in Figure 56. The near exit region of the jet

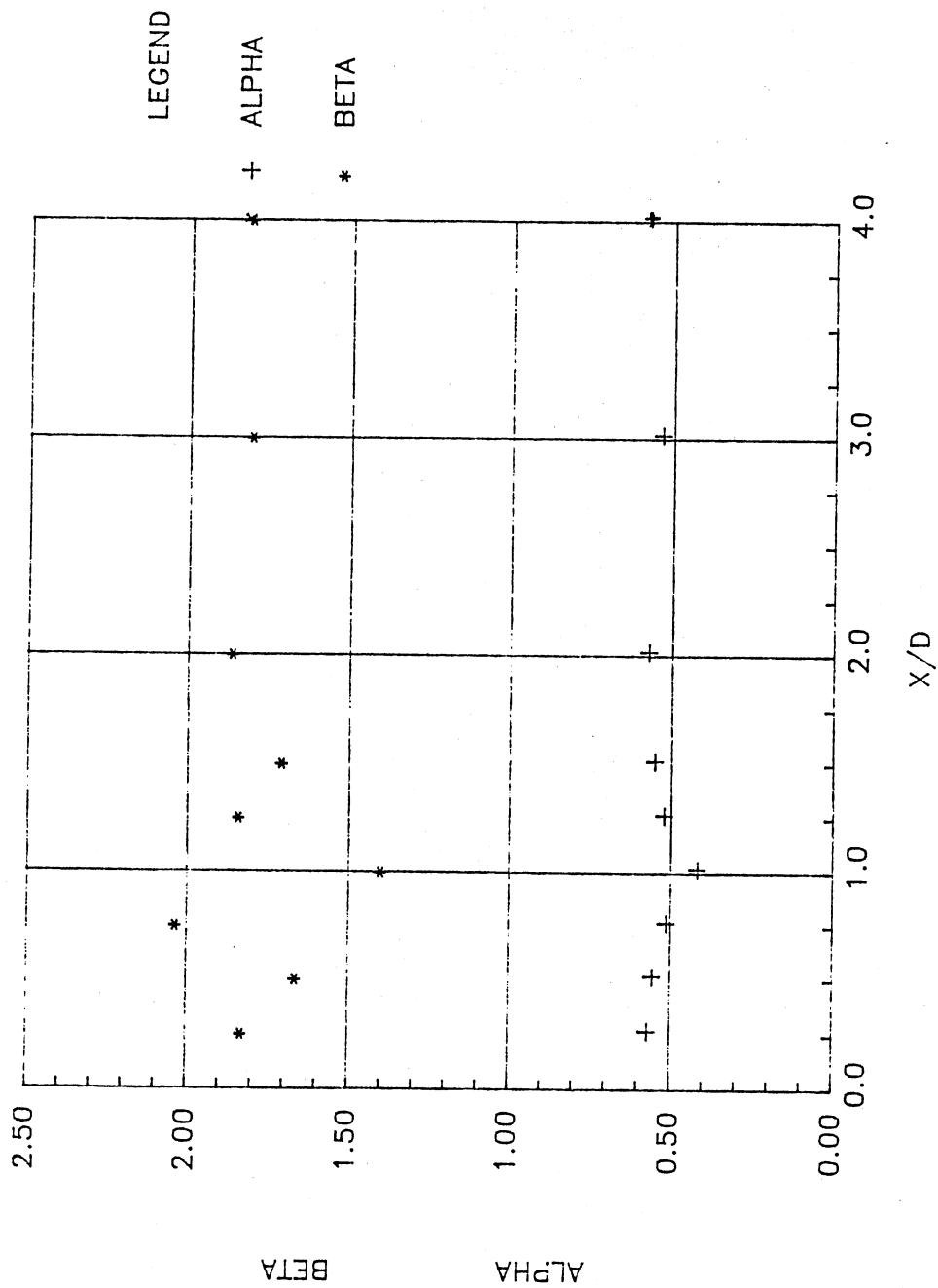


Figure 55. Alpha and Beta Modulation Indices
($f_e = 2650$ Hz)

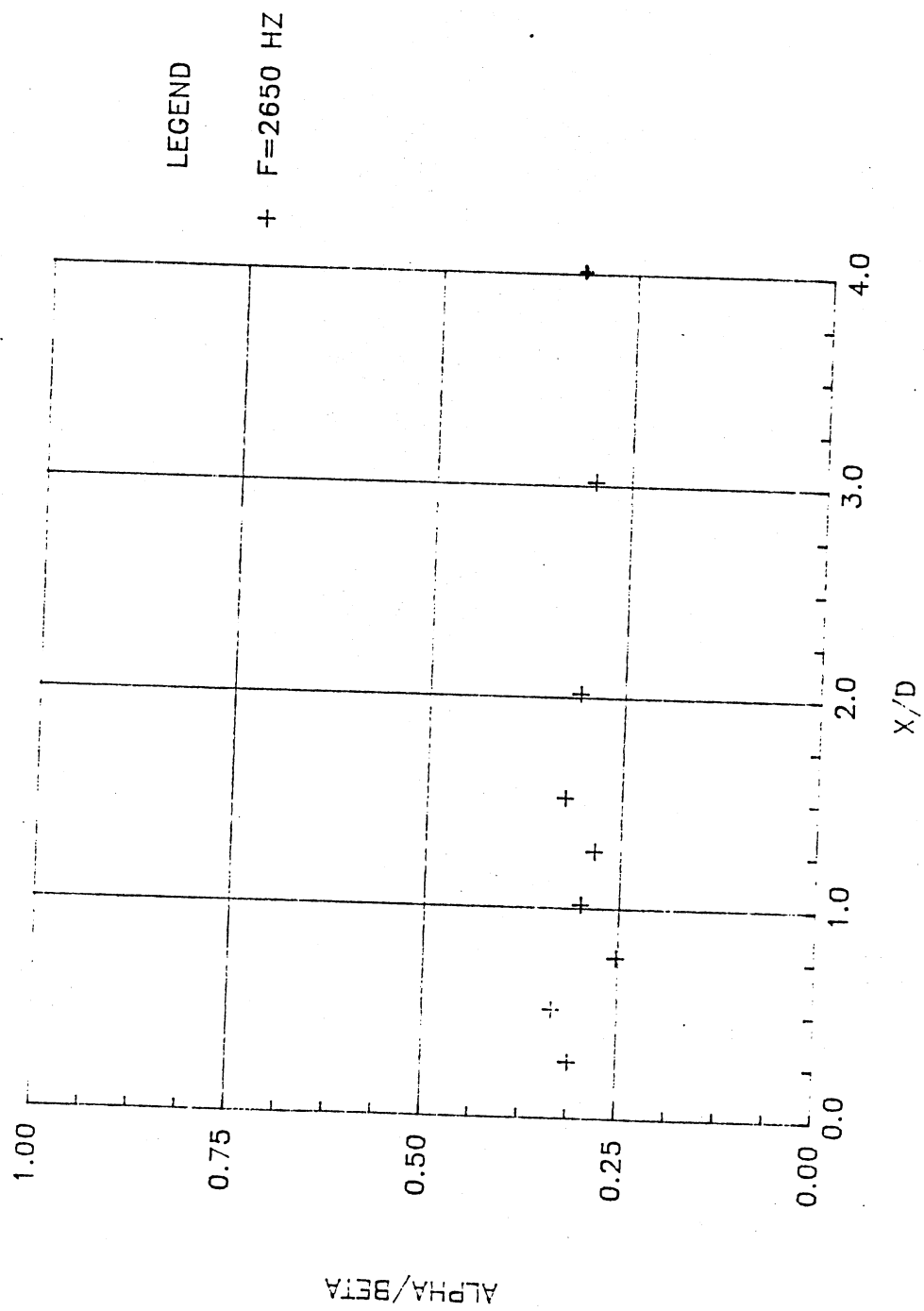


Figure 56. Alpha/Beta Modulations ($f_e = 2650$ Hz)

$(x/D < 2.0)$ shows deviations due to the fact that the phase modulation index (β) is varying with downstream distance while the amplitude modulation index remains relatively constant. The drop of the ratio at $x/D = 1.0$ is interesting. At this point the phase modulation increased significantly. This could be attributed to the fact that the fundamental frequency saturates at this location. At $x/D > 2.0$ locations, the amplitude and phase modulations seem to have become constant.

3.3.3 Digital Complex Demodulation

at $f_m = 2200$ Hz

The jet is now excited at an excitation frequency of $f_m = 2200$ Hz. This frequency is also the frequency of demodulation. The digital filter setting remains the same. Figure 57 shows the amplitude and phase modulations indices. As in the tuned jet, the phase modulation is the dominant modulation. Both indices remain relatively constant throughout downstream distances. Figure 58 shows the ratio of the two modulation indices. At $x/D = 1.0$ the ratio of the two indices drops comparably to that in the tuned jet.

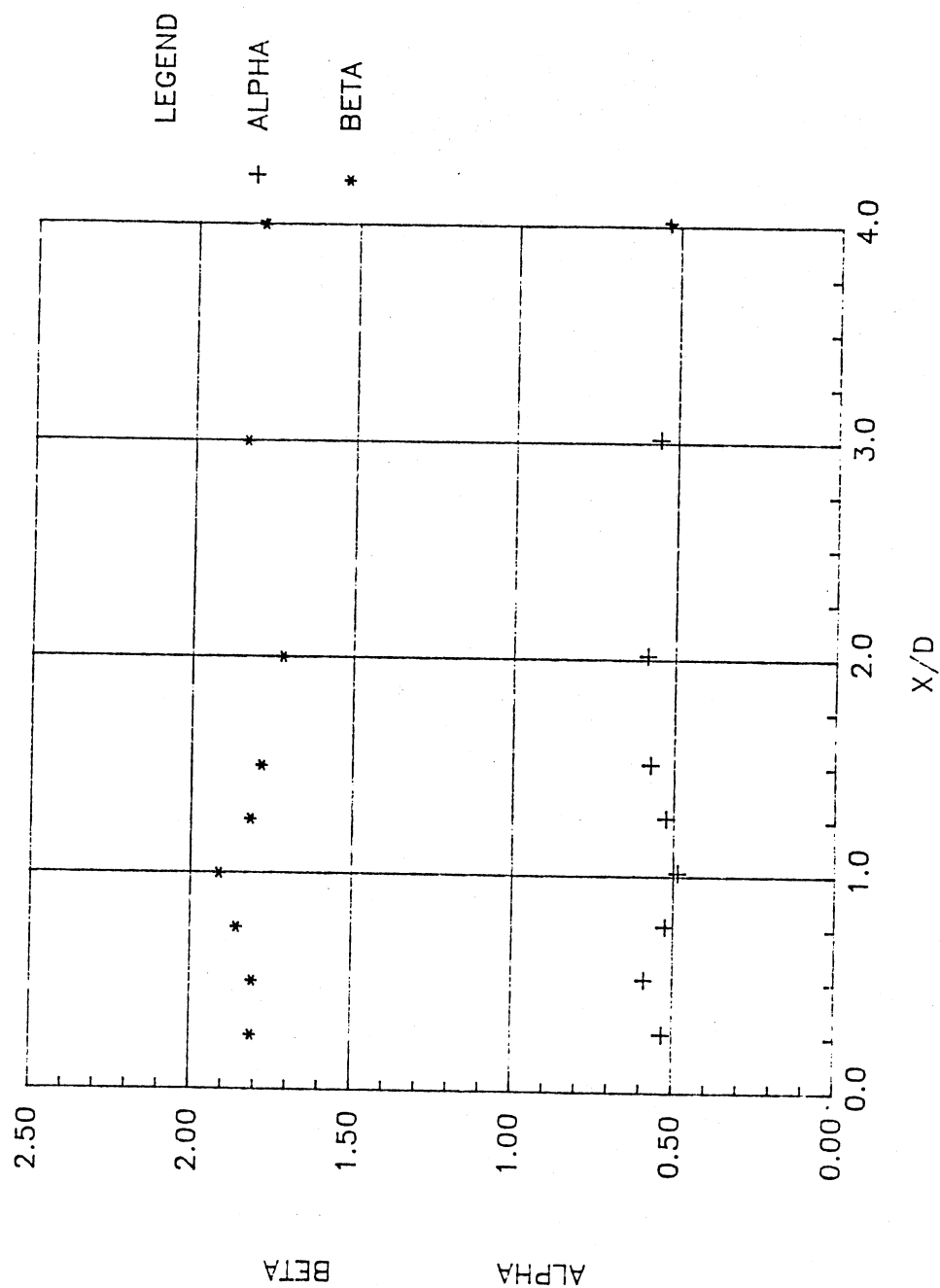


Figure 57. Alpha and Beta Modulation Indices
($f_e = 2200$ Hz)

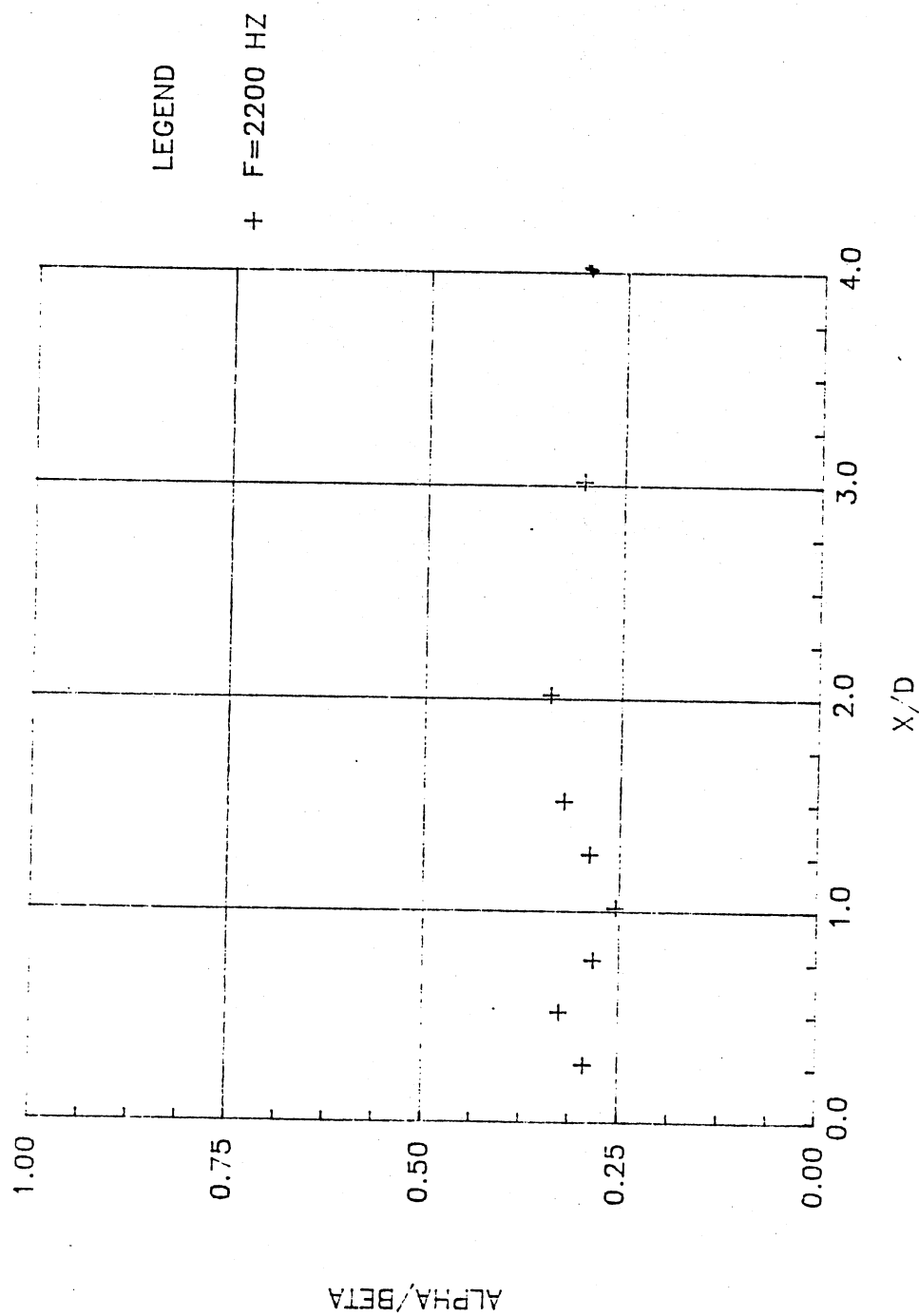


Figure 58. Alpha/Beta Modulations ($f_e = 2200$ Hz)

The power spectrum and demodulation techniques are useful tools for looking at the energy distributions in the flow field. However, neither provides information on the interactions between the modes observed. The bicoherence spectrum is used to determine whether the waves are coupled nonlinearly or are coupled linearly. The next section will provide information regarding the nonlinear interactions in the developing jet flow via use of this bicoherence spectrum.

3.4 Bicoherence Spectra Measurements

This section presents bicoherence measurements documenting the nonlinear wave reactions of the jet under excited conditions ($f_{\omega} = 2650$ Hz and $f_{\omega} = 2200$ Hz). Bicoherence measurements are obtained in the shear layers for x/D locations 0.5 to 4.0. Background information on the bicoherence technique and theory is presented before the results are documented.

3.4.1 Bispectral Techniques

To distinguish between nonlinear coupled waves and linear independent waves, a higher order spectrum than the power spectrum is used. This spectrum is referred to as the bispectrum, which is a cube spectral density function. A nonzero bispectrum is indicative of nonlinear interactions between instability waves. Kim and Powers

(1979) and Kim et al. (1980) describe the bispectrum in detail. Use of the bispectrum along with the previously presented power spectrum can provide quantitative information on the nature of the nonlinear interactions invoked during transition.

Consider the longitudinal velocity fluctuation measured at a point which has a Fourier representation

$$x(t) = \sum_{k=-\infty}^{\infty} X_{k_c} e^{-i2\pi f_{k_c} t} \quad (3.28)$$

where X_{k_c} is the complex Fourier amplitude at frequency f_{k_c} defined by

$$X_{k_c} = \lim_{T \rightarrow \infty} \frac{1}{T} \int_{-T/2}^{T/2} x(t) e^{i2\pi f_{k_c} t} dt \quad (3.29)$$

where T is the total record length of $x(t)$. The degree to which frequencies f_i and f_j are coupled to wave f_{k_c} can be determined by the bispectrum. The bicoherence spectrum is the normalized version of the bispectrum and is defined by Kim and Powers (1979) as

$$b^2(i, j) = \frac{|B(i, j)|^2}{E[|X_i X_j|^2] E[|X_{i+j}|^2]} \quad (3.30)$$

where $E[\]$ denotes an expected value, i and j are integers representing the frequencies $f_i = (i-1)\Delta f$ and $f_j = (j-1)\Delta f$ (Δf represents the frequency resolution), and $B(i, j)$ is

the discrete bispectrum defined as

$$B(i, j) = E[X_i X_j X_{i+j}^*] \quad (3.31)$$

The bicoherence spectrum measures the phase coherence among a wave triad. If three spectral components are nonlinearly coupled, a phase coherence will exist between them. The bicoherence spectrum is bounded by $0 \leq b^2 \leq 1$. A value near 1 indicates that the wave at frequency f_k is nonlinearly coupled with waves f_i and f_j . A value near zero indicates a lack of phase coherence between the waves suggesting f_k is a linearly independent wave not related to waves f_i and f_j .

The bicoherence spectrum is plotted only in the triangular region of the f_i, f_j which is defined as follows: $0 \leq f_i \leq f_N/2$, $f_i \leq f_j \leq f_N/2 - f_i$, where f_N is the Nyquist frequency. Each bicoherence plot shows lines of constant frequency $f_k = f_i + f_j$. A schematic of the bicoherence plot is shown in Figure 59. Values along these lines can be interpreted as nonlinear interactions between different pairs of instabilities with a sum frequency equal to f_k . However, due to the symmetry properties of the bispectrum, difference-mode interaction of the form $f_k - f_i = f_j$ and $f_k - f_j = f_i$ are also mapped into the $b^2(i, j)$ interaction. To determine which of the three possible interactions is taking place, the corresponding power spectrum should be referenced. The computer program

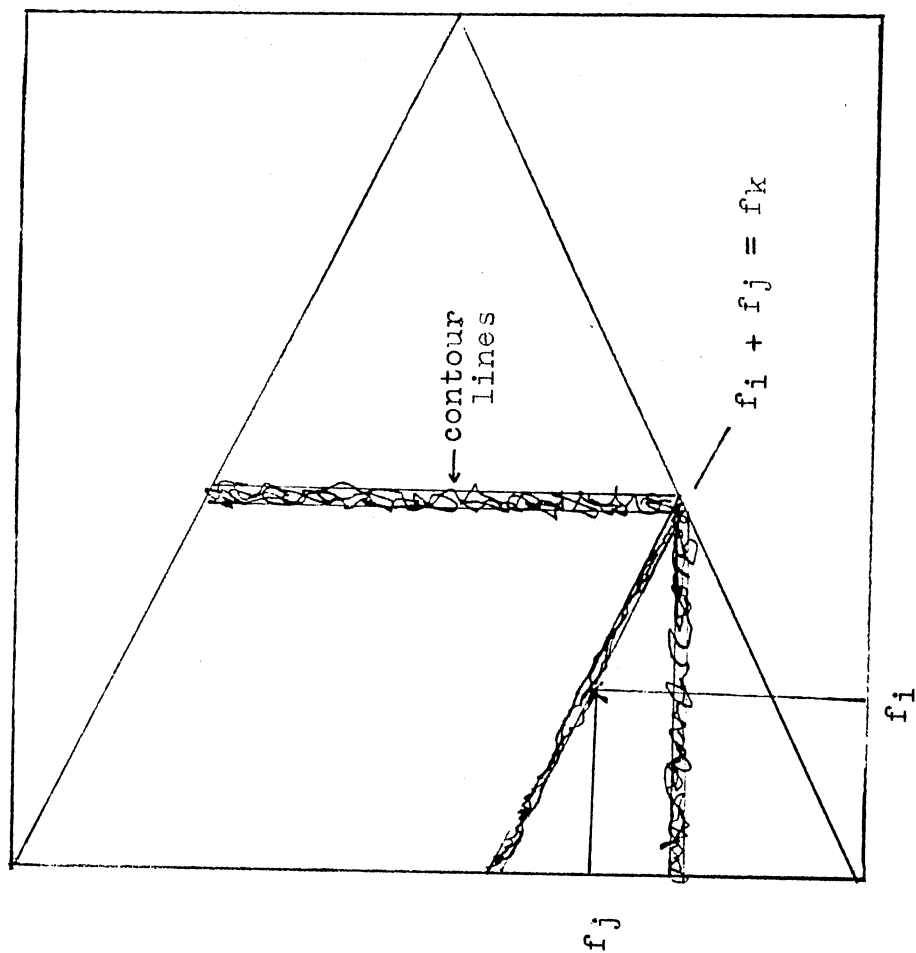


Figure 59. Eicoherence Schematic

used to take the bicoherence measurements can be viewed in Appendix A.

3.4.2 Bicoherence measurements

at $f_w = 2650$ Hz.

Bicoherence measurements are taken at locations $x/D = 0.5$ to 4.0 in the shear layer where $U/U_{free} = 0.6$. Measurements are also taken on the jet centerline at locations $x/D = 4.0$ to 10.0 . The excitation frequency for each measurement is $f_w = 2650$ Hz. The Nyquist frequency for each case is $f_N = 6000$ Hz. Figure 60 shows the bicoherence measurement at location $x/D = 0.5$. The major peak in the plot occurs at $b^2(f_w/2, f_w/2) = 0.729$. This peak represents the subharmonic production through a nonlinear interaction of the form $f_w - f_w/2 \rightarrow f_w/2$. The symbol " \rightarrow " is to be read "undergo nonlinear interaction to yield". This peak showing complete phase coherence indicates that the spectral mode at $f_w/2$ is truly the subharmonic of the excitation frequency and not a linear independent mode. An important mode at $f_w - f_c$ is formed by the nonlinear interaction of the form $f_w - f_c \rightarrow (f_w - f_c)$. This is shown on the plot as an observable peak at $b^2(f_c, f_w - f_c) = 0.221$. Two other elevated peaks are also noticeable. The first occurs at $b^2(f_w/2 - f_c, f_w/2 + f_c) = 0.261$. This corresponds to the nonlinear interaction of the form $f_w - (f_w/2 - f_c) \rightarrow (f_w/2 + f_c)$. This interaction shows

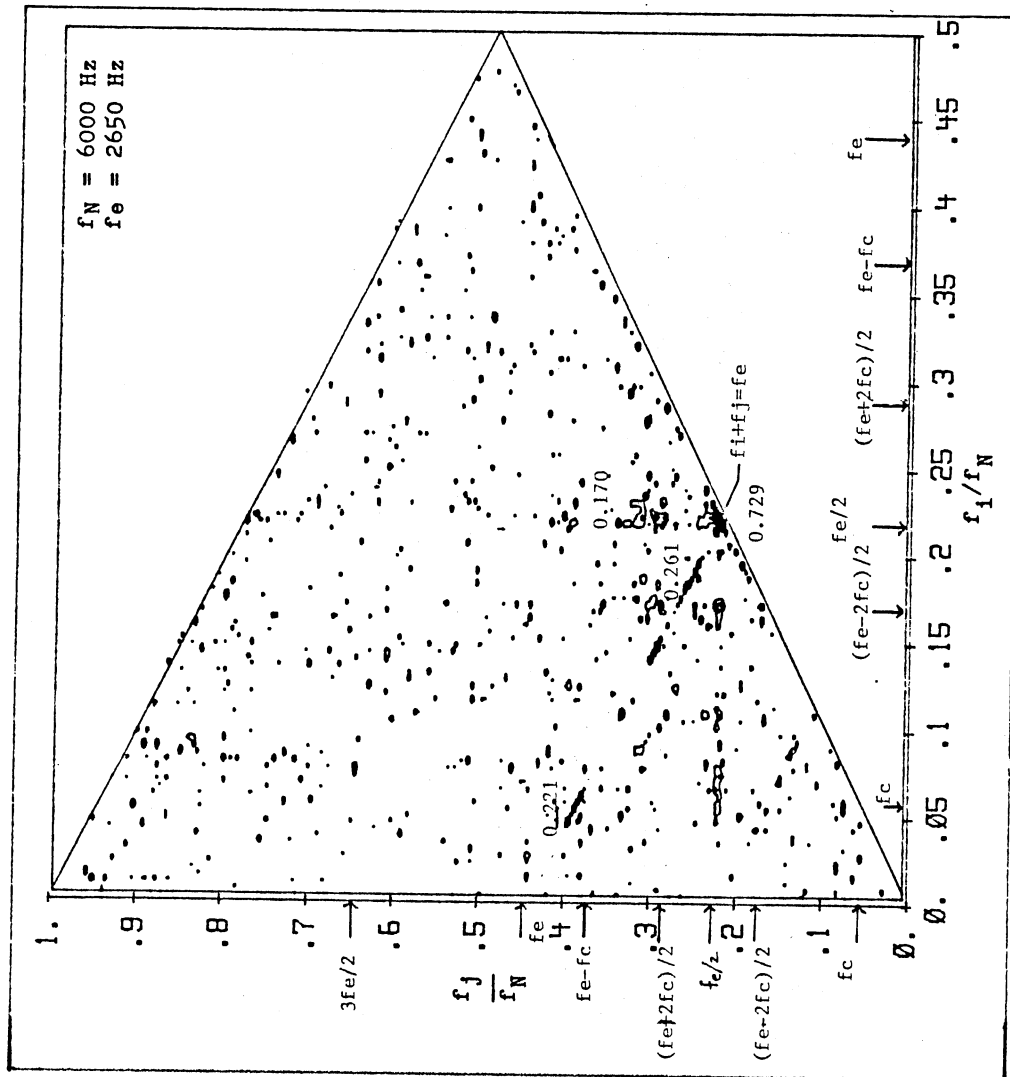


Figure 60. Bicoherence Spectrum at $x/D = 0.5$
($f_e = 2650 \text{ Hz}$)

that the upper sideband of the subharmonic is produced by the nonlinear interaction of the excitation frequency with the lower sideband of the subharmonic. The second observable peak at $b^2(f_{sw}/2, f_{sw}-f_{sc}) = 0.170$ shows how the lower sideband of the subharmonic is formed. The lower sideband of the subharmonic is formed through the nonlinear interaction $(f_{sw}-f_{sc})-f_{sw}/2 \rightarrow f_{sw}/2-f_{sc}$. It is interesting to note the interaction of the jet column mode at this near exit case. This indicates that the jet column mode exerts an upstream influence on the near exit flow field. These nonlinear interactions occurring at this near exit case help to explain the deviations observed in the application of the linear theory in section 3.1 at $x/D = 0.5$. In addition to these noticeable major peaks contours along the line $f_{sc} = f_{sw}$ are observable. The line $f_{sc} = f_{sw}$ indicates that multiple modes between $f_{sw}/2$ and $(f_{sw}/2-f_{sc})$ are also involved in the subharmonic resonance.

The bicoherence spectrum at $x/D = 0.75$ is shown in Figure 61. The dominant peak occurs at $b^2(f_{sw}, f_{sw}) = 0.890$ which indicates harmonic production through a nonlinear interaction of the form $f_{sw}+f_{sw} \rightarrow 2f_{sw}$. The power spectrum at location $x/D = 0.75$ (Figure 36) shows the harmonic frequency occurring due to this nonlinear interaction. Contours extending in the $f_{sc} = f_{sw}$ and $f_{sc} = f_{sw}$ directions represent nonlinear interactions between the excitation frequency and nearby modes to strengthen the neighboring

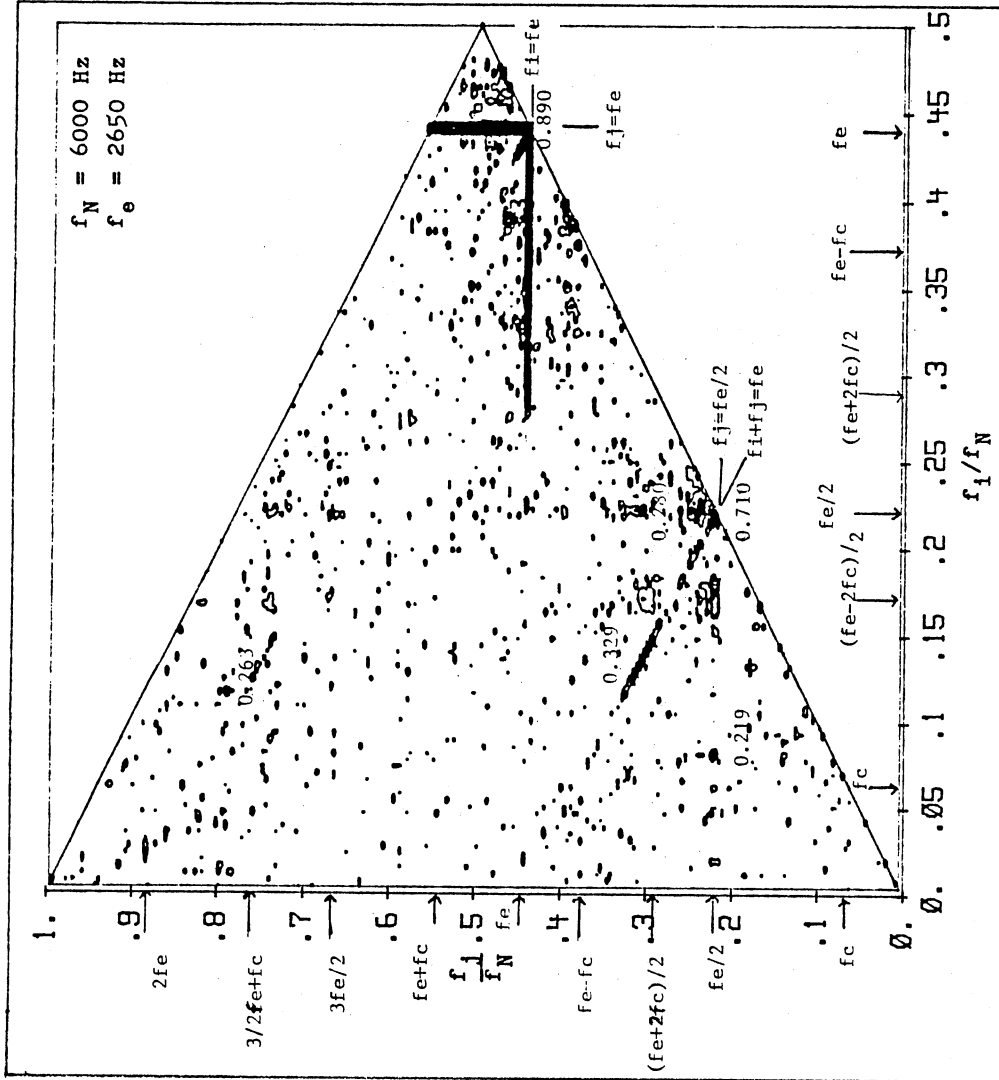


Figure 61. Bicoherence Spectrum at $x/D = 0.75$
($f_e = 2650$ Hz)

modes around the harmonic frequency. A contour line is beginning to form in the direction $f_j = f_{ex}/2$. This contour represents nonlinear interactions between the subharmonic frequency and nearby modes to enrich the modes around the excitation mode. The peak at $b^2(f_{ex}/2, f_{ex}/2)$ has decreased slightly from a value of 0.730 to 0.710. The contour line $f_{ic} = f_{ex}$ is still evident.

Figure 62 shows the bicoherence spectrum at location $x/D = 1.0$. It is evident from this plot that numerous nonlinear interactions are taking place at this x/D location. The peaks at $b^2(f_{ex}, f_{ex})$ and $b^2(f_{ex}/2, f_{ex}/2)$ are still very dominant peaks, showing almost perfect coherence. Contour lines extend from these peaks in the directions $f_i = f_{ex}$, $f_j = f_{ex}$, $f_j = f_{ex}/2$, $f_{ic} = f_{ex}$, and $f_{ic} = 2f_{ex}$. With the exception of $f_{ic} = 2f_{ex}$, the contour lines extending in the other directions have strengthened over previous locations. The contour line $f_{ic} = 2f_{ex}$ represents the interactions of multiple modes between f_{ex} and f_{ex} to help form the harmonic mode.

Figure 63 shows the bicoherence spectrum at location $x/D = 1.25$. The contour lines extending in the directions $f_i = f_{ex}$, $f_j = f_{ex}$, $f_j = f_{ex}/2$, and $f_{ic} = f_{ex}$, are still evident. The peak at $b^2(f_{ex}, f_{ex})$ has decreased from a value of 0.883 to 0.607 while the peak at $b^2(f_{ex}/2, f_{ex}/2)$ has increased from 0.733 to 0.933. The power spectrum at this location shows the subharmonic frequency as the dominant

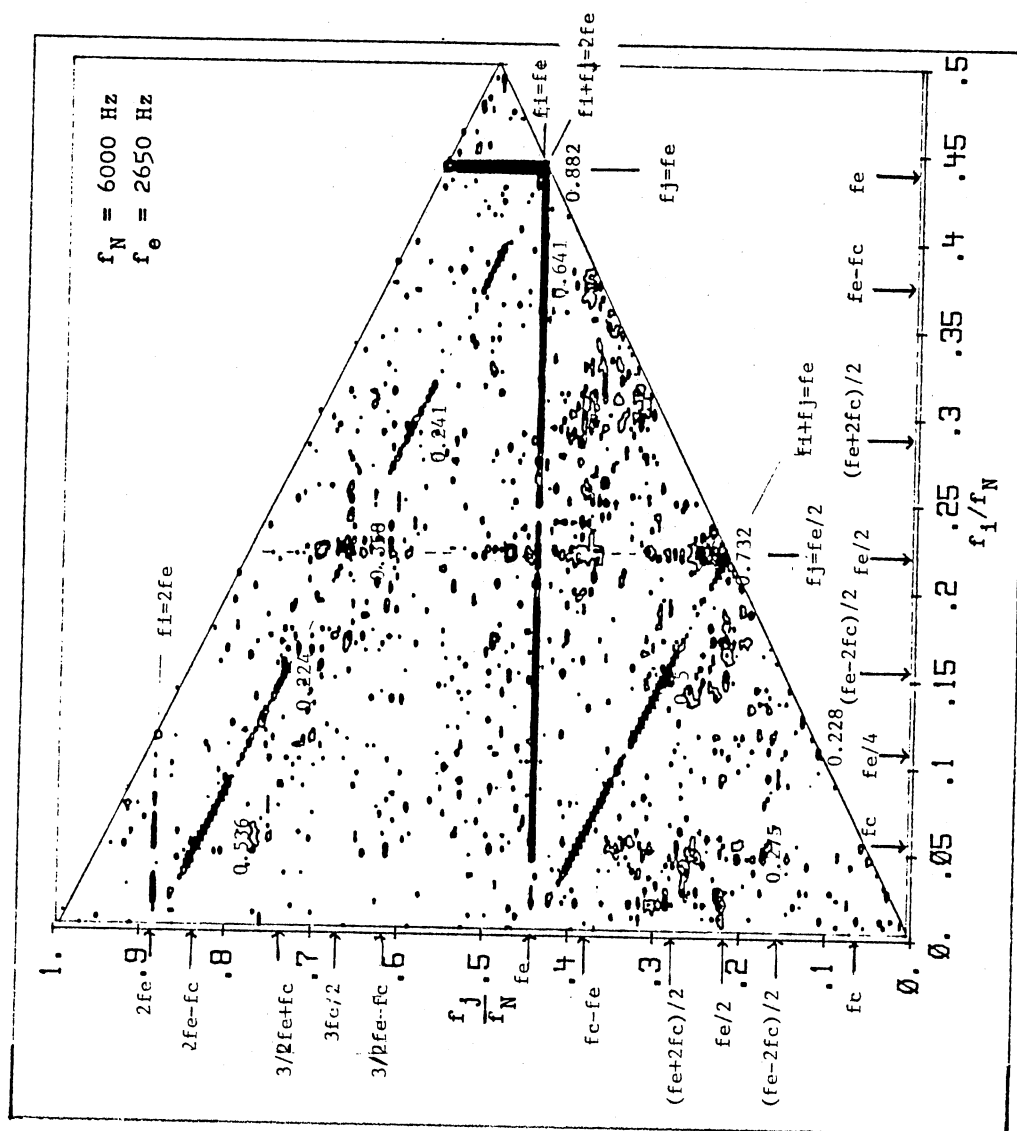


Figure 62. Bicoherence Spectrum at $x/D = 1.0$
($f_e = 2650 \text{ Hz}$)

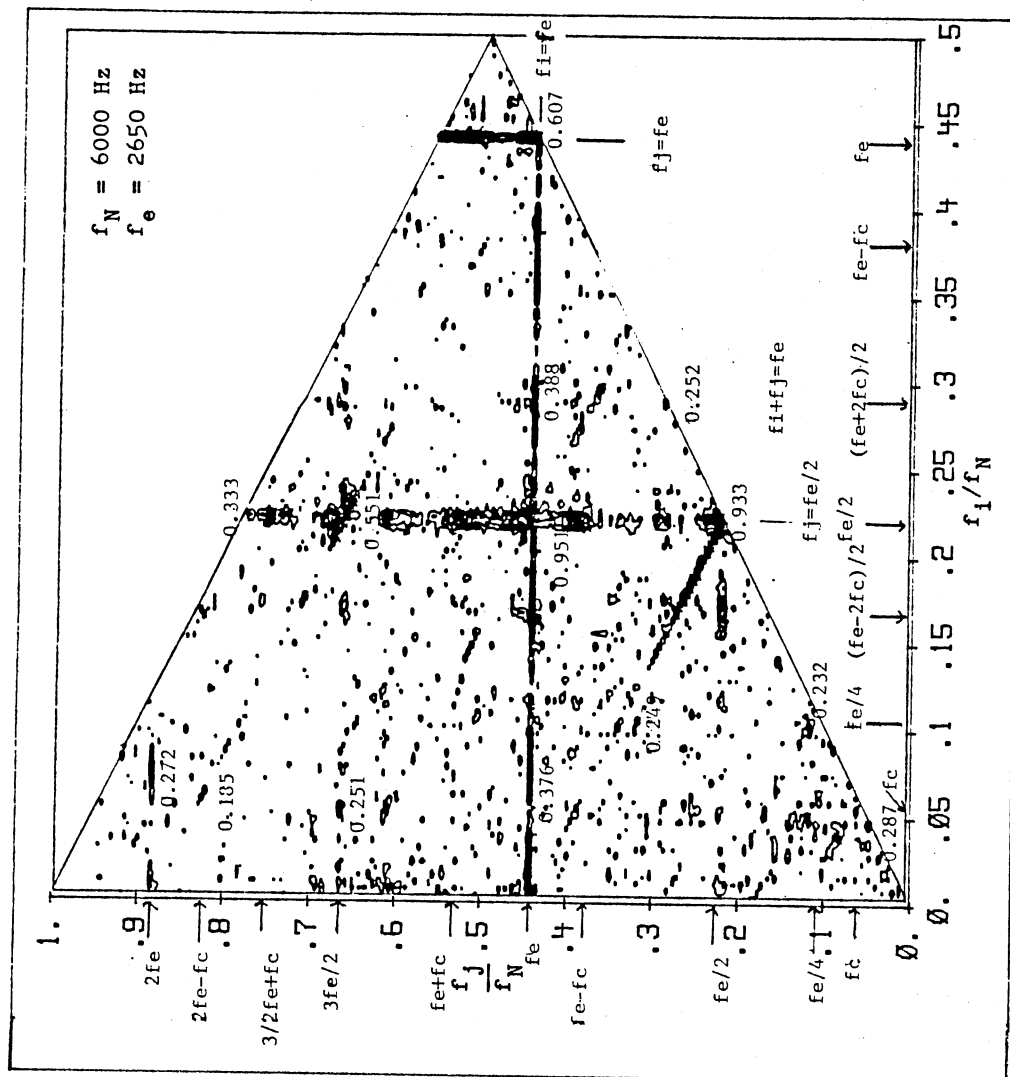


Figure 63. Bicoherence Spectrum at $x/D = 1.25$
($f_e = 2650 \text{ Hz}$)

frequency agreeing with the information provided in the bicoherence spectrum. A small peak at $b^2(f_{\omega}/4, f_{\omega}/4) = 0.233$ shows the nonlinear interaction $f_{\omega}/2 - f_{\omega}/4 \rightarrow f_{\omega}/4$. This is the second subharmonic frequency beginning to form. Other nonlinear interactions are also occurring at this location. As an example, $b^2(f_{\omega}, 3f_{\omega}/2) = 0.251$ shows the nonlinear interaction $(3f_{\omega}/2 + f_{\omega}) - f_{\omega} \rightarrow 3f_{\omega}/2$ occurring.

Figure 64 shows the bicoherence spectrum at location $x/D = 1.5$. Contour lines $f_i = f_{\omega}$, $f_j = f_{\omega}$, $f_j = f_{\omega}/2$, and $f_{\omega} = f_{\omega}$ still show dominant interactions among these frequencies. Newly appearing contours can be seen in directions $f_i = f_{\omega}/2$ and $f_{\omega} = f_{\omega}/2$; the first contour representing nonlinear interactions between the subharmonic frequency and nearby modes to strengthen the subharmonic mode. The second contour line represents interactions of multiple modes between $f_{\omega}/4$ and f_{ω} to enrich the mode $f_{\omega}/4$. Both peaks at $b^2(f_{\omega}, f_{\omega})$ and $b^2(f_{\omega}/2, f_{\omega}/2)$ have decreased in magnitude. Very few peaks are present that show the formulation of the harmonic frequency $2f_{\omega}$.

Figure 65 shows the bicoherence spectrum at location $x/D = 1.75$. It is interesting to note from this figure that the contour lines $f_i = f_{\omega}$ and $f_j = f_{\omega}$ seem to be scattering to neighboring modes. Contour lines $f_j = f_{\omega}/2$ and $f_{\omega} = f_{\omega}$ are still dominant lines even though they have lessened in intensity from the previous location. The

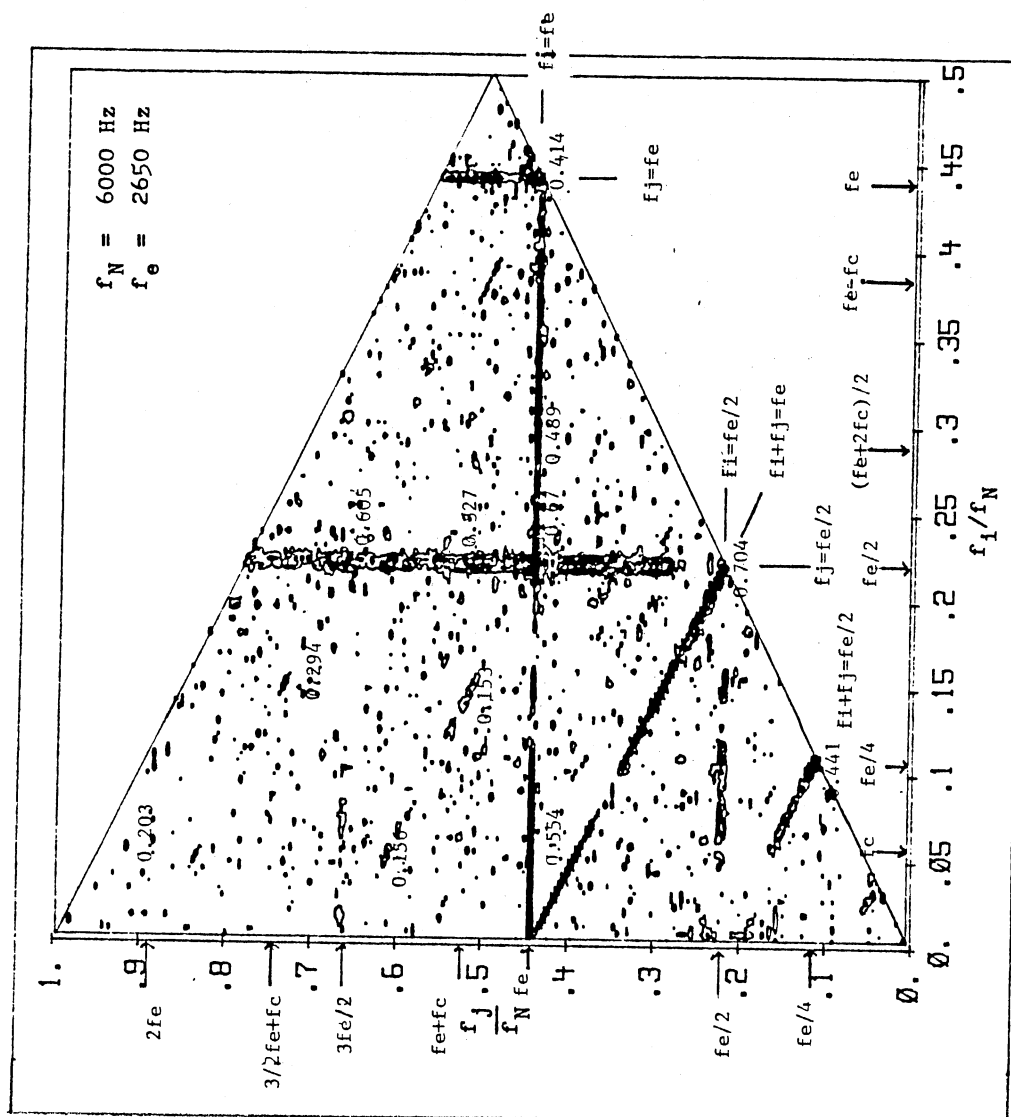


Figure 64. Bicoherence Spectrum at $x/D = 1.75$
($f_e = 2650$ Hz)

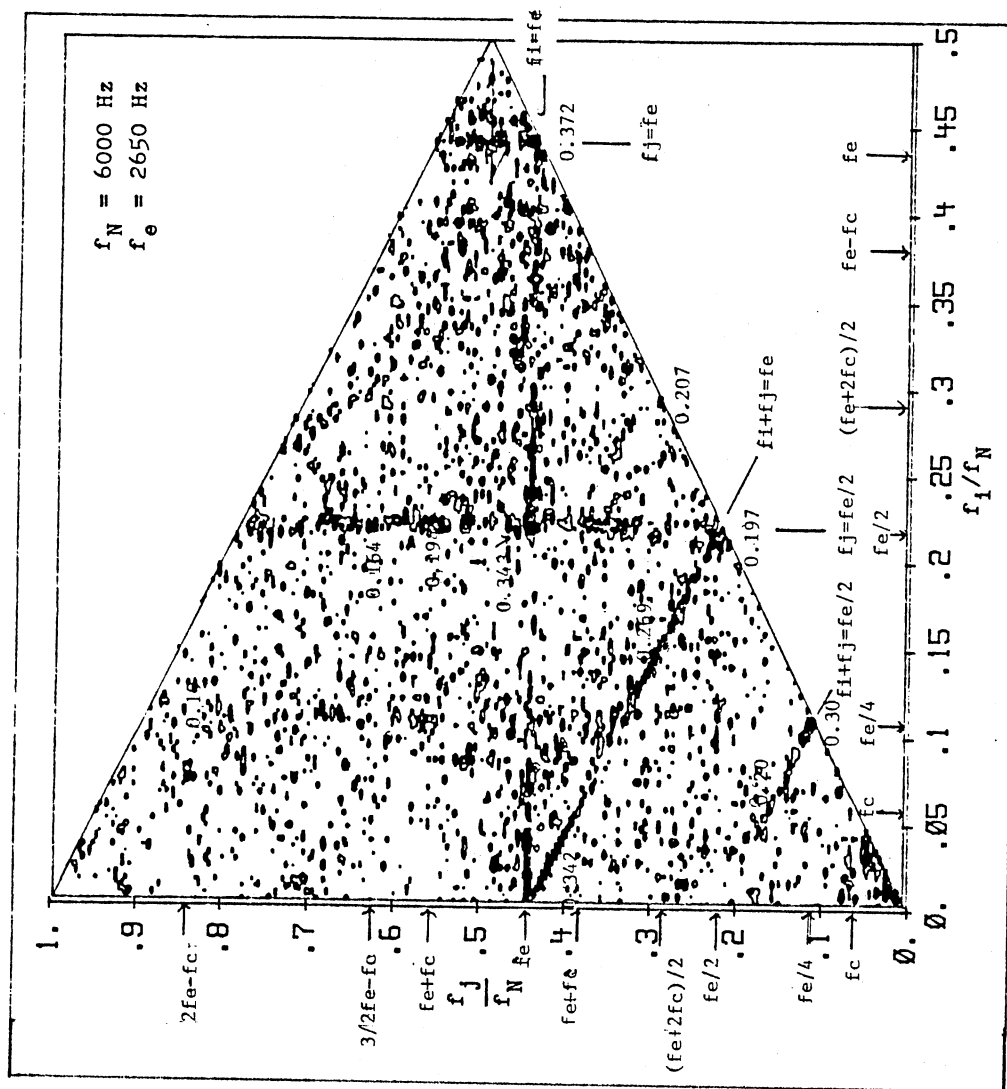


Figure 65. Bicoherence Spectrum at $x/D = 1.75$
($f_e = 2650 \text{ Hz}$)

peak showing the interaction $f_{\omega} - f_{\omega}/2 \rightarrow f_{\omega}/2$ has decreased in phase coherence significantly from a value of 0.704 to a value of 0.197. Also of interest is the increase of the peak at location $b^2(f_{\omega}, f_{\omega})$ from a coherence value of 0.414 to a value of 0.572. This explains the dominance of the excitation frequency shown in the power spectrum at this location (see Figure 38). Both the peak at location $b^2(f_{\omega}/4, f_{\omega}/4)$ and the contour line at $f_{\omega} = f_{\omega}/2$ are still evident. Both of these features of the plot produce the mode $f_{\omega}/4$.

Figure 66 shows the bicoherence spectrum at location $x/D = 2.0$. The alone contour line remaining by this location is the line given by $f_{\omega} = f_{\omega}/2$. The remaining peaks present show nonlinear interactions producing the dominant mode at $f_{\omega}/4$. Figure 67 shows the bicoherence at location $x/D = 2.5$. The contour line at $f_{\omega} = f_{\omega}/2$ is still present showing the interactions to produce the subharmonic mode. A peak at $b^2(f_{\omega}/4, f_{\omega}/4)$ is still present showing the interaction to form a mode at $f_{\omega}/4$. No other peaks are present.

The bicoherence spectrum at location $x/D = 3.0$ can be viewed in Figure 68. Again the contour line $f_{\omega} = f_{\omega}/2$ is still present. The only peak observable besides those showing up in the contour line is the peak at $b^2(f_{\omega}/4, f_{\omega}/4)$. By $x/D = 4.0$ the bicoherence spectrum shows a complete random plot due to a turbulent flow field

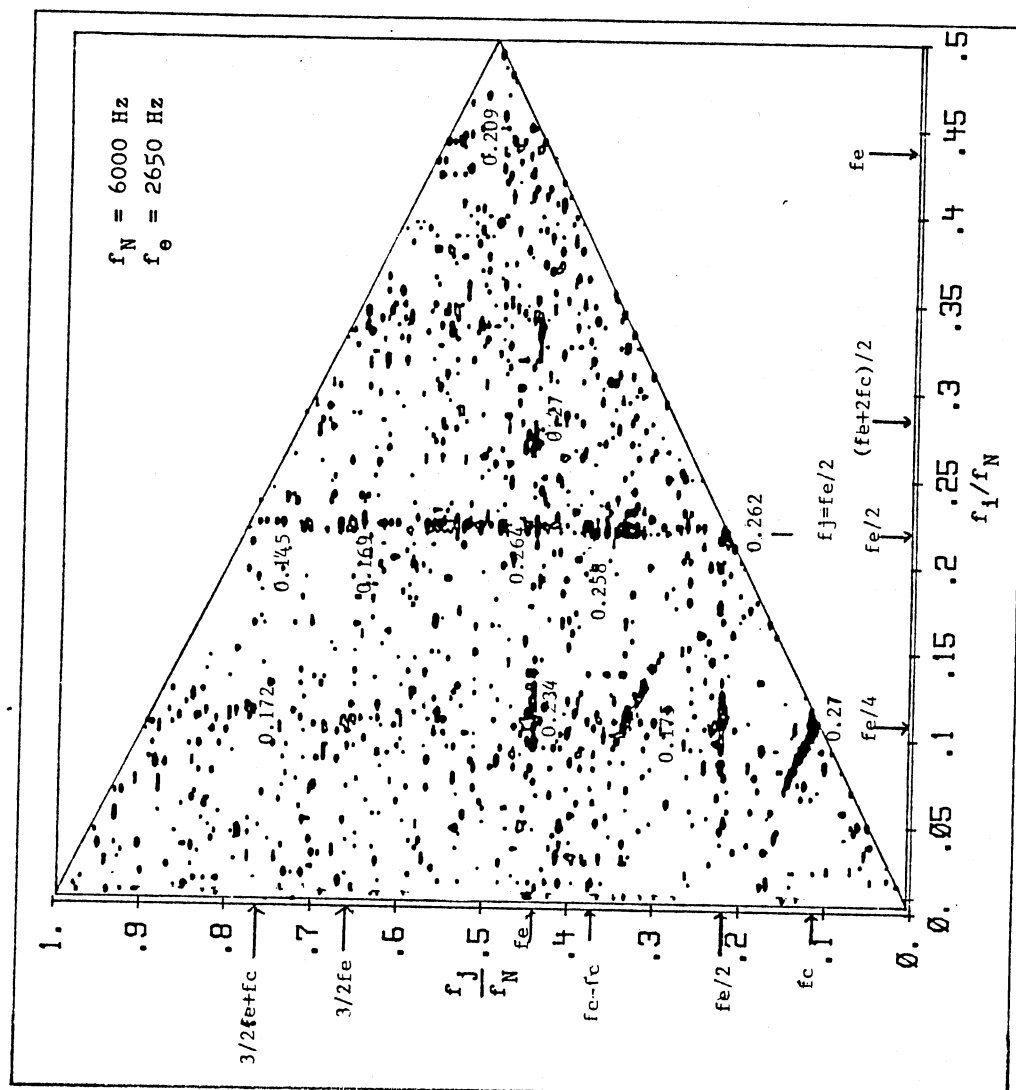


Figure 66. Bicoherence Spectrum at $x/D = 2.0$
($f_e = 2650 \text{ Hz}$)

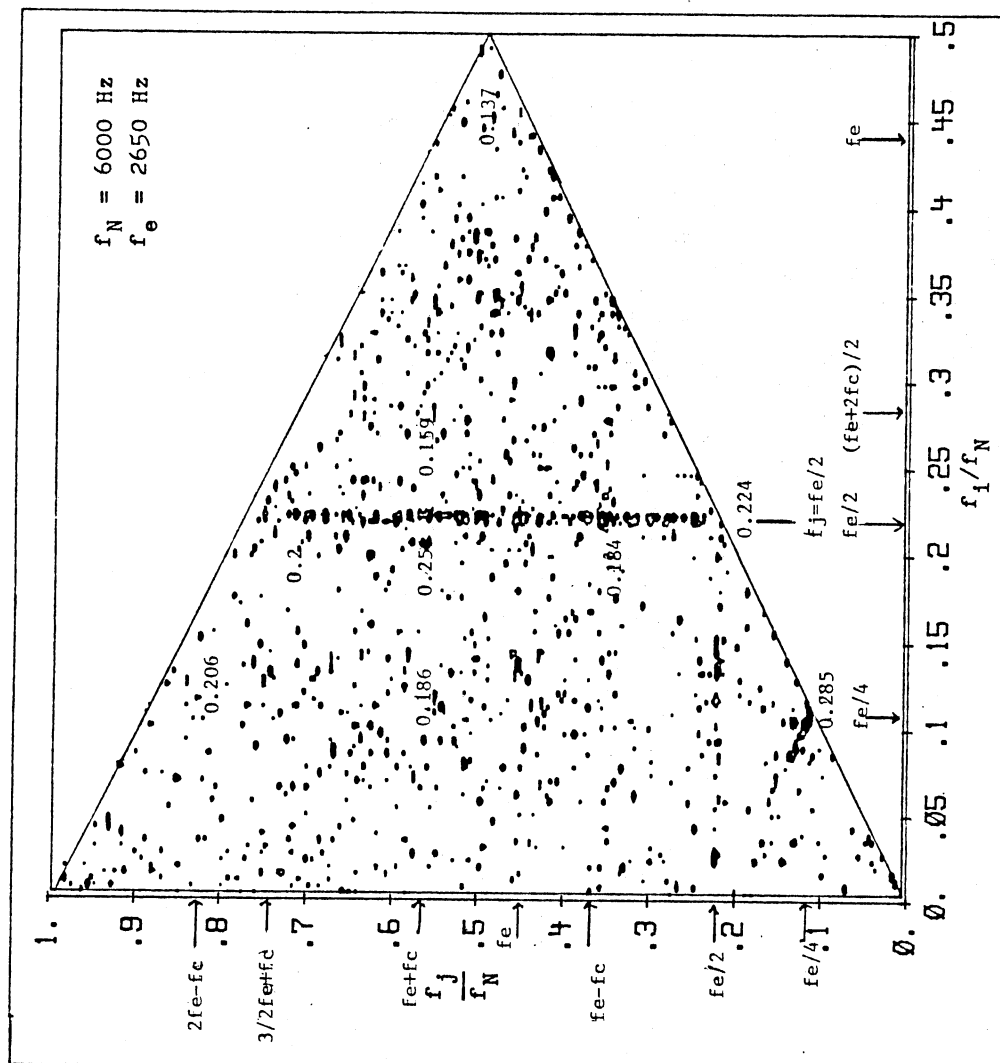


Figure 67. Bicoherence Spectrum at $x/D = 2.5$
($f_e = 2650 \text{ Hz}$)

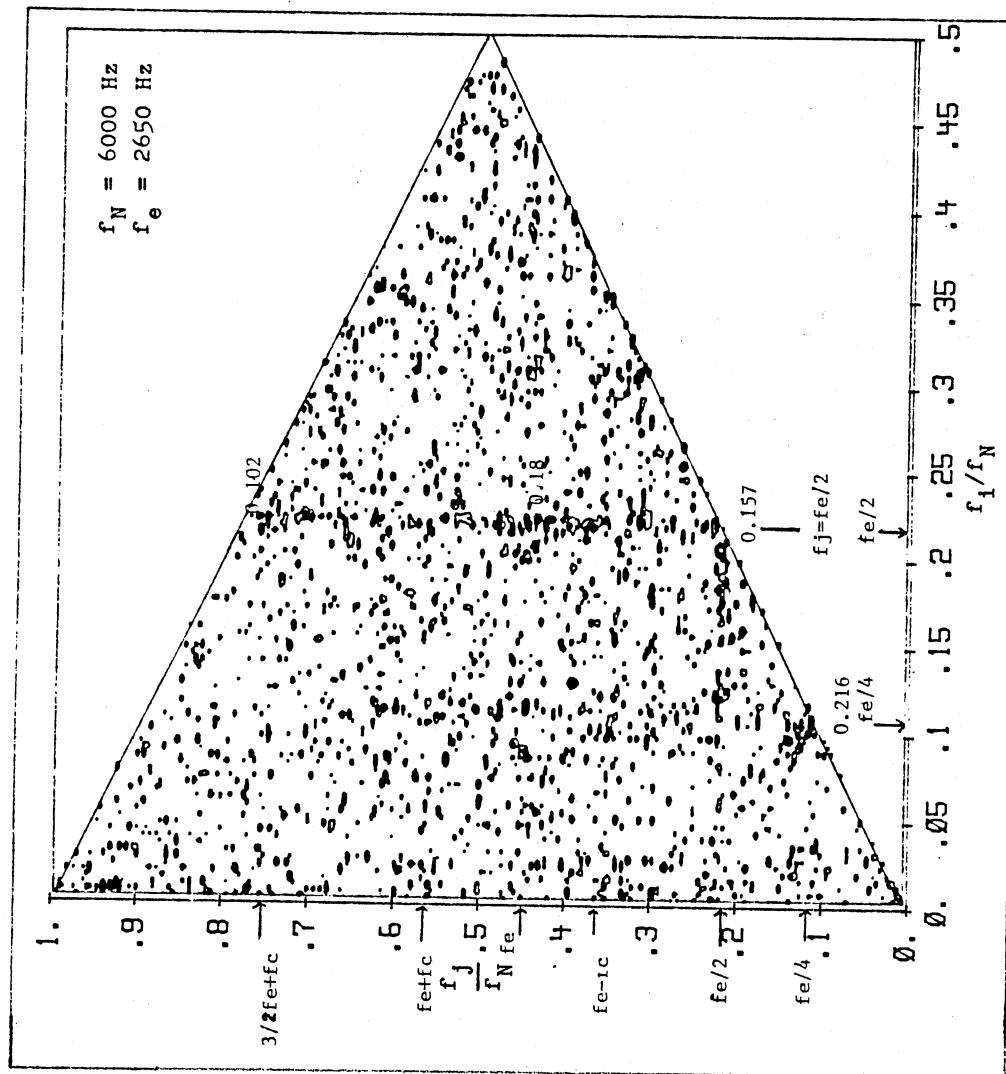


Figure 68. Bicoherence Spectrum at $x/D = 3.0$
 ($f_e = 2650 \text{ Hz}$)

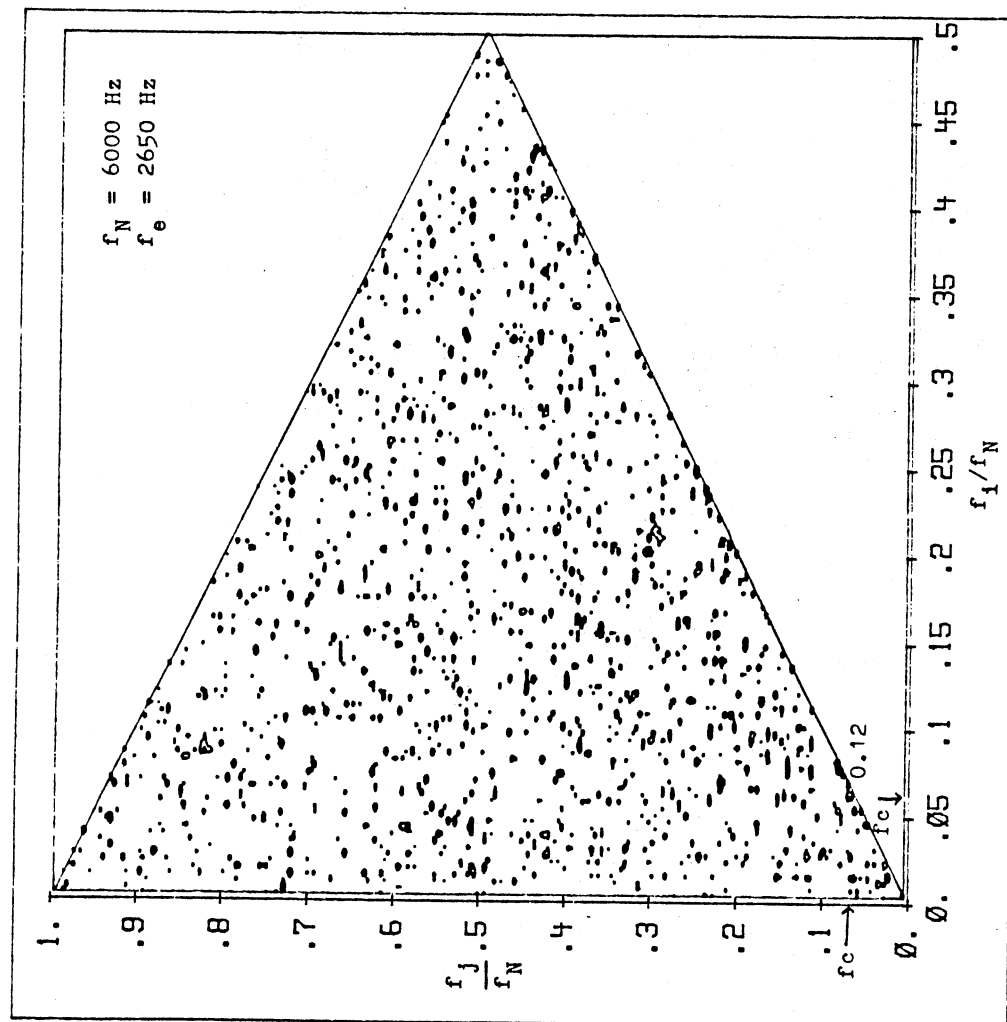


Figure 69. Bicoherence Spectrum at $x/D = 4.0$
 ($f_e = 2650 \text{ Hz}$)

(Figure 69).

The next section presents bicoherence measurements for the untuned jet. These measurements will determine the nonlinear interactions for the case of $f_w = 2200$ Hz.

3.4.3 Bicoherence Measurements

at $f_w = 2200$ Hz

Figure 70 shows the bicoherence plot at $x/D = 1.0$. Locations closer to the nozzle exit do not show any phase coherence. The peaks in this plot are very broad agreeing with the power spectrum plots that show the energy to be spread out over a wider frequency band. Dominant peaks are observable at locations $b^2((f_w+3f_c)/2, (f_w+3f_c)/2)$ and $b^2(f_w-f_c/4, f_w-f_c/2)$. It is interesting to note the dual peak arrangement instead of the one dominant peak in the tuned case. Also it is important to notice that no peak shows up at the excitation frequency. This suggests that there is no true harmonic production in the untuned case. Contour lines extend from these modes in the directions $f_1 = f_2 = (f_w+3f_c)/2$ and $f_1 = f_2 = f_w-f_c/4$. These contour lines show multiple interactions to strengthen the modes $(f_w+3f_c)/2$ and $f_w-f_c/4$. A strong mode is shown at location $b^2(f_w/2, f_w/2)$. This mode corresponds to the interaction $f_w - f_w/2 \rightarrow f_w/2$. Another mode is at $b^2(2f_c, (f_w-f_c)/2)$ showing the non-linear interaction $2f_c + (f_w-f_c)/2 \rightarrow (f_w+3f_c)/2$. A contour line extends in the

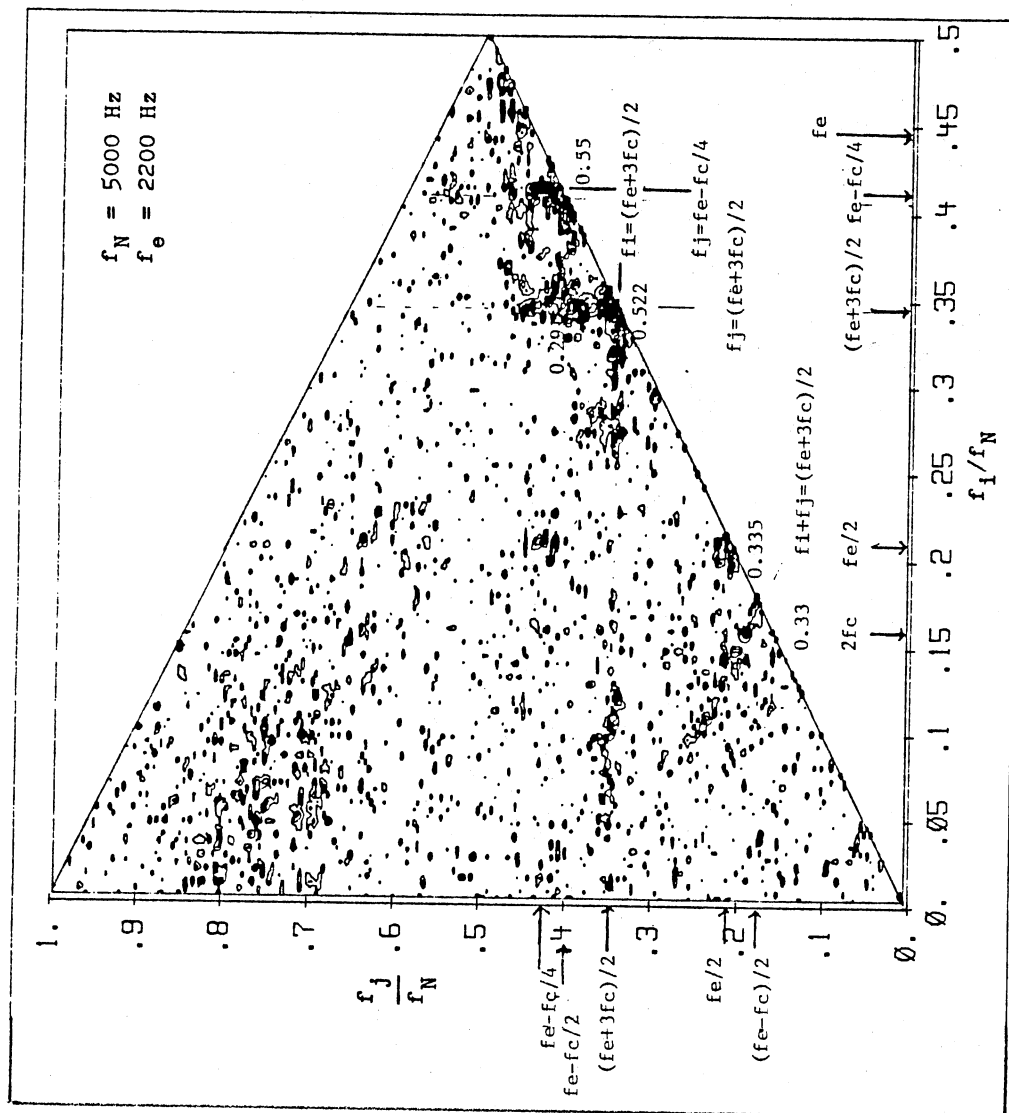


Figure 70. Bicoherence Spectrum at $x/D = 1.0$
($f_e = 2200 \text{ Hz}$)

direction $f_{\omega} = f_{\omega} - f_{\omega}$ starting from this mode. This corresponds to interactions strengthening the mode at $(f_{\omega} + 3f_{\omega})/2$. The last strong mode is found at $b^2(f_{\omega}/2, f_{\omega} - f_{\omega}/2)$.

Figure 71 shows the bicoherence plot at $x/D = 1.25$. Very little change is shown at this location. The mode at $b^2((f_{\omega} + 3f_{\omega})/2, (f_{\omega} + 3f_{\omega})/2)$ is strengthened slightly while the mode at $b^2(f_{\omega} - f_{\omega}/4, f_{\omega} - f_{\omega}/2)$ is decreased in coherence slightly. A new mode is shown at $b^2(f_{\omega}/2, (f_{\omega} + 3f_{\omega})/2)$.

Figure 72 shows the bicoherence plot at $x/D = 1.5$. Major changes are shown from the previous location. The only modes at this location that were seen previously are the modes at $b^2(f_{\omega}/2, f_{\omega}/2)$, $b^2(f_{\omega}/2, (f_{\omega} + 3f_{\omega})/2)$, and $b^2(f_{\omega}/2, f_{\omega} - f_{\omega}/2)$. A new peak is now seen at $b^2(f_{\omega}/4, f_{\omega}/4)$ showing the interaction $f_{\omega}/2 - f_{\omega}/4 \rightarrow f_{\omega}/4$. This is the first interaction to produce the second subharmonic frequency.

As in the power spectrum, the bicoherence spectrum at locations further downstream ($x/D > 1.5$) show a random spectrum. This contrasts with the "tuned" jet which did not show a random spectrum until the potential core ended at $x/D = 4.0$. This suggests that the untuned jet has considerably more turbulence inherent in the shear layers due to the jet trying to redistribute the energy to become in tune with the jet column mode.

The next section presents coherence measurements

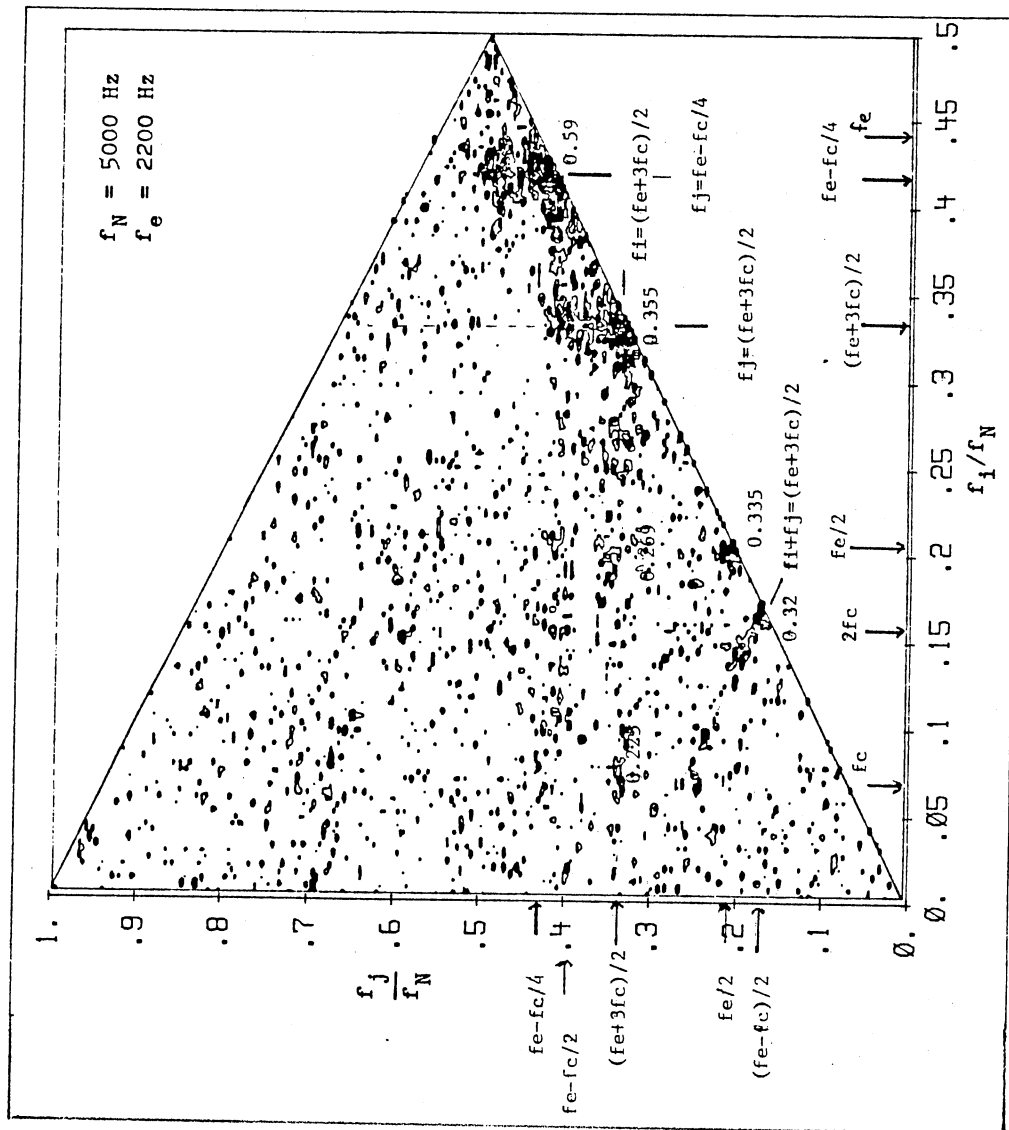


Figure 71. Bicoherence Spectrum at $x/D = 1.25$
($f_e = 2200 \text{ Hz}$)

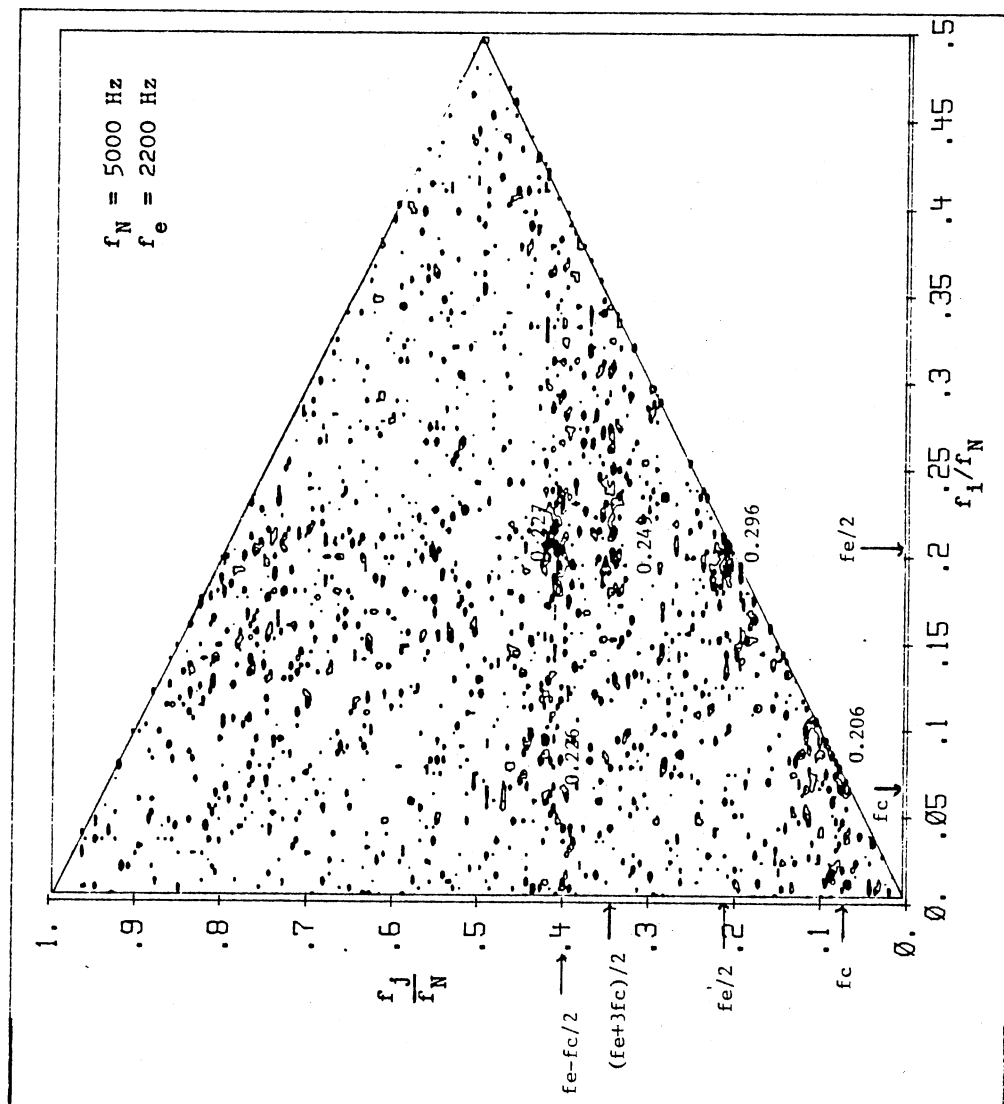


Figure 72. Bicoherence Spectrum at $x/D = 1.5$
 ($f_e = 2200 \text{ Hz}$)

between the fluctuations in the two jet shear layers for x/D locations 0.5 to 4.0. The coherence measurements should give further information on the mechanism by which the jet column mode interacts with shear layer unstable modes.

3.5 Coherence and Phase Angle Measurements

This section presents coherence and phase angle measurements documenting the coherence of fluctuations between the two shear layers. Coherence and phase angle measurements are obtained for x/D locations 0.5 to 4.0. Background information on the coherence technique and theory is presented before the results are presented.

3.5.1 Coherence and Phase Angle Techniques

The coherence function is derived from the cross-spectral density function. The cross-spectral density function is generally a complex number defined by

$$G_{xy} = C_{xy}(f) - jQ_{xy}(f) \quad (3.32)$$

where the real part, $C_{xy}(f)$, is called the coincident spectral density function and the imaginary part, $Q_{xy}(f)$, is called the quadrature spectral density function. In frequency terms, the coincident spectral density function is the average product of $x(t)$ and $y(t)$ within a narrow frequency interval f and $f+\Delta f$, divided by the frequency

interval. The quadrature spectral density function is the same except that either $x(t)$ or $y(t)$, not both, is shifted in time sufficiently to produce a 90-degree shift at frequency f .

Expressing the cross-spectral density function in complex polar notation gives the relationship

$$G_{xy}(f) = |G_{xy}(f)| e^{-j\theta_{xy}(f)} \quad (3.33)$$

where

$$|G_{xy}(f)| = [C_{xy}^2(f) + Q_{xy}^2(f)]^{1/2} \quad (3.34)$$

$$\theta_{xy}(f) = \tan^{-1}[Q_{xy}(f)/C_{xy}(f)] \quad (3.35)$$

Another useful relationship is

$$|G_{xy}(f)|^2 \leq G_x(f)G_y(f) \quad (3.36)$$

The coherence function can now be defined by

$$\gamma_{xy}^2(f) = \frac{|G_{xy}(f)|^2}{G_x(f)G_y(f)} \leq 1 \quad (3.37)$$

where $\gamma_{xy}^2(f)$ is called the coherence function, and $G_x(f)$ and $G_y(f)$ are power spectral density functions. When $\gamma_{xy}^2(f) = 0.0$, the two signals $x(t)$ and $y(t)$ are said to be incoherent at that frequency. When $\gamma_{xy}^2(f) = 1.0$, the signals $x(t)$ and $y(t)$ are said to be fully coherent at that frequency. In-between values give partial coherence

at that frequency.

Spectral coherence measurements were made at selected x/D locations between 0.5 and 4.0. The hot-wire probes were placed on opposite sides of the centerline in the shear layers at a location $U/U_{free} = 0.6$. Each coherence and phase angle spectrum represents an ensemble average over 100 samples of 512 points each. The program used can be viewed in Appendix A. Figure 73 shows the placement of the hot-wire probes in the flow field.

3.5.2 Coherence and Phase Development

at $f_{jet} = 2650$ Hz

Figure 74 presents the coherence function at an x/D location of 0.5. Five distinct peaks of coherence can be seen at $x/D = 0.5$. The peak centers occur at 200 Hz, 1125 Hz, 1525 Hz, 2250 Hz, and 3450 Hz. The peak at 200 Hz is centered at half the jet column mode, $f_{jet}/2$. This mode is phase coupled on opposite sides of the jet shear layers. The peaks at 1125 Hz and 1525 Hz show very high coherence. It is interesting to note that these peaks occur at a frequency of $f_{jet}/2 \pm f_{jet}/2$. Half the jet column mode is interacting with the subharmonic frequency to produce highly coherent peaks within the shear layers. The peak at 2250 Hz, showing lower coherence than the other mentioned peaks, shows coherence of the mode produced by the interaction $f_{jet} - f_{jet}$. The fifth peak is at a

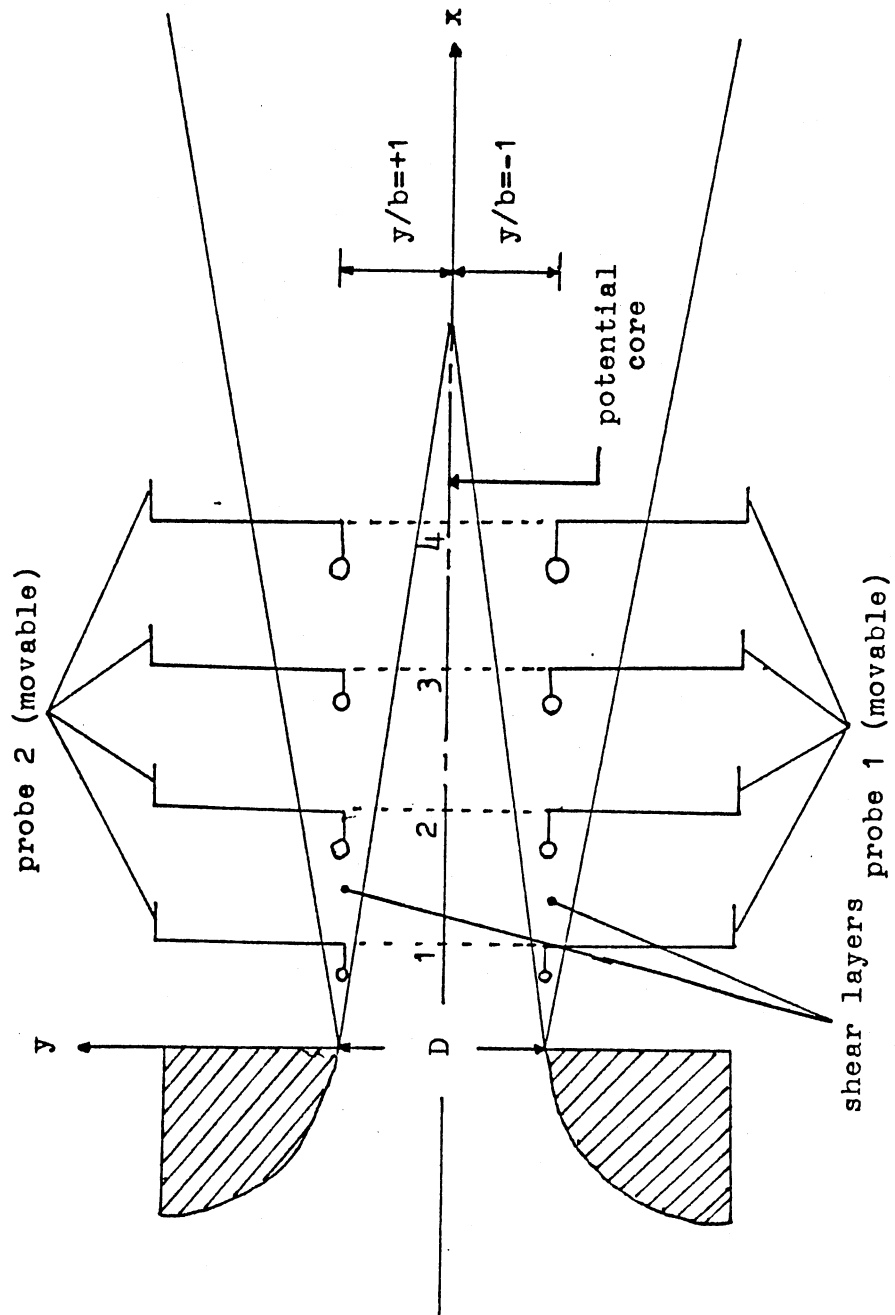


Figure 73. Schematic for Coherence Probe Placement

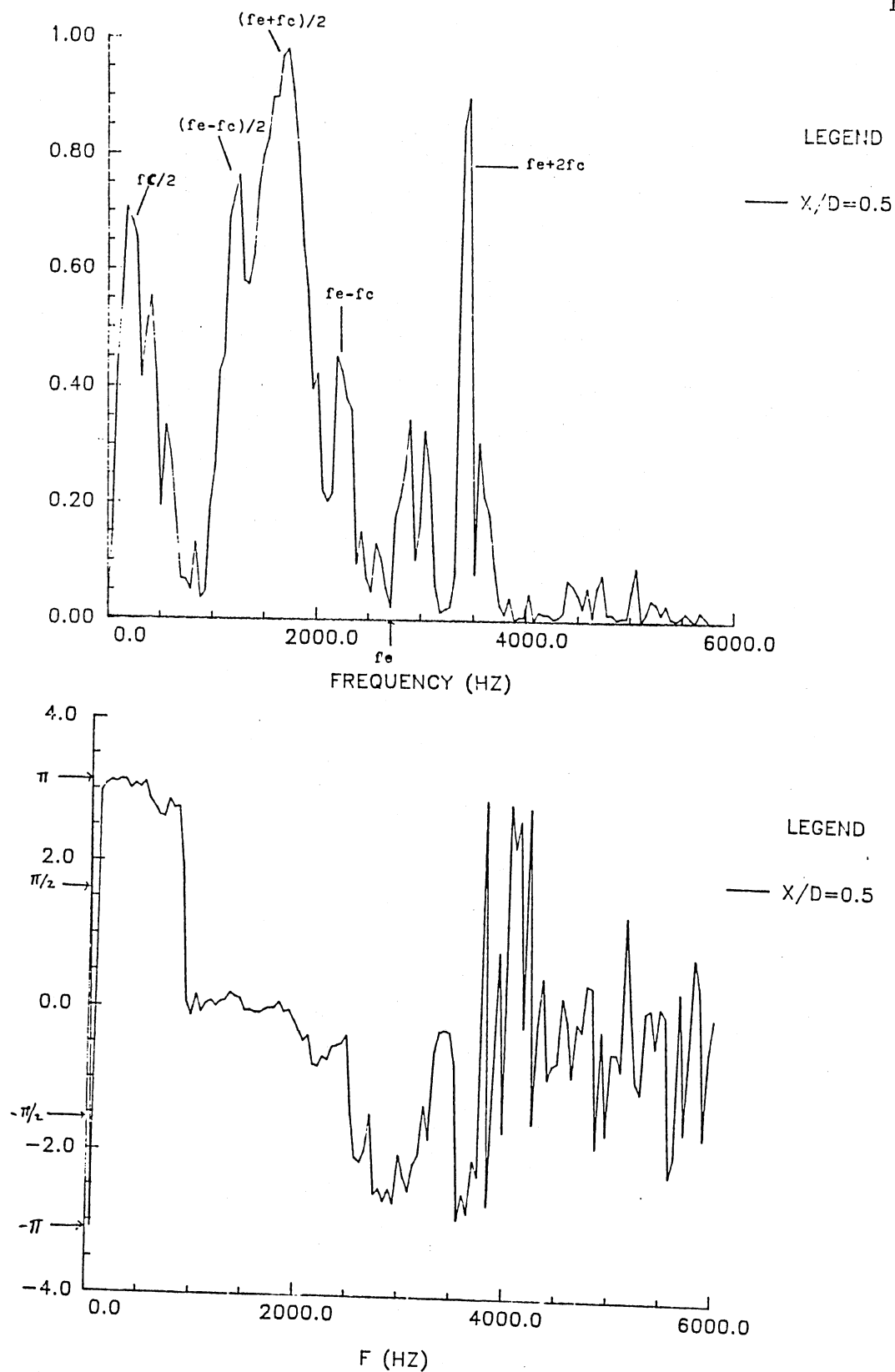


Figure 74. Coherence and Phase at $x/D = 0.5$
($f_e = 2650$ Hz)

frequency produced by the interaction $f_{\omega} + 2f_{\omega}$. All the coherent peaks are peaks formed by interactions with the jet column mode. Another point of interest is that the excitation frequency shows almost no coherence.

The phase coherence spectrum for $x/D = 0.5$ shows the shear layers are π out of phase for frequencies $f = 0-1000$ Hz. This shows that the shear layers are undergoing lateral oscillations. The shift to being completely in phase occurs where the coherence becomes a minimum in the coherence plot. A second phase shift occurs at the frequency $f = 2250$ Hz. The phase is shifted to being $-\pi$ out of phase. At $f = 3050$ Hz another shift of phase is noted. This relates to the interaction $f_{\omega} + f_{\omega}$. A fourth shift is noted at $f = 3450$ corresponding to the mode at $f_{\omega} + 2f_{\omega}$. At higher frequencies the phase coherence is slightly random due to low coherence levels. As with the coherence spectrum, the phase coherence seems to be governed by the interactions of instability modes with the jet column mode.

Figure 75 shows the coherence and phase for $x/D = 1.0$. Basically the same peaks as in the previous upstream location ($x/D = 0.5$) are observable. The peaks at 200 Hz, 1125 Hz, and 2250 Hz show much lower coherence. The coherence at frequencies 1525 Hz and 3450 Hz still show very high coherence. A new coherence peak has formed at a frequency of 5100 Hz. This is the peak given by $2f_{\omega} - f_{\omega}$.

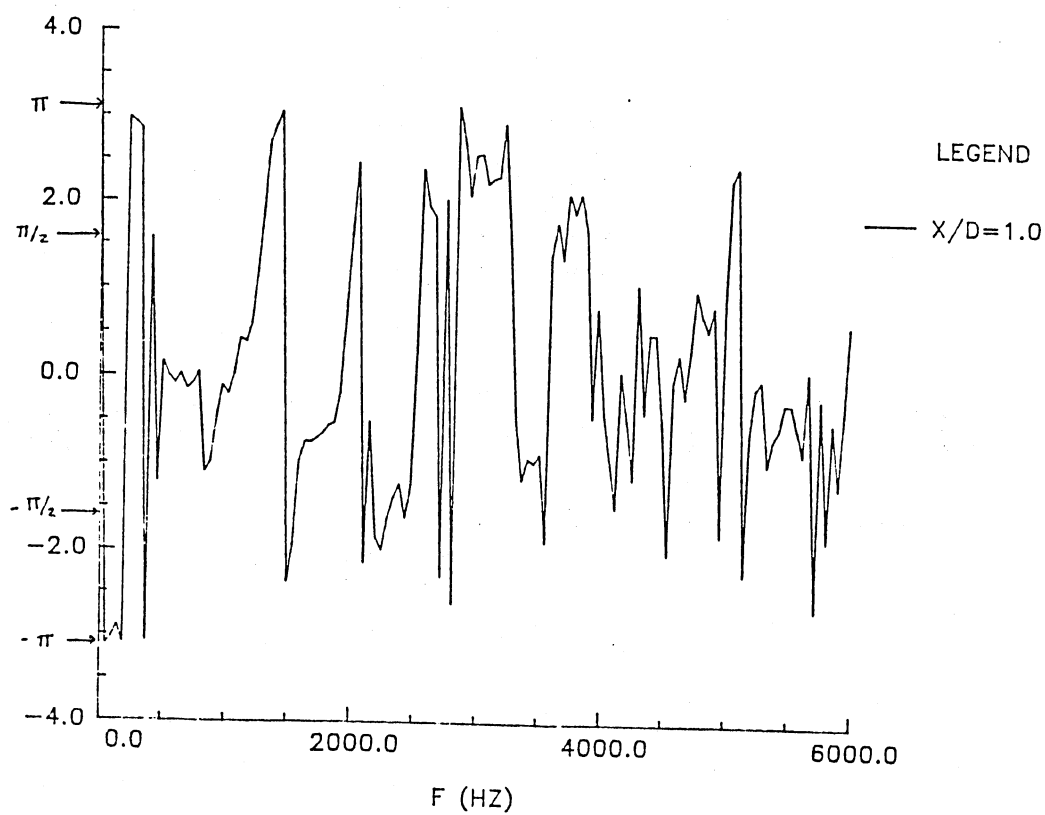
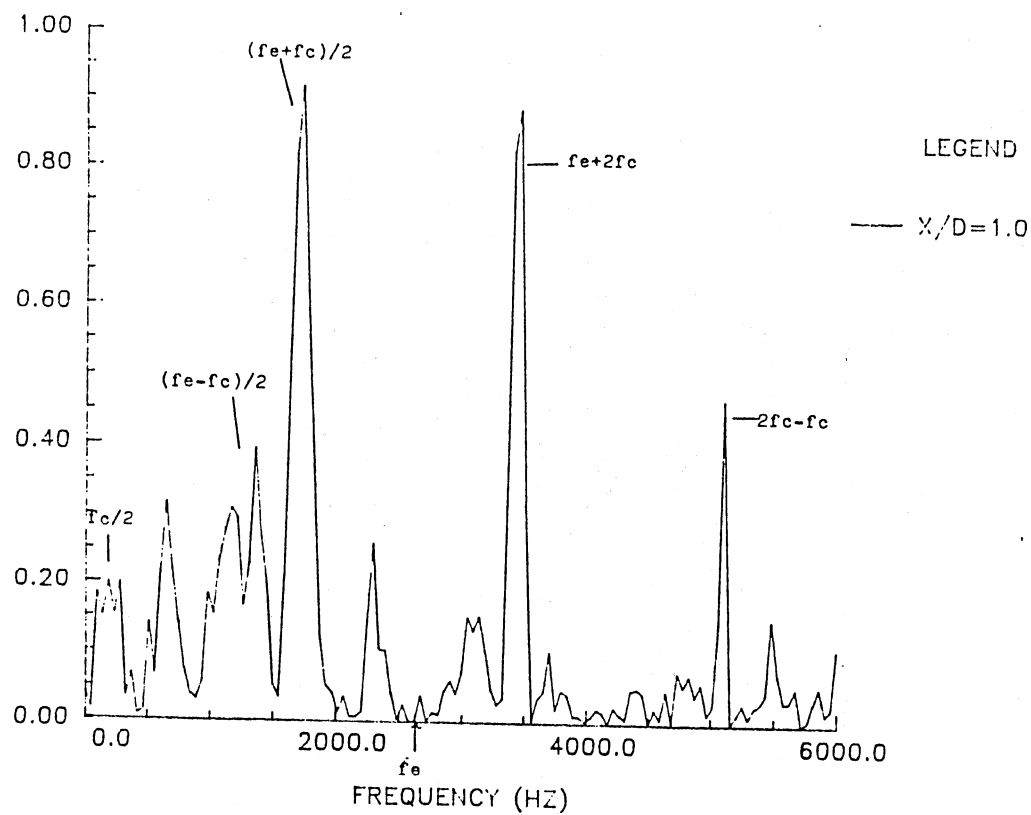


Figure 75. Coherence and Phase at $x/D = 1.0$
($f_e = 2650$ Hz)

Phase coherence at $x/D = 1.0$ shows the shear layers are π out of phase for frequencies $f = 0-400$ Hz. Again this phase shift occurs where the coherence becomes a minimum. As in the previous location, the phase shifts occur where the coherence peaks form. These shifts occur at frequencies 1125 Hz, 1525 Hz, 2250 Hz, 3450 Hz, and 3975 Hz. All of these modes involve the jet column mode. The influence of the jet column mode again can be seen to affect the upstream flow.

Further downstream at $x/D = 1.5$ (coherence and phase is shown in Figure 76), three distinct peaks are visible. Peaks occur at 1525 Hz, 3450 Hz, and 5100 Hz. These peaks are present in upstream locations but have decreased in coherence due to increased turbulence in the shear layers. The phase coherence plot for $x/D = 1.5$ can also be viewed in Figure 76. Again, the phase shifts can be related to the peaks of coherence. As in the cases of $x/D = 0.5$ and $x/D = 1.0$, the peaks of coherence and phase shifts occur at modes that involve the jet column mode.

By $x/D = 2.0$, see Figure 77, only two coherent peaks exist. The peaks are at 1525 Hz and 3450 Hz. By $x/D = 3.0$, also shown in Figure 78, the only peak that shows any amount of coherence is the peak at 1525 Hz. Due to increasing turbulence levels, no coherent peaks are observable any farther downstream. At these downstream locations the phase coherence is becoming hard to

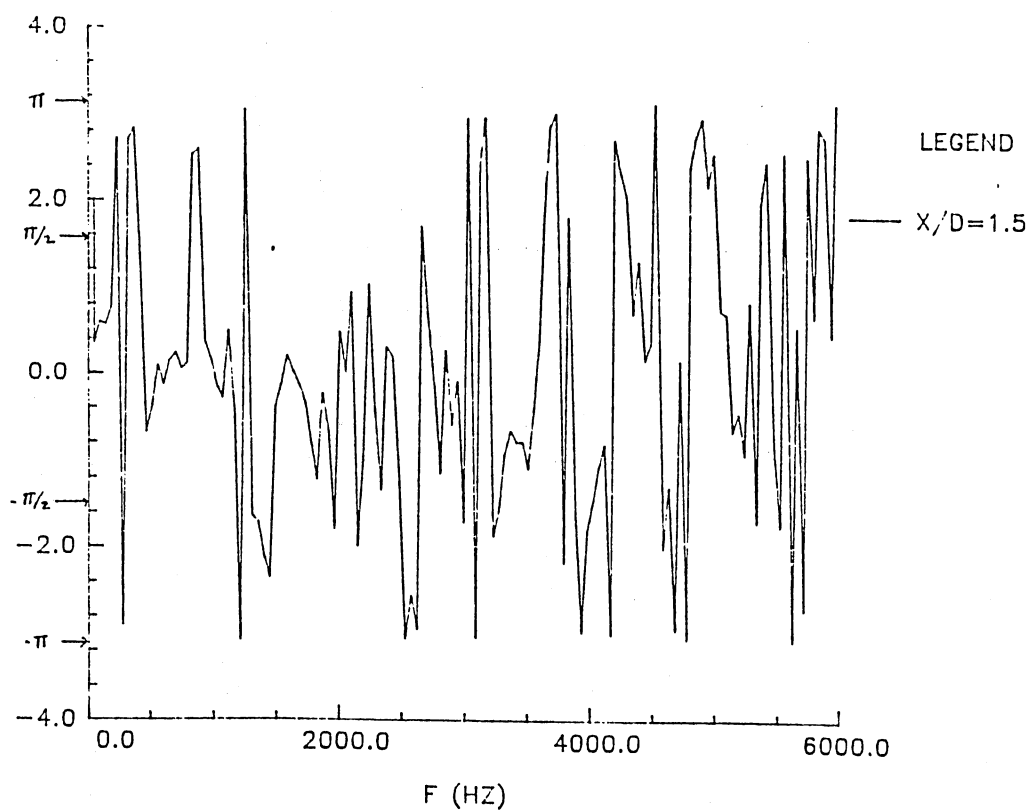
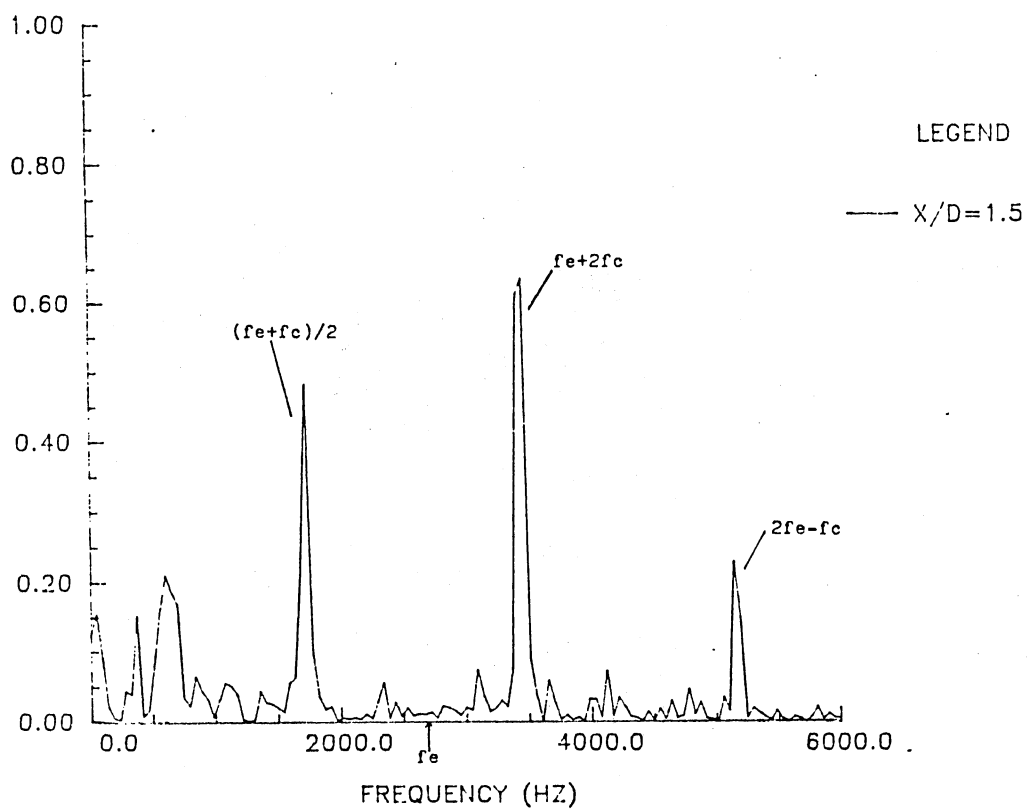


Figure 76. Coherence and Phase at $x/D = 1.5$
($fe = 2650$ Hz)

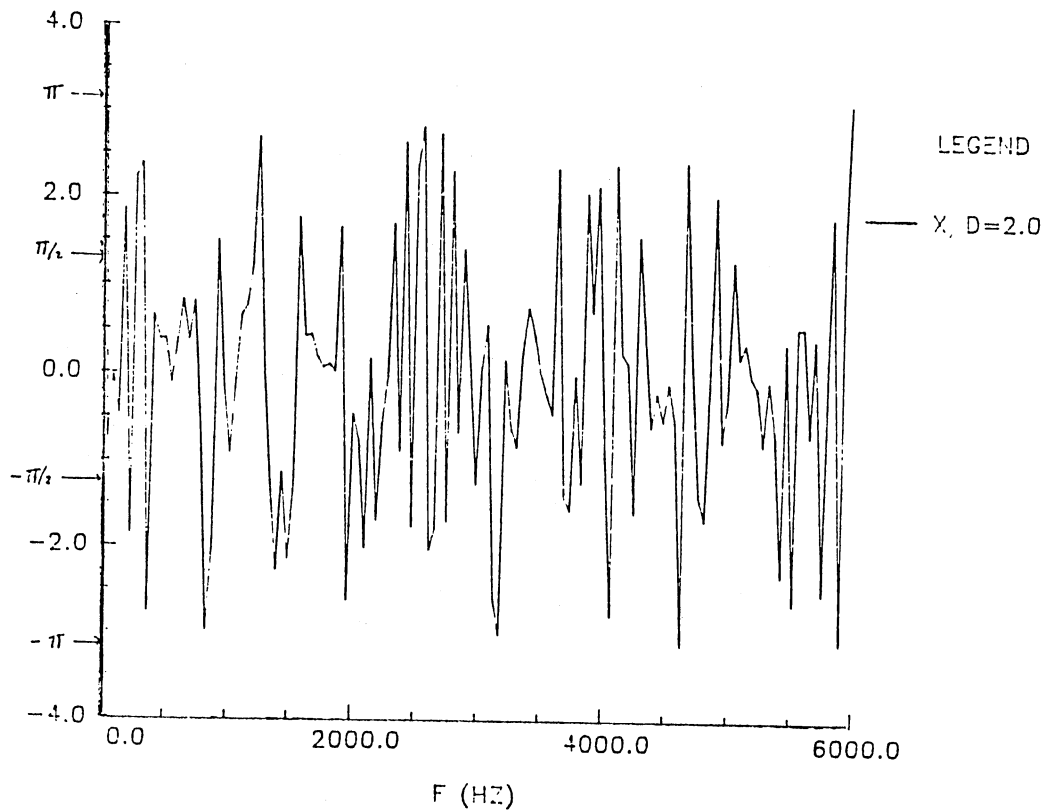
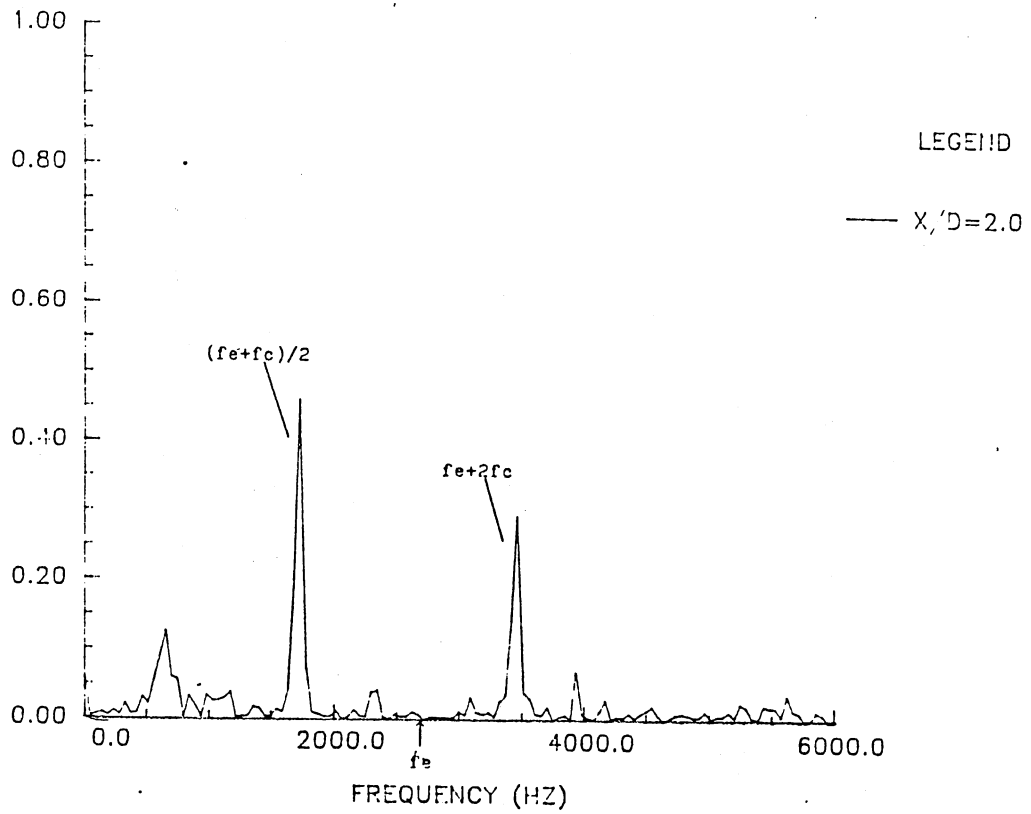


Figure 77. Coherence and Phase at $x/D = 2.0$
($f_e = 2650$ Hz)

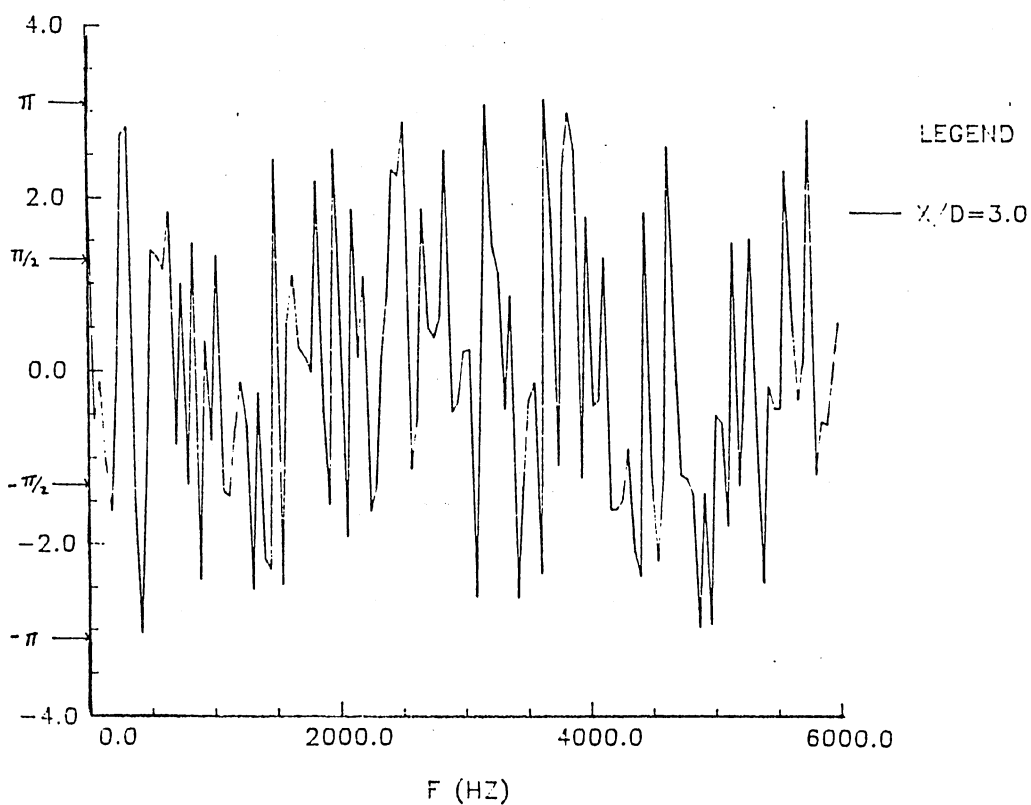
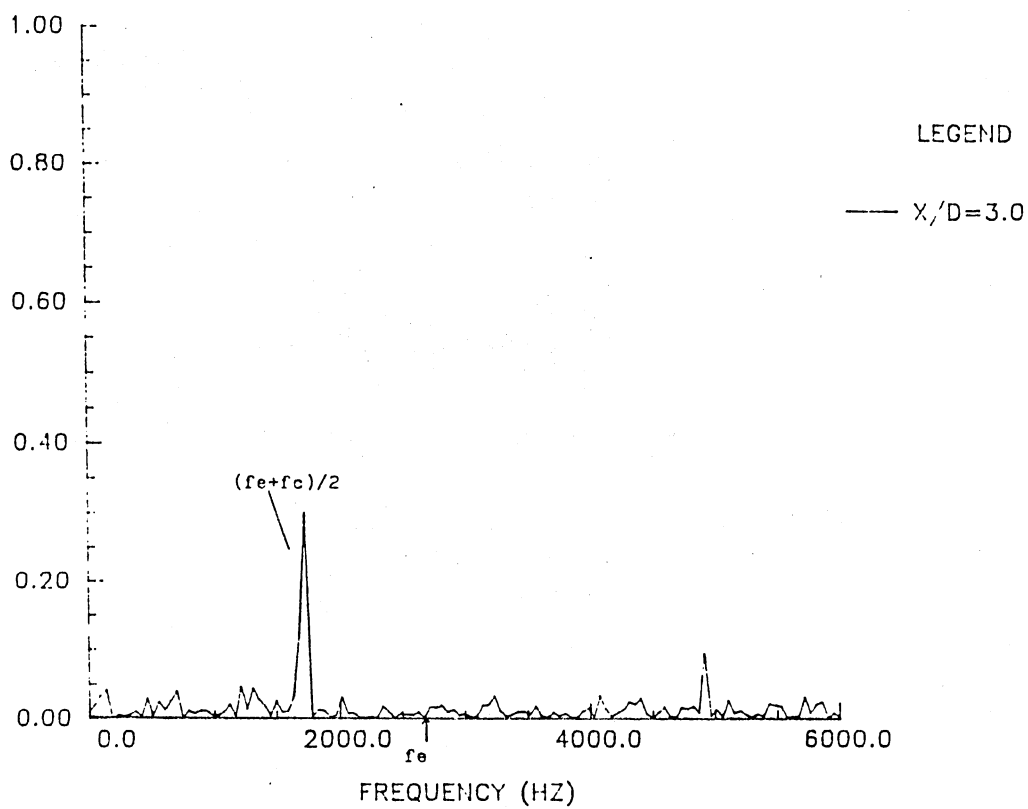


Figure 78. Coherence and Phase at $x/D = 3.0$
($f_e = 2650$ Hz)

determine where the phase shifts take place due to low levels of coherence between the shear layers

Chang (1987) has shown that the coherence between the two shear layers can be reasonably modeled by using two complex cosine waves of the form

$$A_1 = a_c [\cos(\omega_1 t) + \cos(\omega_2 t)] \cos(\omega_3 t + \phi) + n(t) \quad (3.38)$$

$$A_2 = a_c [\cos(\omega_1 t) + \cos(\omega_2 t)] \cos(\omega_3 t) + n(t) \quad (3.39)$$

where $a_c = 1.0$, ϕ = arbitrary phase angle to account for the possibility of asymmetry in the low frequency component, $n(t)$ is small amplitude random noise which is never larger than $0.1a_c$, and ω_1 , ω_2 , ω_3 are frequencies determined by the bicoherence spectrum. Certainly the actual shear layer anemometer signals are more complex than these, but the bicoherence measurements indicate that the strongest interactions that occur in the developing jet shear layers will involve some multiple of the excitation frequency and some multiple of the jet column mode. This modeling technique has been shown to capture the dominant features of the coherence spectrum.

An explanation for the influence of the jet column mode on the upstream flow is given by Prakash (1986). The model described by Prakash is shown in Figure 79. In this figure two large-scale vortical structures with opposite rotation interact with one another at the end of the potential core. This generates a pressure field that

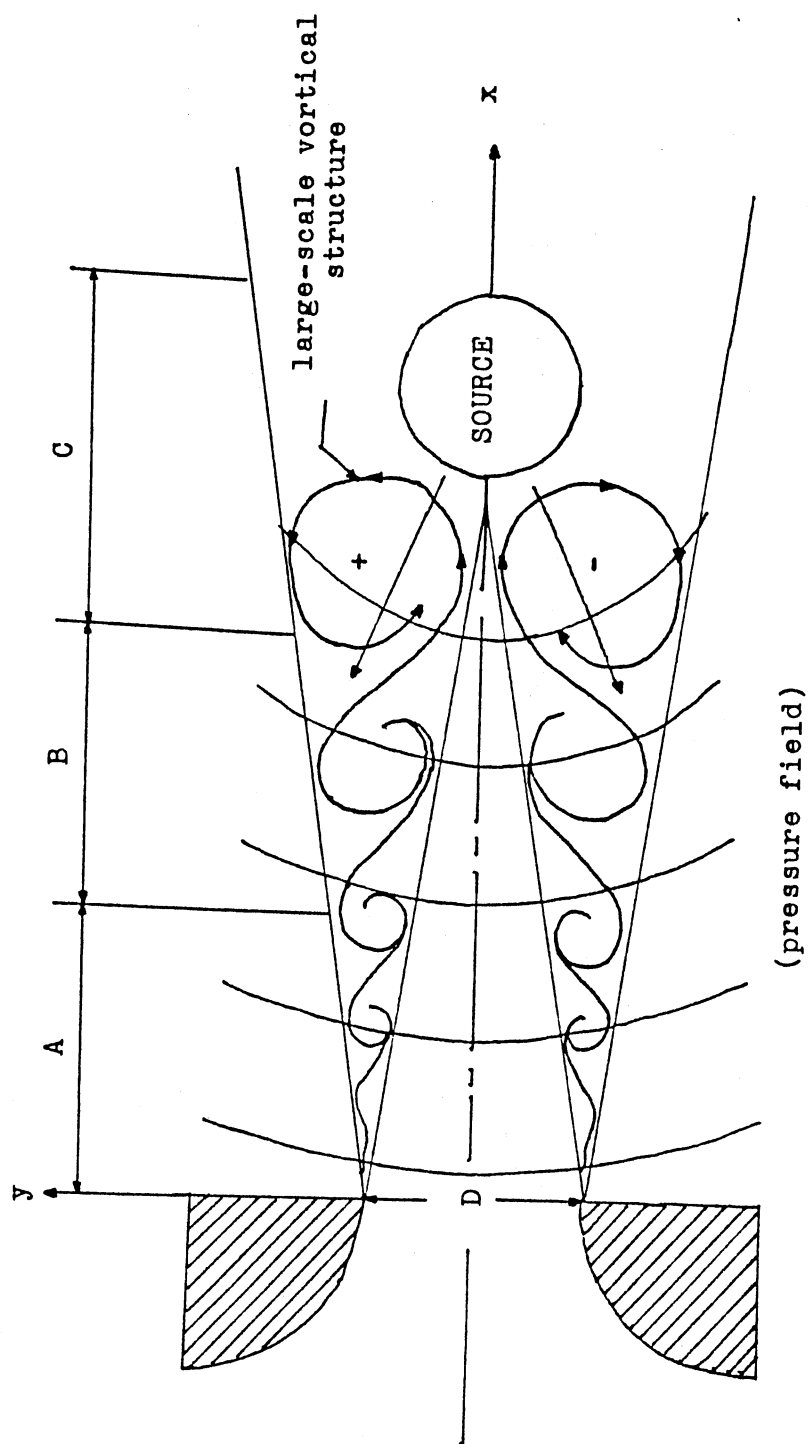


Figure 79. Model of Upstream Influence

travels upstream and interacts with initial shear layer instabilities. The interactions will then generate the periodic structures that are convected to downstream locations to complete the feedback loop. In region "A", the coherence measurements exhibit higher values since both shear layers are equally influenced by the "source" in section C immediately upon leaving the jet nozzle. Coherence values lessen in region "B" due to increasing downstream disturbances.

The coherence measurements in this section show that the initial excited jet shear layer development is coupled to the vortical interactions downstream. This coupling of near exit conditions to the downstream interactions (the jet passage frequency f_m) has been suggested by both the power spectrum and the bicoherence spectrum. In the next section the coherence functions will be examined for the untuned jet.

3.5.3 Coherence and Phase Development

at $f_m = 2200$ Hz

The "untuned" coherence measurements, like the "untuned" power spectra and bicoherence measurements, are vastly different from the "tuned" measurements. Figure 80 shows the coherence and phase measurements at $x/D = 0.5$. The only coherence at $x/D = 0.5$ occurs at the lower frequencies of 0-400 Hz. This corresponds to frequencies

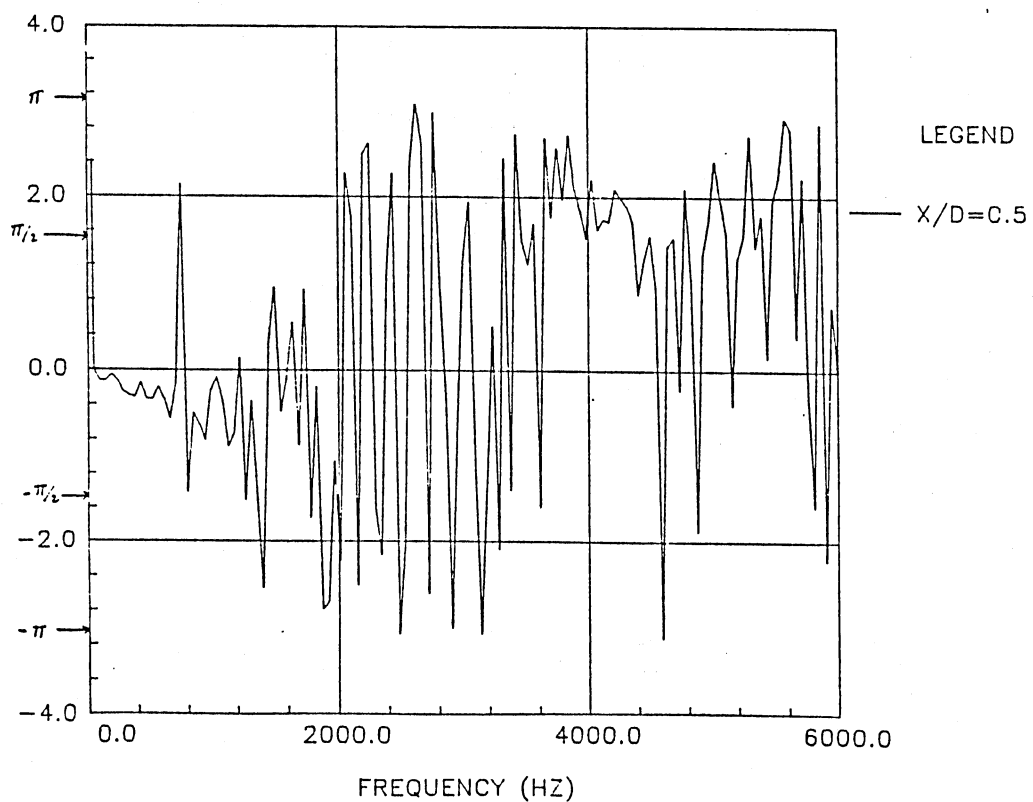
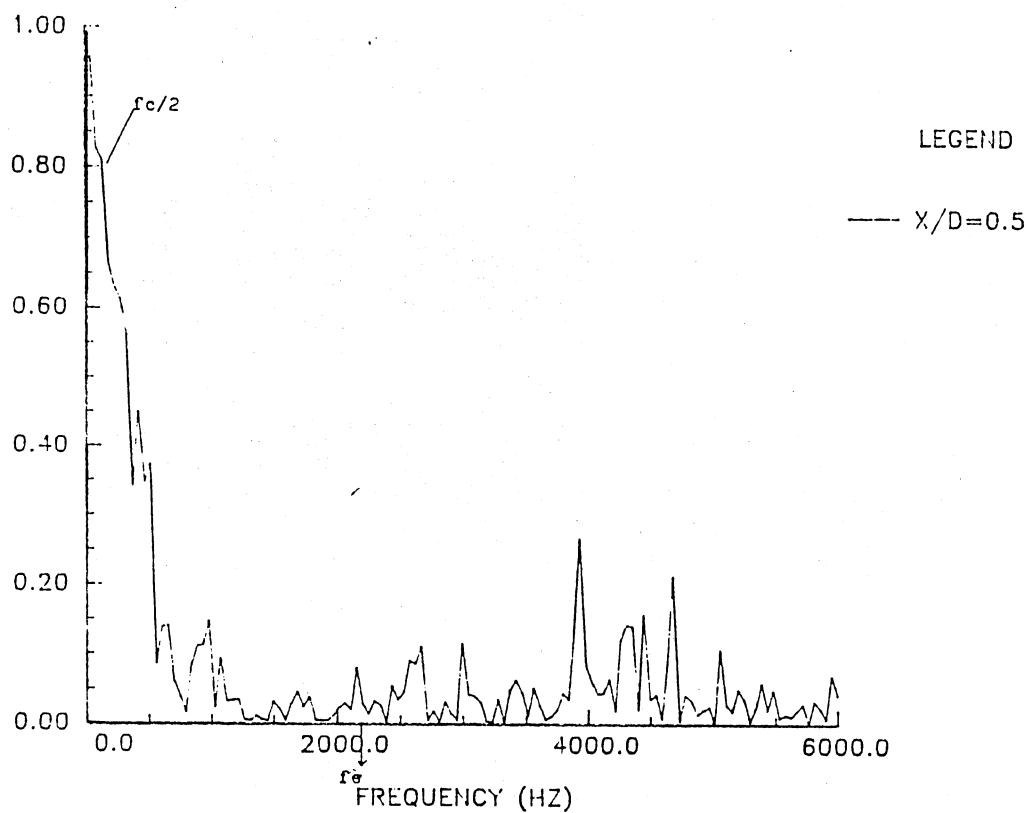


Figure 80. Coherence and Phase at $x/D = 0.5$
($f_e = 2200$ Hz)

less than the jet column mode. The coherence of these low frequencies is seen to be very high. The phase coherence at $x/D = 0.5$ shows the shear layers to be completely in phase from 0-600 Hz. This is contradictory of what is expected to happen at this location. It is expected that the shear layers should be π out of phase to indicate lateral oscillations. A phase shift occurs at 600 Hz. Another phase shift occurs at 1100 Hz. The higher frequencies show random phase due to nonexistent coherence levels.

By $x/D = 1.0$ (coherence and phase shown in Figure 81), higher frequencies show coherence. Coherence peaks are located at frequencies 0-400 Hz, 900-1300 Hz, 2100-2300 Hz, and 2700-2900 Hz. These coherence peaks are centered around $f_{c1}/2$, $f_{c2}/2$, f_{c3} , and $f_{c3}+3f_{c1}/2$. The phase coherence at $x/D = 1.0$ shows zero phase angle from 0-200 Hz. Again this is difficult to explain as to why the phase angle is not π out of phase. From 200 Hz until 4000 Hz the phase coherence shows steady drift from zero phase angle to π out of phase.

Figure 82 shows the coherence and phase at $x/D = 1.5$. The peaks at $x/D = 1.5$ show that coherence between the two shear layers occurs between the frequencies 900-1700 Hz. This relates to the frequencies between $(f_{c3}-f_{c1})/2$ and $(f_{c3}+3f_{c1})/2$. The phase coherence for $x/D = 1.5$ shows a steady drift for frequencies 0 to 2400 Hz. The drift is

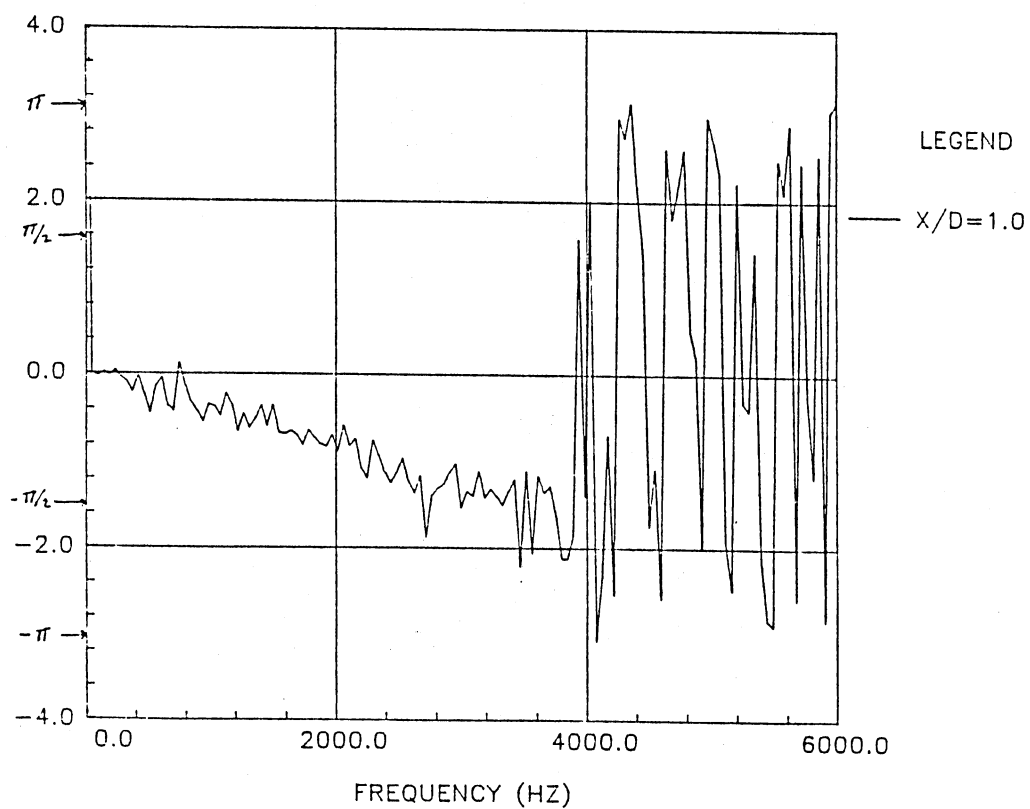
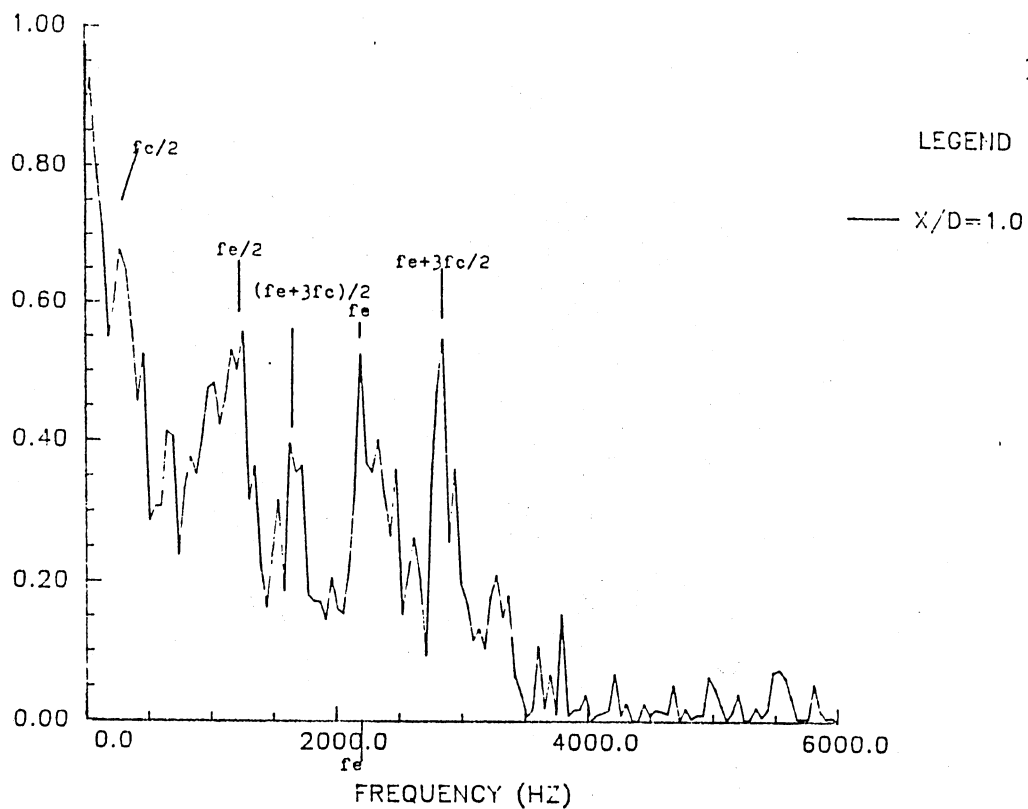


Figure 81. Coherence and Phase at $x/D = 1.0$
($f_e = 2200$ Hz)

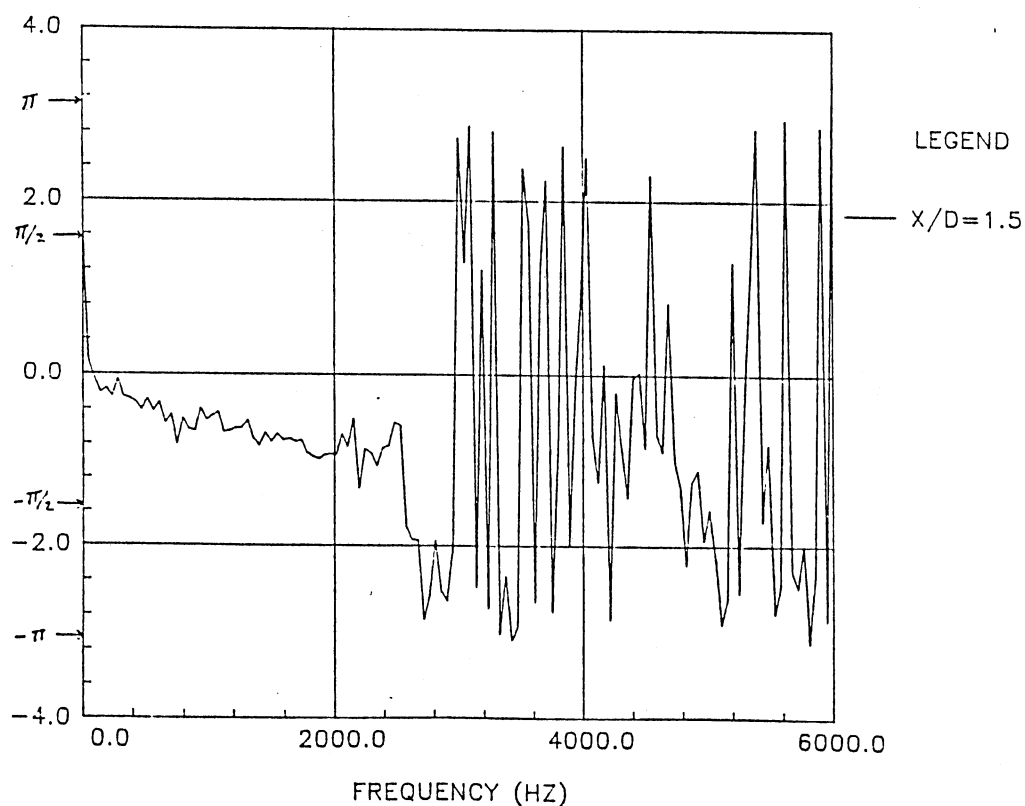
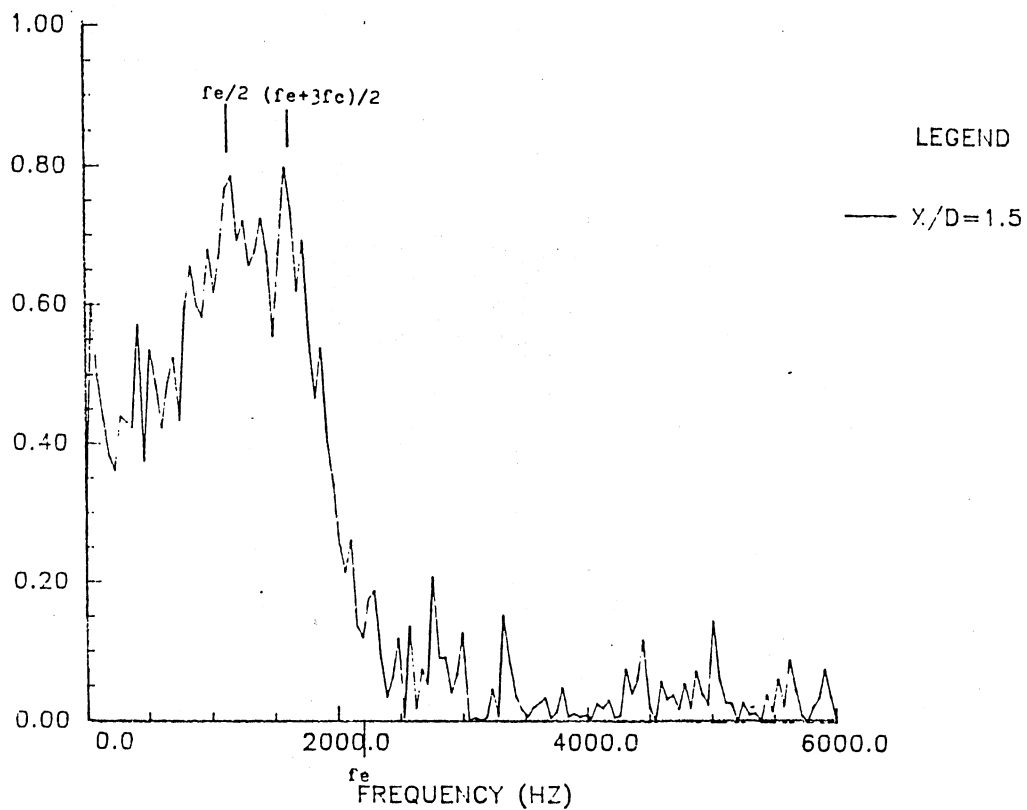


Figure 82. Coherence and Phase at $x/D = 1.5$
($f_e = 2200$ Hz)

from zero phase angle to $\pi/2$ out of phase. A phase shift to π out of phase occurs at 2400 Hz. This phase shift occurs at mode $f_{ac} + f_{ac}/2$.

By $x/D = 3.0$, Figure 83, the coherence has shifted to lower frequencies. Frequencies 0-900 Hz show very high coherence. Frequencies higher than 2200 Hz show almost no coherence. The phase coherence for $x/D = 3.0$ is very similar to that of $x/D = 1.5$. By the end of the potential core, $x/D = 4.0$, the entire frequency range shows no coherence (coherence plot at this location not shown).

In the next section correlation measurements will be taken to examine the correlation between the two shear layers.

3.6 Correlation Measurements

This section presents lateral space-time correlations between the two shear layers. The correlation measurements will provide additional information concerning structural patterns in the jet. Correlation measurements are obtained for x/D locations 0.5 to 7.5. Background information on the correlation technique and theory is presented before the results are presented.

3.6.1 Correlation Techniques

The correlation function of two sets of random data describes the general dependence of the values of one set

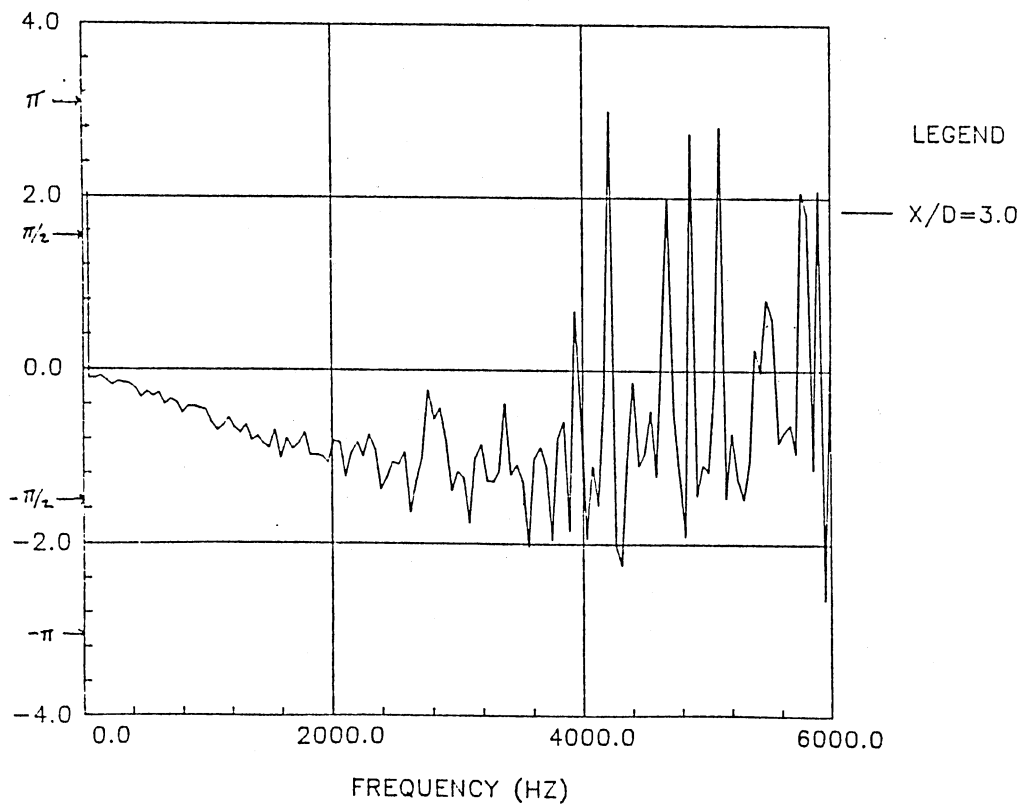
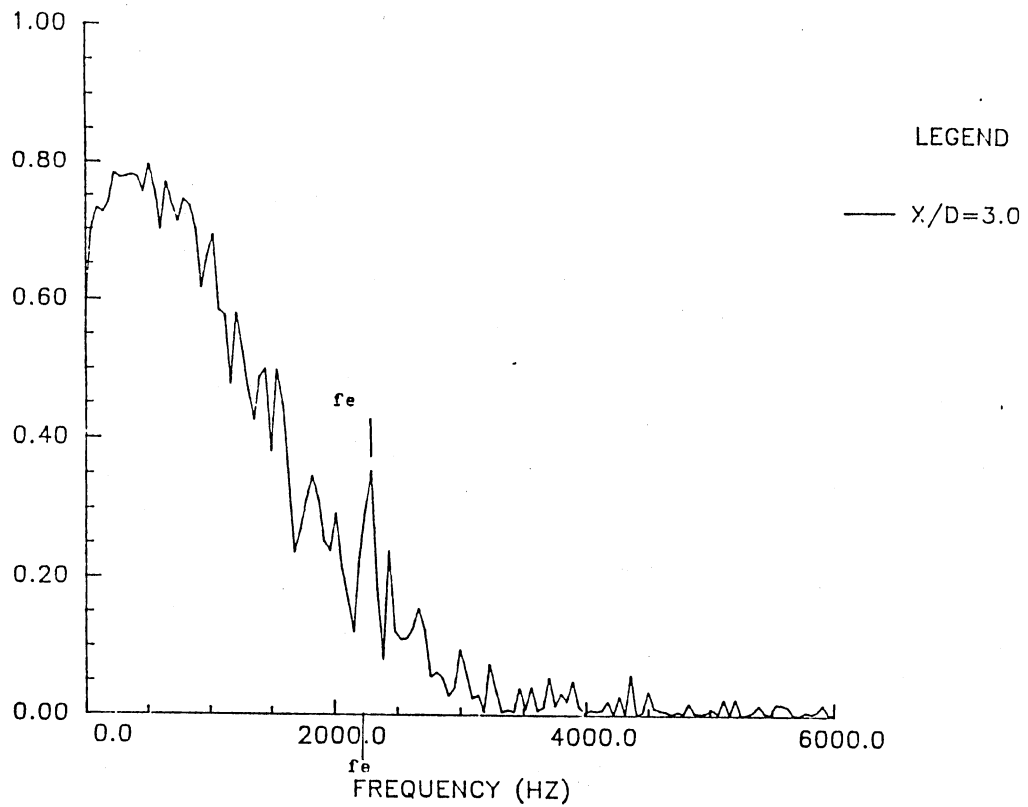


Figure 83. Coherence and Phase at $x/D = 3.0$
($f_e = 2200$ Hz)

of data on the other. An estimate for the correlation function between two real signals of $x(t)$ and $y(t+\tau)$, where τ is a time delay, may be obtained by taking the average product of the two values over a sufficiently large observation time T . The resulting average product will approach an exact correlation function as T approaches infinity:

$$R_{xy}(\tau) = \lim_{T \rightarrow \infty} \frac{1}{T} \int_0^T x(t)y(t+\tau)dt \quad (3.40)$$

The function $R_{xy}(\tau)$ is always a real-valued function which may be either positive or negative. $R_{xy}(\tau)$ does not necessarily have a maximum at $\tau = 0$. $R_{xy}(\tau)$ displays symmetry about the ordinate when x and y are interchanged. That is,

$$R_{xy}(-\tau) = R_{yx}(\tau) \quad (3.41)$$

Two useful relationships which bound the absolute value of the correlation function are

$$|R_{xy}(\tau)| \leq R_{xx}(0)R_{yy}(0) \quad (3.42)$$

$$|R_{xy}(\tau)| \leq \frac{1}{2}[R_{xx}(0) + R_{yy}(0)] \quad (3.43)$$

When $R_{xy}(\tau) = 0$, $x(t)$ and $y(t)$ are said to be uncorrelated. If $x(t)$ and $y(t)$ are statistically independent, then $R_{xy}(\tau) = 0$ for all time displacements. $R_{xy}(\tau)$ is then normalized by the RMS fluctuations to give

a correlation coefficient that is bounded between 0 and 1.

Correlation measurements were made at selected x/D locations between 0.25 and 7.5. The hot-wire probes were placed on opposite sides of the centerline in the shear layers at a location $U/U_{\text{ref}} = 0.6$ as in Figure 73. Each correlation measurement represents an ensemble average over 100 samples. The time delay is $\tau = \pm 0.01$ seconds. The program used can be viewed in Appendix A.

3.6.2 Correlation Measurements at

$$\underline{f_{\text{ref}} = 2650 \text{ Hz}}$$

The correlation at $x/D = 0.25$ is shown in Figure 84. The maximum correlation between the shear layers occurs at a zero time delay. The peak at zero time delay is positive and shows a value of 0.88. This is a very high value of correlation meaning the two shear layers at this point are dependent to one another. The positive value of correlation means the flow is in a symmetric pattern. This contradicts the coherence measurements taken. From the coherence measurements an antisymmetric pattern is expected. Since the correlation measurements do not show correlation of particular frequencies it is suggested that the reason a symmetric pattern is indicated is that the higher frequencies that are in phase overshadow the lower π out of phase frequencies thereby indicating symmetric patterns in the near exit case. At $x/D = 0.5$ (Figure 85)

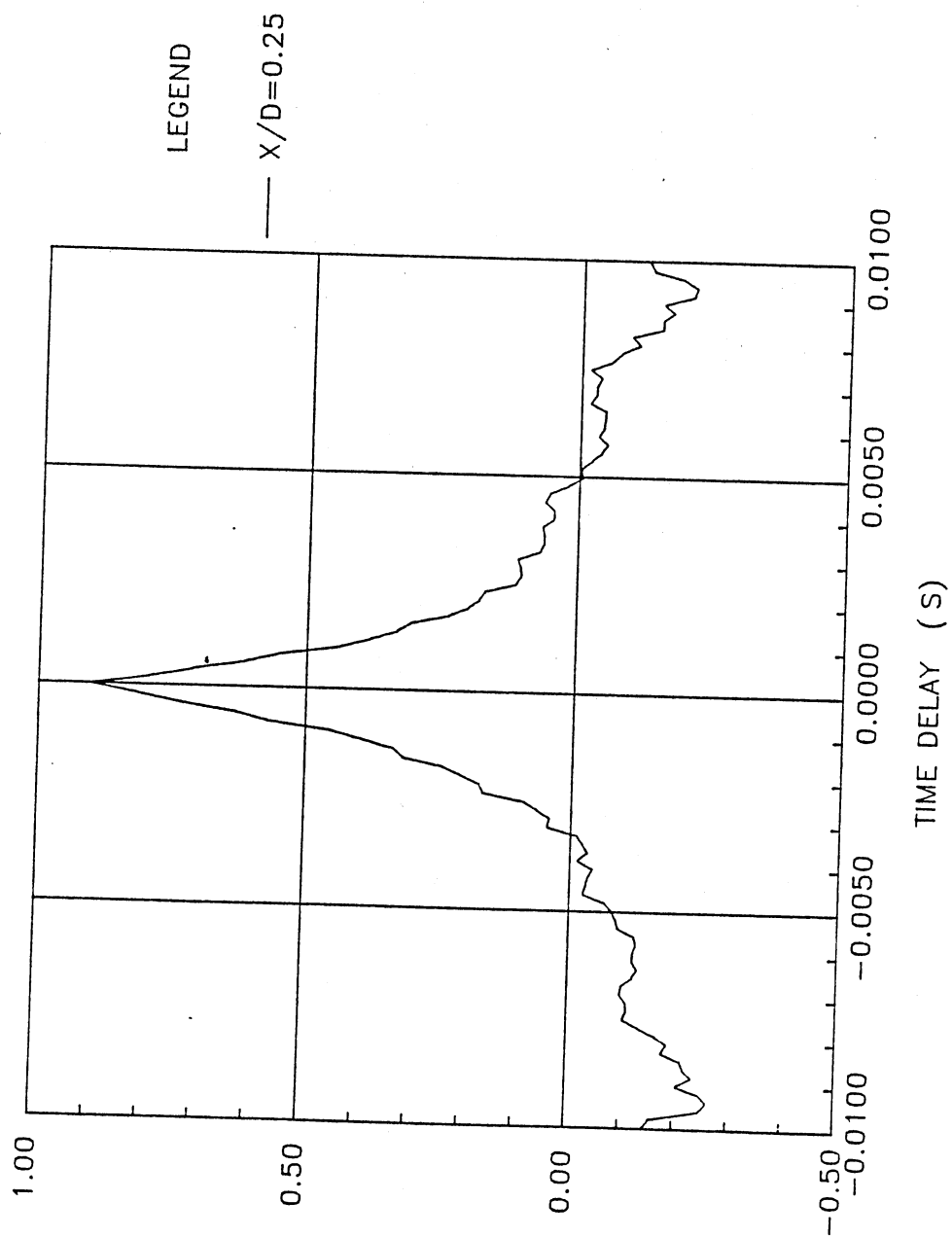


Figure 84. Correlation at $x/D = 0.25$ ($f_e = 2650$ Hz)

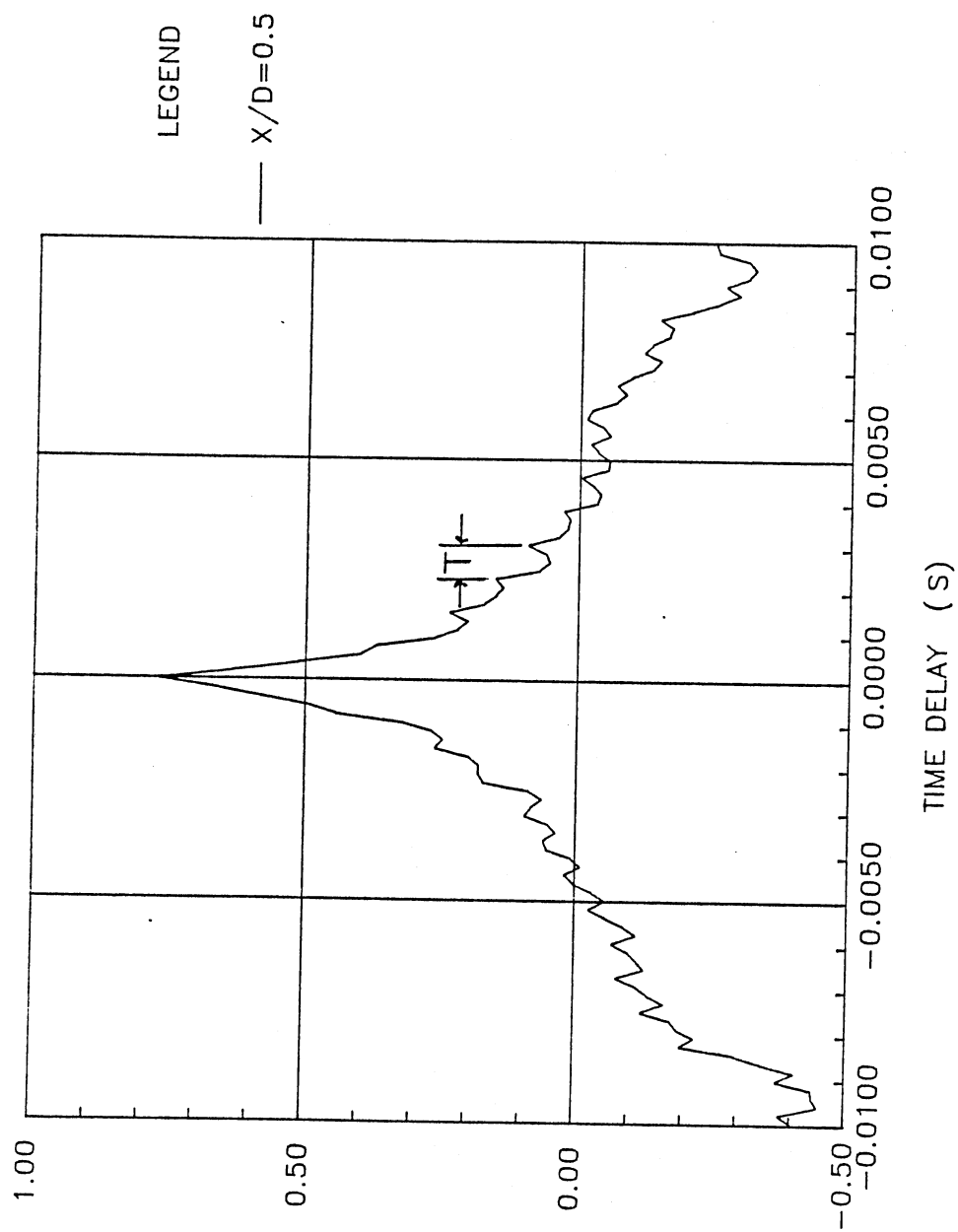


Figure 85. Correlation at $x/D = 0.5$ ($f_e = 2650$ Hz)

the flow is still symmetric with a strong dependence showing between the shear layers at a zero time delay. The correlation coefficient at this point is 0.78. Also noticeable at this location are smaller correlation peaks at nonzero time delays. Average frequencies can be associated to these oscillations by using the relationship

$$f = 1/T \quad (3.44)$$

where T is the time period between peaks. The frequency associated with the time period between each of the oscillations is $f = 1325$ Hz.

The trend of the correlation value getting smaller with downstream distance continues as shown in Figure 86, which shows the correlation plot at $x/D = 1.5$. This figure does not show one peak at zero time delay as do the other previous plots. A positive correlation is shown approximately every 0.0008 second time delay (1325 Hz), while a negative correlation is shown 0.0004 second time delay (2650 Hz) between the positive peaks. The absolute values of the correlation coefficients are approximately equal at a value of 0.15. This is not a very strong value of correlation, meaning the two shear layers at this point are almost independent of one another.

Farther downstream at a location $x/D = 2.5$ (Figure 87), the correlation plot again shows a distinct peak at a zero time delay. The value at this point is 0.12. Again

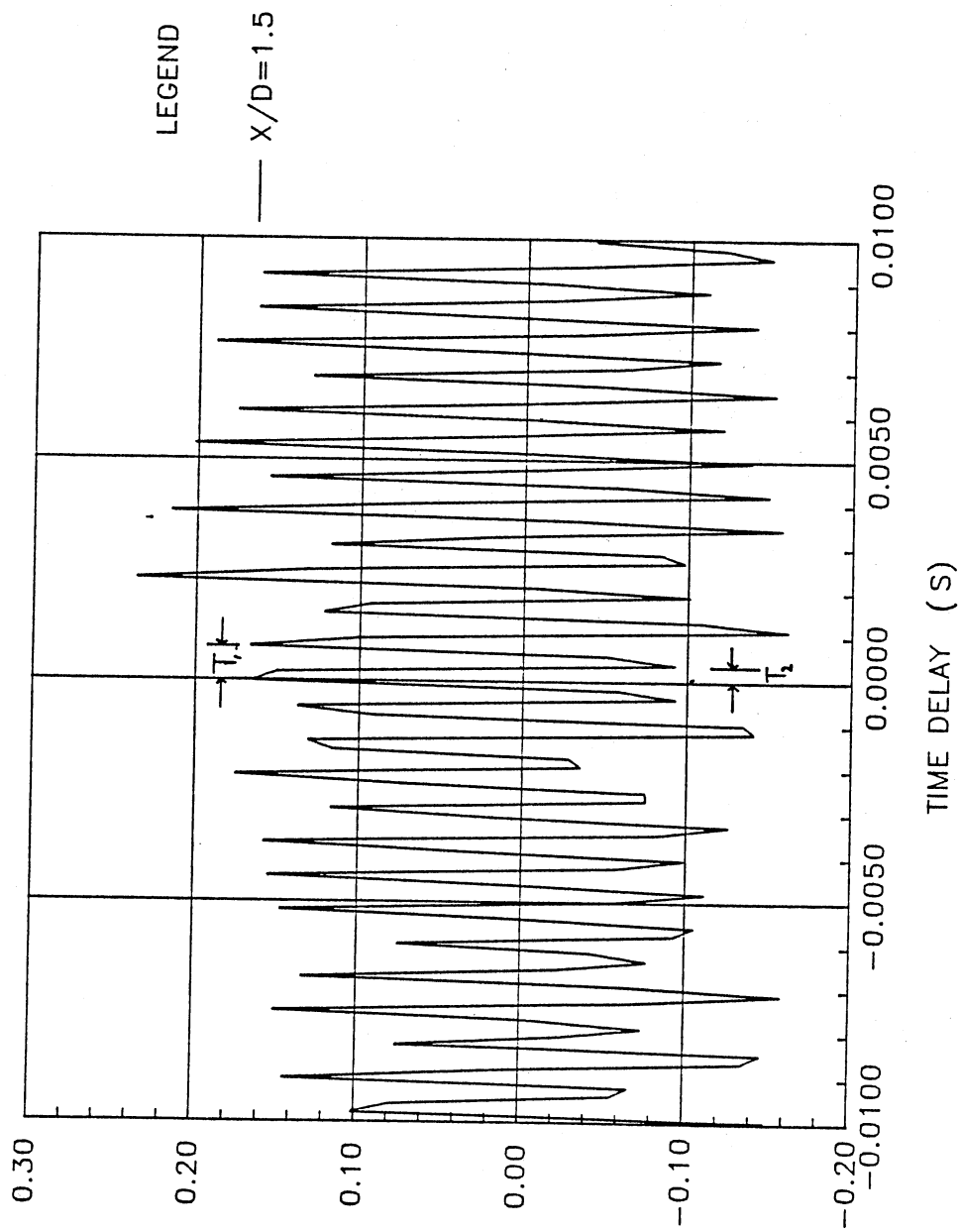


Figure 86. Correlation at $x/D = 1.5$ ($f_e = 2650$ Hz)

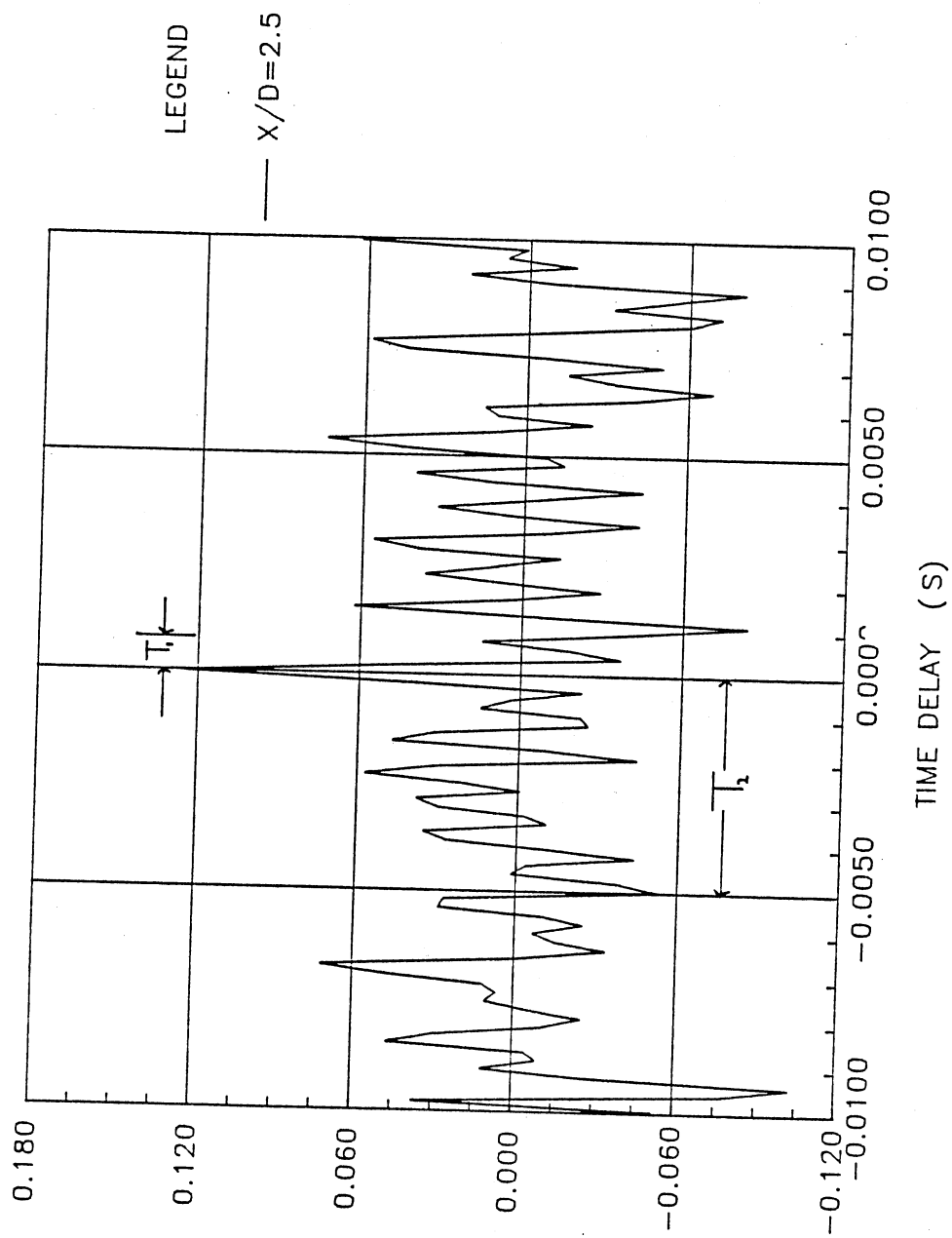


Figure 87. Correlation at $x/D = 2.5$ ($f_e = 2650$ Hz)

this low of a value indicates a slight dependence between the two shear layers. The frequency associated with the time delay between positive peaks is 1325 Hz. The frequency associated with the correlation peak at 0.0055 second time delay is 200 Hz. This corresponds to half of the jet column mode. From the previous section pertaining to coherence, it was noticed that half of the jet column mode is very important in the transition of the jet.

At $x/D = 4.0$, the end of the potential core, the correlation plot (Figure 88) shows a slight negative correlation. This corresponds to a switch from a symmetric to an antisymmetric pattern caused by the merging of the shear layers. This switch is also observed by other authors: Antonia et al. (1983) and Thomas & Goldschmidt (1986). Average frequencies can be associated with time delays at 0.0025 seconds and -0.0052 seconds: 390 Hz and 195 Hz respectively. Since $x/D = 4.0$ is at the end of the potential core it is not surprising that the jet column mode and half the jet column mode show correlation between the shear layers.

At all locations downstream from the potential core, the correlation function is similar to that shown in Figure 89 which shows the correlation of the two shear layers at $x/D = 7.5$. A negative correlation at zero time delay is noted. Although the value of the correlation is not a large value, it still suggests an antisymmetric

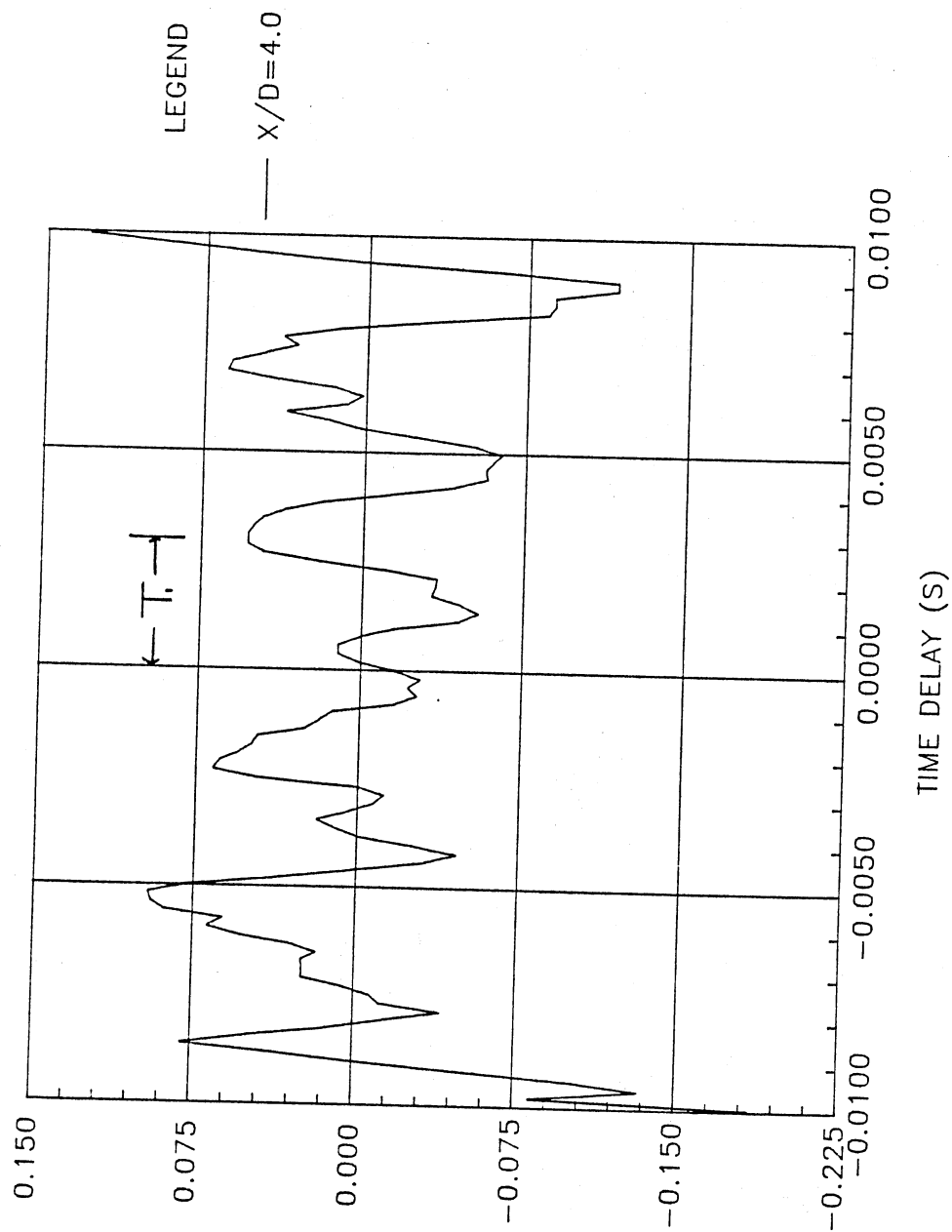


Figure 88. Correlation at $x/D = 4.0$ ($f_e = 2650$ Hz)

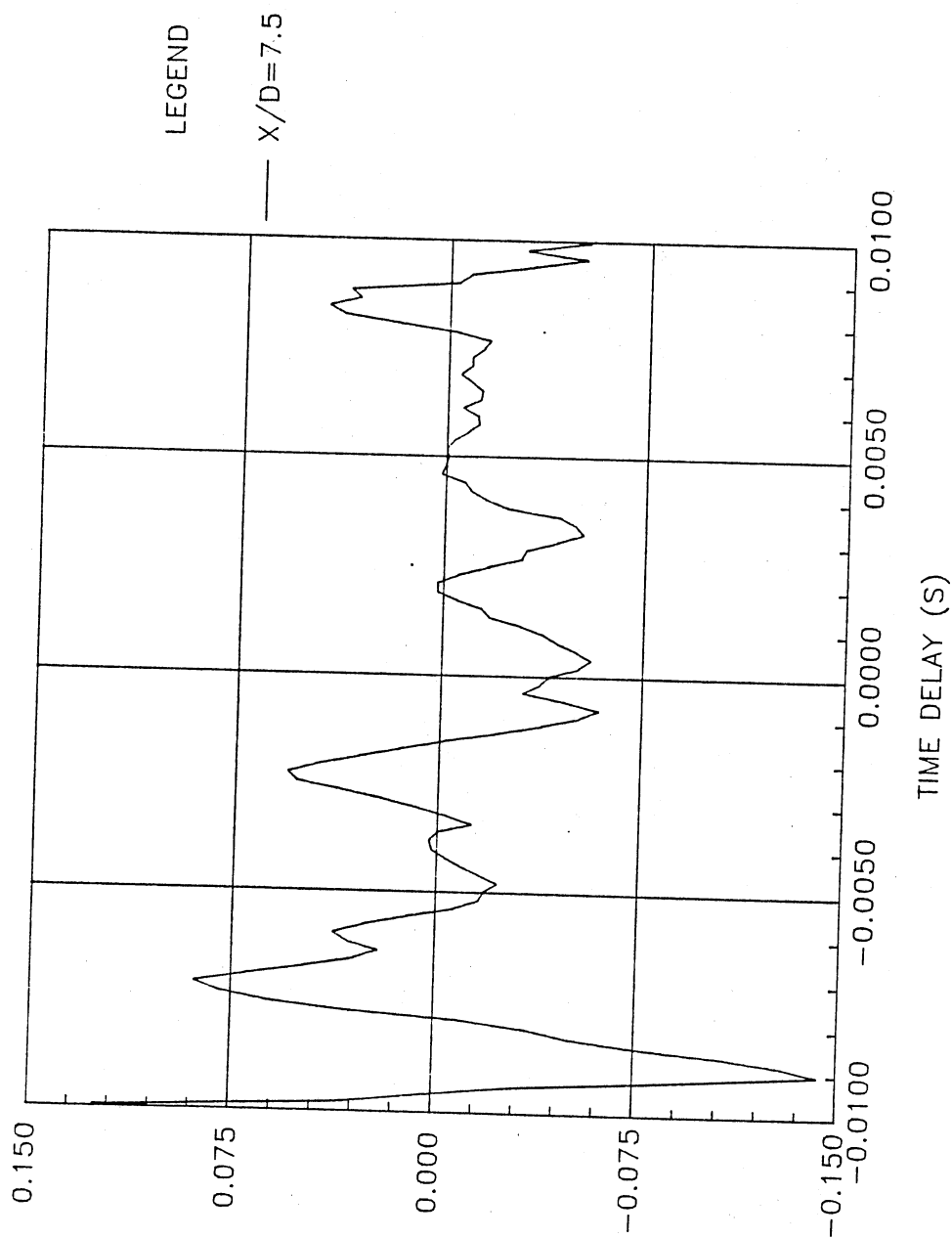


Figure 89. Correlation at $x/D = 7.5$ ($f_e = 2650$ Hz)

structural arrangement in the flow. This antisymmetric structural pattern agrees with the model presented in the previous section shown in Figure 79. The low value of the correlation is due to the random turbulence that occurs downstream of the potential core. Thomas and Brehob (1986) have shown that the antisymmetric structures can be tracked as far downstream as $x/D = 120$. They also showed that the frequency of oscillations associated with the structures are given by the relationship

$$fb/U_{\text{rms}} = 0.1 \quad (3.45)$$

where f is the frequency of oscillation, b is the mean velocity half-width, and U_{rms} is the maximum mean velocity.

3.6.3 Correlation Measurements at

$$\underline{f_{\text{osc}} = 2200 \text{ Hz}}$$

Figure 90 shows the correlation at $x/D = 0.25$. This figure shows negative correlation at the exit of the jet. Negative correlation corresponds to an antisymmetric structural pattern. This antisymmetric pattern at the jet exit is expected since it shows lateral oscillations between the shear layers. It is interesting that the untuned case showed negative while the tuned case did not. This would seem to suggest that the upstream influence of the untuned jet is greater than that of the tuned jet.

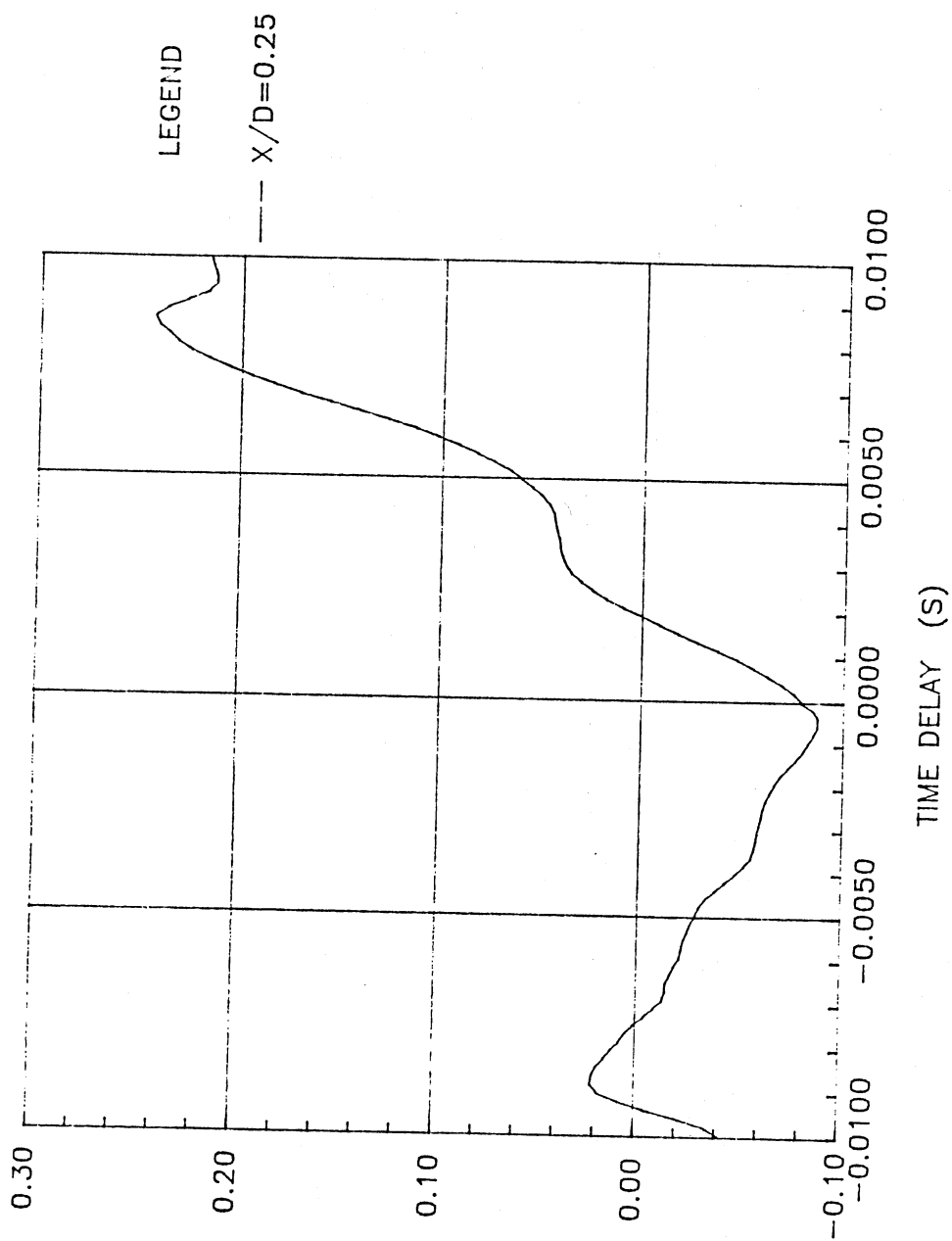


Figure 90. Correlation at $x/D = 0.25$ ($f_e = 2200$ Hz)

The correlation at $x/D = 0.5$ is shown in Figure 91. At zero time delay almost no correlation is shown between the two shear layers. The frequency associated with the correlation peak at 0.0025 second time delay is 390 Hz. Again the jet column mode is shown to play a major role in the transition of the jet. By $x/D = 1.0$, Figure 92, low correlation is shown at zero time delay. The average frequency associated with the alternating correlation peaks is 1100 Hz. The trend of low correlation at zero time delay continues downstream to the end of the potential core (see Figures 93 and 94). It is interesting to note in Figure 93 ($x/D = 3.0$) that the time delay associated with half the jet column mode (0.005 seconds) shows negative correlation. Downstream from the end of the potential core, negative correlation is shown for all x/D locations. This again indicates antisymmetric structural patterns.

The bispectral, coherence, and correlation measurements have all indicated a definite coupling of the near exit shear layers with that of the jet column mode at the end of the potential core. If the antisymmetric patterns shown at the jet exit are caused by the coherent structures at the end of the potential core, one would expect correlation between the shear layers at the near exit to that at the end of the potential core. Figure 95 shows the probe placement used to determine if the

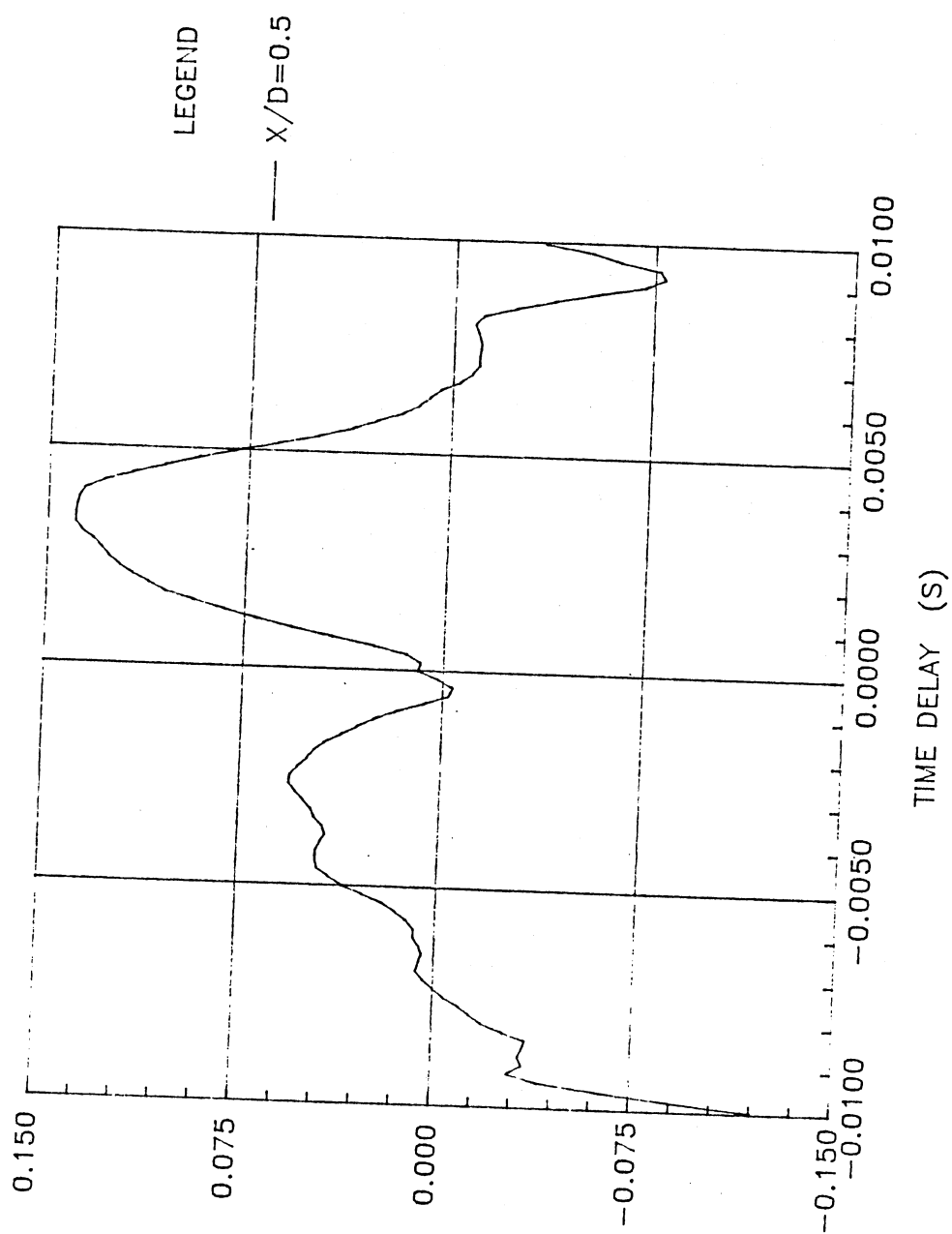


Figure 91. Correlation at $x/D = 0.5$ ($f_e = 2200$ Hz)

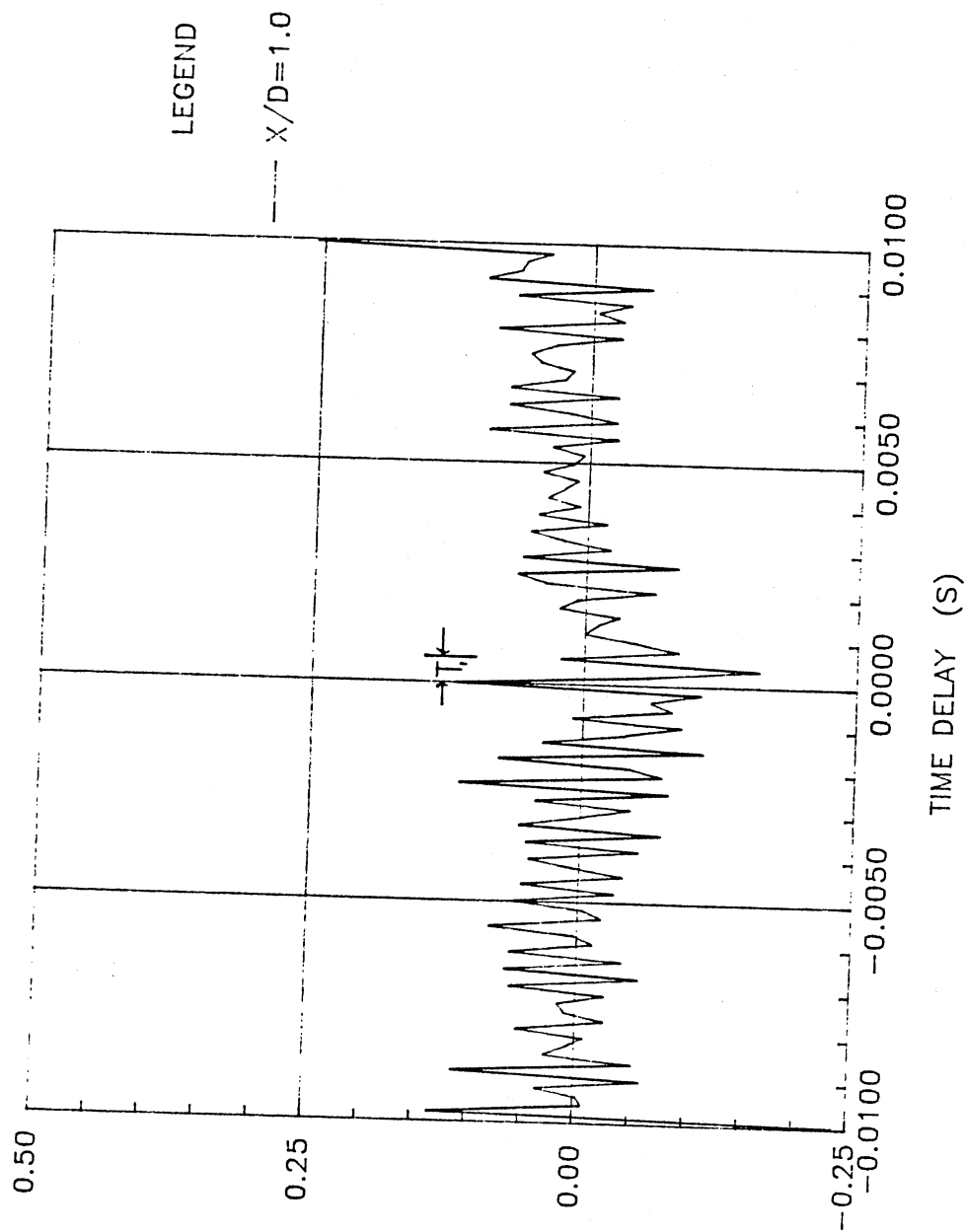


Figure 92. Correlation at $x/D = 1.0$ ($f_e = 2200$ Hz)

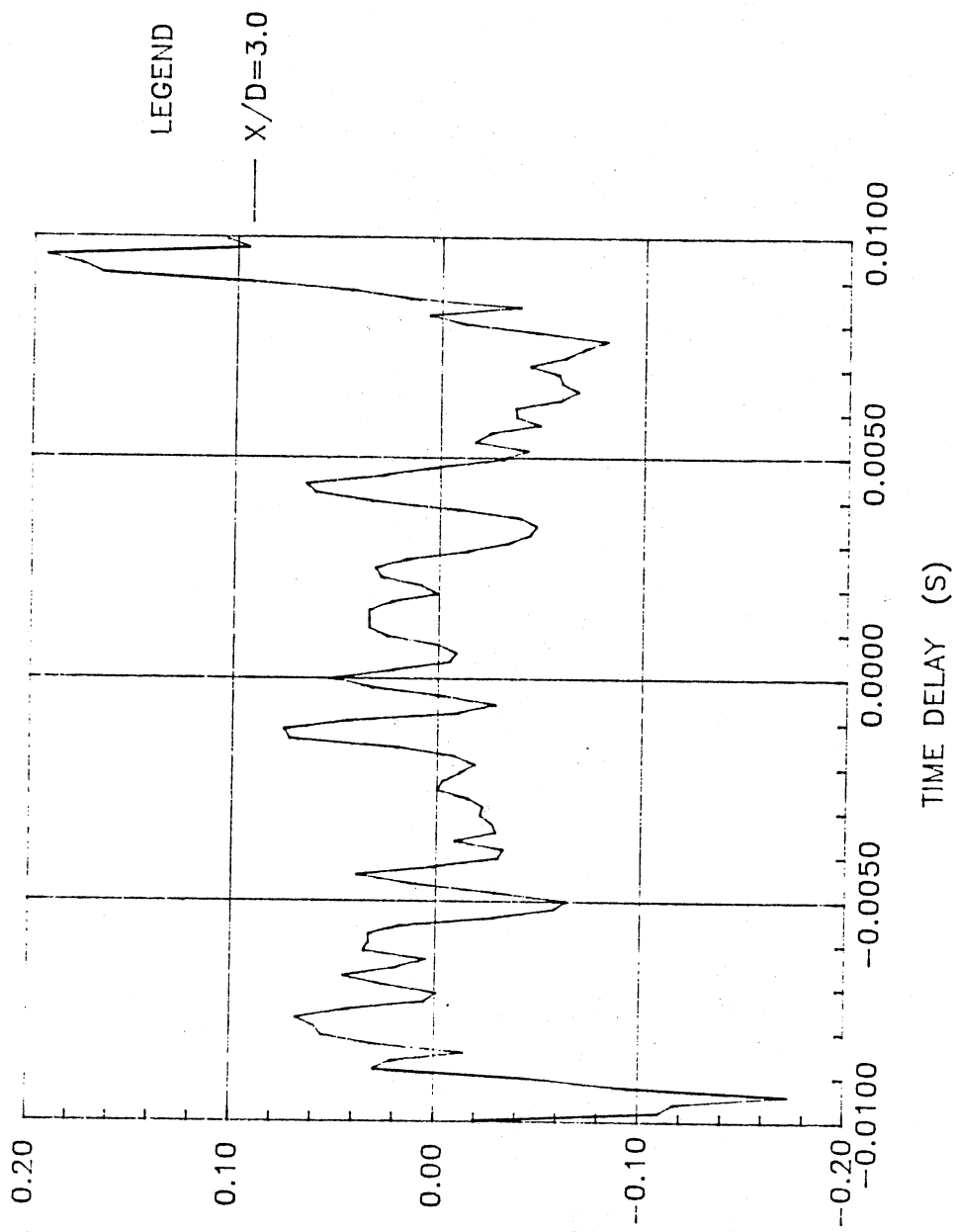


Figure 93. Correlation at $x/D = 3.0$ ($f_e = 2200$ Hz)

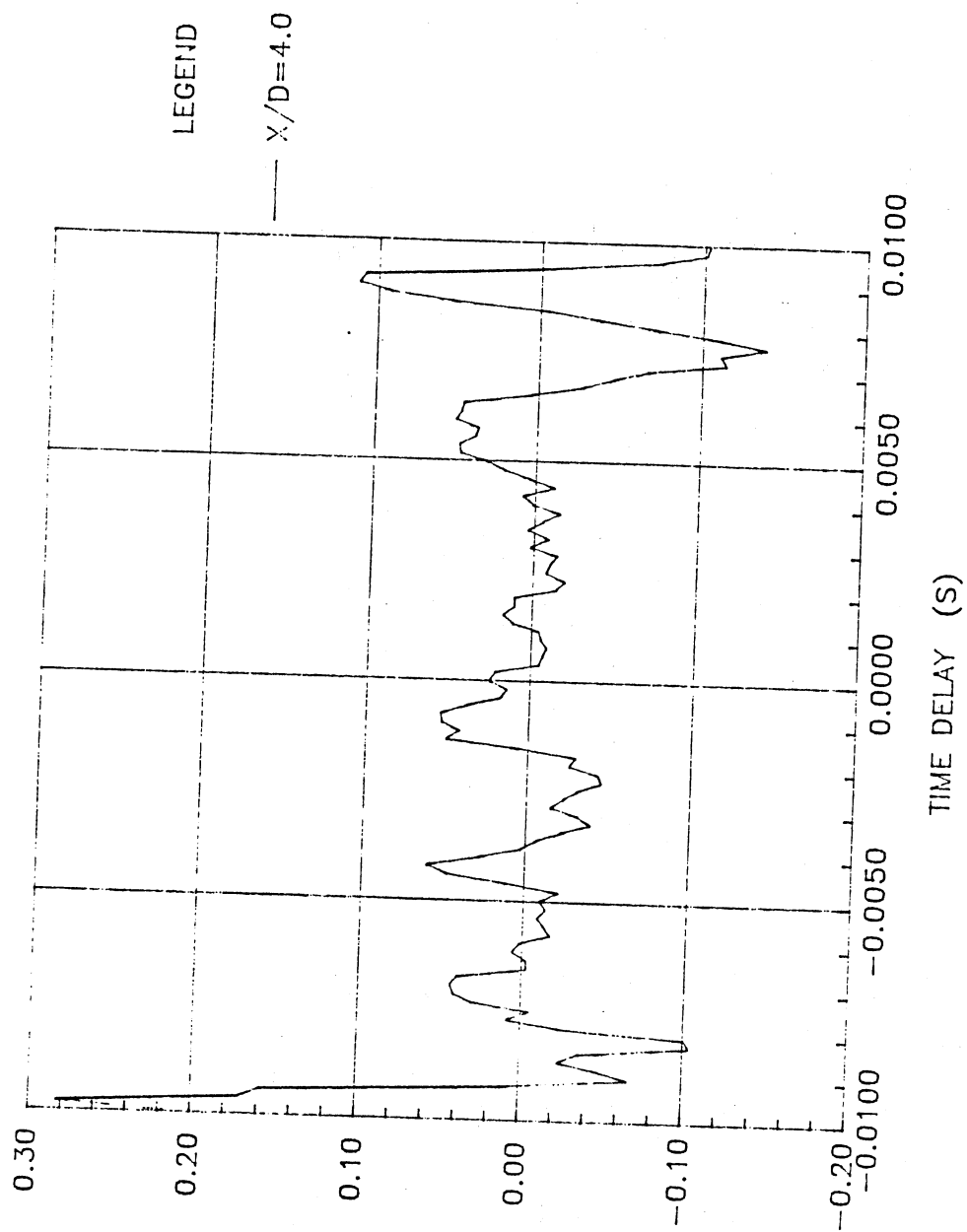


Figure 94. Correlation at $x/D = 4.0$ ($f_e = 2200$ Hz)

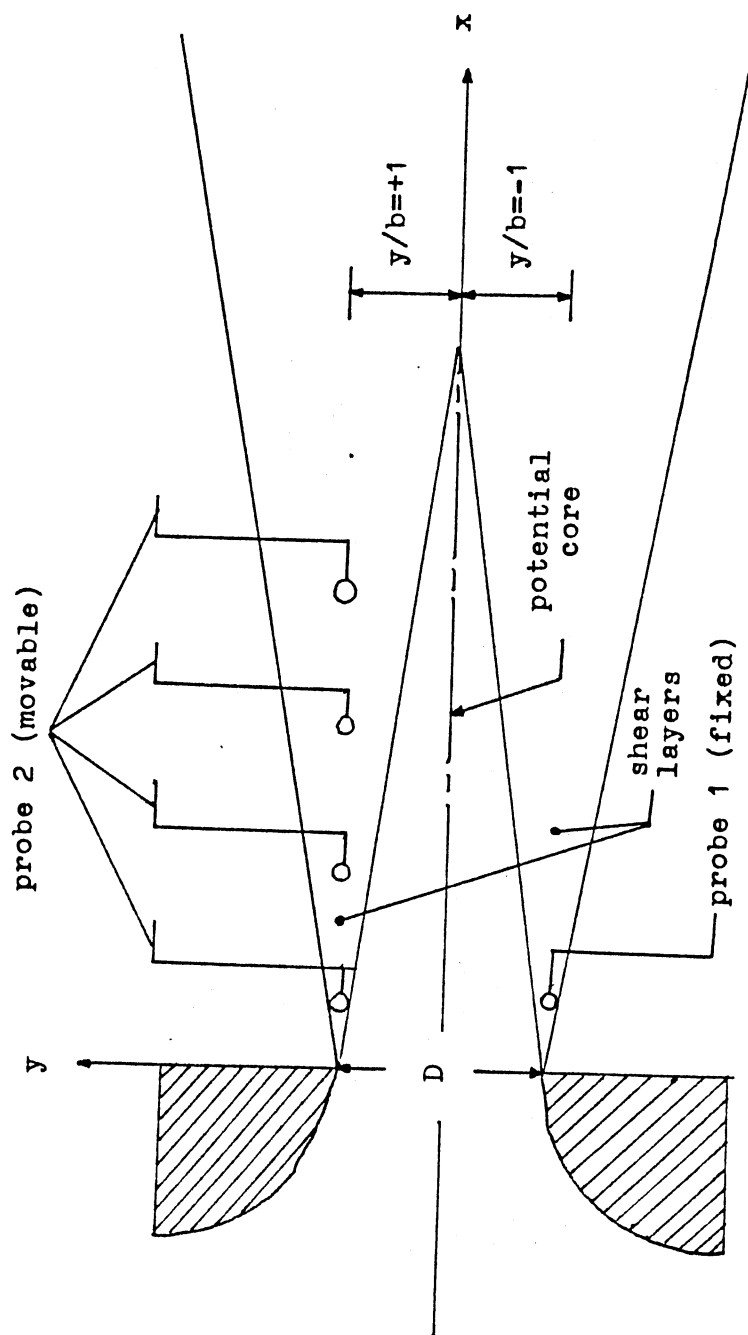


Figure 95. Probe Schematic for Upstream Influence

coherent structures at the end of the potential core influence the jet at upstream locations.

Figures 96-98 show the results of placing one probe at $x/D = 0.25$ and the other probe at $x/D = 3.0$, 3.5 , and 4.0 respectively. These figures show a definite correlation at zero time delay. These figures prove that the downstream coherent structures produced a significant effect on the near exit conditions of the untuned jet.

The next chapter will discuss the conclusions to be drawn from the measurements presented in this chapter.

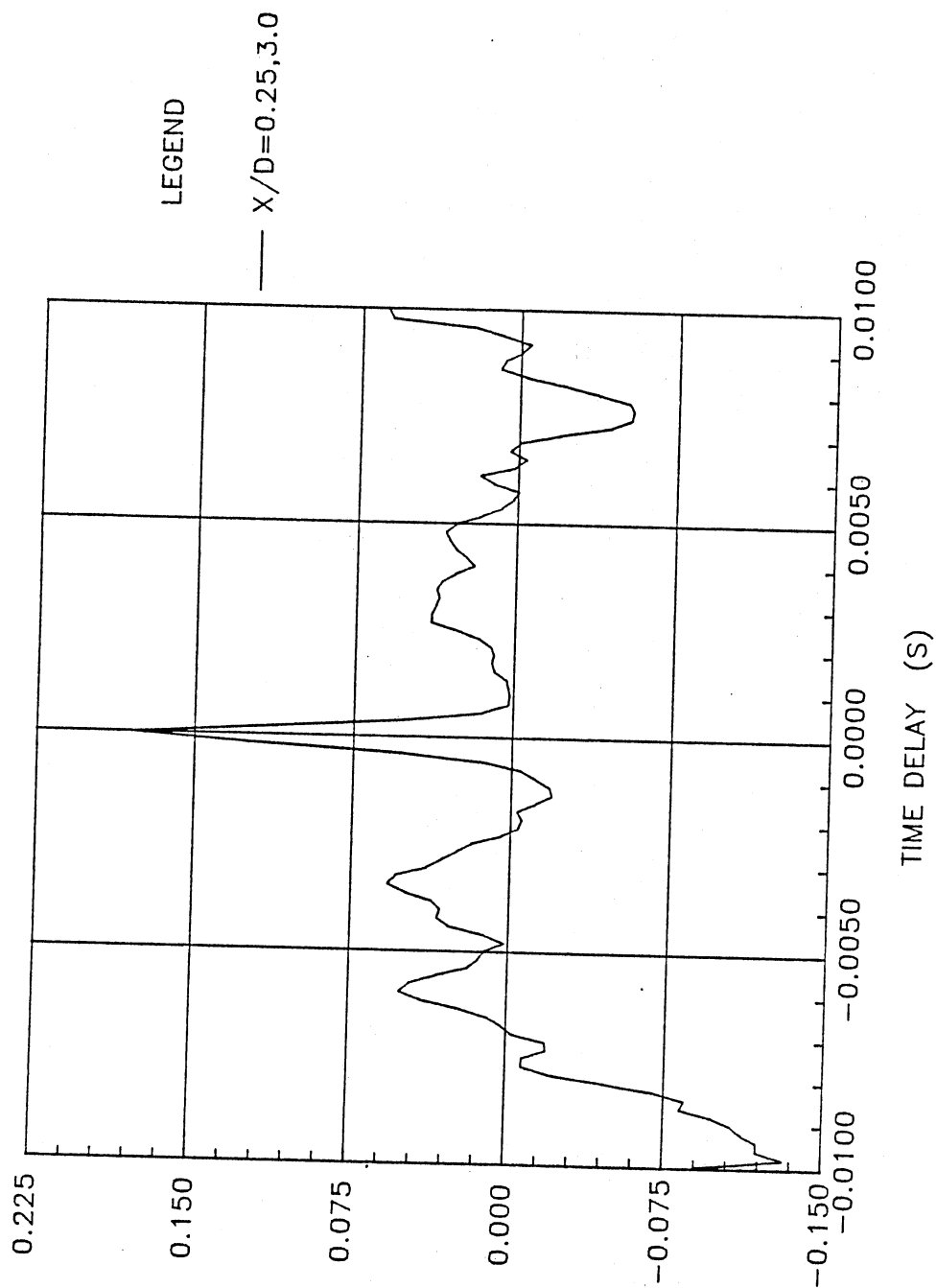


Figure 96. Correlation at $x/D = 0.25$ and 3.0
($f_e = 2200$ Hz)

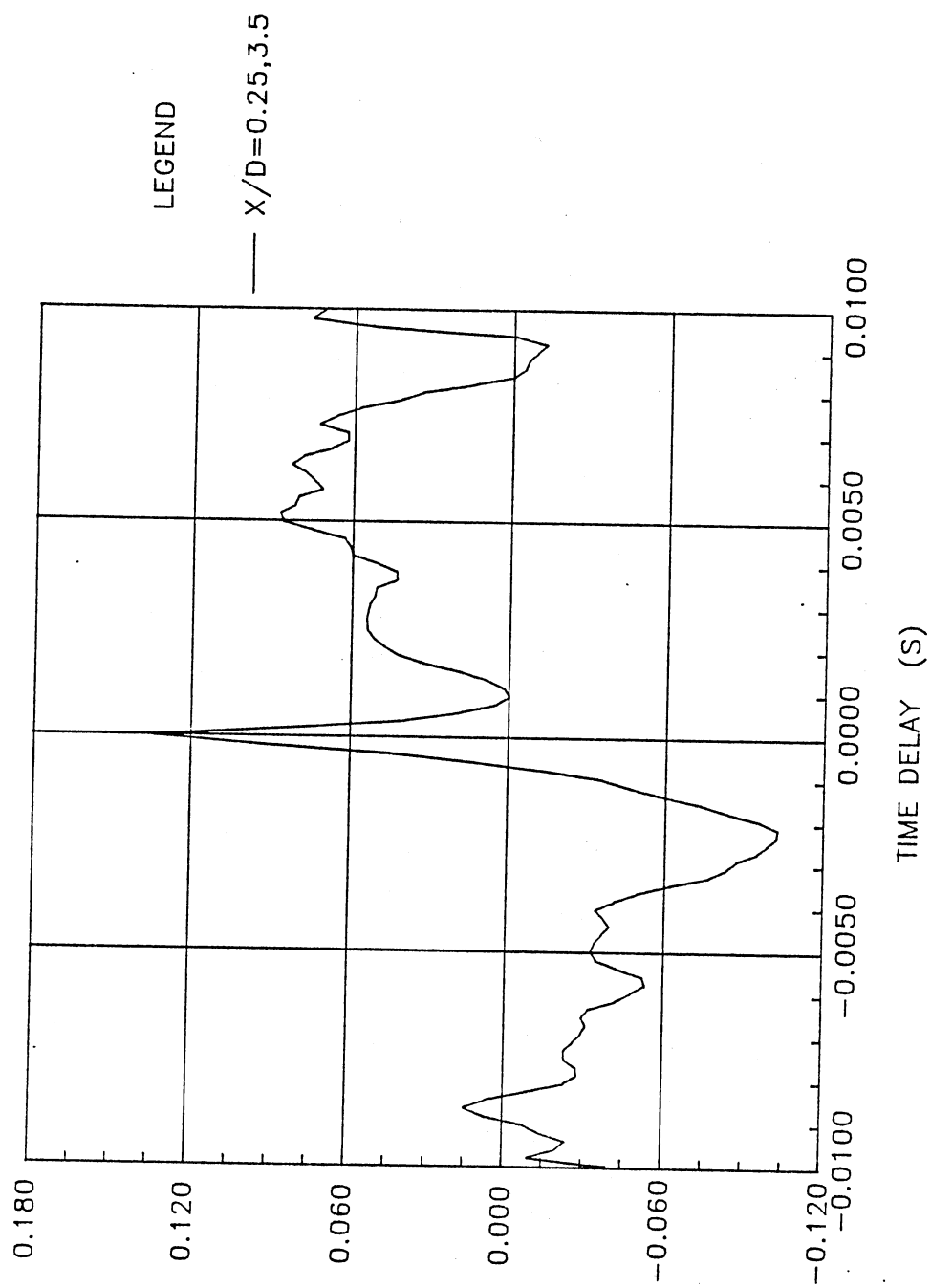


Figure 97. Correlation at $x/D = 0.25$ and 3.5
($f_e = 2200$ Hz)

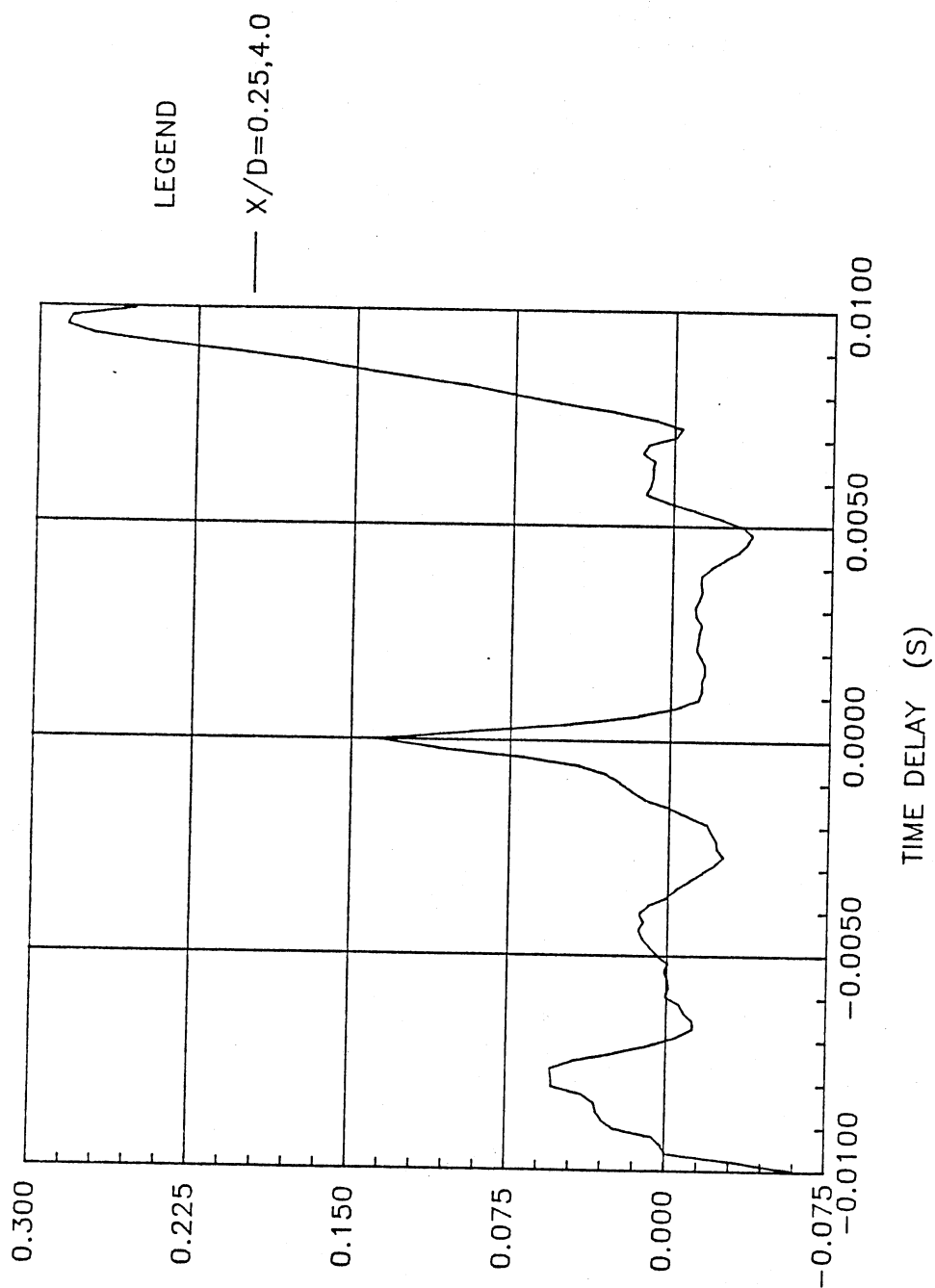


Figure 98. Correlation at $x/D = 0.25$ and 4.0
($f_e = 2200$ Hz)

CHAPTER IV

CONCLUSION AND RECOMMENDATIONS

In this chapter the sum total results of the measurements will be discussed for both the tuned ($f_{\text{exc}} = 2650$ Hz) and the untuned ($f_{\text{exc}} = 2200$ Hz) jet. Conclusions will be presented and recommendations for further studies will be suggested.

4.1 Discussion of Results

4.1.1 The "Tuned" Jet

The "tuned" jet refers to the jet under excited conditions in which the excitation frequency is a close multiple of the jet column mode f_c . In this research the tuned jet case is achieved by the sinusoidal excitation of the flow at a frequency $f_{\text{exc}} = 2650$ Hz. The measurements taken at this excitation frequency will be discussed in this section.

The power spectrum, bicoherence spectrum, and coherence measurements show the most obvious feature of transition in the jet. The power spectrum and bicoherence spectrum measurements strongly indicate the importance of the jet column mode f_c in determining the initial spectral development and energy transfer which characterizes the

jet transition, while the coherence measurements show that the modes created by the jet column mode interactions are coherent across the jet. By a downstream location of $x/D = 1.0$, the jet column mode has formed new modes by interacting with the excitation frequency and both its subharmonic and harmonic modes. The modes formed by these interactions are shown in the power spectrum to be $2f_{\text{jet}} - f_c$, $f_{\text{jet}} \pm f_c$, and $(f_{\text{jet}} \pm f_c)/2$. The bicoherence measurements show that these modes are created by nonlinear interactions of the form: $2f_{\text{jet}} - f_c \rightarrow 2f_{\text{jet}} - f_c$, $f_{\text{jet}} - f_c \rightarrow f_{\text{jet}} - f_c$, $f_{\text{jet}} + f_c \rightarrow f_{\text{jet}} + f_c$, $f_{\text{jet}} - (f_{\text{jet}}/2 - f_c) \rightarrow (f_{\text{jet}}/2 + f_c)$, and $(f_{\text{jet}} - f_c) - f_{\text{jet}}/2 \rightarrow f_{\text{jet}}/2 - f_c$. These modes can be traced as far downstream as $x/D = 1.75$.

Digital demodulation techniques show that modes generated about the excitation frequency at these near exit locations are produced by amplitude and phase modulation, with phase modulation being the dominant modulation. Miksad, et al. (1982) has shown that amplitude and phase modulations are produced by nonlinear interactions involving a low-frequency mode, in our case the jet column mode f_c . Further they found that the larger the nonlinear effects, the larger the phase modulations will become. The presence of high levels of phase modulation at the near exit of the jet again shows that nonlinear effects are occurring in the initial development of the shear layers.

The results of the coherence measurements suggest that the initial excited jet shear layer is also strongly affected by downstream vortical interactions which couple the near exit flow with that of downstream locations. These measurements indicate that a global resonance mechanism operates in the jet flow, exerting upstream influence on the near exit shear layers. This influence is determined to involve the jet column mode, f_c , and half the jet column mode, $f_c/2$ (also seen in the power spectra and bicoherence spectra). This influence by the jet column mode and half the jet column mode is seen only at $x/D < 1.0$. It is expected that the streamwise evolution of the disturbance induced near the nozzle exit results in a loss of coherence downstream.

Since nonlinear interactions are shown to exist at locations right at the nozzle lip, it is understandable why the application of linear stability theory had limited success. Good agreement between linear theory and measurements was shown for locations $x/D < 1.25$, but even at these locations the nonlinear effects, along with high amplitudes of instability fluctuations, were strong enough to produce discrepancies. In order to achieve better agreement between theory and measurements, the stability theory needs to incorporate nonlinear effects.

As the measurements progress downstream from the nozzle exit, the importance of "pairing" in transition can

be seen. Interactions take place whereby two neighbouring vortices coalesce to form a single, larger vortex. This process is seen as a halving of frequency. Continuous repetition of this pairing process is responsible for the entrainment of surrounding fluid which allows the mixing layer to grow. The first pairing can be seen as early as $x/D = 0.25$ where the subharmonic frequency ($f_{\omega}/2$) is first noticed in the power spectrum. This pairing is produced by the nonlinear interaction $f_{\omega} - f_{\omega}/2 \rightarrow f_{\omega}/2$ (determined by the bicoherence measurements). A second pairing is seen to occur at $x/D = 1.50$. This is the location where the frequency $f_{\omega}/4$ first occurs in the power spectrum. This pairing is brought about by the nonlinear interaction $f_{\omega}/2 - f_{\omega}/4 \rightarrow f_{\omega}/4$ documented in the bicoherence spectrum.

By $x/D = 3.0$ the jet column mode becomes apparent in the power spectra and by $x/D = 4.0$ the jet column mode contains nearly all of the energy in the power spectra. The shift of energy in the power spectra to the jet column mode, which is defined as structural passage frequency near the end of the potential core, indicates the end of the potential core. Correlation measurements at this location indicate the presence of antisymmetric large-scale coherent structures by showing negative correlation between symmetric points on either side of the jet centerline. This contrasts with correlation measurements upstream. Measurements upstream showed strongly

correlated symmetric structures. The symmetric structures at the near exit case were not expected, but it is believed that the higher frequencies that are in phase (symmetric) are overshadowed by the lower frequencies that were shown to be antisymmetric (oscillating π out of phase) by the coherence measurements. The switch from symmetric to antisymmetric structures at the end of the potential core indicate the rearrangement of the structures to some form similar to a Karman-Vortex-Street. Correlation measurements taken further downstream of the potential core continue to indicate antisymmetric coherent structures.

A simple dynamic model of the transition in the jet can be presented now that the importance of the individual measurements have been determined. Transition in the tuned jet occurs as follows:

1. A global resonance mechanism operating in the jet exerts influence upstream to the shear layers at the nozzle lip in the form of the jet column mode and half the jet column mode.

2. The jet column mode and half the jet column mode nonlinearly interact with the excitation frequency to produce sum and difference modes.

3. The nonlinear interactions trigger amplitude and phase modulations involving the excitation frequency and the jet column mode. Phase modulations are dominant

because phase modulations are more effective in transferring energy across the frequency spectrum when large nonlinear effects are present.

4. Increasing nonlinear interactions cause two neighbouring vortices to coalesce and form a single larger vortex. This pairing process allows entrainment of surrounding fluid which permits the mixing layers to grow. A similar process is occurring in the second shear layer creating coherent structures across the potential core of the jet.

5. These symmetric coherent structures meet at the end of the potential core where the structures realign themselves into antisymmetric structures. These antisymmetric structures remain coherent and travel downstream.

6. The rearrangement of the coherent structures at the end of the potential core and their interactions are responsible for the upstream influence in 1.

The differences in the untuned jet will be noted in the next section.

4.2.2 The "Untuned" Jet

The "untuned" jet refers to the jet under excited conditions in which the excitation frequency is not a close multiple of the jet column mode f_c . The untuned jet in this research is obtained by a sinusoidal excitation at

$f_w = 2200$ Hz.

The power spectra and bicoherence spectra show that the jet column mode is also an important feature of transition in the untuned jet. By $x/D = 1.25$ the following modes involving the jet column mode have formed: $(f_w \pm f_c)/2$, $(f_w + 3f_c)/2$, $f_w + f_c$, and $(3f_w + 2f_c)/2$. The bicoherence measurements show that these modes are indeed formed by nonlinear interactions.

Digital demodulation techniques show predominantly the same results as in the tuned jet. Amplitude and phase modulation exists with phase modulation being the stronger modulation. The phase modulation again shows how important nonlinear effects are in the shear layer transition process.

The nonlinear effects producing pairing are also apparent in the untuned jet. However, the pairing is not as easily noticed in the untuned jet. The nonlinear interactions with the jet column mode are strong enough to produce modes on either side of the subharmonic that contain significantly more energy than that of the subharmonic. Therefore it is difficult to notice where the first pairing takes place. The second pairing to produce $f_w/4$ is noticed at $x/D = 2.0$. These pairing are brought about by the nonlinear interactions $f_w - f_w/2 \rightarrow f_w/2$ and $f_w/2 - f_w/4 \rightarrow f_w/4$ as shown in the bispectrum.

The coherence measurements show a very different

picture in the untuned jet than they did in the tuned jet. These measurements show that the only coherent frequency at the near exit ($x/D = 0.5$) is the frequency at half the jet column mode $f_c/2$. The influence of the global resonance at this point is strong enough to provide disturbances which prohibit coherence at other frequencies. The coherence measurements at $x/D = 1.0$ show coherence at other frequencies involving the excitation frequency, subharmonic frequency, the jet column mode, and half the jet column mode as did the tuned jet. A slight discrepancy is seen in the phase coherence measurements because they do not show lateral fluctuations occurring (shown by the shear layers being π out of phase).

The correlation measurements at the jet exit document the "flapping" phenomenon discussed in the introduction. The correlation measurements show antisymmetric coherent structures to exist at $x/D = 0.25$. These antisymmetric structures at the jet exit have been shown to be correlated with the antisymmetric structures located at the end of the potential core. The correlation coefficient in fact has been shown to be greater for the correlation of the near exit to the end of the potential core than for any symmetric correlation across the jet centerline.

The method of transition for the untuned jet seems to agree with the model presented for the tuned jet. The

major difference lies in the role the global resonance plays in the transition. The vortical interactions at the end of the potential core produce much stronger influence on the initial exit shear layers. This influence is strong enough to produce antisymmetric structures right at the jet exit. The strong influence on the initial jet shear layers is necessary to redistribute the energy in the flow to allow efficient passage at the end of the potential core.

4.2 Conclusions

The planar turbulent jet's method of transition has been studied for both a "tuned" case ($f_{\text{osc}} = 2650$ Hz) and an "untuned" case ($f_{\text{osc}} = 2200$ Hz). The measurement techniques used to document the transition are as follows: application of linear stability theory, power spectrum measurements, bicoherence measurements, coherence measurements, correlation measurements, and digital demodulation measurements. The analysis of these measurements can be summed up briefly by the following statements:

1. Nonlinear interactions at the near exit of the jet with those of the jet column mode are important in determining the initial spectral development and subsequent energy transfer.
2. Phase modulation is the predominant form of

modulation which redistributes the energy during transition.

3. Vortical interactions at the end of the potential core produce upstream influence in the form of the jet column mode and half the jet column mode.

4. Further nonlinear interactions produce pairing of neighboring vortices to provide growth of the mixing layers.

5. The coherent structures at the end of the potential core are forced to realign themselves in an antisymmetric pattern thereby producing the upstream effects in #3.

The major difference in the transition of the untuned jet from that of the tuned jet comes in the amount of upstream influence imparted to the initial jet shear layers. The untuned jet receives a larger amount of influence since the jet has to be forced to redistribute the energy of the shear layers into the jet column mode frequency by the end of the potential core. This is easily accomplished in the tuned jet since the majority of the energy at any given location is at a frequency that is a multiple of the jet column mode.

The next section gives some recommendations that could further this study of the near exit region of the turbulent planar jet.

4.3 Recommendations

1. Freymuth (1966) suggests for high Strouhal numbers that the characteristics of the jet will more readily agree with temporal amplification rather than that of spatial amplification. Inviscid linear theory could be applied to the jet using temporal amplification assumptions. The results could then be compared to those compiled in this thesis for the assumption of spatial amplification.

2. Weakly nonlinear theory could be applied to the near exit of the jet instead of the linear theory used. It would be interesting to compare the applicability of the two separate theories to the planar turbulent jet under high Reynolds numbers.

3. A new quantitative measurement called the cross-bispectrum could be used. This technique would give insights regarding the phase coherence between two developing shear layers with different frequency modes. This technique could also be used to measure the growth of three-dimensional effects which are inherent in the large-scale vortical structures in the shear layer.

4. A new technique presented by Ritz and Powers (1986) could be used for the experimental determination of transfer functions. The authors present a method by which linear and quadratically nonlinear transfer functions are to be computed based on the measurement of the

fluctuations at two points in space and time. This method is extremely useful in that the nonlinear transfer function eliminates the need for physical interpretation of the bicoherence spectrum by reference to power spectra. This means that the interactions $f_i + f_j \rightarrow f_k$, $f_k - f_j \rightarrow f_i$, and $f_k - f_i \rightarrow f_j$ are each mapped into three different regions when the nonlinear transfer function is computed.

5. The Reynolds stresses could be calculated and plotted using an x-wire probe. This information would be helpful in further understanding the transition of the jet.

6. The experimental measurements used in this thesis could be repeated with varying parameters of the jet. For example, change the Reynolds number, change the frequency and amplitude of sinusoidal excitation, or perhaps change the physical dimensions of the jet nozzle. These experiments would give insight into independent and dependent factors of transition.

REFERENCES

- Antonia, R. A., Browne, L. W. B., Rajagopalan, S., and Chambers, A. J., "On the Organized Motion of a Turbulent Plane Jet," J. Fluid Mech., 134, pp. 49-66, 1983.
- Bechert, D. W., "Excitation of Instability Waves in free Shear Layers. Part 1. Theory," J. Fluid Mech., 186, pp. 47-62, 1988.
- Bendat, J. S., and Piersol, A. G., Random Data: Analysis and Measurement Procedures. Wiley-Interscience, 1971.
- Bradbury, L. J. S., "The Structure of a Self-Perserving Turbulent Plane Jet," J. Fluid Mech., 23, Part 1, pp. 31-63, 1965.
- Bradshaw, P., "The Effects of Initial Conditions on the Development of a Free Shear Layer," J. Fluid Mech., 26, pp. 225-236, 1966.
- Browand, F. K., "An Experimental Investigation of the Instability of an Incompressible, Separated Shear Layer," J. Fluid Mech., 26, pp. 281-307, 1966.
- Browand, F. K., and Weidman, P. D., "Large Scales in the Developing Mixing Layer," J. Fluid Mech., 76, pp. 127-144, 1976.
- Brown, G. L., and Roshko, A., "The Effect of Density Difference on the Turbulent Mixing Layer," Turbulent Shear Flows, pp. 23(1-12), AGARD-CP-93, 1971.
- Brown, G. L., and Roshko, A., "On Density Effects and Large Structure in Turbulent Mixing Layers," J. Fluid Mech., 64, pp. 775-816, 1974.
- Cervantes De Gortari, J. G., "An Experimental Study of the Flapping Motion of a Turbulent Plane Jet," Ph.D. Thesis, School of Mech. Engng., Purdue University, 1978.

- Cervantes De Gortari, J. G., "The Apparent Flapping of a Turbulent Plane Jet-Further Experimental Results," A.S.M.E. Paper, 80-WA-FE-13, 1980.
- Chambers, F. W., "Acoustic Interaction With a Turbulent Plane Jet," Ph.D. Dissertation, Purdue University, 1977.
- Chang, C., "Quantitative Measurement of Nonlinear Wave Interactions Characterizing the Transition of a Planar Turbulent Jet," M.S. Thesis, Oklahoma State University, 1987.
- Clenshaw, C. W., and Elliott, D., "A Numerical Treatment of the Orr-Sommerfield Equation in the Case of a Laminar Jet," Quart. J. Mech. Appl. Math., 13, pp. 300-330, 1960.
- Cohen, J., and Wygnanski, I., "The Evolution of Instabilities in the Axisymmetric Jet. Part 1. The Linear Growth of Disturbances Near the Nozzle," J. Fluid Mech., 176, pp. 191-219, 1987.
- Crow, S. C., and Champagne, F. H., "Orderly Structure in Jet Turbulence," J. Fluid Mech., 48, pp. 547-591, 1971.
- Curle, N., "Stability Calculations of a Two-Dimensional Jet," Proc. Roy. Soc., 238, pp. 489-499, 1957.
- Everitt, K. W., and Robins, A. G., "The Development and Structure of Turbulent Plane Jets," J. Fluid Mech., 88, pp. 563-568, 1978.
- Fiedler, H. E., and Mensing, P., "The Plane Turbulent Shear Layer with Periodic Excitation," J. Fluid Mech., 150, pp. 281-309, 1985.
- Flora, J. J. Jr., and Goldschmidt, V. W., "Virtual Origins of a Free Plane Turbulent Jet," AIAA Journal, 7, 12, pp. 2344-2346, 1969.
- Foss, F. J., "A Study of Incompressible Bounded Turbulent Jets," Ph.D. Dissertation, Purdue University, 1965.
- Freythuth, P., "On Transition in a Separated Laminar Boundary Layer," J. Fluid Mech., 69, pp. 683-704, 1966.
- Goldschmidt, V. W., and Bradshaw, P., "Flapping of a Plane Jet," Phys. Fluids, 16, pp. 354-355, 1973.

- Gutmark, E., and Wygnanski, I., "The Planar Turbulent Jet," *J. Fluid Mech.*, 73, pp. 465-495, 1976.
- Ho, C. M., and Huang, L. S., "Subharmonics and Vortex Merging in Mixing Layers," *J. Fluid Mech.*, 119, pp. 443-473, 1982.
- Huerre, P., and Monkewitz, P. A., "Absolute and Convective Instabilities in Free Shear Layers," *J. Fluid Mech.*, 159, pp. 151-168, 1985.
- Jenkins, P. E. and Goldschmidt, V. M., "Study of the Intermittent Region of a Two-Dimensional Plane Jet," Herrick Lab Report, JL 74-75, Purdue University, 1974.
- Jordinson, R., "Design of Wind Tunnel Contractions," *Aircraft Eng.*, 33, pp. 294-297, 1961.
- Kaiser, K. F., "An Experimental Investigation of Interaction of an Acoustic Field and a Plane Turbulent Jet," M.S. Thesis, Purdue University, 1971.
- Kelly, R. E., "On the Stability of an Inviscid Shear Layer which is Periodic in Space and Time," *J. Fluid Mech.*, 27, pp. 657-689, 1967.
- Michalke, A., "On Spatially Growing Disturbances in an Inviscid Shear Layer," *J. Fluid Mech.*, 23, pp. 521-544, 1965.
- Michalke, A., and Hermann, G., "On the Inviscid Instability of a Circular Jet with External Flow," *J. Fluid Mech.*, 114, pp. 343-359, 1982.
- Miksad, R. W., "Experiments on the Nonlinear Stages of Free Shear Layer Transition," *J. Fluid Mech.*, 56, pp. 695-719, 1972.
- Miksad, R. W., "Experiments on Nonlinear Interactions in the Transition of a Free Shear Layer," *J. Fluid Mech.*, 59, pp. 1-21, 1973.
- Miksad, R. W., Jones, F. L., Powers, E. J., Kim, Y. C., and Khadra, L., "Digital Complex Demodulation of Unsteady Fluid Flow Measurements," *Phys. Fluids*, 24, pp. 219-222, 1981.
- Miksad, R. W., Jones, F. L., Powers, E. J., Kim, Y. C., and Khadra, L., "Experiments on the Role of Amplitude and Phase Modulations During Transition to Turbulence," *J. Fluid Mech.*, 123, pp. 1-29, 1982.

- Miksad, R. W., Jones, F. L., and Powers, E. J., "Measurement of Nonlinear Interactions During natural Transition of a Symmetric Wake," *Phys. Fluids*, 26, pp. 1402-1409, 1983.
- Mulej, D. J., "The Velocity of the Interface," M.S. Thesis, Purdue University, 1975.
- Mumford, J. C., "The Structures of the Large Eddies in Fully Developed Turbulent Shear Flows. Part 1. The Plane Jet," *J. Fluid Mech.*, 118, pp. 241-268, 1982.
- Oler, J. W., and Goldschmidt, V. W., "A Vortex-street Model of the Flow in the Similarity Region of a Two-Dimensional Free Turbulent Jet," *J. Fluid Mech.*, 123, pp. 523-535, 1982.
- Ott, E. S., "Convective Velocities in a Turbulent Plane Jet," M.S. Thesis, Purdue University, 1972.
- Peterka, J. A., and Richardson, P. D., "Effects of Sound on Separated Flows," *J. Fluid Mech.*, 37, pp. 265-287, 1969.
- Prakash, K. M. K., "Influence of a Global Resonance Mechanism on the Structural Development of a Planar Turbulent Jet," M.S. Thesis, Oklahoma State University, 1986.
- Ritz, C. P. and Powers, E. J., "Estimation of Nonlinear Transfer Functions for Fully Developed Turbulence," *Physica* 20D, pp. 320-334, 1986.
- Ruelle, D. and Takens, F., "On the Nature of Turbulence," *commun. Math. Phys.*, 20, pp. 167-192, 1971.
- Saffman, P. G., and Schatzman, J. C., "Stability of a Vortex Street of finite Vortices," *J. Fluid Mech.*, 117, pp. 171-185, 1982.
- Sato, H., "Transition of a Two-dimension Jet," *J. Fluid Mech.*, 7, pp. 53-80, 1960.
- Sato, H., "An Experimental Study of Non-linear Interaction of Velocity Fluctuations in the Transition Region of a Two-dimensional Wake," *J. Fluid Mech.*, 44, pp. 741-765, 1970.
- Sato, H., and Kuriki, K., "The Mechanism of Transition in the Wake of a Thin Flat Plate Placed Parallel to a Uniform Flow," *J. Fluid Mech.*, 11, pp. 321-352, 1970.

- Sato, H., and Okada, O., "The Stability and Transition of an Axisymmetric Wake," J. Fluid Mech., 26, pp. 237-250, 1966.
- Sato, H., and Saito, H., "Fine-structure of Energy Spectra of Velocity Fluctuations in the Transition Region of a Two-Dimensional wake," J. Fluid Mech., 67, pp. 539-559, 1975.
- Sato, H., and Saito, H., "Artificial Control of the Laminar-Turbulent Transition of a Two-Dimensional Wake by External Sound," J. Fluid Mech., 84, pp. 657-672, 1978.
- Sato, H., and Sakao, F., "An Experimental Investigation of a Two-Dimensional Jet at Low Reynolds Numbers," J. Fluid Mech., 20, pp. 337-352, 1964.
- Tatsumi, T., and Kakutani, T., "The Stability of a Two-dimensional Laminar Jet," J. Fluid Mech., 4, pp. 261-280, 1958.
- Thomas, F. O., "Effect of Nozzle Geometry of Acoustic Interaction With a Turbulent Jet," M.S. Thesis, Purdue University, 1980
- Thomas, F. O., "Development of a Two-Dimensional Turbulent Jet Under Natural and Excited Condition," Ph.D. Dissertaton, Purdue University, 1983.
- Thomas, F. O., and Brehob, E. G., "An Investigation of Large-Scale Structure in the Similarity Region of a Two-Dimensional Turbulent Jet," Phys. of Fluids, 29, pp. 1788-1795, 1986.
- Thomas, F. O., and Goldschmidt, V. W., "The Possibility of a Resonance Mechanism in the Developing Two-Dimensional Jet," Phys. of Fluids, 28, pp. 3510-3514, 1985.
- Thomas, F. O., and Goldschmidt, V. W., "Structural Characteristics of a Deveoping Turbulent Planar Jet," J. Fluid Mech., 163, pp. 227-256, 1986.
- Townsend, A. A., The Structure of Turbulent Shear Flow. Cambridge University Press, 1956.
- Winant, C. D., and Browand, F. K., "Vortex Pairing: the Mechanism of Turbulent Mixing Layer Growth at Moderate Reynolds Number," J. Fluid Mech., 63, pp. 237-255, 1974.

Van Der Hegge Zijnen, B. G., "Measurements of Turbulence in a Plane Jet of Air by the Diffusion Method and by the Hot-Wire Method," Applied Science Rec., Section A, 7, pp. 256-276, 1958.

APPENDIXES

APPENDIX A

COMPUTER PROGRAM LISTINGS

EIGENVALUE CALCULATION PROGRAM

```

program stable(input,output,TXT1,TXT2,TXT3,TXT4);
LABEL 20,30;
(THIS PROGRAM COMPUTES THE EIGENVALUES AND EIGENFUNCTIONS FOR THE :
INVISCID INSTABILITY OF A HYPERBOLIC TANGENT TYPE VELOCITY PROFILES)
(INPUT PROFILE USING A TABLE OF VALUES -- Y,U)

type
LILARRAY=ARRAY[0..100] OF REAL;
PARRAY=ARRAY[1..750] OF REAL;
PARRAY=PACKED ARRAY[1..17] OF CHAR;
var
a,b,c,d,e,f,g,h,i1,h2,hm1,hm2,j,k,l,m,n,aa,bb,cc,dd,ee,ff,r,ii,gg,
hh,p,q,t,u,u1,ddu,v,w,dphir1,dphir2,dphii1,dphii2,ddphir1,ddphir2,
ddphii1,ddphii2,ar,ai,beta,z4,dz1,dz2,freal,fimag,difmin,delar,
delai,alphamin,fr1,fi1,alphaimin,armax,armin,aimax,aimin,tolerance,
dum1,dum2,amult, y2,y3,uppl,upp2,uuml,delp,delpq:real;

iii,testfind,i,i1,i2,i3,i4,nd,nd1,nd2,
DSIZE,JJ,KK,XSIZE,YSIZE,ERRSTAT:INTEGER;
txt1,txt2,txt3,txt4:text;

filename1,filename2,filename3:PARRAY;

phir1,phir2,phii1,phii2,dphir,dphii,d2phir,d2phii,d3phir,d3phii,d4phir,
y1,d4phii,z3,z,upp,dz,uum:PARRAY;

arr,ail,fdif,fdif1:LILARRAY;

function Fr(xr,xi,z4,ddu,u1:real):real;
begin
(writeln('b=',b:7:5,' c=',c:7:5,' e=',e:7:5,' g=',g:7:5);)
(writeln('a=',a:7:5,' d=',d:7:5,' n=',n:7:5,' beta=',beta:7:5);)
(writeln('xr=',xr:7:5,' xi=',xi:7:5,' z4=',z4:7:5,' ddu=',ddu:7:5,' u1=',)
( u1:7:5);)
fr1:=(a-sqr(xr)+sqr(xi))/(1-sqr(z4));
fr1:=fr1+(ddu*u1*d-ddu*n)/((1-sqr(z4))*(sqr(u1)*d-2*u1*n+sqr(beta)));
fr:=fr1;
(writeln('Fr=',fr1);)
end;

function Fi(xr,xi,z4,ddu,u1:real):real;
begin
(writeln('f=',f:7:5,' m=',m:7:5,' d=',d:7:5,' n=',n:7:5,' beta=',beta:7:5);)
(writeln('xr=',xr:7:5,' xi=',xi:7:5,' z4=',z4:7:5,' ddu=',ddu:7:5,' u1=',)
( u1:7:5);)
fi1:=(f-2*xi*xr)/(1-sqr(z4));
fi1:=fi1+m*ddu/((1-sqr(z4))*(d*sqr(u1)-2*u1*n+sqr(beta)));
fi:=fi1;
(writeln('Fi=',fi1);)
end;

begin
tolerance:=0.0001;
(*****
***** read velocity profile *****
writeln('ENTER THE FILENAME FOR THE VELOCITY PROFILE COEFF. ');
writeln;
readln(filename3);
writeln;
BIND(txt3,filename3,ERRSTAT);
reset(txt3);
il:=0;
while not EOF(txt3) do begin

```

```

    ii:=ii+1;
    readln(txt0,y1[i1],sum[i1],upp[i1]);
    z0[i1]:=(exp(y1[i1])-exp(-y1[i1]))/(exp(y1[i1])+exp(-y1[i1]));
    IF (ABS(Y1[i1])<0.0095) THEN ND1:=i1;
end;
nd:=ii-1;
(writein('nd=',nd);)

nd2:=nd-nd1;
close (txt3);

difmin:=1000;
writein('ENTER THE FREQUENCY BETA');
readln(beta);
testfind:=0;
jj:=1;
delc:=0.19314;
delq:=0.05174;

(EIGENVALUE SEARCH USING PATTERN SEARCH)

writein('ENTER THE INITIAL VALUE OF ar ');
writein;
readln(armin);
writein;
writein('ENTER THE INITIAL VALUE OF ai ');
writein;
readln(aimin);
writein;
writein('ENTER THE INITIAL VALUE OF STEP SIZE MULTIPLIER');
writein;
readln(amult);
delp:=delp*amult;
delq:=delq*amult;

20:arr[1]:=armin;      aii[1]:=aimin;
arr[2]:=armin+delp;   aii[2]:=aimin+delq;
arr[3]:=armin+delq;   aii[3]:=aimin+delp;

while difmin>tolerance do
begin

30:ai:=aii[jj];
ar:=arr[jj];
(-----COMPUTE CONSTANTS-----)
a:=(sqr(ar)-sqr(ai));
b:=(2*sqr(ar)+2*sqr(ai));
c:=(2*sqr(ar)-4*beta*ar+2*sqr(ai));
d:=(sqr(ar)+sqr(ai));
e:=(sqr(ar)-4*beta*ar+sqr(ai)+4*sqr(beta));
f:=(2*ai*ar);
g:=(4*ai*beta);
h:=beta-sqr(ar)+sqr(ai)-ar+beta*ar;
j:=beta*ai-ai-2*ar*ai;
k:=(beta+beta*ar);
l:=-ar*beta*(1+ar)-sqr(ai)*beta;
m:=-ai*beta;
n:=ar*beta;
aa:=sqr(ar)-sqr(ai)+2*ar*beta;
bb:=2*ar*ai+2*ai*beta;
cc:=sqr(ar)-sqr(ai)+sqr(beta)-2*ar*beta;
dd:=2*ar*ai-2*beta*ai;
ee:=(aa*cc)+(bb*dd);
ff:=(bb*cc)-(aa*dd);
r:=(h*ar+j*ai)/(sqr(h)+sqr(j));
ii:=(h*ai-l*ar)/(sqr(h)+sqr(j));

```

```

gg:=(0.5*sqr(a)-0.5*sqr(i)+(ar*r)-(ai*i)-(0.5*ea;
hh:=-r*i1)+(ar*r)-(ar*i1)-0.50*ai;
o:=1/(sqr(k)+sqr(m));
q:=m/(sqr(k)+sqr(m));
t:=(sqr(ar)-sqr(ai)-2*beta*ar)/(2*sqr(beta));
u:=(2*ar*ai-2*beta*ai)/(2*sqr(beta));
v:=(0.5*sqr(q)-(0.5*sqr(p)-(ar*p)+(ai*q)-t;
w:=p*q+ai*p+ar*q+u;

```

(ZERO ALL ARRAYS)

for i:=1 to nd do begin

```

  phi1[i]:=0.0; phir2[i]:=0.0; phi1[i]:=0.0; phi2[i]:=0.0;
  d1phi1[i]:=0.0; d1phi1[i]:=0.0; d2phir[i]:=0.0; d2phi1[i]:=0.0;
  d3phir[i]:=0.0; d3phi1[i]:=0.0; d4phir[i]:=0.0; d4phi1[i]:=0.0;
end;

```

(CALCULATE DERIVATIVES FOR TAYLOR SERIES EXPANSION)

```

dphir1:=(h*ar+j*ai)/(sqr(h)+sqr(j));
dphir2:=1/(sqr(k)+sqr(m));
dphi1:=(h*ai-j*ar)/(sqr(h)+sqr(j));
dphi2:=m/(sqr(k)+sqr(m));
ddphir1:=(gg*(1+0.5*ar)+hh*(0.5*ai))/(sqr(1+0.5*ar)+sqr(0.5*ai));
ddphi1:=(hh*(1+0.5*ar)-gg*(0.5*ai))/(sqr(1+0.5*ar)+sqr(0.5*ai));
ddphir2:=(v*(1+0.5*ar)-w*(0.5*ai))/(sqr(1+0.5*ar)+sqr(0.5*ai));
ddphi2:=(w*(1+0.5*ar)-v*(0.5*ai))/(sqr(1+0.5*ar)+sqr(0.5*ai));

```

(CALCULATE INITIAL "PHI" VALUES BY TAYLOR SERIES)

```

dz1:=abs(z3[2]-z3[1]);
dz2:=abs(z3[nd]-z3[nd-1]);
phir1[1]:=-ar-dphir1*dz1+0.50*ddphir1*sqr(dz1);
phir2[nd]:=ar+dphir2*dz2+0.50*ddphir2*sqr(dz2);
phi1[1]:=-ai-dphi1*dz1+0.50*ddphi1*sqr(dz1);
phi2[nd]:=ai+dphi2*dz2+0.50*ddphi2*sqr(dz2);
(writeln(dz1,dz2);)
(writeln(phir1[1],phir2[nd],phi1[1],phi2[nd]);)

```

(INTEGRATE BOTH THE REAL AND IMAGINARY DIFFERENTIAL EQUATIONS)
(PERFORM NUMERICAL INTEGRATION VIA A RUNGE-KUTTA PROCEDURE)

```

for i:=1 to nd1 do begin
  dz[i+1]:=z3[i+1]-z3[i];
  upp1:=(upp[i]+upp[i+1])/2;
  upp2:=upp[i+1];
  uum1:=0.5*(uum[i]+uum[i+1]);

  d1phir[i]:=dz[i+1]*fr(phir1[i],phi1[i],z3[i],upp[i],uum[i]);
  d1phi[i]:=dz[i+1]*fi(phir1[i],phi1[i],z3[i],upp[i],uum[i]);

  d2phir[i]:=dz[i+1]*fr(phir1[i]+0.5*d1phir[i],phi1[i]+0.5*d1phi[i],
    z3[i]+0.5*dz[i+1],upp1,uum1);
  d2phi[i]:=dz[i+1]*fi(phir1[i]+0.5*d1phir[i],phi1[i]+0.5*d1phi[i],
    z3[i]+0.5*dz[i+1],upp1,uum1);

  d3phir[i]:=dz[i+1]*fr(phir1[i]+0.5*d2phir[i],phi1[i]+0.5*d2phi[i],
    z3[i]+0.5*dz[i+1],upp2,uum1);
  d3phi[i]:=dz[i+1]*fi(phir1[i]+0.5*d2phir[i],phi1[i]+0.5*d2phi[i],
    z3[i]+0.5*dz[i+1],upp2,uum1);

  d4phir[i]:=dz[i+1]*fr(phir1[i]+d3phir[i],phi1[i]+d3phi[i],
    z3[i]+dz[i+1],upp2,uum1);
  d4phi[i]:=dz[i+1]*fi(phir1[i]+d3phir[i],phi1[i]+d3phi[i],
    z3[i]+dz[i+1],upp2,uum1);
  (writeln(d1phir[i]:7:5,d1phi[i]:7:5,d2phir[i]:7:5,d2phi[i]:7:5);)

```

```

d3phir[i]:=d3, d3phii[i]:=7:5, d4phir[i]:=7:5, d4phii[i]:=7:5;

phir1[i+1]:=phir1[i]+((d1phir[i]+2*d2phir[i]+2*d3phir[i]+d4phir[i])/6);
phii1[i+1]:=phii1[i]+((d1phii[i]+2*d2phii[i]+2*d3phii[i]+d4phii[i])/6);
writeln('i=', i, phir1[i+1]:7:5, phii1[i+1]:7:5);
end;

for i2:=1 to nd2-1 do begin
  i:=nd-i2+1;
  dz[i-1]:=z3[i-1]-z3[i];
  upp1:=(upp[i]+upp[i-1])/2;
  upp2:=upp[i-1];
  uum1:=0.5*(uum[i]+uum[i-1]);
  writeln(i, ' dz=', dz[i-1]:7:4, ' z3=', z3[i]:7:4, ' upp=', upp[i]:7:4,
    ' uum=', uum[i]:7:4, ' upp1=', upp1:7:4, ' upp2=', upp2:7:4);
  d1phir[i]:=dz[i-1]*fr(phir2[i], phii2[i], z3[i], upp[i], uum[i]);
  d1phii[i]:=dz[i-1]*fi(phir2[i], phii2[i], z3[i], upp[i], uum[i]);

  d2phir[i]:=dz[i-1]*fr(phir2[i]+0.5*d1phir[i], phii2[i]+0.5*d1phii[i],
    z3[i]+0.5*dz[i-1], upp1, uum1);
  d2phii[i]:=dz[i-1]*fi(phir2[i]+0.5*d1phir[i], phii2[i]+0.5*d1phii[i],
    z3[i]+0.5*dz[i-1], upp1, uum1);

  d3phir[i]:=dz[i-1]*fr(phir2[i]+0.5*d2phir[i], phii2[i]+0.5*d2phii[i],
    z3[i]+0.5*dz[i-1], upp1, uum1);
  d3phii[i]:=dz[i-1]*fi(phir2[i]+0.5*d2phir[i], phii2[i]+0.5*d2phii[i],
    z3[i]+0.5*dz[i-1], upp1, uum1);

  d4phir[i]:=dz[i-1]*fr(phir2[i]+d3phir[i], phii2[i]+d3phii[i],
    z3[i]+dz[i-1], upp2, uum[i-1]);
  d4phii[i]:=dz[i-1]*fi(phir2[i]+d3phir[i], phii2[i]+d3phii[i],
    z3[i]+dz[i-1], upp2, uum[i-1]);
  writeln(i, ' d1phir[i]:8:5, d1phii[i]:8:5, d2phir[i]:8:5, d2phii[i]:8:5,
    d3phir[i]:8:5, d3phii[i]:8:5, d4phir[i]:8:5, d4phii[i]:8:5);
  phir2[i-1]:=phir2[i]+((d1phir[i]+2*d2phir[i]+2*d3phir[i]+d4phir[i])/6);
  phii2[i-1]:=phii2[i]+((d1phii[i]+2*d2phii[i]+2*d3phii[i]+d4phii[i])/6);
  writeln('i=', i, phir2[i-1]:7:5, phii2[i-1]:7:5);
end;

for iii:=40 to 60 do begin
  writeln('i=', iii, ' phir1=', phir1[iii]:7:5, ' phir2=', phir2[iii]:7:5,
    ' phii1=', phii1[iii]:7:5, ' phii2=', phii2[iii]:7:5);
end;

freal:=phir1[nd+1]-phir2[nd-nd2+1];
fimag:=phii1[nd+1]-phii2[nd-nd2+1];
writeln('fr=', freal:7:5, ' fi=', fimag:7:5);
WRITELN('TESTFIND', TESTFIND, 'JJ', JJ);
fdif[jj]:=sqrt(sqr(freal)+sqr(fimag));
difmin:=fdif[jj];
fdif1[testfind]:=fdif[jj];
testfind:=testfind+1;

writeln;
writeln('delp=', delp:7:5, ' delq=', delq:7:5);
writeln(jj, ' FDIF = ', difmin:7:5, ' FOR Ar = ', ar:7:5, ' AND Ai = ', ai:7:5);
writeln;
if (testfind<3) then jj:=jj+1;
if (testfind<3) then goto 30;
if (fdif1[testfind-1]=fdif1[testfind-3]) then begin delp:=0.2*delp;
  delq:=0.2*delq;
  testfind:=0; armin:=ar; aimin:=ai; jj:=1;
  goto 20; end;

if (fdif[1]>fdif[2]) and (fdif[1]>fdif[3]) then begin
  arr[1]:=arr[2]+arr[3]-arr[1];
  aii[1]:=aii[2]+aii[3]-aii[1];
  jj:=1;

```

```

end;
if (fdiF[2] > fdiF[1]) and (fdiF[2] > fdiF[3]) then begin
    arr[2] := arr[1] + arr[3] - arr[2];
    aii[2] := aii[1] + aii[3] - aii[2];
    jj := 2;
end;
if (fdiF[3] > fdiF[2]) and (fdiF[3] > fdiF[1]) then begin
    arr[3] := arr[1] + arr[2] - arr[3];
    aii[3] := aii[1] + aii[2] - aii[3];
    jj := 3;
end;

end;

writeln(' BETA = ', BETA:7:4);
writeln(' REAL AT ZERO = ', PHIR1[ND1]:7:5);
writeln(' IMAGINARY AT ZERO = ', PHII1[ND1]:7:5);
writeln('ENTER THE FILENAME FOR THE REAL EIGENFUNCTION');
writeln;
readln(filename1);
BIND(txt1, filename1, ERRSTAT);
rewrite(txt1);
for i:=1 to nd1+1 do begin
    writeln(txt1, z3[i]:7:5, ' ', phir1[i]:7:5);
end;
for i:=nd1+2 to nd do begin
    writeln(txt1, z3[i]:7:5, ' ', phir2[i]:7:5);
end;
close (txt1);
writeln;
writeln('ENTER THE FILENAME FOR THE IMAGINARY EIGENFUNCTION');
readln(filename2);
BIND(txt2, filename2, ERRSTAT);
rewrite(txt2);
for i:=1 to nd1+1 do begin
    writeln(txt2, z3[i]:7:5, ' ', phii1[i]:7:5);
end;
FOR I:=ND1+2 TO ND DO BEGIN
    writeln(txt2, z3[i]:7:5, ' ', phii2[i]:7:5);
end;
close (txt2);
END.II;

```

EIGENFUNCTION CALCULATION PROGRAM

```

PROGRAM EIGEN(INPUT,OUTPUT,TXT1,TXT2,TXT3);
  (THIS PROGRAM COMPUTES THE EIGENFUNCTIONS FOR THE INVISCID )
  (INSTABILITY OF THE HYPERBOLIC TANGENT VELOCITY PROFILE)

  TYPE

    RARRAY=ARRAY[1..500] OF REAL;
    MIDARRAY=ARRAY[1..20] OF REAL;
    PARRAY=PACKED ARRAY[1..17] OF CHAR;

  VAR

    D1PHIR,D2PHIR,D3PHIR,D4PHIR,D1PHII,D2PHII,D3PHII,D4PHII,
    D1PR,D2PR,D3PR,D4PR,D1PI,D2PI,D3PI,D4PI,YUPPER,YLOWER,
    upp1,upp2,ddu1,u1,dum1,dum2,z,DY,dy1,dy2,A,B,BETA,AR,AI:REAL;

    DSIZE,I,i1,i3,J,ii,nd,nd1,ERRSTAT:INTEGER;

    TXT1,TXT2,txt3:TEXT;

    FILENAME1,FILENAME2,filename3:PARRAY;

    PHIR1,PHII1,PR1,PI1,PHIR2,PHII2,PR2,PI2,Y1,Y2,ddu,u,z3:RARRAY;

    a1:MIDARRAY;

  FUNCTION GR(X,upp,u2:REAL):REAL;
  BEGIN
    GR:=A+((upp*AR*(u2*AR-BETA)+u2*upp*SQR(AI))/(SQR(u2*AR-BETA)+
      SQR(u2)*SQR(AI)));
  END;

  FUNCTION GI(X,upp,u2:REAL):REAL;
  BEGIN
    GI:=B+((upp*AI*(u2*AR-BETA)-AR*AI*upp*u2)/(SQR(u2*AR-BETA)+
      SQR(u2)*SQR(AI)));
  END;

  FUNCTION FR(X,Y,Z,upp,u2:REAL):REAL;
  BEGIN
    FR:=GR(X,upp,u2)*Y-GI(X,upp,u2)*Z;
  END;

  FUNCTION FI(X,Y,Z,upp,u2:REAL):REAL;
  BEGIN
    FI:=GI(X,upp,u2)*Y+GR(X,upp,u2)*Z;
  END;

  BEGIN
    (*****
    (*****      read velocity profile      *****)
    writeln('ENTER THE FILENAME FOR THE VELOCITY PROFILE COEFF. ');
    writeln;
    readln(filename3);
    writeln;
    BIND(txt3,filename3,ERRSTAT);
    reset(txt3);
    i1:=0;
    while not EOF(txt3) do begin
      i1:=i1+1;
      readLN(txt3,y1[i1],u1[i1],ddu1[i1]);
    
```



```

      IF (Y11111<0.0005) AND (Y11111>-0.0005) THEN nd:=11;
end;
nd1:=11-1;
writeln('nd=',nd,' nd1=',nd1);
close (txt3);

WRITELN('ENTER FREQUENCY "BETA"');
WRITELN;
READLN(BETA);
WRITELN('ENTER THE EIGENVALUE AR');
WRITELN;
READLN(AR);
WRITELN;
WRITELN('ENTER THE EIGENVALUE AI');
WRITELN;
READLN(AI);
WRITELN;
A:=SQR(AR)-SQR(AI);
B:=2*AI*AR;
(*INITIALIZE VALUES AT Y=0*)
PHIR1[nd]:=1.0; PHII1[nd]:=0.0; PHIR2[nd]:=1; PHII2[nd]:=0.0;
WRITELN('ENTER THE VALUE OF PHI REAL AT Y=0');
READLN(PR1[nd]);
WRITELN;
WRITELN('ENTER THE VALUE OF PHI IMAGINARY AT Y=0');
WRITELN;
READLN(PI1[nd]);
PR2[nd]:=PR1[nd];
PI2[nd]:=PI1[nd];
WRITELN('*****');
WRITELN('          RUNGE-KUTTA INTEGRATION IN PROGRESS          ');
WRITELN('*****');
WRITELN;

FOR i:= nd downto 2 DO BEGIN
  DY:=y1[i-1]-y1[i];
  ddu1:=(ddu[i]+ddu[i-1])/2;
  u1:=(u[i]+u[i-1])/2;

  D1PHIR:=DY*PR1[i];
  D1PHII:=DY*PI1[i];
  D1PR:=DY*FR(Y1[i],PHIR1[i],PHII1[i],ddu[i],u[i]);
  D1PI:=DY*FI(Y1[i],PHIR1[i],PHII1[i],ddu[i],u[i]);

  D2PHIR:=DY*(PR1[i]+0.5*D1PR);
  D2PHII:=DY*(PI1[i]+0.5*D1PI);
  D2PR:=DY*FR(Y1[i]+0.5*DY,PHIR1[i]+0.5*D1PHIR,PHII1[i]+0.5*D1PHII,ddu1,u1);
  D2PI:=DY*FI(Y1[i]+0.5*DY,PHIR1[i]+0.5*D1PHIR,PHII1[i]+0.5*D1PHII,ddu1,u1);

  D3PHIR:=DY*(PR1[i]+0.5*D2PR);
  D3PHII:=DY*(PI1[i]+0.5*D2PI);
  D3PR:=DY*FR(Y1[i]+0.5*DY,PHIR1[i]+0.5*D2PHIR,PHII1[i]+0.5*D2PHII,ddu1,u1);
  D3PI:=DY*FI(Y1[i]+0.5*DY,PHIR1[i]+0.5*D2PHIR,PHII1[i]+0.5*D2PHII,ddu1,u1);

  D4PHIR:=DY*(PR1[i]+D3PR);
  D4PHII:=DY*(PI1[i]+D3PI);
  D4PR:=DY*FR(Y1[i]+DY,PHIR1[i]+D3PHIR,PHII1[i]+D3PHII,ddu[i-1],u[i-1]);
  D4PI:=DY*FI(Y1[i]+DY,PHIR1[i]+D3PHIR,PHII1[i]+D3PHII,ddu[i-1],u[i-1]);

  PHIR1[i-1]:=PHIR1[i]+((D1PHIR+2*D2PHIR+2*D3PHIR+D4PHIR)/6);
  PHII1[i-1]:=PHII1[i]+((D1PHII+2*D2PHII+2*D3PHII+D4PHII)/6);
  PR1[i-1]:=PR1[i]+((D1PR+2*D2PR+2*D3PR+D4PR)/6);
  PI1[i-1]:=PI1[i]+((D1PI+2*D2PI+2*D3PI+D4PI)/6);

```

```

FOR i:= nd to nd1-1 DO BEGIN
  dy:=y1[i+1]-y1[i];
  ddu1:=(ddu[i]+ddu[i+1])/2;
  u1:=(u[i]+u[i+1])/2;

  D1PHIR:=DY*PR2[i];
  D1PHII:=DY*PI2[i];
  D1PR:=DY*FR(Y1[i],PHIR2[i],PHI2[i],ddu[i],u[i]);
  D1PI:=DY*FI(Y1[i],PHIR2[i],PHI2[i],ddu[i],u[i]);

  D2PHIR:=DY*(PR2[i]+0.5*D1PR);
  D2PHII:=DY*(PI2[i]+0.5*D1PI);
  D2PR:=DY*FR(Y1[i]+0.5*DY,PHIR2[i]+0.5*D1PHIR,PHI2[i]+0.5*D1PHII,ddu1,u1);
  D2PI:=DY*FI(Y1[i]+0.5*DY,PHIR2[i]+0.5*D1PHIR,PHI2[i]+0.5*D1PHII,ddu1,u1);

  D3PHIR:=DY*(PR2[i]+0.5*D2PR);
  D3PHII:=DY*(PI2[i]+0.5*D2PI);
  D3PR:=DY*FR(Y1[i]+0.5*DY,PHIR2[i]+0.5*D2PHIR,PHI2[i]+0.5*D2PHII,ddu1,u1);
  D3PI:=DY*FI(Y1[i]+0.5*DY,PHIR2[i]+0.5*D2PHIR,PHI2[i]+0.5*D2PHII,ddu1,u1);

  D4PHIR:=DY*(PR2[i]+D3PR);
  D4PHII:=DY*(PI2[i]+D3PI);
  D4PR:=DY*FR(Y1[i]+DY,PHIR2[i]+D3PHIR,PHI2[i]+D3PHII,ddu[i+1],u[i+1]);
  D4PI:=DY*FI(Y1[i]+DY,PHIR2[i]+D3PHIR,PHI2[i]+D3PHII,ddu[i+1],u[i+1]);

  PHIR2[i+1]:=PHIR2[i]+((D1PHIR+2*D2PHIR+2*D3PHIR+D4PHIR)/6);
  PHI2[i+1]:=PHI2[i]+((D1PHII+2*D2PHII+2*D3PHII+D4PHII)/6);
  PR2[i+1]:=PR2[i]+((D1PR+2*D2PR+2*D3PR+D4PR)/6);
  PI2[i+1]:=PI2[i]+((D1PI+2*D2PI+2*D3PI+D4PI)/6);

END;
WRITELN;
writeln('ENTER THE FILENAME FOR THE REAL EIGENFUNCTION');
writeln;
readln(filename1);
BIND(txt1,filename1,ERRSTAT);
rewrite(txt1);
for i:=1 to nd do begin
  writeln(txt1,Y1[i]:7:5,' ',phir1[i]:7:5,' ',PR1[i]:7:5);
end;
for i:=nd+1 to nd1 do begin
  writeln(txt1,Y1[i]:7:5,' ',phir2[i]:7:5,' ',PR2[i]:7:5);
end;
close (txt1);
writeln('ENTER THE FILENAME FOR THE IMAGINARY EIGENFUNCTION');
readln(filename2);
BIND(txt2,filename2,ERRSTAT);
rewrite(txt2);
for i:=1 to nd DO BEGIN
  writeln(txt2,Y1[i]:7:5,' ',phii1[i]:7:5,' ',PI1[i]:7:5);
end;
for i:=nd+1 to nd1 DO BEGIN
  writeln(txt2,Y1[i]:7:5,' ',phii2[i]:7:5,' ',PI2[i]:7:5);
end;
close (txt2);
END.

```

STABILITY DATA PROGRAM

```

program spectS2(input,output);
label 5;
{This program samples a time varying voltage and computes the frequency}
{spectrum by the Fast Fourier Transform method. The spectrum is written}
{to disk as "SPECTDATA.TEXT". This program assumes that the D.C. component}
{of the signal has been removed prior to A/D conversion.}
{Voltage is phase correlated with the peak of an input signal from channel 2}
import iodeclarations;
import general_2;
import measurement_lib;

```

```

const

```

```

    name = 'ADC';
    model = '98640A';
    select_code = 18;
    error = 'NO';
    units = 'STANDARD';
    multiplier = 1.0;
    offset = 0.0;
    p_size = 2;
    q_size = 2;
    c_size = 2;
    n=512; n1=511; n=9; pi=3.14159265;
    d_size = 60000;
    rept = 30000;

```

```

type

```

```

    r_array = ARRAY[1..150000] of real;
    r_ptr = ^r_array;
    i_array = ARRAY[1..7] of shortint;
    i_ptr = ^i_array;
    d_ptr = ^i_array;
    complex=record x,y: real end;
    datta = ARRAY[0..n1] of complex;
    c_ptr = ^datta;
    a_array=ARRAY[0..n1] of real;
    l_array = array[1..n1] of real;

```

```

var

```

```

    channel: i_ptr;
    signal: d_ptr;
    gain: i_ptr;
    pace: r_ptr;
    data: r_ptr;
    i,j,k,m,c,p,nn,n2,n5,msamp,gane,imin,imax,ilow: integer;
    NSCALE,sig,fmax,time,nsamp,pase1,pase2,sc,deltaf,
    trap,qan,FEX,BAND: real;
    w,a: c_ptr;
    txt1,txt: text;
    amp,freq: a_array;
    filename1,filename: packed array[1..20] of char;

```

```

procedure reord(var a: c_ptr);

```

```

var

```

```

    i,j,k,l: integer;
    q: complex;

```

```

begin

```

```

    for i:=1 to n1 do begin
        l:=i;
        k:=0;
        for j:=0 to (n-1) do begin

```

```

        k:=(2*k)+1 mod 2;
        l:=l div 2
      end;
    if i<k then begin
      q:=a[i];
      a[i]:=a[k];
      a[k]:=q
    end
  end
end; {reord}

procedure sum(z,w:complex; var s:complex);
begin
  with s do begin
    x:=z.x+w.x;
    y:=z.y+w.y
  end
end;

procedure dif(z,w:complex; var s:complex);
begin
  with s do begin
    x:=z.x-w.x;
    y:=z.y-w.y
  end
end;

procedure prod(z,w:complex; var s:complex);
begin
  with s do begin
    x:=z.x*w.x-z.y*w.y;
    y:=z.x*w.y+z.y*w.x
  end
end;

procedure neg(u:complex; var w:complex);
begin
  w.x:=-u.x;
  w.y:=-u.y
end;

procedure trf(var x:c_ptr);
var
  lvl,tl,tll,expon,p,i,j,k:integer;
  s,z:complex;

{tl = 2^lvl}
{tll=2^(lvl-1)}
{p=2^(n-lvl)}
{expon=j*p}

begin
  tl:=2; tll:=1;
  for lvl:=1 to n do
    begin
      p:=n div tl; expon:=0;
      for j:=0 to tll-1 do
        begin
          i:=j; s:=w[expon];
          while i<n do
            begin
              k:=i+tll;
              if j=0 then z:=a[k]
              else prod(a[k],s,z);
              dif(a[i],z,a[k]);
            end
          end
        end
      end
    end
  end
end;

```

```

        sum(a^[1],z,a^[1]);
        i:=i+1;
    end;
    expon:=expon+p;
    end;
    t1:=2*t1; t11:=2*t11;
    end;
end; {trf}

function mag(z:complex):real;
begin
    with z do
        mag:=sqr(x)+sqr(y);
    end;
end;

begin {MAIN PROGRAM}
    new(w);
    new(a);
    rewrite(txt1,'JIM:XDDATA.TEXT');
    writeln('CHANNEL 1 MUST BE CONNECTED TO HOT WIRE SIGNAL WITH THE ');
    writeln('DC COMPONENT REMOVED');
    writeln;
    writeln('CHANNEL 2 MUST BE CONNECTED TO THE DESIRED FREQ GENERATOR');
    writeln;
    writeln('ENTER THE EXCITATION FREQUENCY');
    writeln;
    readnumber(1,fex);
    writeln;
    writeln('ENTER THE MAXIMUM FREQUENCY COMPONENT OF THE HOT WIRE SIGNAL');
    readnumber(1,fmax);
    writeln;
    pase1:=0.000025;
    pase2:=(1.0/(2.0*fmax));
    if(pase2 < 0.000018) then
    begin
        writeln('THE PACE VALUE IS TOO SMALL FOR THE HP-98640A!!');
        writeln('*****');
        writeln('IF ALLOWED TO CONTINUE PACE WILL BE SET TO THE VALUE 0.000018');
        pase2:=0.000018;
    end;
    if (pase2>0.0393336) then
    begin
        writeln('THE PACE VALUE IS TOO LARGE FOR THE HP-98640A!!');
        writeln('*****');
        writeln('IF ALLOWED TO CONTINUE PACE WILL BE SET TO THE VALUE 0.0393336');
        pase2:=0.0393336;
    end;
    writeln('THE PACE RATE ON THE HP-98640A WILL BE SET TO:',pase2:9:7);
    deltaf:=(2*(1/(2*(pase1+pase2))))/n;
    writeln('THE FREQUENCY RESOLUTION WILL BE ',deltaf:6:4,' HZ');
    writeln;
    writeln('ENTER THE BAND WIDTH TO BE VIEWED');
    writeln;
    readnumber(1,band);
    writeln;
    writeln('ENTER THE NUMBER OF SAMPLES TO FORM THE SMOOTHED SPECTRUM');
    writeln;
    readnumber(1,nsamp);
    writeln;
    writeln('THE NUMBER OF ELEMENTS STORED IS 30000 *****');
    writeln;
    WRITELN;
    WRITELN('ENTER THE SCALE READING');
    READNUMBER(1,NSCALE);
    new(channel);
    channel^[1]:=2;

```

```

channel'[2]:=1;
new(pace);
pace'[1]:=pace2;
pace'[2]:=pace1;
new(gain);
writeln('ENTER THE GAIN SETTING FOR THE HP-98640A ADC BOARD');
writeln('THE AVAILABLE CHOICES ARE 1, 8, 64, 512');
writeln('channel 1');
readnumber(1,gan);
gane:=round(gan);
gain'[2]:=gane;
writeln('channel 2');
readnumber(1,gan);
gane:=round(gan);
gain'[1]:=gane;
meas_lib_init;
config_0(name,model,select_code,1,0.02,error,units,multiplier,offset);
init(name);
sc:=(8*arctan(1)/n);
for i:=0 to n1 do
  with w'[i] do begin
    x:=cos(sc*i);
    y:=sin(sc*i);
  end;
for i:=0 to n1 do begin
  amp[i]:=0.0;
end;
calibrate(name,3,0.0001,1000);
new(data);
new(signal);
for i:=1 to 512 do begin
  signal'[i]:= 0.0;
end;
n5:=0;
while n5<nsamp do begin
  writeln('FFT DATA SAMPLING IN PROGRESS*****');
  random_scan(name,c_size,channel,d_size,data,rept,p_size,pace,g_size,gain);
  writeln(' 30000 data points taken ');

  for i:=3 to (d_size-2) do begin
    if (data'[i]>data'[i-2]) and (data'[i]>data'[i+2]) and (data'[i]>0) then
      begin
        m:=1;
        for k:=(i+1) to (i+1023) do begin
          signal'[m]:=signal'[m]+data'[k];
          m:=m+1;
          k:=k+1;
        end;
        n5:=n5+1;
        if (n5 >= nsamp) then goto 5;
        i:=i+1022;
      end;
    if (d_size-2-i < 1550) then goto 5;
    i:=i+1;
  end;
5:
  writeln(n5:3,' samples taken ');
end;
nsamp:=n5;
for m:= 1 to 512 do begin
  sig:=signal'[m]/round(nsamp);
  writeln(txt1,m:6,' ',sig:8:5);
end;
close(txt1,'save');
for i:=1 to 51 do begin
  signal'[i]:=signal'[i]*(1-cos(5*pi*(i-1)/512));

```

```

        end;
        writeln('1');
        for i:=461 to 512 do begin
            signal[i]:=signal[i]*(1+cos(5*pi*i/512));
        end;
        writeln('2');
        (ASSIGN REAL DATA TO ONE COMPONENT OF COMPLEX NUMBER "a")
        for i:=0 to n1 do
            with a[i] do begin x:=signal[i+1]; y:=0.0 end;
        reord(a);
        trf(a);
        writeln('3');
        for i:=0 to n1 do begin
            amp[i]:=amp[i]+mag(a[i])
        end;
        rewrite(txt,'JIM:SPECTDATA.TEXT');
        nn:=round(n/2);
        {WRITELN(TXT,NN:4)}
        for i:=0 to n1 do begin
            amp[i]:=amp[i]*(2*(pase1+pase2)/n)*1.14286;
            amp[i]:=amp[i]/nsamp;
            amp[i]:=amp[i]*1.0E08;
            freq[i]:=i*deltaf;
        end;
        for i:=0 to nn do begin
            IF (ROUND(FREQ[I])=710) THEN BEGIN WRITELN(TXT); WRITELN(TXT,NSCALE:4:2); END;
            writeln(txt,freq[i]:8:4,' ',amp[i]:20:17);
        end;
        imin:=round((fex-band)/deltaf);
        imax:=round((fex+band)/deltaf);
        writeln;
        writeln(nscale:8:4);
        for i:=imin to imax do begin
            writeln(freq[i]:8:4,' ',amp[i]:20:17);
        end;
        ilow:=round((fex-2*deltaf)/deltaf);
        trap:=deltaf/2*(amp[ilow]+2*amp[ilow+1]+2*amp[ilow+2]+2*amp[ilow+3]
            +amp[ilow+4]);
        writeln;
        writeln('INTEGRATED AREA BY TRAP RULE:');
        writeln;
        writeln(trap:15:4);
        writeln;
        writeln('INPUT ANY NUMBER TO VIEW SUBHARMONIC VALUES');
        readnumber(1,nscale);
        writeln;
        writeln('SUBHARMONIC FREQUENCY DISPLAYED');
        fex:=fex/2;
        imin:=round((fex-band)/deltaf);
        imax:=round((fex+band)/deltaf);
        for i:=imin to imax do begin
            writeln(freq[i]:8:4,' ',amp[i]:20:17);
        end;
        ilow:=round((fex-2*deltaf)/deltaf);
        trap:=deltaf/2*(amp[ilow]+2*amp[ilow+1]+2*amp[ilow+2]+2*amp[ilow+3]
            +amp[ilow+4]);
        writeln;
        writeln('INTEGRATED AREA BY TRAP RULE:');
        writeln;
        writeln(trap:15:4);
        close(txt,'SAVE');
        end.

```


POWER SPECTRUM PROGRAM

```

program spectrum(input,output);
  {This program samples a time varying voltage and computes the frequency}
  {spectrum by the Fast Fourier Transform method. The spectrum is written}
  {to disk as "SPECTDATA.TEXT". This program assumes that the D.C. component}
  {of the signal has been removed prior to A/D conversion. If this is not the}
  {case then program spectrum2 should be used.}
  import iodeclarations;
  import general_2;
  import measurement_lib;

  const
    name = 'ADC';
    model = '98S40A';
    select_code = 18;
    error = 'NO';
    units = 'STANDARD';
    multiplier = 1.0;
    offset = 0.0;
    o_size = 1;
    q_size = 1;
    c_size = 1;
    n=1024; n1=1023; r=10; pi=3.14159265;

  type
    r_array = ARRAY[1..15000] of real;
    r_ptr = ^r_array;
    i_array = ARRAY[1..7] of shortint;
    i_ptr = ^i_array;
    complex=record x,y: real and;
    datta = ARRAY[0..n1] of complex;
    c_ptr = ^datta;
    a_array=ARRAY[0..n1] of real;

  var
    channel: i_ptr;
    gain: i_ptr;
    pace: r_ptr;
    data: r_ptr;
    d_size, rept, i, m, c, p, nn, gane: integer;
    reschan, fmax, time, nsamp, pase, sc, deltaf, gan: real;
    w, a: c_ptr;
    txt: text;
    amp, freq: a_array;

  procedure reord(var a: c_ptr);
  var
    i, j, k, l: integer;
    q: complex;
  begin
    for i:=1 to n1 do begin
      l:=1;
      k:=0;
      for j:=0 to (n-1) do begin
        k:=(2*k)+1 mod 2;
        l:=l div 2;
      end;
      if i<k then begin
        q:=a[i];

```

```

    a[k]:=a
  end
end
end: (record)

procedure sum(z,w:complex; var s:complex);
begin
  with s do begin
    x:=z.x+w.x;
    y:=z.y+w.y
  end
end:

procedure dif(z,w:complex; var s:complex);
begin
  with s do begin
    x:=z.x-w.x;
    y:=z.y-w.y
  end
end:

procedure prod(z,w:complex; var s:complex);
begin
  with s do begin
    x:=z.x*w.x-z.y*w.y;
    y:=z.x*w.y+z.y*w.x
  end
end:

procedure neg(u:complex; var w:complex);
begin
  w.x:=-u.x;
  w.y:=-u.y
end:

procedure trf(var x:c_ptr);

var
  lvl,tl,tll,expon,p,i,j,k:integer;
  s,z:complex;

{tl = 2lvl}
{tll=2(lvl-1)}
{p=2(n-lvl)}
{expon=j*p}

begin
  tl:=2; tll:=1;
  for lvl:=1 to n do
    begin
      p:=n div tl; expon:=0;
      for j:=0 to tll-1 do
        begin
          i:=j; s:=w[expon];
          while i<n do
            begin
              k:=i+tll;
              if j=0 then z:=a[k]
              else prod(a[k],s,z);
              dif(a[i+1],z,a[k]);
              sum(a[i+1],z,a[i]);
              i:=i+tll
            end;
            expon:=expon+p
          end;
          i:=i+1; z:=a[i];
        end;
      end;
    end;
  end;
end:

```

```

    end
end; (trf)

function mag(z:complex):real;
begin
    with z do
        mag:=sqrt(x)+sqrt(y)
    end;
end;

begin (MAIN PROGRAM)
    new(w);
    new(a);
    writeln('ENTER THE MAXIMUM FREQUENCY COMPONENT OF THE SIGNAL');
    readnumber(1,fmax);
    writeln;
    pasc:=(1.0/(2.0*fmax));
    if(pasc < 0.000018) then
    begin
        writeln('THE PACE VALUE IS TOO SMALL FOR THE HP-98640A!!');
        writeln('*****');
        writeln('IF ALLOWED TO CONTINUE PACE WILL BE SET TO THE VALUE 0.000018');
        pasc:=0.000018;
    end;
    if (pasc>0.0393336) then
    begin
        writeln('THE PACE VALUE IS TOO LARGE FOR THE HP-98640A!!');
        writeln('*****');
        writeln('IF ALLOWED TO CONTINUE PACE WILL BE SET TO THE VALUE 0.0393336');
        pasc:=0.0393336;
    end;
    writeln('THE PACE RATE ON THE HP-98640A WILL BE SET TO:',pasc:9:7);
    writeln;
    d_size:=n;
    writeln('THE NUMBER OF ELEMENTS STORED IS ',d_size:5);
    rept:=d_size;
    writeln;
    deltaf:=(2*fmax)/n;
    writeln('THE FREQUENCY RESOLUTION WILL BE ',deltaf:6:4,' HZ');
    writeln;
    writeln('ENTER THE NUMBER OF SAMPLES TO FORM THE SMOOTHED SPECTRUM');
    writeln;
    readnumber(1,nsamp);
    new(channel);
    writeln;
    writeln('ENTER THE CHANNEL DESIRED FOR THE SPECTRAL MEASUREMENT');
    writeln;
    readnumber(1,realchan);
    channel^[1]:=round(realchan);
    new(pace);
    pace^[1]:=pasc;
    new(gain);
    writeln('ENTER THE GAIN SETTING FOR THE HP-98640A ADC BOARD');
    writeln('THE AVAILABLE CHOICES ARE 1, 8, 64, 512');
    writeln;
    readnumber(1,gan);
    gane:=round(gan);
    gain^[1]:=gane;
    meas_lib_init;
    config_0(name,model,select_code:1,0.02,error,units,multiplier,offset);
    init(name);
    sc:=(8*arctan(1)/n);
    for i:=0 to n1 do
        with w^[i] do begin
            x:=cos(sc*i);
            y:=sin(sc*i)

```

```

end;
for i:=0 to n1 do begin
  amp[i]:=0.0
end;
calibrate(name,3.0.0001.1000);
new(data);
for p:=1 to round(nsamp) do begin
  writein(chr(12));
  writein('DATA SAMPLING IN PROGRESS*****SAMPLE ',p:3,' OF ',nsamp:4:0);
  random_scan(name,c_size,channel,d_size,data,rept,p_size,pase,q_size,gain);
  {APPLY COSINE WINDOWING TO THE SAMPLED DATA}
  for i:=1 to round(d_size/10) do begin
    data[i]:=data[i]*(1-cos(5*pi*(i-1)/d_size));
  end;
  for i:=round(9*d_size/10) to d_size do begin
    data[i]:=data[i]*(1+cos(5*pi*(i-1)/d_size));
  end;
  {ASSIGN REAL DATA TO ONE COMPONENT OF COMPLEX NUMBER "a"}
  for i:=0 to n1 do
    with a[i] do begin x:=data[i+1]; y:=0.0 end;
  reord(a);
  trf(a);
  for i:=0 to n1 do begin
    amp[i]:=amp[i]+mag(a[i])
  end;
end;
rewrite(txt,'KIRK:SPECTDATA.TEXT');
nn:=round(n/2);
for i:=0 to n1 do begin
  amp[i]:=amp[i]*(2*pase/n)*1.14286;
  amp[i]:=amp[i]/nsamp;
  amp[i]:=amp[i]*1.0E08;
  freq[i]:=i*deltaf;
end;
for i:=0 to nn do begin
  writein(txt,freq[i]:8:4,'      ',amp[i]:20:17);
end;
close(txt,'SAVE');
end.

```

DIGITAL COMPLEX DEMODULATION PROGRAM

```

program demodulate(input,output);
LABEL S0;
{This program samples data at a user specified rate and a }
{digital complex demodulation technique is used to obtain both}
{the phase and amplitude modulates }
import iodeclarations;
import general_1;
import general_2;
import measurement_lib;

const
    name = 'ADC';
    model = '98640A';
select_code = 18;
    error = 'NO';
    units = 'STANDARD';
multiplier = 1.0;
    offset = 0.0;
    p_size = 1;
    q_size = 1;
    c_size = 1;
    pi = 3.14159265;

type
    an_array = ARRAY[0..200] of real;
    i_array = ARRAY[1..7] of shortint;
    i_ptr = ^i_array;
    complex = record x,y :real end;
    r_array = ARRAY[1..5000] of real;
    r_ptr = ^r_array;
    c_array = ARRAY[1..5000] OF COMPLEX;
    c_ptr = ^c_array;
    l1lr_array = ARRAY [1..7] of real;
    lr_ptr = ^l1lr_array;

var
    txt:text;
    test:char;
    channel:i_ptr;
    q,w,f:c_ptr;
    gain:i_ptr;
    pace:lr_ptr;
    b:an_array;
    data,xx,yy:r_ptr;
    msamp,d_size,rept,i,j,k,np:integer;
    rgain,t,sumx,sumy,a,p,beta,delta,fmax,pase,time,sumv,tavg,meanv
    ,fcarry,al,ptot,pbar:real;
    alpha,betal,atot,atsq,ptsq,abar,atsqbar,atsqrt,ratio:real;

procedure prod(z,w:complex; var s:complex);
begin
    with s do begin
        x:=x*w.x-z.v*w.v;

```

```

        y:=z.x*w.y+z.y*w.x
    end
end;

function mag(z:complex):real;
begin
    with z do
        mag:=sqrt(sqr(x)+sqr(y));
    end;
end;

function phase(z:complex):real;
begin
    with z do begin
        if (x=0.0) and (y>0.0) then phase:=1.570796327;
        if (x=0.0) and (y<0.0) then phase:=-1.570796327;
        if (x>0.0) and (y>0.0) then phase:=arctan(y/x);
        if (x<0.0) and (y>0.0) then phase:=pi+arctan(y/x);
        if (x>0.0) and (y<0.0) then phase:=arctan(y/x);
        if (x<0.0) and (y<0.0) then phase:=arctan(y/x)-pi;
        if (x<0.0) and (y=0.0) then phase:=pi;
        (PHASE:=ARCTAN(Y/X));
    end;
end;

procedure ners(al,be,de:real;var np:integer;var bk:an_array);
{THIS PROCEDURE COMPUTES THE COEFFICIENTS OF A NEARLY EQUIRIPPLE LINEAR}
{PHASE SMOOTHING FILTER WITH AN ODD NUMBER (2NP+1) OF TERMS AND EVEN SYMMETRY}

const
    pi = 3.141592654;

type
    an_array = ARRAY[1..200] of real;

var
    fk,et,qp,fla,gk,flk,ge,e:real;
    fnp,k,i,j,n:integer;

procedure ino(x:real;var s:real);
LABEL 1;
{THIS PROCEDURE EVALUATES THE MODIFIED BESSEL FUNCTION OF ZEROth ORDER}
{AT THE REAL VALUES OF THE ARGUMENT}

var
    ds,d:real;
begin
    s:=1.0;
    ds:=1.0;
    d:=0.0;
    i:=d+2.0;
    ds:=ds*x*x/(d*d);
    s:=s+ds;
    if (ds>0.2E-08*s) then goto 1;
end;

begin
    fk:=1.8445;
    if (al>21.0) then fk:=0.13927*(al-7.95);
    et:=0.58417*(exp(0.4*ln(al-21.0))+0.07886*(al-21.0));
    if (al<21.0) then et:=0.0;
    if (al>50.0) then et:=0.1102*(al-8.7);
    np:=trunc((fk/(2.0*de))+0.75);
    {TEST NP AGAINST DIMENSION LIMIT}
    if (np>149) then np:=149;
    fnp:=np;
    np:=np+1;

```



```

      ino(et,fia);
      for k:=1 to np do begin
        flk:=(2*k-1)/2;
        gk:=pi*k;
        ge:=et*sqrt(1.0-sqr(k/fnp));
        ino(ge,e);
        bk[k]:=(sin(be*gk)/gk)*(e/fia);
      end;
      bk[np]:=bk[np]/2.0;
      n:=np+1;
      for i:=2 to n do begin
        k:=n-i+2;
        j:=k-1;
        bk[k]:=bk[j];
      end;
      bk[1]:=be;
    end;

begin(MAIN PROGRAM)

  new(f);
  new(w);
  new(data);
  new(q);
  writeln('ENTER THE MAXIMUM FREQUENCY COMPONENT OF THE DATA (Hz)');
  writeln;
  readln(fmax);
  writeln;
  pase:=1.0/(2.0*fmax);
  writeln('ENTER THE TOTAL SAMPLE TIME (sec)');
  writeln;
  readln(time);
  d_size:=round(time/pase)+1;
  writeln('THE TOTAL NUMBER OF ELEMENTS STORED IS ',d_size:5);
  rept:=d_size;
  new(channel);
  channel^[1]:=1;
  new(pace);
  pace^[1]:=pase;
  new(gain);
  writeln('ENTER THE GAIN SETTING FOR THE MEASUREMENT');
  write('CHOICES ARE: 1,8,64,256 ----> ');
  readln(rgain);
  gain^[1]:=round(rgain);
  meas_lib_init;
  config_0(name,model,select_code,1,0.02,error,units,multiplier,offset);
  init(name);
  {calibrate(name,3,0.0001,1000);}
  writeln('*****');
  writeln('NOW CALCULATING THE MEAN VOLTAGE TO BE SUBTRACTED ');
  writeln('FROM ALL TIME SERIES ELEMENTS ');
  writeln('*****');
  writeln;
  writeln('ENTER THE AVERAGING TIME FOR COMPUTING THE MEAN VOLTAGE');
  writeln;
  readln(tavg);
  IF (TAVG<0.0) THEN BEGIN MEANV:=0.0; GOTO 50; END;
  msamp:=round(tavg/(pase*d_size));
  sumv:=0.0;
  for i:=1 to msamp do begin
    writeln(chr(12));
    writeln;
    writeln('MEAN VOLT CALCULATION IN PROGRESS..REPETITION ',i:3,' OF ',msamp:3);
    random_scan(name,c_size,channel,d_size,data,rept,p_size,pase,q_size,gain);
    for j:=1 to d_size do begin
      sumv:=sumv+data^[j];
    end;
  end;

```

```

end;
end;
meanv:=sumv/(d_size*msamp);
writeln;
S0:writeln('MEAN VOLTAGE HAS BEEN COMPUTED: MEAN VOLTAGE = ',MEANV:9:6);
writeln('PRESS "C" WHEN READY TO SAMPLE SIGNAL FOR COMPLEX DEMODULATION');
repeat
  readchar(1,test);
  until ord(test) = 67;
writeln;
random_scan(name,c_size,channel,d_size,data,rept,p_size,pase,q_size,gain);
writeln;
  for i:=1 to d_size do begin
    data^[i]:=data^[i]-meanv;
  end;
writeln('SIGNAL HAS BEEN SAMPLED AND THE MEAN SUBTRACTED FROM ALL TIME-');
writeln('SERIES ELEMENTS');
writeln;
  for i:=1 to d_size do begin
    with f^[i] do begin
      x:=data^[i];
      y:=0.0;
    end;
  end;
end;
writeln('DATA NOW FORMS THE REAL PART OF COMPLEX NUMBER "f"');
writeln;
writeln('ENTER THE CARRIER FREQUENCY (in Hz) AS DETERMINED FROM PREVIOUS');
writeln('POWER SPECTRAL MEASUREMENTS');
writeln;
readln(fcarry);
  for i:=1 to d_size do begin
    with w^[i] do begin
      x:=2*cos(2*pi*i*fcarry*pase);
      y:=-2*sin(2*pi*i*fcarry*pase);
    end;
  end;
end;
  for i:=1 to d_size do begin
    prod(w^[i],f^[i],q^[i]);
  end;
beta:=fcarry/fmax;
writeln;
write('ENTER THE TRANSITION BANDWIDTH DELTA ---> ');
readln(delta);
writeln;
write('ENTER THE STOPBAND LOSS IN dB ---> ');
readln(al);
writeln;
writeln('APPLYING THE NERS DIGITAL FILTER');
ners(al,beta,delta,np,b);
writeln;
writeln('EXIT NERS....NP = ',np:4);
writeln;
dispose(w);
new(xx);
new(yy);
  for i:=1 to d_size do begin
    with q^[i] do begin
      xx^[i]:=x;
      yy^[i]:=y;
    end;
  end;
end;
  for i:= np to (d_size-np+1) do begin
    sumx:=0.0;
    sumy:=0.0;
    for k:=2 to np do begin
      sumx:=sumx+bfk*1e((xx^[i-k+1]+xx^[i+k-1]));

```

```

        sumy:=sumy+b[k]*(yy^[i-k+1]+yy^[i+k-1]);
    end;
    sumx:=sumx+b[i]*xx^[i];
    sumy:=sumy+b[i]*yy^[i];
    with q^[i] do begin
        x:=sumx;
        y:=sumy;
    end;
end;
rewrite(txt,'V20: SIGNAL.TEXT');
t:=0.0;
for i:=np to (d_size-np+1) do begin
    with f^[i] do begin
        writeln(txt,t:10:7,' ',x:10:7);
    end;
    t:=t+pase;
end;
close(txt,'SAVE');
rewrite (txt,'V20: AMP.TEXT');
t:=0.0;
atot:=0.0;
ptot:=0.0;
atsq:=0.0;
ptsq:=0.0;
for i:=np to (d_size-np+1) do begin
    with q^[i] do begin
        a:=mag(q^[i]);
        atot:=atot+a;
        p:=phase(q^[i]);
        ptot:=ptot+p;
    end;
    writeln(txt,t:10:7,' ',a:10:7);
    t:=t+pase;
end;
close(txt,'SAVE');

abar:=atot/(d_size-2*np+2);
pbar:=ptot/(d_size-2*np+2);
WRITELN('MEAN PHASE = ',PBAR:10:6);
WRITELN;
for i:=np to (d_size-np+1) do begin
    with q^[i] do begin
        a:=mag(q^[i]);
        atsq:=atsq+sqr(a-abar);
    end;
end;
atsqbar:=atsq/(d_size-2*np+2);
atsqrt:=sqrt(atsqbar);
alpha:=atsqrt/abar;

rewrite(txt,'V20: FAZE.TEXT');
t:=0.0;
for i:=np to (d_size-np+1) do begin
    with q^[i] do begin
        p:=phase(q^[i]);
        {if (pbar<0.0) then begin}
        {pbar:=abs(pbar);}
        {p:=p+pbar;}
        {end}
        {else}
        p:=p-pbar;
        ptsq:=ptsq+sqr(p);
    end;
    writeln(txt,t:10:7,' ',p:10:7);
    t:=t+pase;
end;

```

```
beta1:=sqrt(ptsq/(d_size-2*np+2));
ratio:=alpha/beta1;

close(txt,'SAVE');
writeln;
writeln('*****');
writeln('DIGITAL COMPLEX DEMODULATION OUTPUT RESULTS:');
writeln('RMS AMPLITUDE MODULATION INDEX (alpha) = ',alpha:8:4);
writeln('RMS PHASE MODULATION INDEX (beta)      = ',beta1:8:4);
writeln('THE RATIO OF alpha/beta =                ',ratio:8:4);
writeln('*****');
end.
```

BICOHERENCE PROGRAM

```
PROGRAM SIGNAL_BIAB(INPUT,OUTPUT);
```

```
IMPORT IODECLARATIONS;
IMPORT GENERAL_2;
IMPORT MEASUREMENT_LIB;
```

```
CONST
```

```
    NAME = 'ADC';
    MODEL = '98640A';
    SELECT_CODE = 18;
    ERROR = 'NO';
    UNITS = 'STANDARD';
    MULTIPLIER = 1.0;
    OFFSET = 0.0;
    P_SIZE = 1;
    G_SIZE = 1;
    C_SIZE = 1;
    N = 512;
    N1 = 511;
    N2 = 256;
    N4 = 128;
```

```
TYPE
```

```
    R_ARRAY = ARRAY[1..512] OF REAL;
    R_PTR = ^R_ARRAY;
    I_ARRAY = ARRAY[1..7] OF SHORTINT;
    I_PTR = ^I_ARRAY;
    A_ARRAY = ARRAY[0..N1] OF REAL;
```

```
VAR
```

```
    CHANNEL : I_PTR;
    GAIN : I_PTR;
    PACE : R_PTR;
    DATA : R_PTR;
    GANE,D_SIZE,REPT,I,II,J,K,L,M,C,T,MSAMP,NSAMP,NN: INTEGER;
    GAN,FMAX,FL,FK,DELTA F,TIME,NUMSAMP,PASE,SC,DELTA,SUMV,MEANV: REAL;
    TXTS: TEXT;
    FILENAME : PACKED ARRAY[1..20] OF CHAR;
```

```
BEGIN {MAIN PROGRAM}
```

```
    WRITELN('ENTER THE MAXIMUM FREQUENCY COMPONENT OF THE SIGNAL');
    READNUMBER(1,FMAX);
    WRITELN;
    PASE := (1.0/(2.0*FMAX));
    IF (PASE<0.000018) THEN
        BEGIN
            WRITELN('THE PACE VALUE IS TOO SMALL FOR THE HP-98640A!!');
            WRITELN('*****');
            WRITELN('IF ALLOWED TO CONTINUE PACE WILL BE SET TO THE VALUE');
            WRITELN('0.000018');
            PASE := 0.000018;
        END;
    IF (PASE<0.0333336) THEN
```



```

PROGRAM DISK_BI(INPUT,OUTPUT);
{THIS IS PART A BICOHERENCE SPECTRUM COMPUTATION}
{THIS PART SAMPLES A TIME VARYING VOLTAGE & COMPUTES THE COMPLEX FOURIER}
{COEFFICENTS BY THE FFT METHOD AND ALL THESE DATA ARE READ FROM HARD DISK}
{THE BICOHERENCE COEFFICENTS ARE WRITTEN TO FIVE DATAFILES}

IMPORT IODECLARATIONS;
IMPORT GENERAL_2;
IMPORT MEASUREMENT_LIB;

CONST
    N = 512;
    N1 = 511;
    N2 = 256;
    N4 = 128;
    R = 9;
    PI = 3.14159265;

TYPE
    R_ARRAY = ARRAY[1..512] OF REAL;
    R_PTR = ^R_ARRAY;
    I_ARRAY = ARRAY[1..71] OF SHORTINT;
    I_PTR = ^I_ARRAY;
    COMPLEX = RECORD X,Y: REAL END;
    DATTA = ARRAY[0..N1] OF COMPLEX;
    C_PTR = ^DATTA;
    A_ARRAY = ARRAY[0..N1] OF REAL;
    B_ARRAY = ARRAY[1..N4,1..N2] OF COMPLEX;
    B_PTR = ^B_ARRAY;

VAR
    DATA : R_PTR;
    GANE,D_SIZE,REPT,I,II,J,K,L,M,C,T,MSAMP,NSAMP,NN,SAM: INTEGER;
    GAN,FMAX,FL,FK,DELTA F,TIME,NUMSAMP,PASE,SC,DELTA,SUMV,MEANV: REAL;
    PASE2,PASE3,PASE4,PASE5: REAL;
    B: B_PTR;
    P: COMPLEX;
    W,A,D: C_PTR;
    TXT1,TXT2,TXT3,TXT4,TXT5,TXT6,TXT7,TXT8,TXT9,TXT0: TEXT;
    AMP: A_ARRAY;
    FILENAME1,FILENAME2,FILENAME3,FILENAME4,FILENAMES
    : PACKED ARRAY[1..20] OF CHAR;

```

```

procedure reord(var a: c_ptr);
var
    i,j,k,l: integer;
    q: complex;
begin
    for i:=1 to n1 do begin
        l:=i;
        k:=0;
        for j:=0 to (n-1) do begin
            k:=(2*k)+1 mod 2;
            l:=l div 2

```

```

    end;
    if i<k then begin
        q:=a[i];
        a[i]:=a[k];
        a[k]:=q
    end
end
end; {reord}

procedure sum(z,w:complex; var s:complex);
begin
    with s do begin
        x:=z.x+w.x;
        y:=z.y+w.y
    end
end;

procedure dif(z,w:complex; var s:complex);
begin
    with s do begin
        x:=z.x-w.x;
        y:=z.y-w.y
    end
end;

procedure prod(z,w:complex; var s:complex);
begin
    with s do begin
        x:=z.x*w.x-z.y*w.y;
        y:=z.x*w.y+z.y*w.x
    end
end;

procedure neg(u:complex; var w:complex);
begin
    w.x:=-u.x;
    w.y:=-u.y
end;

procedure conj(u:complex; var w:complex);
begin
    w.x:=u.x;
    w.y:=-u.y;
end;

procedure trf(var x:c_ptr);
var
    lvl,tl,tll,expon,t,i,j,k:integer;
    s,z:complex;

{tl = 2^lvl}
{tll=2^(lvl-1)}
{p=2^(r-lvl)}
{expon=j*p}

begin
    tl:=2; tll:=1;
    for lvl:=1 to r do
        begin
            t:=n div tl; expon:=0;
            for j:=0 to tll-1 do
                begin
                    i:=j; s:=w[expon];
                    while i<n do

```

```

begin
    k:=1+t11;
    if j=0 then z:=a[k];
    else prod(a[k],s,z);
    dif(a[i],z,a[k]);
    sum(a[i],z,a[k]);
    i:=i+t1
end;
expon:=expon+t
end;
t1:=2*t1; t11:=2*t11
end
end; {trf}

function mag(z:complex):real;
begin
    with z do
        mag:=sqr(x)+sqr(y)
    end;
end;

BEGIN (MAIN PROGRAM)
    NEW(W);
    NEW(A);
    new(B);
    NEW(D);
    WRITELN('ENTER THE INPUT DATAFILE **** 1');
    READLN(FILENAME1);
    RESET(TXT1,FILENAME1);
    READ(TXT1,PASE);
    WRITELN;
    WRITELN('ENTER THE INPUT DATAFILE **** 2');
    READLN(FILENAME2);
    RESET(TXT2,FILENAME2);
    READ(TXT2,PASE2);
    WRITELN;
    WRITELN('ENTER THE INPUT DATAFILE **** 3');
    READLN(FILENAME3);
    RESET(TXT3,FILENAME3);
    READ(TXT3,PASE3);
    WRITELN;
    WRITELN('ENTER THE INPUT DATAFILE **** 4');
    READLN(FILENAME4);
    RESET(TXT4,FILENAME4);
    READ(TXT4,PASE4);
    WRITELN;
    WRITELN('ENTER THE INPUT DATAFILE **** 5');
    READLN(FILENAME5);
    RESET(TXT5,FILENAME5);
    READ(TXT5,PASE5);
    WRITELN;
    WRITELN(' THE PACE RATE READ FROM 1 IS ',PASE:9:7);
    WRITELN(' THE PACE RATE READ FROM 2 IS ',PASE2:9:7);
    WRITELN(' THE PACE RATE READ FROM 3 IS ',PASE3:9:7);
    WRITELN(' THE PACE RATE READ FROM 4 IS ',PASE4:9:7);
    WRITELN(' THE PACE RATE READ FROM 5 IS ',PASE5:9:7);
    WRITELN;
    D_SIZE:=N;
    WRITELN('THE NUMBER OF ELEMENTS STORED IS ',D_SIZE:5);
    REPT:= D_SIZE;
    WRITELN;
    DELTAF:=1/(N*PASE);
    WRITELN('THE FREQUENCY RESOLUTION WILL BE ',DELTAF:6:4,' HZ ');
    WRITELN;
    WRITELN('ENTER THE NUMBER OF SAMPLES TO FORM THE BISPECTRAL');
    WRITELN('MEASUREMENT');
    WRITELN;
    READNUMBER(1,NUMSAMP);

```



```

=====
II := 1;
IF SAM=1 THEN REWRITE(TXT6,'KIRK:BICOH1.TEXT');
IF SAM=2 THEN REWRITE(TXT7,'KIRK:BICOH2.TEXT');
IF SAM=3 THEN REWRITE(TXT8,'KIRK:BICOH3.TEXT');
IF SAM=4 THEN REWRITE(TXT9,'KIRK:BICOH4.TEXT');
IF SAM=5 THEN REWRITE(TXT0,'KIRK:BICOH5.TEXT');
FOR L := 1 TO ROUND(N/4) DO BEGIN
  FOR K := L TO (ROUND(N/2)-L) DO BEGIN
    IF (II <= 9) THEN BEGIN
      WITH B^[L,K] DO BEGIN
        IF SAM=1 THEN WRITE(TXT6,' ',X:7:5);
        IF SAM=2 THEN WRITE(TXT7,' ',X:7:5);
        IF SAM=3 THEN WRITE(TXT8,' ',X:7:5);
        IF SAM=4 THEN WRITE(TXT9,' ',X:7:5);
        IF SAM=5 THEN WRITE(TXT0,' ',X:7:5);
      END;
    END
  END
ELSE
  BEGIN
    WITH B^[L,K] DO BEGIN
      IF SAM=1 THEN BEGIN
        WRITELN(TXT6);
        WRITE(TXT6,' ',X:7:5);
      END;
      IF SAM=2 THEN BEGIN
        WRITELN(TXT7);
        WRITE(TXT7,' ',X:7:5);
      END;
      IF SAM=3 THEN BEGIN
        WRITELN(TXT8);
        WRITE(TXT8,' ',X:7:5);
      END;
      IF SAM=4 THEN BEGIN
        WRITELN(TXT9);
        WRITE(TXT9,' ',X:7:5);
      END;
      IF SAM=5 THEN BEGIN
        WRITELN(TXT0);
        WRITE(TXT0,' ',X:7:5);
      END;
    END;
  END
  II := II+1;
END;
END;
IF SAM=1 THEN CLOSE(TXT6,'SAVE');
IF SAM=2 THEN CLOSE(TXT7,'SAVE');
IF SAM=3 THEN CLOSE(TXT8,'SAVE');
IF SAM=4 THEN CLOSE(TXT9,'SAVE');
IF SAM=5 THEN CLOSE(TXT0,'SAVE');
END;
<=====>
END.

```

BICOHERENCE PLOTTING ROUTINE

02234567

```

COMMON X(128), Y(255), Z(128,255), WORK(128,255)
REAL  LOWEST,HIGHEST,XTICVAL,YTICVAL,SMOOL,ADJ,OD,FRE,PASE
REAL  FX, FY,XWINMIN,XWINMAX,YWINMIN,YWINMAX,AUTO
INTEGER FXX,FYY,N,N1,N2,N3,N4
REAL PENS(7),INCRE
CHARACTER NAME*20,XTITLE*20,YTITLE*20,TITLE*20
DATA PENS/ 1.0,2.0,3.0,4.0,3.0,2.0,1.0/
C*****
C  THIS PROGRAM IS USING X AND Y ONE-DIMENSIONAL ARRAY TO DRAW  *
C  THE CONTOURS OF A FUNCTION OF TWO VARIABLES  $Z = F(X,Y)$ , WHERE  *
C  Z IS DEFINED ON A RECTANGULAR MESH  *
C*****
C  DEFINITION OF INPUT VARIABLES:  *
C  XC J      ONE-DIMENSIONAL ARRAY READ FROM DATAFILE  *
C  YC J      ONE-DIMENSIONAL ARRAY READ FROM DATAFILE  *
C  NAME      DATAFILE NAME (USER INPUT)  *
C  FX        THE NUMBER OF "COLUMN" OF POINTS IN THE X DIRECTION  *
C            AS WELL AS THE LEADING DIMENSION OF Z FUNCTION.(REAL)  *
C  FY        THE NUMBER OF "ROW" OF POINTS IN THE Y DIRECTION AS  *
C            WELL AS THE SECOND DIMENSION OF Z FUNCTION.(REAL)  *
C  XWINMIN   USERS DEFINE THE X-AXIS MINIMUM WINDOW VALUE  *
C  XWINMAX   USERS DEFINE THE X-AXIS MAXIMUM WINDOW VALUE  *
C  YWINMIN   USERS DEFINE THE Y-AXIS MINIMUM WINDOW VALUE  *
C  YWINMAX   USERS DEFINE THE Y-AXIS MAXIMUM WINDOW VALUE  *
C  LOWEST    LOWEST CONTOUR LEVEL  *
C  HIGHEST   HIGHEST CONTOUR LEVEL  *
C  INCRE     CONTOUR INCREMENT VALUE  *
C  N         THE NUMBER OF CONTOUR LABEL INCREMENT  *
C  XTITLE    X AXIS LABEL  *
C  YTITLE    Y AXIS LABEL  *
C  TITLE     THE PLOT TITLE  *
C*****
0234567
PRINT*, '*****'
PRINT*, 'THIS PROGRAM IS USING TEMPLATE PACKAGE ROUTINE (UPCNTR)'
PRINT*, 'TO DRAW TWO-DIMENSIONAL CONTOUR LINES'
PRINT*, '*****'
PRINT*, 'PLEASE ENTER DATA FILENAME'
READ(3, '(A20)') NAME
PRINT*, 'ENTER THE MAX FREQUENCY'
READ(3, *) FRE
PASE=1.0/(2.0*FRE)
OPEN(UNIT=122, FILE=NAME)

C
N=512
N1=N-1
N2=N/2
N4=N/4

C
DO 1400 I=1,N4
X(I)=0.0
DO 1400 J=1,(N2-1)
Y(J)=0.0
Z(I,J)=0.0
1400 CONTINUE

C
DO 1510 I=1,N4
X(I)=I/(N*PASE)
1510 CONTINUE
DO 1520 J=1,(N2-1)
Y(J)=J/(N*PASE)

```



```

      READ(122,*) Z(I,J) = Z(I,N2-1), I=1,N4)

C
      PRINT*, 'AUTO CALCULATION OF THE CONTOUR LEVEL OR NOT'
      PRINT*, '.1. FOR YES ; .2. FOR NO'
      READ(3,*)ADJ

C
      IF (ADJ .EQ. 2) THEN
        PRINT*, 'ENTER THE LOWEST CONTOUR LEVEL'
        READ(3,*)LOWEST
        PRINT*, 'ENTER THE HIGHEST CONTOUR LEVEL'
        READ(3,*)HIGHEST
        PRINT*, 'ENTER THE CONTOUR INCREMENT VALUE'
        READ(3,*)INCRE
        PRINT*, 'ENTER THE NUMBER OF CONTOUR LABEL INCREMENT'
        READ(3,*)N
      ELSE
        ENDIF

C
      PRINT*, 'ENTER THE PLOT TITLE'
      READ(3,*(A20))TITLE
C
      PRINT*, 'ENTER X-AXIS TITLE'
      READ(3,*(A20))XTITLE
C
      PRINT*, 'ENTER Y-AXIS TITLE'
      READ(3,*(A20))YTITLE
C
      PRINT*, 'DO YOU WANT TO USE THE DEFAULT DEVICE VIEWPORT'
      PRINT*, 'ENTER .1. FOR YES .2. FOR NO'
C
      READ(3,*)ADJ
      PRINT*, 'USING AUTOSCALING OR NONAUTOSCALING FOR X-Y AXES'
      PRINT*, 'ENTER .1. FOR AUTO ; .2. FOR NON AUTO'
      READ(3,*)AUTO
      IF (AUTO .EQ. 2.) THEN
        PRINT*, 'PLEASE ENTER X-AXIS MINIMUM AND MAXIMUM WINDOW VALUE'
        READ(3,*)XWINMIN,XWINMAX
        PRINT*, 'PLEASE ENTER Y-AXIS MINIMUM AND MAXIMUM WINDOW VALUES'
        READ(3,*)YWINMIN,YWINMAX
        PRINT*, 'PLEASE ENTER X AND Y AXES TICVALUES'
        READ(3,*)XTICVAL,YTICVAL
      ELSE
        ENDIF

C
      PRINT*, 'DO YOU WANT CONTOUR LINES ARE SMOOTHED OR NOT'
      PRINT*, '.1. FOR YES ; .2. FOR NO'
      READ(3,*)SMOO

C
      PRINT*, 'DO YOU WANT CONTOUR PLOT IN 2-D OR 3-D'
      PRINT*, '.1. FOR 2-D ; .2. FOR 3-D'
      READ(3,*)DD

C
      FX = N4 * 1.0
      FY = (N2-1)*1.0

C
      DO 10 I = 1,N4
      DO 10 J = 1,(N2-1)
      WORK(I,J) = 0.0
10    CONTINUE

C
      XMIN = X(1)
      XMAX = X(1)
      YMIN = Y(1)
      YMAX = Y(1)
      ZMIN = Z(1,1)
      ZMAX = Z(1,1)
C234567
      DO 20 I = 2, N4
      IF (X(I) .GT. XMAX) XMAX = X(I)

```

```

20  CONTINUE
C
DO 30 J = 1, (N2-1)
  IF (Y(J) .GT. YMAX) YMAX = Y(J)
  IF (Y(J) .LT. YMIN) YMIN = Y(J)
30  CONTINUE
C
DO 32 I=1,N4
  X(I)=X(I)/FRE
32  CONTINUE
C
DO 35 I=1, N2-1)
  Y(I)=Y(I)/FRE
35  CONTINUE
C
DO 40 I=1,N4
DO 40 J=1, (N2-1)
  IF (Z(I,J) .GT. ZMAX) ZMAX=Z(I,J)
  IF (Z(I,J) .LT. ZMIN) ZMIN=Z(I,J)
40  CONTINUE
C
DO 45 I=1,N4
DO 45 J=1, (N2-1)
  Z(I,J)=Z(I,J)/ZMAX
45  CONTINUE
C
C*****
C
C   START TO USE TEMPLATE GRAPHICS
C
C*****
C
C   CALL USTART
C
C
C*****
C   ADJUST AND OUTLINE THE DEVICE VIEWPORT
C*****
C   CALL UOUTLN
C
C*****
C   PLOT THE X-Y AXES AND LABEL
C*****
C   CALL USET('ERROR')
C   CALL USET('LARGE')
C
C
C   CALL UPSET('XLABEL', 'X-Fx/FN')
C   CALL UPSET('YLABEL', 'Y-Fy/FN')
C   CALL USET('XBOTH')
C   CALL USET('YBOTH')
C*****
C
C   USING AUTOSCAL(1) OR OWNSCALE(2)
C
C***** 1
C   CALL USET('XYAXES')
C
C   IF (AUTO.EQ. 1.) THEN
C   CALL USET('AUTOSCALE')
C   CALL USET('BESTFORMAT')
C ----- 2
C   ELSE
C   CALL USET('OWNSCALE')

```

```

      CALL UPSET('CLOW',LOWEST)
      CALL UWINDO(XWINMIN,XWINMAX,YWINMIN,YWINMAX)
      ENDIF
C*****
C**** DRAW THE CONTOUR LINES FROM THE ORIGIN
      CALL USET('ORIGIN')

C**** CONTOUR SMOOTHING
      IF(SMOO.EQ. 1) THEN
        CALL USET('SMOOTH')
      ELSE
        CALL USET('NOSMOOTH')
      ENDIF
C**** MINMAX LABELS
      CALL USET('MINMAX')

C**** CONTOUR DIMENSION
      IF (DD.EQ. 1) THEN
        CALL UPOINT(0.0,0.0,1.0)
        CALL USET('2DCONTOURS')
      ELSE
        CALL USET('3DCONTOURS')
      ENDIF
C      CALL UPOINT(X,Y,Z)
C**** UNIFORMITY
      CALL USET('UNIFORM')

C**** VIEWING RESET OR NOT
      CALL USET('RESET')
C
C*****
C      CONTOUR GENERATION AUTO OR USERS GIVE
C*****
C
      IF(ADJ.EQ. 1) THEN
        CALL USET('CONTOURS')
C *****
      ELSE
        CALL UPSET('CLOW',LOWEST)
        CALL UPSET('CHIG',HIGHEST)
        CALL UPSET('CINC',INCR)
      ENDIF

C**** CONTOUR LABEL INCREMENT
      CALL UPSET('CBOT', 0.0)
      CALL UPSET('CTOP', 0.5)
      CALL UPSET('CLABEL',FLOAT(N))
C
C***** CONTOUR ROUTINE *****
C
      CALL UPCNTR(Z,X,Y,WORK,FX,FY,PENS)
C
C*****
C
      CALL UEND
C *****
      STOP
      END

```

COHERENCE PROGRAM

```

program COHERENCE(input,output);
  {This program uses the FFT method to compute the coherence}
  {function between two sampled anemometer signals}
  import iodeclarations;
  import general_2;
  import measurement_lib;

  const
    name = 'ADC';
    model = '98640A';
    select_code = 18;
    error = 'NO';
    units = 'STANDARD';
    multiplier = 1.0;
    offset = 0.0;
    p_size = 2;
    q_size = 2;
    c_size = 2;
    n = 256;
    n1 = 255;
    r = 8;
    pi = 3.14159265;

  type
    r_array = ARRAY[1..2*n] of real;
    r_ptr = ^r_array;
    i_array = ARRAY[1..7] of shortint;
    i_ptr = ^i_array;
    complex = record x,y: real end;
    datta = ARRAY[0..(2*n)-1] of complex;
    c_ptr = ^datta;
    a_array = ARRAY[0..n1] of real;
    l_array = ARRAY[1..n] of real;

  var
    channel: i_ptr;
    gain: i_ptr;
    pace: r_ptr;
    data: r_ptr;
    d_size, rept, i, j, m, c, p, msamp, k: integer;
    fmax, time, nsamp, pasc1, pasc2, sc, sumv1, sumv2, meanv1, meanv2, temp, tau,
    f: real;
    w, a, b, g: c_ptr;
    txt: text;
    theta, sumx, sumy, qxy, qx, qy, gamma: a_array;
    q, qq: complex;
    v: l_array;

  procedure reord1(var a: c_ptr);
  var
    i, j, k, l: integer;
    q: complex;
  begin
    for i := 1 to n1 do begin

```

```

l:=1;
k:=0;
for j:=0 to (n-1) do begin
  k:=(2*k)+1 mod 2;
  l:=l div 2
end;
if i<k then begin
  q:=a[l];
  a[l]:=a[k];
  a[k]:=q
end
end
end; {reord1}

procedure reord2(var b:c_ptr);
var
  i,j,k,l:integer;
  q:complex;
begin
  for i:=1 to n1 do begin
    l:=1;
    k:=0;
    for j:=0 to (n-1) do begin
      k:=(2*k)+1 mod 2;
      l:=l div 2
    end;
    if i<k then begin
      q:=b[l];
      b[l]:=b[k];
      b[k]:=q
    end
  end
end; {reord2}

procedure sum(z,w:complex; var s:complex);
begin
  with s do begin
    x:=z.x+w.x;
    y:=z.y+w.y
  end
end;

procedure dif(z,w:complex; var s:complex);
begin
  with s do begin
    x:=z.x-w.x;
    y:=z.y-w.y
  end
end;

procedure prod(z,w:complex; var s:complex);
begin
  with s do begin
    x:=z.x*w.x-z.y*w.y;
    y:=z.x*w.y+z.y*w.x
  end
end;

procedure neg(u:complex; var w:complex);
begin
  w.x:=-u.x;
  w.y:=-u.y
end;

```

```

var
  lvl,tl,tll,expon,p,i,j,k:integer;
  s,z:complex;

{tl = 2^lvl}
{tll=2^(lvl-1)}
{p=2^(r-lvl)}
{expon=j*p}

begin
  tl:=2; tll:=1;
  for lvl:=1 to r do
    begin
      p:=n div tl; expon:=0;
      for j:=0 to tll-1 do
        begin
          i:=j; s:=w[expon];
          while i<n do
            begin
              k:=i+tll;
              if j=0 then z:=a[k];
              else prod(a[k],s,z);
              dif(a[i],z,a[k]);
              sum(a[i],z,a[i]);
              i:=i+tll;
            end;
            expon:=expon+p;
          end;
          tl:=2*tl; tll:=2*tll;
        end
      end;
    end; {trf1}

  procedure trf2(var x:c_ptr);

  var
    lvl,tl,tll,expon,p,i,j,k:integer;
    s,z:complex;

    {tl = 2^lvl}
    {tll=2^(lvl-1)}
    {p=2^(r-lvl)}
    {expon=j*p}

  begin
    tl:=2; tll:=1;
    for lvl:=1 to r do
      begin
        p:=n div tl; expon:=0;
        for j:=0 to tll-1 do
          begin
            i:=j; s:=w[expon];
            while i<n do
              begin
                k:=i+tll;
                if j=0 then z:=b[k];
                else prod(b[k],s,z);
                dif(b[i],z,b[k]);
                sum(b[i],z,b[i]);
                i:=i+tll;
              end;
              expon:=expon+p;
            end;
            tl:=2*tl; tll:=2*tll;
          end
        end;
      end;
    end; {trf2}

```

```

procedure conj(u:complex; var w:complex);
begin
  w.x:=u.x;
  w.y:=-u.y
end;

function mag(z:complex):real;
begin
  with z do
    mag:=sqr(x)+sqr(y)
  end;

function phase(y1,x1:real):real;
begin
  if (x1=0.0) and (y1>0.0) then phase:=1.570796327;
  if (x1=0.0) and (y1<0.0) then phase:=-1.570796327;
  if (x1>0.0) and (y1>0.0) then phase:=arctan(y1/x1);
  if (x1<0.0) and (y1>0.0) then phase:=pi+arctan(y1/x1);
  if (x1>0.0) and (y1<0.0) then phase:=arctan(y1/x1);
  if (x1<0.0) and (y1<0.0) then phase:=arctan(y1/x1)-pi;
  if (x1<0.0) and (y1=0.0) then phase:=pi;
end;

begin {MAIN PROGRAM}
  new(w);
  new(a);
  new(data);
  new(b);
  new(g);
  writeln('ENTER THE MAXIMUM FREQUENCY COMPONENT OF THE DATA (HZ)');
  writeln;
  readnumber(1,fmax);
  writeln;
  pase1:=0.000025;
  pase2:=1.0/(2.0*fmax);
  d_size:=2*n;
  writeln('THE TOTAL NUMBER OF ELEMENTS STORED IS ',d_size:5);
  writeln;
  rept:=n;
  writeln('ENTER THE NUMBER OF SAMPLES TO FORM THE AVERAGE COHERENCE');
  writeln;
  readnumber(1,nsamp);
  new(channel);
  for i:= 1 to 2 do
  begin
    channel^[i]:=1
  end;
  new(pace);
  pace^[1]:=pase2;
  pace^[2]:=pase1;
  new(gain);
  gain^[1]:=1;
  gain^[2]:=1;
  meas_lib_init;
  config_0(name,model,select_code,1,0.02,error,units,multiplier,offset);
  init(name);
  calibrate(name,3,0.0001,1000);
  sc:=(8*arctan(1)/n);
  for i:=0 to n1 do
    with w^[i] do begin
      x:=cos(sc*i);
      y:=sin(sc*i)
    end;
  writeln('* * * * *');
  writeln('NOW CALCULATING THE MEAN VOLTAGE TO BE SUBTRACTED FROM ALL ');

```



```

writeln('TIME SERIES DATA ELEMENTS');
writeln('* * * * *');
writeln;
writeln('ENTER THE AVERAGING TIME FOR COMPUTING THE MEAN VOLTAGE');
writeln;
readnumber(1,time);
msamp:=round((2*time)/((pasel+pase2)*d_size));
sumv1:=0.0;
sumv2:=0.0;
for i:= 1 to msamp do begin
    writeln(chr(12));
    writeln;
    writeln('MEAN VOLT CALCULATION IN PROGRESS...REPETITION ',i:3,' OF',msamp:3);
    random_scan(name,c_size,channel,d_size,data,rept,p_size,pase,q_size,gain);
    for j:=1 to (d_size-1) do begin
        sumv1:=sumv1+data^[j];
        sumv2:=sumv2+data^[j+1];
        j:=j+1;
    end;
end;
meanv1:=(2.0*sumv1)/(d_size*msamp);
meanv2:=(2.0*sumv2)/(d_size*msamp);
(* * * * * *)
for k:=0 to n1 do begin
    gxy[k]:=0.0;
    gx[k]:=0.0;
    gy[k]:=0.0;
    theta[k]:=0.0;
    gamma[k]:=0.0;
end;
for p:=1 to round(nsamp) do begin
    writeln(chr(12));
    writeln('*****');
    writeln('COHERENCE MEASUREMENT IN PROGRESS.....');
    writeln('SAMPLE ',p:3,' OF ',nsamp:4:0);
    writeln('*****');
    writeln;
    random_scan(name,c_size,channel,d_size,data,rept,p_size,pase,q_size,gain);
    for i:=1 to (d_size-1) do begin
        data^[i]:=data^[i]-meanv1;
        data^[i+1]:=data^[i+1]-meanv2;
        i:=i+1;
    end;

    i:=1;
    for j:=1 to round(d_size/2) do begin
        v[j]:=data^[i];
        i:=i+2;
    end;
    for i:=1 to round(d_size/20) do begin
        v[i]:=v[i]*(1-cos(10*pi*(i-1)/d_size));
    end;
    for i:=round(9*d_size/20) to round(d_size/2) do begin
        v[i]:=v[i]*(1+cos(10*pi*i/d_size));
    end;
    i:=1;
    for j:=1 to round(d_size/2) do begin
        data^[i]:=v[j];
        i:=i+2;
    end;
    i:=1;
    for j:=1 to round(d_size/2) do begin
        v[j]:=data^[i+1];
        i:=i+2;
    end;
    for i:=1 to round(d_size/20) do begin

```

```

v[i1]:=v[i1]*(1-cos(10*pi*(i-1)/d_size));
end;
for i:=round(9*d_size/20) to round(d_size/2) do begin
v[i1]:=v[i1]*(1+cos(10*pi*i/d_size));
end;
i:=1;
for j:=1 to round(d_size/2) do begin
data^[i+1]:=v[j];
i:=i+2
end;

j:=1;
for i:=0 to n1 do begin
with a^[i1] do begin x:=data^[j]; y:=0.0; j:=j+2 end;
end;

j:=1;
for i:=0 to n1 do begin
with b^[i1] do begin x:=data^[j+1]; y:=0.0; j:=j+2 end;
end;

reord1(a);
trf1(a);
reord2(b);
trf2(b);
for k:=0 to n1 do begin
gx[k]:=gx[k]+mag(a^[k]);
gy[k]:=gy[k]+mag(b^[k]);
end;
for i:=0 to n1 do begin
conj(a^[i1],q);
prod(q,b^[i1],q^[i1]);
with q^[i1] do begin sumx[i1]:=sumx[i1]+x;
sumy[i1]:=sumy[i1]+y end;
end;
end;
for i:=0 to n1 do begin
gxy[i1]:=sqrt(sqr(sumx[i1])+sqr(sumy[i1]));
theta[i1]:=phase(sumy[i1],sumx[i1]);
end;
writeln;
for k:=0 to n1 do begin
gx[k]:=gx[k]*(2*pase2/n)*1.14286*1/nsamp;
gy[k]:=gy[k]*(2*pase2/n)*1.14286*1/nsamp;
gxy[k]:=gxy[k]*(2*pase2/n)*1.14286*1/nsamp;
gamma[k]:=sqr(gxy[k])/(gx[k]*gy[k]);
end;

rewrite(txt,'V20:COHERENCE.TEXT');
for j:=0 to round(n/2) do begin
f:=j/(n*pase2);
writeln(txt,f:9:6,' ',gamma[j]:9:6);
end;
close(txt,'SAVE');
rewrite(txt,'V20:FAZE.TEXT');
for j:=0 to round(n/2) do begin
f:=j/(n*pase2);
writeln(txt,f:9:6,' ',theta[j]:9:6);
end;
close(txt,'SAVE');
end.

```

CORRELATION PROGRAM

```

program corr(input,output);
{This program computes the space-time correlation function between}
{two sampled hot-wire anemometer signals. The time-delay is from }
{minus "tau" to plus "tau" and is user selectable.                }
import iodeclarations;
import general_2;
import measurement_lib;

const
    name = 'ADC';
    model = '98640A';
    select_code = 18;
    error = 'NO';
    units = 'STANDARD';
    multiplier = 1.0;
    offset = 0;
    p_size = 2;
    q_size = 2;

type
    r_array = ARRAY[1..15000] of real;
    r_ptr = ^r_array;
    i_array = ARRAY[1..7] of shortint;
    i_ptr = ^i_array;
    corr_array = ARRAY[0..7500] of real;
    corr_ptr = ^corr_array;

var
    data: r_ptr;
    cor, corn: corr_ptr;
    channel: i_ptr;
    gain: i_ptr;
    pace: r_ptr;
    c_size, d_size, rept, n, ns, i, j, k, np, p, msamp: integer;
    GAN1, GAN2, fmax, m, time, size, tavg, totaltime, sumsqv1, sumsqv2, sumv1, sumv2, tau,
    meanv1, meanv2, pase1, pase2, samplelength, rms1, rms2, d, rns: real;
    x: text;

begin {MAIN PROGRAM}

    pase1:=0.000025;
    writeln('ENTER THE MAXIMUM FREQUENCY COMPONENT OF THE SIGNAL');
    readnumber(1,fmax);
    writeln;
    writeln('ENTER THE PARAMETER "m" WHICH IS A MULTIPLIER OF THE');
    writeln('MINIMUM PACE RATE REQUIRED TO SATISFY THE NYQUIST CRITERION');
    writeln('NOTE: FOR GOOD DISCRETIZATION "m" SHOULD BE AT LEAST 5');
    readnumber(1,m);
    pase2:=(1.0/((1.0*m)))*(1.0/(2.0*fmax));
    if(pase2 < 0.000018) then
    begin
        writeln('THE PACE VALUE IS TOO SMALL FOR THE HP-98640A!!');
        writeln('*****');
        writeln('IF ALLOWED TO CONTINUE PACE WILL BE SET TO THE VALUE 0.000018');
        pase2:=0.000018;
    end;
    if (pase2 > 0.0393336) then
    begin
        writeln('THE PACE VALUE IS TOO LARGE FOR THE HP-98640A!!');
    end;

```

```

writein('*****');
writein('IF ALLOWED TO CONTINUE PACE WILL BE SET TO THE VALUE 0.0393336');
pace2:=0.0393336;
end;
writein('THE PACE RATE ON THE HP-98640A WILL BE SET TO:',pace2:9:7);
writein;
writein('ENTER THE MAXIMUM TIME-LAG (seconds)');
readnumber(1,time);
d_size:=round((time/(pace2+pace1))+1.0);
d_size:=(2*d_size);
if (d_size mod 4 = 0) then d_size:=d_size+2;
writein;
writein('d_size:= ',d_size:4);
writein;
if (d_size > 7500) then begin
writein('THE INCREMENTAL TIME IS TOO LARGE!!');
writein('*****');
writein('STOP PROGRAM EXECUTION AND RESTART WITH A SMALLER INCREMENTAL');
writein('TIME.....');
writein;
end;
rept:=round(d_size/2.0);
writein('ENTER THE NUMBER OF ENSEMBLES FOR COMPUTING THE AVERAGE');
writein('SPACE-TIME CORRELATION FUNCTION');
writein;
readnumber(1,rns);
ns:=round(rns);
writein;
c_size:=2;
new(channel);
channel^[1]:=2;
channel^[2]:=1;
new(pace);
pace^[1]:=pace2;
pace^[2]:=pace1;
new(gain);
writein('ENTER THE GAIN SETTING FOR CHANNEL 1');
readnumber(1,gan1);
writein('ENTER THE GAIN SETTING FOR CHANNEL 2');
readnumber(1,gan2);
gain^[1]:=round(gan2);
gain^[2]:=round(gan1);
meas_lib_init;
config_0(name,model,select_code,1,0.02,error,units,multiplier,offset);
init(name);
calibrate(name,3,0.0001,1000);
new(cor);
new(corn);
new(data);
sumv1:=0.0;
sumv2:=0.0;
sumsqv1:=0.0;
sumsqv2:=0.0;
for i:= 0 to (round(d_size/2)-1) do begin
cor^[i]:=0.00;
corn^[i]:=0.00
end;
writein;
writein('NOW CALCULATING THE MEAN VOLTAGE TO BE SUBTRACTED FROM ALL');
writein('TIME SERIES DATA ELEMENTS');
writein;
writein('ENTER THE AVERAGING TIME FOR COMPUTING THE MEAN VOLTAGE');
writein;
readnumber(1,tavg);
msamp:=round(tavg/((pace2+pace1)*d_size));
for i:= 1 to msamp do begin

```

```

        writeln(chr(12));
        writeln;
        writeln('MEAN VOLT CALCULATION IN PROGRESS...REPETITION ',i:3,' OF ',msamp:3);
        random_scan(name,c_size,channel,d_size,data,rept,p_size,pase,pase2,gain);
        for j:=1 to d_size do begin
            sumv1:=sumv1+data^[j];
            sumv2:=sumv2+data^[j+1];
            sumsqv1:=sumsqv1+sqr(data^[j]);
            sumsqv2:=sumsqv2+sqr(data^[j+1]);
            j:=j+1;
        end;
    end;
    meanv1:=(2.0*sumv1)/(d_size*msamp);
    meanv2:=(2.0*sumv2)/(d_size*msamp);
    sumsqv1:=(sumsqv1/(((d_size/2.0))*msamp))-(sqr(meanv1));
    sumsqv2:=(sumsqv2/(((d_size/2.0))*msamp))-(sqr(meanv2));
    rms1:=sqrt(sumsqv1);
    rms2:=sqrt(sumsqv2);

    writeln('*****BEGIN CORRELATION MEASUREMENT*****');
    for i:=1 to ns do
        begin
            writeln(chr(12));
            writeln;
            writeln('CORRELATION SAMPLE NUMBER ',i:4,' OF ',ns:4);
            random_scan(name,c_size,channel,d_size,data,rept,p_size,pase,pase2,gain);
            for k:=1 to (d_size-1) do begin
                data^[k]:=data^[k]-meanv1;
                data^[k+1]:=data^[k+1]-meanv2;
                k:=k+1;
            end;

            for k:= 0 to (round(d_size/2)-1) do begin
                p:=1;
                for j:=1 to (round(d_size/2)-k) do begin
                    cor^[k]:=cor^[k]+data^[p]*data^[p+(2*k)+1];
                    p:=p+2;
                end;
            end;
            for k:=0 to (round(d_size/2)-2) do begin
                p:=2;
                for j:=1 to (round(d_size/2)-k-1) do begin
                    corn^[k]:=corn^[k]+(data^[p]*data^[p+(2*k)+1]);
                    p:=p+2;
                end;
            end;
            for k:= 0 to (round(d_size/2)-1) do begin
                cor^[k]:=cor^[k]/(ns*((d_size/2)-k))/(rms1*rms2);
            end;
            for k:=0 to (round(d_size/2)-2) do begin
                corn^[k]:=corn^[k]/(ns*((d_size/2)-1-k))/(rms1*rms2);
            end;
            for k:=0 to (round(d_size/2)-1) do begin
                cor^[k+round(d_size/2)]:=cor^[k];
            end;
            {SHIFT DATA ONE ELEMENT TO THE LEFT}
            for k:=(round(d_size/2)-1) to (d_size-2) do begin
                cor^[k]:=cor^[k+1];
            end;
            for k:=0 to (round(d_size/2)-2) do begin
                corn^[k]:=corn^[round(d_size/2)-2-k];
            end;
            rewrite(x,'KIRK:CORRDATA.TEXT');
            tau:=--((d_size/2)-1)*(pase1+pase2);

```

```
np:=d_size-1;  
writeln(x,np);  
for k:=0 to d_size-2 do begin  
  writeln(x,tau:9:6,' ',con[k1:7:4]);  
  tau:=tau+(pase2+pase1);  
end;  
close(x,'SAVE');  
end.
```

APPENDIX B

UNCERTAINTY ANALYSIS

An experimental uncertainty analysis was performed to determine uncertainties in certain measurements. The method of Kline and McClintock (1953) was used to obtain the results

1. Uncertainty in setting the Reynolds Number

$$Re_D = \pm 3.6\%$$

2. Uncertainty in Mean Velocity Measurements

$$U = U \pm 2.5\%$$

3. Uncertainty in RMS Velocity Measurements

$$\langle u^2 \rangle^{1/2} = \pm 5\%$$

2
VITA

William Kirk Bryza

Candidate for the Degree of
Master of Science

Thesis: TRANSITION AND STRUCTURAL DEVELOPMENT OF THE NEAR
FIELD OF A PLANAR TURBULENT JET UNDER LOW LEVEL
ACOUSTIC EXCITATION

Major Field: Mechanical Engineering

Biographical:

Personal Data: Born in Ft. Chaffee, Arkansas,
March 9, 1963, the son of William V. and
Margaret Bryza

Education: Graduated from Chisholm High School, Enid,
Oklahoma, in May 1981; received Bachelor of
Science Degree in Mechanical Engineering from
University of Oklahoma State in May, 1987;
completed requirements for the Master of Science
degree at Oklahoma State University in
May, 1989.

Professional Experience: Teaching Assistant,
Department of Mechanical Engineering, Oklahoma
State University, August, 1987, to December,
1988.